



Tan, Minghu (2018) *Low energy capture of near-Earth asteroids in the circular restricted three-body problem*. PhD thesis.

<https://theses.gla.ac.uk/30779/>

Copyright and moral rights for this work are retained by the author

A copy can be downloaded for personal non-commercial research or study, without prior permission or charge

This work cannot be reproduced or quoted extensively from without first obtaining permission in writing from the author

The content must not be changed in any way or sold commercially in any format or medium without the formal permission of the author

When referring to this work, full bibliographic details including the author, title, awarding institution and date of the thesis must be given

Enlighten: Theses

<https://theses.gla.ac.uk/>
research-enlighten@glasgow.ac.uk



University
of Glasgow

**Low energy capture of near-Earth
asteroids in the circular restricted three-
body problem**

Minghu Tan

School of Engineering
College of Science and Engineering
University of Glasgow

June 2018

ABSTRACT

Near-Earth Asteroids (NEAs) can provide useful resources in terms of feedstock for spacecraft propellant, crew logistic support and a range of useful metals. The possibility of capturing small NEAs using low energy transfers would therefore be of significant scientific and commercial interest. Although NEAs may make close approaches to the Earth, and so represent a potential impact threat, the exploitation of their resources has long been proposed as a necessary element for future space exploration.

The objective of the research presented in this thesis is to develop methodologies for the trajectory design of capturing NEAs in the neighbourhood of the Earth. Firstly aimed at capturing NEAs around the Earth-Moon L_2 point, a new type of lunar asteroid capture is defined, termed direct capture. In this capture strategy, the transfer trajectory for capturing a NEA into the Earth-Moon system is modelled in the Sun-Earth-Moon restricted four-body. A Lambert arc in the Sun-asteroid two-body problem is used as an initial guess and a differential corrector used to generate the transfer trajectory from the asteroid's initial orbit to the stable manifold associated with Earth-Moon L_2 point. The direct asteroid capture strategy requires a shorter flight time compared to an indirect asteroid capture strategy, which couples capture in the Sun-Earth circular restricted three-body problem and subsequent transfer to the Earth-Moon circular restricted three-body problem. Finally, the direct and indirect asteroid capture strategies are also applied to consider capture of asteroids at the triangular libration points in the Earth-Moon system.

As ideal locations for space science missions and candidate gateways for future crewed interplanetary missions, the Sun-Earth libration points L_1 and L_2 are also preferred locations for the captured asteroids. Therefore, the concept of coupling together a flyby of the Earth and then capturing small NEAs onto Sun-Earth L_1 or L_2 periodic orbits is proposed. A periapsis map is then employed to determine the required perigee of the Earth flyby. Moreover, depending on the perigee distance of the flyby, Earth flybys with and without aerobraking are investigated to design a transfer trajectory capturing a small NEA from its initial orbit to the stable manifolds associated with Sun-Earth L_1 and L_2 periodic orbits. NEA capture strategies using an Earth flyby with and without aerobraking both have the potential to be of lower cost in terms of energy requirements than a direct NEA

capture strategy without the Earth flyby. Moreover, NEA capture with an Earth flyby also has the potential for a shorter flight time compared to the NEA capture strategy without the Earth flyby. Following by this work, a more general analysis of aerobraking is undertaken and the low energy capture of near-Earth asteroids into bound orbits around the Earth using aerobraking is then investigated. Two asteroid capture strategies utilising aerobraking are defined, termed single-impulse capture and bi-impulse capture, corresponding to two approaches to raising the perigee height of the captured asteroid's orbit after the aerobraking manoeuvre. A Lambert arc in the Sun-asteroid two-body problem is again used as an initial estimate for the transfer trajectory to the Earth and then a global optimisation is undertaken, using the total transfer energy cost and the retrieved asteroid mass ratio (due to ablation) as objective functions. It is shown that aerobraking can in principle enable candidate asteroids to be captured around the Earth with, in some cases, extremely low energy requirements.

The momentum exchange theory is also applied to the capture of small near-Earth asteroids into bound periodic orbits at the Sun-Earth L_1 and L_2 points. A small asteroid is first manoeuvred to engineer a flyby with a larger asteroid. Two strategies are then considered: when the small asteroid approaches the vicinity of the large asteroid, it will either impact the large asteroid or connect to it with a tether. In both strategies, momentum exchange can be used to effect the capture of one of the asteroids. Then, a two-impulse Lambert arc is utilised to design a post-encounter transfer trajectory to the stable manifolds of the Sun-Earth L_1 or L_2 points. By investigating the outcome of the impact on the small asteroid, or the tension of the tether, the maximum velocity increment available using these momentum exchange strategies is investigated. Again the capture strategies using momentum exchange in principle have the potential to deliver low-energy capture of asteroids.

The methods presented in this thesis are intended to be used as a preliminary analysis for these asteroid capture strategies. Although some significant practical challenges remain, the transfer in the CRTBP models can serve as a good approximation for the trajectory in a more accurate dynamical model.

TABLE OF CONTENTS

Abstract	I
Table of Contents	III
List of Figures	VII
List of Tables.....	XIII
Acknowledgement.....	XV
Nomenclature	XVI
Chapter 1 Introduction	1
1.1 Asteroid exploration and capture missions	2
1.1.1 Asteroid capture around the Sun-Earth libration points L_1/L_2	7
1.1.2 Asteroid capture into the vicinity of the Moon	8
1.1.3 Asteroid capture into bound orbits around the Earth	9
1.2 Low-energy strategies of capturing asteroids	11
1.2.1 Multi-body and invariant manifold theory.....	11
1.2.2 Gravity assist manoeuvres.....	13
1.2.3 Aerobraking and aerocapture	14
1.2.4 Momentum exchange theory.....	16
1.2.5 Advanced propulsion technologies	17
1.3 Objectives.....	18
1.4 Thesis outline	19
1.5 Publications	21
Chapter 2 Dynamical models.....	24
2.1 Two-body problem.....	25
2.1.1 Orbital elements	26

2.1.2	Lambert arc	28
2.2	Circular restricted three-body problem	29
2.2.1	Libration points and Jacobi constant.....	31
2.2.2	Zero-velocity surfaces.....	33
2.2.3	State Transition and Monodromy Matrices.....	36
2.2.4	Periodic orbits around L_1/L_2	37
2.2.5	Periodic orbits around L_4/L_5	39
2.2.6	Invariant manifolds	40
2.3	Sun-Earth-Moon four-body problem	42
2.3.1	Patched three-body model.....	43
2.3.2	Four-body problem in Sun-centred inertial frame	43
Chapter 3	Capture of small NEAs in the vicinity of the Moon	45
3.1	Direct capture of NEAs in the Earth-Moon system	46
3.1.1	Target periodic orbits in the Earth-Moon system	46
3.1.2	Strategy for direct capture.....	47
3.1.3	Target point filter	50
3.1.4	Differential correction for the Sun-Earth-Moon four-body problem.....	55
3.1.5	Candidate asteroid selection.....	57
3.1.6	Approach date and departure date guess.....	60
3.1.7	Design procedure	62
3.1.8	Optimisation and discussion	63
3.2	Indirect capture of NEAs to Earth-Moon L_2 periodic orbits.....	66
3.3	Direct and indirect capture of NEAs to Earth-Moon system triangular points....	74
3.4	Discussions.....	79
Chapter 4	Capture of NEAs around Sun-Earth libration points using Earth flyby and aerobraking	81
4.1	Target periodic orbits and stable manifolds.....	82
4.2	Strategies for Earth flyby	83
4.2.1	Aerobraking model.....	84

4.2.2	Earth flyby without aerobraking	88
4.3	Asteroid capture opportunities	89
4.3.1	Asteroid hazard analysis	89
4.3.2	Candidate asteroids selection	90
4.3.3	Asteroid capture window	92
4.4	Asteroid capture using Earth flyby without aerobraking	92
4.4.1	Problem statement.....	92
4.4.2	Initial guess and differential correction.....	94
4.4.3	Design Procedure	95
4.4.4	Optimisation.....	97
4.4.5	Comparison of the results of asteroid capture with and without Earth flyby ..	99
4.5	Asteroid capture using aerobraking	102
4.5.1	Problem statement.....	102
4.5.2	Aerobraking phase	104
4.5.3	Aerobraking opportunities for periodic orbits.....	106
4.5.4	Aerobraking window.....	108
4.5.5	Design Procedure and Optimisation.....	109
4.6	Discussion	115
Chapter 5	Capture of small NEAs at the Earth using direct aerobraking	117
5.1	Capture conditions	118
5.2	Asteroid capture around the Earth using aerobraking.....	120
5.2.1	Asteroid capture opportunities and initial guess	120
5.2.2	Modes of aerobraking	124
5.2.3	Two approaches to raise the perigee height after aerobraking.....	125
5.2.4	Bi-impulse capture of asteroids at the Earth	128
5.2.5	Single impulsive capture of asteroids around the Earth.....	132
5.3	Maximum mass ratio of the captured asteroid and spacecraft	137
5.4	Discussion	141
Chapter 6	Capture of NEAs using momentum exchange strategies.....	142

6.1	Target periodic orbits and invariant manifolds	143
6.2	Candidate asteroid selection.....	144
6.2.1	Capture windows.....	144
6.2.2	Candidate asteroid filter	144
6.3	Small asteroid capture through impact of a large asteroid.....	145
6.3.1	Problem statement.....	146
6.3.2	Collision geometry	147
6.3.3	Analysis of impact mechanics.....	150
6.3.4	Selection of candidate large asteroids	153
6.3.5	Design procedure and optimisation.....	154
6.4	Small asteroid capture by tether-assisted flyby of large asteroids	161
6.4.1	Statement of the problem	162
6.4.2	Dynamical model during tether-assisted flyby	162
6.4.3	Analysis of the tether forces.....	164
6.4.4	Selection strategy for candidate asteroids	165
6.4.5	Design procedure and optimisation.....	166
6.5	Conclusions	172
Chapter 7	Conclusions	174
7.1	Summary of thesis.....	174
7.2	Current limitations	177
7.3	Remarks on future work.....	177
7.3.1	Trajectory refinement.....	178
7.3.2	Optimisation for maximum economic return.....	178
7.3.3	NEA transfer vehicle design and mission operations	179
References	181

LIST OF FIGURES

Fig. 1.1 Orbital distribution of NEAs: (a) semi-major and eccentricity and (b) semi-major and inclination.....	2
Fig. 1.2 Decision tree for potential options and methods of capturing asteroids.....	5
Fig. 2.1 Geometry of the two-body problem.	26
Fig. 2.2 Geometry of the orbital elements.	27
Fig. 2.3 Schematic diagram of the Lambert problem.....	29
Fig. 2.4 Geometry of the CRTBP system in the frame xyz and in an inertial frame XYZ	31
Fig. 2.5 Geometry of the libration points in the Earth-Moon CRTBP system.	33
Fig. 2.6 Zero-velocity surface in the Earth-Moon CRTBP system with Jacobi constant $C = 3.16$: (a) 3D view; (b) x - y projection; (c) x - z projection.....	34
Fig. 2.7 Zero-velocity curve, possible region of motion (white) and forbidden region (grey) in the Earth-Moon CRTBP system with (a) $C = C_1$; (b) $C_2 < C < C_1$; (c) $C = C_2$; (d) $C = C_3$; (e) $C_4 = C_5 < C < C_3$; (f) $C = C_4 = C_5$	35
Fig. 2.8 A Lyapunov orbit with an initial guess when $A_x = 0.15$, $A_z = 0$ in Eq. (2.28).	38
Fig. 2.9 Halo orbits with an initial guess when $A_x = 0.15$, $A_z = 0.38$ in Eq. (2.28): (a) 3D view; (b) x - y projection; (c) x - z projection; (d) y - z projection.....	39
Fig. 2.10 Short-period orbits around the triangular points L_4 and L_5 points in the Earth-Moon system ($\kappa_1 = 0$, $\kappa_2 = 0.1$).....	42
Fig. 2.11 Stable and unstable manifolds associated with a Lyapunov orbit around the Earth-Moon L_2 point in Fig. 2.8.....	42
Fig. 2.12 Geometry of the Sun-Earth-Moon restricted four-body problem.	44
Fig. 3.1 Planar Lyapunov orbits with Jacobi constant [3.01017213, 3.17205221] and (b) halo orbits with Jacobi constant [3.06733209, 3.15211497] around L_2 point in the Earth-Moon system.	46
Fig. 3.2 Stable manifolds associated with a Lyapunov orbit ($C = 3.15415202$) around the Earth-Moon L_2 point.	47
Fig. 3.3 Direct capture of a NEA: (a) initial impulse Δv_1 for the asteroid to leave its orbit; (b) second impulse Δv_2 to insert the asteroid onto the stable manifold associated with the periodic orbit around the Earth-Moon L_2 point.	48

Fig. 3.4 (a) Jacobi constant of Lyapunov orbits with different x -amplitudes around the Earth-Moon L_2 point; (b) Jacobi constant of halo orbits with different z -amplitudes around the Earth-Moon L_2 point.	49
Fig. 3.5 (a) Period T_p of Lyapunov orbits with different x -amplitudes around the Earth-Moon L_2 point; (b) Period T_p of halo orbits with different z -amplitudes around the Earth-Moon L_2 point.	50
Fig. 3.6 Earth-Moon L_2 stable manifolds inside the 3BSOI.	51
Fig. 3.7 Maximum and minimum values of (a) f_{sm} and (b) f_{em} with different values of r_s ...	53
Fig. 3.8 $t_{threshold}$ with different amplitude variables A_p (a) stable manifold associated with Earth-Moon L_2 Lyapunov orbits; (a) stable manifold associated with Earth-Moon L_2 halo orbits.....	54
Fig. 3.9 Differential correction with an initial guess using a Lambert transfer.	55
Fig. 3.10 Given $T_f = 63000$ [MJD], the three-dimensional orbital element space of target points on the stable manifolds associated with Earth-Moon L_2 Lyapunov orbits (red) and halo orbits (black): (a) 3D view; (b) $a-e$ projection; (c) $e-i$ projection. .	58
Fig. 3.11 Three-dimensional orbital element space of the stable manifold associated with Earth-Moon L_2 Lyapunov orbits with a Δv threshold of 500 m/s: (a) 3D view; (b) $a-e$ projection; (c) $e-i$ projection.	59
Fig. 3.12 Three-dimensional orbital element space of the stable manifold associated with Earth-Moon L_2 halo orbits with a Δv threshold of 500 m/s: (a) 3D view; (b) $a-e$ projection; (c) $e-i$ projection..	60
Fig. 3.13 Approach date guess by using MOMD (2018 AV2).	61
Fig. 3.14 The first impulse δv_1 (m/s) as a function of T_0 and T_f (2018 AV2).	62
Fig. 3.15 Given $T_0 = 65833.1$ [MJD], $T_f = 66495.5$ [MJD], $A_p = -0.04994$, $t_p = 0.255$, $t_{sm} = 4.10$, direct capture trajectory (phase I) for 2018 AV2 to an Earth-Moon L_2 halo orbit and stable manifold (phase II) associated with the target halo orbit in the J2000 Sun-centred inertial frame: (a) 3D view; (b) $x-y$ projection; (c) $x-z$ projection; (d) $y-z$ projection.....	64
Fig. 3.16 (a) Planar Lyapunov orbits with x -amplitude $[0, 0.0080998]$ (corresponding to Jacobi constant $[2.99991065, 3.00089301]$) and (b) halo orbits with z -amplitude $[-0.0050595, 0.0050595]$ (corresponding to Jacobi constant $[3.00022207, 3.00083043]$) around L_1 and L_2 points in the Sun-Earth system.	67
Fig. 3.17 Part of indirect asteroid capture by patching together the Lambert arc in the Sun-asteroid two-body problem and Sun-Earth stable manifolds.....	68
Fig. 3.18 Part of Indirect asteroid capture by patching together Sun-Earth unstable manifold and Earth-Moon stable manifold with the Poincaré section.....	68

Fig. 3.19 (a) Unstable manifolds of Sun-Earth L_2 Lyapunov orbit ($A_{SE} = 0.0048497$ AU) and (b) their integration time to the same Poincaré section ($x = 1 - \mu$) with varying $\varepsilon \in [0.4 \times 10^{-6}, 2 \times 10^{-6}]$	70
Fig. 3.20 Indirect capture trajectory for 2018 AV2 to Earth-Moon L_2 Lyapunov orbit in the Sun-Earth rotating frame: (a) the transfer trajectory of Part I (b) the transfer trajectory of Part II.....	71
Fig. 3.21 Intersection of Sun-Earth L_2 manifolds and Earth-Moon L_2 manifolds ($\vartheta = 0.5\pi$) with Poincaré section ($x = 1 - \mu$) in the Sun-Earth rotating frame.....	74
Fig. 3.22 Short-period orbits around the triangular points L_4 in the Earth-Moon system ($\kappa_1 = 0, A_p \leq 0.2$).	75
Fig. 3.23 Two types of asteroid capture strategies to the Earth-Moon triangular points: (a) direct capture strategy; (b) indirect capture strategy.....	76
Fig. 3.24 Optimal direct capture trajectory for 2018 AV2 to the Earth-Moon L_4 periodic orbit in the J2000 Sun-centred inertial frame: (a) 3D view; (b) x - y projection; (c) x - z projection; (d) y - z projection.	78
Fig. 3.25 Optimal indirect capture trajectory for 2018 AV2 to Earth-Moon L_4 periodic orbit in Sun-Earth rotating system.....	78
Fig. 4.1 Stable manifolds associated with a Sun-Earth L_2 periodic orbit ($A_p = 0.0020187$) and the periapsis map.....	83
Fig. 4.2 Schematic diagram of an aerobraking	84
Fig. 4.3 (a) Aerobraking Δv provided by the atmosphere as a function of height h and different relative velocities v_p of the asteroid, given an asteroid diameter of $D = 10$ m; (b) Aerobraking Δv provided by the atmosphere as a function of height h and asteroid diameter D given a perigee speed $v_p = 15$ km/s.	88
Fig. 4.4 Schematic diagram of an Earth flyby without aerobraking	88
Fig. 4.5 Mass loss ratio of a 30 m asteroid after aerobraking with incident velocity with respect to the Earth.....	89
Fig. 4.6 Estimated average natural impact interval of asteroids versus asteroid diameter. .90	
Fig. 4.7 Distribution of candidate asteroids: (a) semi-major and eccentricity and (b) semi-major and inclination.	91
Fig. 4.8 $T_{threshold}$ of candidate asteroids	92
Fig. 4.9 Schematic strategy for asteroid capture using Earth flyby without aerobraking: (a) the candidate asteroid leaves its orbit with the first manoeuvre; (b) the candidate asteroid is inserted onto the stable manifold after the Earth flyby.	94

Fig. 4.10 Given $A_p = 0.0018878$, $t_p = 1.637679$, perigee of the stable manifold associated with the Sun-Earth L_2 Lyapunov orbit: (a) global view; (b) local view.	96
Fig. 4.11 Given $\Delta v_3 = 185.96$ m/s and $T_{fly2} = 270.58$ days, the trajectory prior to Δv_3 obtained by propagating backward from the state at perigee: (a) global view; (b) local view.	96
Fig. 4.12 Given $T_0 = 58977.85$ [MJD], $T_{fly1} = 285.87$ days, the transfer trajectory (x - y projection) to capture 2010 UJ onto a Sun-Earth L_2 Lyapunov orbit in the Sun-Earth rotating frame.	97
Fig. 4.13 Transfer trajectory (x - y projection) for capturing 2010 UJ onto the Sun-Earth L_2 Lyapunov orbit in the Sun-centred inertial frame.	97
Fig. 4.14 Schematic strategy for asteroid capture using aerobraking: (a) the candidate asteroid leaves its orbit with the first manoeuvre; (b) the candidate asteroid is inserted onto the stable manifold after aerobraking.	103
Fig. 4.15 Stable manifolds with Lyapunov orbits around the Sun-Earth L_1 and L_2 points.	106
Fig. 4.16 Relationship between r_{min} and the amplitude variable A_p of Lyapunov orbits around the Sun-Earth L_1 point within a given stable manifold flight time (400 days).	107
Fig. 4.17 Relationship between r_{min} and the amplitude variable A_p of Sun-Earth L_1 halo orbits.	107
Fig. 4.18 Relationship between r_{min} and the amplitude variable A_p of Sun-Earth L_2 Lyapunov orbits.	107
Fig. 4.19 Relationship between r_{min} and the amplitude variable A_p of Sun-Earth L_2 halo orbits.	108
Fig. 4.20 Periapsis map of the stable manifolds of a Sun-Earth L_2 Lyapunov orbit with $A_p = 0.0020187$	108
Fig. 4.21 Relationship between the distance of the perigee of the stable manifolds and the parameter t_p	109
Fig. 4.22 Given $A_p = 0.0028288$ AU, $t_p = 1.478633$, the stable manifold associated with the Sun-Earth L_2 Lyapunov orbit and its perigee: (a) global view; (b) local view.	110
Fig. 4.23 Given $T_{fly2} = 5.64$ days, the trajectory before aerobraking is obtained by propagating backward from the state at perigee.	110
Fig. 4.24 Given $T_0 = 59298.19$ [MJD], $T_{fly1} = 216.31$ days, the transfer trajectory (x - y projection) for capturing 2010 UJ onto the Sun-Earth L_2 Lyapunov orbit in the Sun-Earth rotating frame.	111

Fig. 4.25 Transfer trajectory (x - y projection) for capturing 2010 UJ onto the Sun-Earth L_2 Lyapunov orbit in the Sun-centred inertial frame.....	111
Fig. 5.1 x - y projection of the zero-velocity surface when $C = C_1$ and $C = C_2$	119
Fig. 5.2 Examples of trajectories of an asteroid with (a) $C > C_1$; (b) $C = C_1$; (c) $C = C_2 < C_1$; (d) $C < C_2$	119
Fig. 5.3 Overview of capturing NEAs at the Earth using aerobraking	120
Fig. 5.4 Mass loss ratio of an asteroid caused by aerobraking, with different relative velocity and heights above the Earth's surface.....	122
Fig. 5.5 Estimate of the number of asteroids as a function of Δv threshold.	122
Fig. 5.6 Distribution of candidate asteroids (circled) in the family of NEAs: (a) semi-major and eccentricity and (b) semi-major and inclination.....	123
Fig. 5.7 Optimal capture date T_0 guess for capturing 2012 BK14 with potential capture dates highlighted.	123
Fig. 5.8 Perigee map of the asteroid 2012 BK1 orbit with different initial manoeuvres: (a) x - y projection; (b) x - z projection.....	124
Fig. 5.9 Retrograde orbits and prograde orbits generated from Fig. 5.8: (a) 3D view; (b) x - y projection; (c) x - z projection; (d) y - z projection.	125
Fig. 5.10 Strategies to raise the perigee height after aerobraking: (a) additional manoeuvre at apogee; (b) three-body interaction.	126
Fig. 5.11 Geometry of the captured asteroid and the Sun in the Earth-centred inertial frame XYZ.	128
Fig. 5.12 Transfer trajectory capturing 2012 BK14 including: a) transfer trajectory before aerobraking in the Sun-centred inertial frame; b) orbit around the Earth after aerobraking in the Earth-centred inertial frame.	130
Fig. 5.13 Transfer trajectory of capturing 2012 BK14 before aerobraking in the Sun-centred inertial frame.	133
Fig. 5.14 Capture orbit of 2012 BK14 around the Earth after aerobraking for 1000 days in the Sun-Earth rotating frame: (a) 3D view; (b) x - y projection; (c) x - z projection.	134
Fig. 5.15 Perigee height of the captured asteroid's orbit around the Earth after aerobraking	135
Fig. 5.16 Comparison of the true change and estimated change in the perigee height.....	135
Fig. 6.1 Stable manifolds associated with the Lyapunov orbit ($A_p = 0.0020101$ AU) around Sun-Earth L_2	143
Fig. 6.2 Distribution of candidate large and small asteroids: (a) semi-major and eccentricity and (b) semi-major and inclination.	145

Fig. 6.3 Overview of small asteroid capture through impact of a large asteroid.	146
Fig. 6.4 Collision geometry of the two asteroids.	148
Fig. 6.5 Geometric relationship of the vectors in Eq. (6.6) (a) when $ \Delta \mathbf{v}_{ls}^T \mathbf{n}_c \leq \Delta v_{threshold}$ (b)	
when $ \Delta \mathbf{v}_{ls}^T \mathbf{n}_c > \Delta v_{threshold}$	150
Fig. 6.6 Contour map of $\Delta v_{threshold}$ as a function of S_{s_0} and ρ_a	152
Fig. 6.7 Candidate large asteroids when capturing 2008 JL24 into a Lyapunov orbit with	
$\Delta V/2 = 441.19$ m/s.	154
Fig. 6.8 Transfer trajectory for capturing 2008 JL24 into a Lyapunov orbit by impacting	
2001 QJ142 (a) in the Sun-centred inertial frame; (b) in the Sun-Earth rotating	
frame, assuming that they are metallic asteroids.	155
Fig. 6.9 Overview of small asteroid capture using tether-assisted flyby.	161
Fig. 6.10 Contour map of the Δv_{st} as a function of the small asteroid-to-tether mass ratio	
and the characteristic velocity of the tether.	165
Fig. 6.11 Transfer trajectory for capturing 2008 JL24 into a Lyapunov orbit using the	
carbon nanotube tethered flyby of 2015 KE (a) in the Sun-centred inertial frame;	
(b) in the Sun-Earth rotating frame.	167

LIST OF TABLES

Table 1.1 A brief summary of results and solutions of asteroids capture.....	6
Table 2.1 Coordinates of the libration points in the Earth-Moon and Sun-Earth systems...	33
Table 2.2 Jacobi constant at the libration points of the Earth-Moon and Sun-Earth systems.	35
Table 3.1 Orbital elements of the candidate NEAs.....	61
Table 3.2 Results of optimal direct capture of asteroid to Earth-Moon L_2 periodic orbits using the stable manifolds.....	65
Table 3.3 Results of optimal direct capture of asteroid to Earth-Moon L_2 periodic orbits without using the stable manifolds.....	66
Table 3.4 Results of optimal indirect capture of asteroids to Earth-Moon L_2 periodic orbits	72
Table 3.5 Results of optimal indirect capture of asteroids to Earth-Moon L_2 periodic orbits without using the Earth-Moon stable manifolds.....	73
Table 3.6 Results of optimal direct capture of asteroids to the Earth-Moon triangular point	77
Table 3.7 Results of optimal indirect capture of asteroids to the Earth-Moon triangular point.....	77
Table 4.1 Results of capturing asteroids onto Sun-Earth L_1 or L_2 Lyapunov orbits using an Earth flyby without aerobraking.....	98
Table 4.2 Results of capturing asteroids onto Sun-Earth L_1 or L_2 Halo orbits using an Earth flyby without aerobraking.....	99
Table 4.3 Results of capturing asteroids onto Sun-Earth L_1 or L_2 Lyapunov orbits without using an Earth flyby.....	100
Table 4.4 Results of capturing asteroids onto Sun-Earth L_1 or L_2 halo orbits without using an Earth flyby.....	101
Table 4.5 Results of capturing asteroids onto Sun-Earth Lyapunov orbits using aerobraking	113
Table 4.6 Results of capturing asteroids onto Sun-Earth Halo orbits using aerobraking ..	114

Table 5.1 Optimal results of capturing asteroids around the Earth in the Earth two-body problem	131
Table 5.2 Results of capturing asteroids around the Earth in the Sun-Earth CRTBP.....	136
Table 5.3 Results of bi-impulsive capture of asteroids at the Earth when optimising f_m ...	139
Table 5.4 Results of single impulse capture of asteroids at the Earth when optimising f_m	140
Table 6.1 Results for the capture of metallic asteroids into Lyapunov orbits with and without impacting large metallic asteroids	156
Table 6.2 Results for the capture of basalt asteroids into Lyapunov orbits with and without impacting large basalt asteroids	157
Table 6.3 Results for the capture of metallic asteroids into halo orbits with and without impacting large metallic asteroids.....	158
Table 6.4 Results for the capture of basalt asteroids into halo orbits with and without impacting large basalt asteroids	159
Table 6.5 Results for asteroid capture into Lyapunov orbits with and without the carbon nanotube tether assist	168
Table 6.6 Results for asteroid capture into Lyapunov orbits with and without the Zylon tether assist.....	169
Table 6.7 Results for asteroid capture into halo orbits with and without the carbon nanotube tether assist	170
Table 6.8 Results for asteroid capture into halo orbits with and without the Zylon tether assist.....	171

ACKNOWLEDGEMENT

First and foremost, I must recognise and express my sincerest gratitude to my supervisor Professor Colin McInnes for his incredible support, patience and guidance. He always provides help when needed and he provides valuable advice and suggestions on my research. I thank Professor Colin McInnes for his invaluable scientific guidance and the contribution to many of the ideas in this thesis.

I would also like to express my deepest appreciation to my second supervisor Dr Matteo Ceriotti for his help and support in my research, especially in the field of the trajectory optimisation. His directions and suggestions were of great help towards the achievement of my research goals.

I would like to acknowledge financial support from the China Scholarship Council (CSC) without which I would not be able to pursue my work at the University of Glasgow.

I would like to thank my colleagues in our research group for their assistance and suggestions. They have always been kind and willing to help me in all circumstances.

Thanks to my friends in Glasgow who made my life exciting, wonderful and happy. With their company, I adapted to the new life in Glasgow. I will never forget the good times we had together.

Last, but definitely not the least, I wish to express my love and gratitude to my parents who always encourage and support me, and believed in me no matter what I decided to do. I cannot thank them enough for their support and love.

For these reasons, my experience of PhD research at University of Glasgow must be one of the best and most unforgettable periods in my life. It has broadened and extended my vision. To each of the above, I express my deepest appreciation again.

Thanks to all!

NOMENCLATURE

Acronyms

3BSOI	=	Moon-Sun three-body sphere of influence
ARM	=	Near-earth asteroid redirect mission
AU	=	Astronomical Unit
BVP	=	Boundary value problem
CNSA	=	China national space administration's
CNT	=	Carbon nanotube tether
CRTBP	=	Circular restricted three-body problem
EGA	=	Earth gravity assist
ERO	=	Easily retrievable object
ESA	=	And European Space Agency
JAXA	=	Japan aerospace exploration agency
KAM	=	Kolmogorov–arnold–moser
LEO	=	Low Earth orbit
LPO	=	Libration point orbit
MGAs	=	Multiple gravity assists
MOID	=	Minimum Orbit Intersection Distance
MJD	=	Modified Julian date
NASA	=	National Aeronautics and Space Administration
NEA	=	Near-Earth asteroid
PHA	=	Potentially Hazardous Asteroids
TCA	=	Temporarily captured asteroid
WSB	=	Weak stability boundary
SQP	=	Sequential quadratic programming

Symbols

a	=	Semi-major axis of the orbit, AU
A	=	Constant cross-sectional area, m ²
A/M	=	Area-to-mass ratio of the asteroid, m ² /kg
A_p	=	Amplitude variable of periodic orbits
A_{SE}	=	Amplitude variable of target periodic orbit around Sun-Earth L ₁ /L ₂
A_{EM}	=	Amplitude variable of target periodic orbit around Earth-Moon L ₂ point
A_x	=	Amplitude of the periodic orbit along the x -axis
A_z	=	Amplitudes of the periodic orbit z -axis
B	=	Asteroid ballistic coefficient
C	=	Jacobi constant
C_d	=	Drag coefficient of a sphere
C_i	=	Jacobi constant at the libration point L _{<i>i</i>} ($i = 1 - 5$)
C_-, C_+	=	Jacobi constants of the captured asteroid before and after aerobraking, respectively
D	=	Asteroid diameter, m
e	=	Orbit eccentricity
e_+	=	Eccentricity of post-aerobraking orbit
e_n	=	Eccentricity of the orbit with the perigee raised
E	=	Impact kinetic energy, erg
f	=	Mass loss ratio, %
G	=	Gravitational constant
h	=	Relative angular momentum of the small body per unit mass
$h_{threshold}$	=	Height threshold for aerobraking, km
H	=	Asteroid absolute magnitude
h_0	=	Perigee height when aerobraking, km
H_2	=	Two-body Kepler energy of the asteroid after aerobraking
h_a	=	Magnitude of asteroid's angular momentum before aerobraking
h_j	=	Height of j^{th} perigee with respect to the centre of the Earth after aerobraking, km
H_s	=	Atmosphere scale height, m
i	=	Inclination, deg

J	=	Jacobi constant of the asteroid which is approximated by the Tisserand parameter
k	=	Coefficient of restitution
L	=	Tether length, m
m_1	=	Mass of the central body in the two-body problem, kg
m_2	=	Mass of the small body in the two-body problem, kg
M_1	=	Gravitational parameters of the large primary body, km^3/s^2
M_2	=	Gravitational parameters of the small primary body, km^3/s^2
m_l	=	Mass of large asteroid, kg
m_s	=	Mass of small asteroid, kg
m_{tether}	=	Mass of tether, kg
m_-, m_+	=	Mass of the asteroid before and after aerobraking, respectively, kg
\mathbf{n}	=	Unit normal vector along the mass centres of the asteroids
n	=	Mean angular motion of the captured asteroid around the Earth
\mathbf{O}_l	=	Centre-of-mass of large asteroid
\mathbf{O}_s	=	Centre-of-mass of small asteroid
p_v	=	Asteroid albedo
\mathbf{r}	=	Relative position vector of the small body with respect to the large central body
r_a	=	Distance from the centre of the Earth to the apogee of the captured asteroid's orbit after aerobraking, km
\mathbf{r}_{em}	=	The position vector of the Earth-Moon barycentre respect to the Sun in the two-body problem, km
$\mathbf{r}_e, \mathbf{r}_m$	=	Position vectors of the Earth and Moon, respectively, with respect to the Sun, km
r_{np}	=	Distance from the centre of the Earth to the new perigee of the asteroid's orbit, km
r_p	=	The perigee radius of the flyby orbit from the centre of the Earth, km
$\mathbf{r}_{p-}, \mathbf{r}_{p+}$	=	Position vectors of the asteroid before and after aerobraking in the Earth-centred inertial frame, respectively
r_{sa}	=	Distance between the candidate asteroid at perigee when aerobraking and the centre of the Earth, km
$r_{\text{threshold}}$	=	Distance threshold for aerobraking with respect to the centre of the Earth, km

\mathbf{R}	=	Position vector of the third body in an inertial frame
\mathbf{R}_1	=	Position vector of the third body with respect to the large primary body
\mathbf{R}_2	=	Position vector of the third body with respect to the small primary body
\mathbf{R}_{p1}	=	Position vectors of the large primary body in a inertial frame
\mathbf{R}_{p2}	=	Position vectors of the small primary body in a inertial frame
R_{SOI}	=	Radius of the Moon-Sun three-body sphere of influence, km
S_0	=	Maximum safe working stress, Gpa
S_{s0}	=	Material impact strength of small asteroid, J/m ³
S_s	=	Effective impact strength of small asteroid, J/m ³
S	=	Tether stress, Gpa
t_p	=	Time determining the state on the target periodic orbit where invariant manifold is propagated from
t_{p1}	=	Time determining the point on the Sun-Earth periodic orbit where the stable manifold is propagated backward from
t_{p2}	=	Time determining the point on the Sun-Earth periodic orbit where the unstable manifolds is propagated forward from
t_{p3}	=	Time determining the point on the Earth-Moon periodic orbit where the stable manifold is propagated backwards from
t_{um}	=	Unstable manifold transfer time
t_{sm}	=	Stable manifold transfer time
$t_{threshold}$	=	Maximum stable manifold transfer time of the stable manifolds associated with the periodic orbit
T_0	=	Departure date when the asteroid leaves its initial orbit
T_f	=	Approach date corresponding to the date when the candidate asteroid inserts onto the stable manifold
T_{fly}	=	Transfer time between the asteroid initial orbit and the Earth-Moon stable manifold, day
T_{impact}	=	Natural average impact interval for asteroids, year
T_{tot}	=	Total flight time, day
T_L	=	Tether tension at the small asteroid, N
T_p	=	Period of the periodic orbit.
v_c	=	Characteristic velocity of the tether material, m/s
\mathbf{v}_L	=	Velocity vector of the large asteroid before impact or tether-assisted

		flyby, m/s
\mathbf{v}_{l+}	=	Velocity vector of the large asteroid after impact or tether-assisted flyby, m/s
$\mathbf{v}_{p-}, \mathbf{v}_{p+}$	=	Relative velocity of the asteroid before and after aerobraking at perigee with respect to the Earth, respectively
\mathbf{v}_{s-}	=	Velocity vector of small asteroid before impact or tether-assisted flyby, m/s
\mathbf{v}_{s+}	=	Velocity vector of small asteroid after impact or tether-assisted flyby, m/s
\mathbf{v}_{sl}	=	Relative velocity of small asteroid with respect to the large asteroid, m/s
$\mathbf{V}_{p-}, \mathbf{V}_{p+}$	=	Velocity vectors of the asteroid before and after aerobraking in the Earth-centred inertial frame, respectively
$\mathbf{X}_e^{ro}, \mathbf{X}_m^{ro}$	=	Non-dimensional states of the Earth and Moon in the Sun-Earth rotating frame, respectively.
β	=	Angle of the small primary body with respect to the large primary body, rad
γ	=	Angle determining the Poincaré section in the patched three-body problem, rad
$\delta \mathbf{v}_1$	=	Velocity increments at the beginning of the Lambert arc, m/s
$\delta \mathbf{v}_2$	=	Velocity increments at the endpoint of the Lambert arc, m/s
Δv_{2min}	=	Minimum value of the second impulse, m/s
$\Delta \mathbf{v}_n$	=	Relative velocity between the two asteroids in direction \mathbf{n} , m/s
$\Delta \mathbf{v}_{release}$	=	Relative velocity of small asteroid with respect to the large asteroid when released, m/s
$\Delta v_{threshold}$	=	Threshold value of $\Delta \mathbf{v}_n$, m/s
Δv	=	Total cost, m/s
$\Delta \mathbf{v}_a$	=	Aerobraking manoeuvre, m/s
ε	=	Magnitude of the perturbation, in the direction of the stable/unstable eigenvectors
θ	=	True anomaly of the small body around the central body, measured from the periapsis, deg
θ_1, θ_2	=	Angles which determine the direction of a manoeuvre
$\kappa_1, ..$	=	Amplitudes of the short periodic orbit and long periodic orbit,

		respectively.
μ_1	=	Gravitational parameter of the two-body problem
μ_{Earth}	=	Gravitational parameter of the Earth
μ_{Sun}	=	Gravitational parameter of the Sun
μ_{Moon}	=	Gravitational parameter of the Moon
μ	=	Non-dimensional mass parameter of the CRTBP system
ρ	=	Density of the Earth's atmosphere, kg/m ³
ρ_0	=	Density of the Earth's atmosphere at the surface, kg/m ³
ρ_a	=	Asteroid density, kg/m ³
ρ_{tether}	=	Tether density, kg/m ³
$\Phi(t, t_0)$	=	Is the state transition matrix
Φ_T	=	Monodromy matrix
ϕ	=	Angle determining the Poincaré section, rad
Ω	=	Right ascension of the ascending node, deg
ω	=	Argument of perigee, deg
σ	=	Ablation parameter
ϑ	=	Angle determining the position of the Moon

AUTHOR'S DECLARATION

I declare that this thesis has been composed solely by myself and that it has not been submitted, in whole or in part, in any previous application for a degree. Except where states otherwise by reference or acknowledgment, the work presented is entirely my own.

Parts of this work have been published in

Tan, M., McInnes, C.R., and Ceriotti, M. "Direct and indirect capture of near-Earth asteroids in the Earth–Moon system," *Celestial Mechanics and Dynamical Astronomy*, Vol. 129, pp. 1-32, 2017.

Tan, M., McInnes, C.R., and Ceriotti, M. "Low-Energy Near-Earth Asteroid Capture Using Momentum Exchange Strategies," *Journal of Guidance, Control, and Dynamics*, Vol. 41, pp. 632-643, 2017.

Tan, M., McInnes, C.R., and Ceriotti, M. "Low-energy near Earth asteroid capture using Earth flybys and aerobraking," *Advances in Space Research*, Vol. 61, pp. 2099-2115, 2018.

Tan, M., McInnes, C.R., and Ceriotti, M. "Capture of small near-Earth asteroids to Earth orbit using aerobraking", *Acta Astronautica* (In press), 2018



2018.09.11

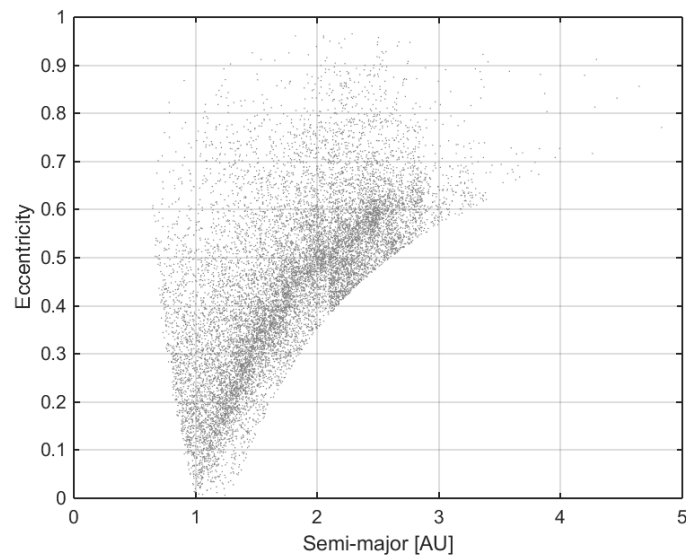
CHAPTER 1

INTRODUCTION

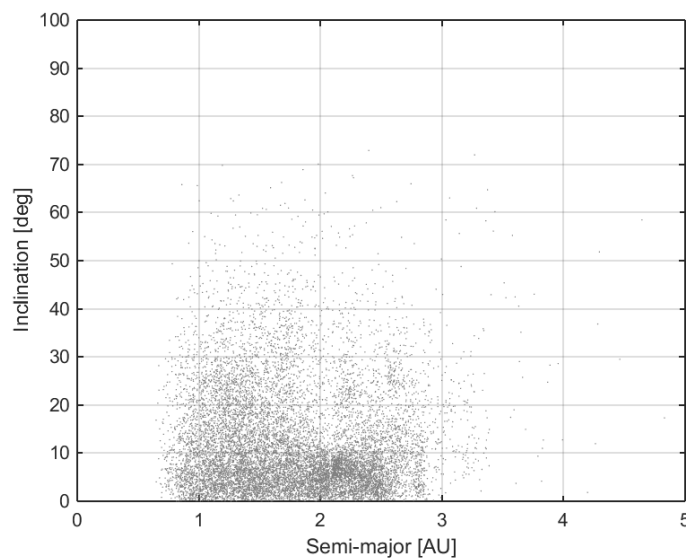
In the last few decades, space agencies such as the National Aeronautics and Space Administration (NASA) and the European Space Agency (ESA) have put a significant effort into the exploration of small solar system bodies, such as asteroids. Generally speaking, asteroids are remnant objects from the formation of the inner solar system and so the exploration of these bodies represents a frontier to extend our knowledge on the formation and evolution of the solar system. Therefore, a series of asteroid exploration missions have been undertaken or are currently planned [1-4]. Among the entire family of asteroids, near-Earth asteroids (NEAs) have gained significant attention due to their accessibility. In general, NEAs typically have orbits that lie between 0.983 and 1.3 Astronomical Units (AU) from the Sun [5], where the JPL Small-Body Database provides the current catalogue of NEAs ¹. Their orbital distribution is shown in Fig. 1.1. Therefore, these asteroids represent the closest potential threats for Earth impact and the easiest targets both to reach from the Earth and to capture in the vicinity of the Earth. Moreover, NEAs are also considered to provide useful resources which can be used to support future space activities, for example in-situ spacecraft propellant manufacturing and logistic support materials [6, 7]. The exploitation of these in-situ resources has long been proposed as a necessary part of long-term space development [7-10]. Furthermore, there is a growing commercial interest in NEA resources [11, 12]. The possibility of mining minerals and metals such as gold, silver and platinum has attracted the attention of some countries and even some companies. For instance, in 2015, U.S. President Barack Obama signed the asteroid mining bill into law which can encourage the commercial exploration and utilisation of the asteroid resources [13]. Then the government of Luxembourg adopted similar legislation in 2017 [14]. In particular, some private enterprises, like Deep Space Industries and Planetary Resources are developing the asteroid-mining technologies and have announced ambitious plans of capturing, returning and then mining asteroids by 2020-2025 [15]. Therefore, the exploitation and utilisation of these resources has generated

¹ Data available online at https://ssd.jpl.nasa.gov/?sb_elem [retrieved 24 February 2018].

a growing interest in low-energy strategies to capture near-Earth asteroids in the vicinity of the Earth, for scientific and potentially commercial purposes [9, 10, 16-19].



(a)



(b)

Fig. 1.1 Orbital distribution of NEAs: (a) semi-major and eccentricity and (b) semi-major and inclination.

1.1 Asteroid exploration and capture missions

The exploration of asteroids can be tracked back for centuries. On 1 January 1801, Giuseppe Piazzi (1746–1826) used a telescope to discover the first asteroid, Ceres, in the Palermo Observatory [20]. Then, visible light observations and near-infrared observations of asteroids have been widely applied to determine detailed information on their structure,

composition, size and shape, etc. [21, 22]. Meanwhile, range-Doppler imaging of asteroids through radio telescopes has been developed to improve the accuracy of shape models of asteroids [23, 24].

More recently, with the development of space technologies, some asteroid exploration missions have already been undertaken, or are planned. In 1989, NASA launched the Galileo spacecraft which passed and imaged the main-belt asteroid Gaspra in 1991, and then another main-belt asteroid Ida in 1993 in route to Jupiter [1, 25]. Then NASA's Clementine spacecraft, which was launched in 1994, extended its mission to transfer to the vicinity of the near-Earth asteroid Geographos and made observations of the asteroid after Clementine completed its primary mission of mapping the surface of the Moon [26]. NASA's third spacecraft for asteroid exploration was the NEAR-Shoemaker mission which was launched in 1996 [27]. After approximately 4 years flight, the spacecraft approached the vicinity of Eros and then made comprehensive observations of the asteroid to measure its physical properties, e.g. mass, composition, structure and shape. Finally, the spacecraft soft-landed on the asteroid's surface in February 2001, and thus became the first spacecraft to land on an asteroid [27]. Then NASA's fourth spacecraft to explore asteroids, Deep Space 1 launched in 1998 and flew by the asteroid Braille in 1999 and Comet Borrelly in 2001 [28]. Moreover, during the Cassini-Huygens mission to Saturn, which was supported by NASA, ESA and Italian Space Agency (ASI), the spacecraft flew past the asteroid Masursky and thereby estimated its size in 2000 [29]. In 1999, NASA launched the Stardust mission spacecraft with a re-entry capsule. This spacecraft firstly flew by the asteroid Anfrank in 2002 and returned information through imaging. After the flyby, the spacecraft approached its target, Comet Wild2, and successfully collected samples. Consequently, these samples were returned to the Earth in 2004 [30].

In May 2003, the Japan Aerospace Exploration Agency (JAXA) launched the Hayabusa spacecraft to target the asteroid Itokawa. The spacecraft rendezvoused with the asteroid in September 2005, and immediately after approached the asteroid in November 2005 for sampling. Finally, Hayabusa returned to Earth with surface samples in June 2010 [31]. On March 2004, ESA's Rosetta mission was launched to its target, Comet 67P/Churyumov-Gerasimenko [4]. Before arriving at the target, the spacecraft flew by the asteroid Steins in September 2008 and the asteroid Lutetia in July 2010. During the flybys, some physical properties of the two asteroids were determined and the origin of asteroid Steins was revealed [32]. On 12 January 2005, NASA launched the Deep Impact spacecraft to explore and analyse the composition of the Comet Tempel 1 [3]. When the spacecraft approached the target, it released an impactor to collide with the comet, thereby successfully completing the first mission to eject material from a comet. After this mission

had been completed, it was proposed to carry out additional comet or asteroid exploration flybys. However, these new missions were cancelled due to the loss of communication between the spacecraft and Earth in September 2013. On 27 September 2007, NASA launched the Dawn mission to explore two of the three known protoplanets in the main asteroid belt, Vesta and Ceres [33]. This was the first spacecraft to orbit two solar system bodies. Similar to the NASA Clementine spacecraft, the China National Space Administration's (CNSA) Chang'e 2 probe performed an extended mission to flyby the asteroid Toutatis in December 2012 after it had finished its initial mission of exploring the surface of the Moon [34]. On its way to the target asteroid, Chang'e 2 was firstly guided to the Sun-Earth Libration point L_2 . As an extension of JAXA's previous Hayabusa mission, Hayabusa 2 was launched in December 2014 and is expected to arrive at the target asteroid 1999 JU3 in July 2018, to study the asteroid, collect samples from it and return to Earth in December 2020 [35]. Furthermore, the latest asteroid exploration and sample return mission is the NASA OSIRIS-Rex mission, which was launched in September 2016. Its mission is to study asteroid 101955 Bennu and then return a sample to Earth in September 2023 [36].

Inspired by the success of asteroid exploration and sample return missions, and with the development of a range of space technologies in recent years, some space agencies (e.g. NASA) have studied the feasibility and possibility of capturing an entire asteroid, instead of sampling material from an asteroid surface. Therefore, in 2011, the Jet Propulsion Laboratory (JPL) and NASA investigated the feasibility of finding, capturing and then returning a NEA to the International Space Station (ISS) [37]. The target asteroid would be used for analysis of its structure, composition and then to evaluate its resource potential. Meanwhile, Fast [38] proposed a mission to capture and return a small NEA with a diameter of approximately 2 m to the ISS and proved the feasibility of capturing such a NEA with current technologies and a typical deep space mission budget. Moreover, in 2012, the Keck Institute for Space Studies (KISS) proposed to capture and return a NEA into a stable lunar orbit, instead of low Earth orbit (LEO) [39]. In this scheme for asteroid capture, a lunar gravity assist (LGA) was used to capture the candidate asteroid and thereby reduce the propellant mass required. Accordingly, these NEAs with a relatively large size became candidate targets. Finally, KISS offered a detailed scheme for capturing and returning the asteroid 2008 HU4 with a diameter of approximately 7 m and a mass of approximately 500 tons to a high lunar orbit. Based on this research, NASA proposed the Near-Earth Asteroid Redirect Mission (ARM) to capture a NEA to a stable lunar orbit in 2013 using solar electric propulsion [40]. This mission was mainly aimed at developing and improving deep space mission capability for the future Mars exploration. Moreover,

the mission would also test the performance of some space technologies and planetary defence techniques. Unfortunately, the mission was cancelled in 2017 [41].

The idea of capturing small NEAs with relatively low energy has been widely investigated in detail by many researchers [9, 16, 18, 42-49]. Most recent research work has investigated the possibility of capturing NEAs in the vicinity of the Earth, including the Sun-Earth libration points L_1 and L_2 [18, 50-52], the neighbourhood of the Moon [39, 45, 53] and bound orbits about the Earth itself [16, 48, 54]. Table 1.1 provides a brief summary of results and solutions of capturing asteroids in these previous works. After studying the accessibility of asteroid resources, Sanchez, et al. [9], [19] estimated the quantity of asteroid resources that can be accessed at relatively low cost and concluded that on the order of 10^{11} tons of material could potentially be harvested with a lower energy cost than that required to access resources from the surface of the Moon. Such materials will no doubt boost the rapid development of space exploration in the future.

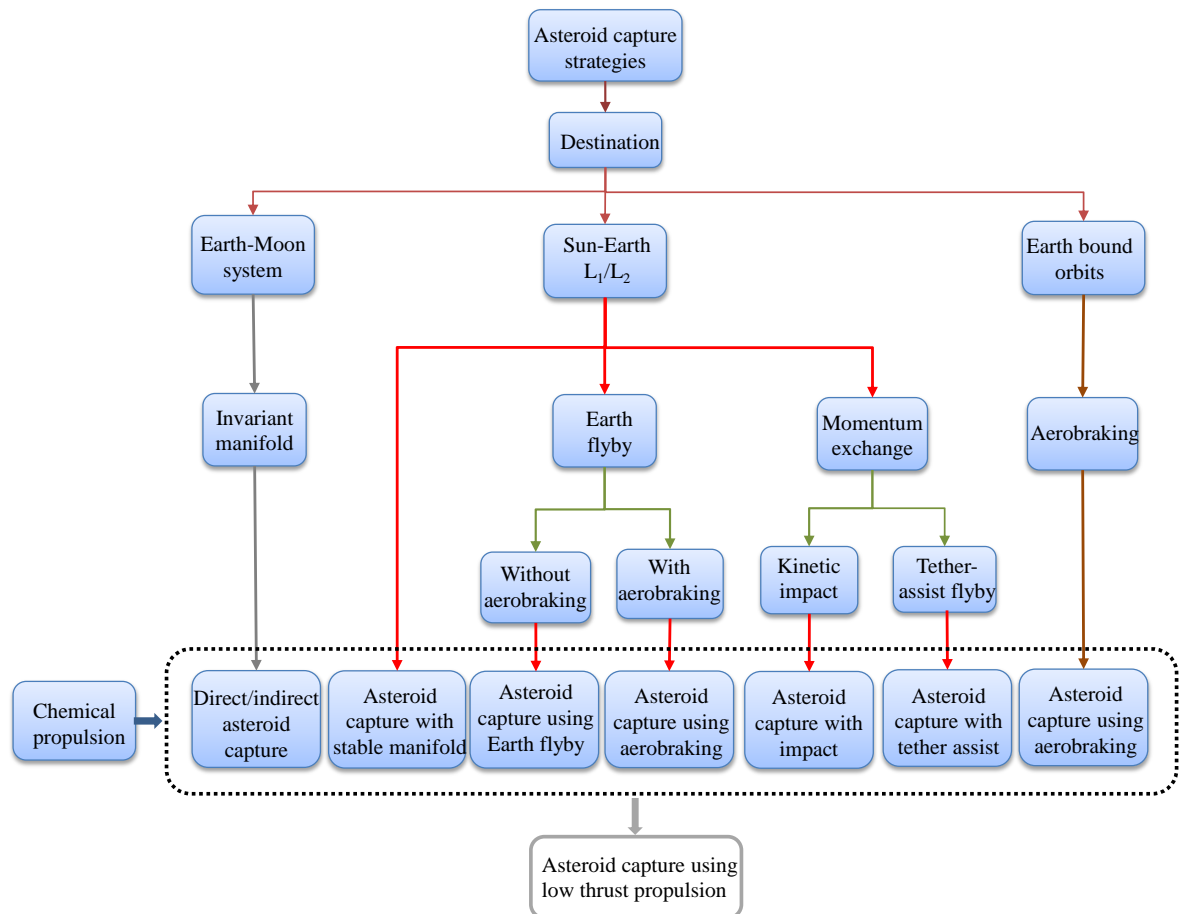


Fig. 1.2 Decision tree for potential options and methods of capturing asteroids.

Therefore, the main objective of this thesis is to investigate asteroid capture strategies in order to achieve low energy capture of NEAs in the vicinity of the Earth, including the neighbourhood of the Moon, the Sun-Earth libration points L_1 and L_2 , and bound orbits

about the Earth itself. Moreover, a decision tree that indicates the potential options and methods of capturing asteroids is shown Fig. 1.2.

Table 1.1 A brief summary of results and solutions of asteroids capture.

Asteroid	Reference	Δv , m/s	Transfer time, day	Destination
2000 SG344	Yárnoz, et al. [50]	443	1223	Sun-Earth L ₁
	Gong and Li [48]	348	-	Earth Hill region
	Sánchez and Yárnoz [18]	470	2602	Sun-Earth L ₁
	Tan, et al. [45]	481	1859	Earth-Moon L ₂
2006 RH120	Yárnoz, et al. [50]	58	2471	Sun-Earth L ₂
	Sánchez and Yárnoz [18]	58	2738	Sun-Earth L ₂
	Tan, et al. [45]	334	2515	Earth-Moon L ₂
	Sanchez, et al. [9]	195	945	Sun-Earth L ₂
2007 UN12	Yárnoz, et al. [50]	199	2675	Sun-Earth L ₂
	Sánchez and Yárnoz [18]	195	2887	Sun-Earth L ₂
	Tan, et al. [45]	347	1292	Earth-Moon L ₂
	Tan, et al. [44]	153	745	Sun-Earth L ₁
2008 EA9	Sanchez, et al. [9]	325	923	Sun-Earth L ₂
	Yárnoz, et al. [50]	328	-	Sun-Earth L ₂
	Sánchez and Yárnoz [18]	341	3048	Sun-Earth L ₂
	Tan, et al. [45]	445	1273	Earth-Moon L ₂
2008 UA202	Sanchez, et al. [9]	416	1245	Sun-Earth L ₂
	Yárnoz, et al. [50]	393	-	Sun-Earth L ₂
	Gong and Li [48]	49	-	Earth Hill region
	Sánchez and Yárnoz [18]	438	3230	Sun-Earth L ₂
2009 BD	Tan, et al. [44]	242	1317	Sun-Earth L ₂
	Yárnoz, et al. [50]	392	-	Sun-Earth L ₂
	Yárnoz, et al. [50]	249	-	Sun-Earth L ₂
2010 UE51	Sánchez and Yárnoz [18]	405	3084	Sun-Earth L ₂
	Tan, et al. [45]	403	2019	Earth-Moon L ₂
	Sánchez and Yárnoz [18]	297	2818	Sun-Earth L ₂
2014 WX202	Tan, et al. [45]	437	1575	Earth-Moon L ₂
	Tan, et al. [44]	279	1379	Sun-Earth L ₁
2015 PS228	Sánchez and Yárnoz [18]	395	3048	Sun-Earth L ₂
	Tan, et al. [44]	614	736	Sun-Earth L ₁

1.1.1 Asteroid capture around the Sun-Earth libration points L_1/L_2

The Sun-Earth L_1 and L_2 points are noteworthy due to their unique locations and dynamical characteristics. The Sun-Earth L_1 point is an ideal location for scientific observations of the Sun-Earth system, such as monitoring the solar wind. Similarly, Farquhar, et al. [55] regarded the Sun-Earth L_2 point as a staging node for interplanetary missions to NEAs and Mars, since it is also a useful location for space-based observatories. Overall, as an ideal location for space science, and a staging node for interplanetary missions in the future, the Sun-Earth L_1 and L_2 points represent potentially beneficial gateways for future space exploration missions [56]. Therefore, capturing asteroids onto periodic orbits around the Sun-Earth L_1 and L_2 points is of particular interest.

Following interest in capturing NEAs onto orbits at the Sun-Earth libration points, Sanchez, et al. [9] regarded the Sun-Earth L_2 region as the final destination for NEA capture missions and investigated the possibility of capturing small NEAs into Lyapunov orbits around the Sun-Earth L_2 point through their invariant manifolds. Moreover, Yárnoz, et al. [50] recently identified a new family of asteroids, termed easily retrievable objects (EROs). EROs are asteroids which can be gravitationally captured into bound periodic orbits around the Sun-Earth L_1 and L_2 points with a total cost of less than 500 m/s. Yárnoz, et al. [50] used a two impulsive Lambert arc to design the transfer trajectory from the candidate asteroid's initial orbit to the stable manifold associated with the target periodic orbit around the Sun-Earth L_1 or L_2 points. Accordingly, Sánchez and Yárnoz [18] updated the list of easily retrievable objects and estimated the largest retrievable mass possible, to investigate the feasibility of asteroid resource utilisation. As the catalogue of asteroids is updated with further observations, it is likely that more easily retrievable objects will be found in the future. Moreover, Tang and Jiang [51], Mingotti, et al. [52] considered the low thrust to design retrieval trajectories in order to increase the retrieval mass and thus improve the feasibility of capturing an entire NEA. Moreover, Ceriotti and Sanchez [57] proposed a strategy to control such ERO retrieval trajectories to solve the issues caused by uncertainties in the asteroid mass and injection manoeuvres. Lladó, et al. [17] have also considered continuous low thrust propulsion to capture NEAs at periodic orbits around the Sun-Earth L_2 point. Tan, et al. [46] have proposed to use momentum exchange theory, including both kinetic impacts and the use of tethered assist for the capture of small asteroids into Lyapunov orbits around the Sun-Earth L_1 and L_2 points. Furthermore, Tan, et al. [44] investigated the combination of a flyby of the Earth and the use of stable manifolds to capture NEAs onto Lyapunov orbits around the Sun-Earth L_1 and L_2 points. Depending on the perigee distance of the flyby, Earth flybys with and without aerobraking can be

considered to design a transfer trajectory capturing a small NEA from its initial orbit to the stable manifolds associated with Sun-Earth L_1 and L_2 periodic orbits [44].

Meanwhile, work on low-energy transfers between periodic orbits around the Sun-Earth libration points and NEAs has also been undertaken. As noted earlier Farquhar, et al. [55] regard the Sun–Earth L_2 point as an important gateway for NEA and Mars exploration missions. For low-energy crewed exploration of NEAs, Zimmer [56] proposed to employ a reusable spacecraft that is stationed on a halo orbit at the Sun-Earth L_1 or L_2 point for such missions. Wang, et al. [58] proposed a perturbation method to search for possible flyby opportunities between Sun-Earth Lissajous orbits and the asteroids Toutatis and 2010 JK1. The method then calculates low-energy transfers between the Lissajous orbit and the asteroids. Then, Gao [59] investigated optimal bi-impulse flyby trajectories from the Sun-Earth L_2 point to the asteroids Toutatis, 2005 NZ6 and 2010 CL19.

1.1.2 Asteroid capture into the vicinity of the Moon

The Earth–Moon libration points are also key to the future of deep space exploration. In 2010, the two ARTEMIS spacecraft became the first vehicles to operate in the vicinity of an Earth-Moon libration point, operating successfully in this dynamical regime from August 2010 to July 2011 [60]. In 2011, NASA released a report on Earth-Moon libration point missions as part of a ‘Global Exploration Roadmap’ [61]. NASA has identified the Earth-Moon L_1 and L_2 points as potential locations of interest for future human space exploration [62].

Meanwhile, as noted earlier, NASA has also considered a potential future mission (ARM) to rendezvous with and then capture a small near-Earth asteroid (later a boulder from a near-Earth asteroid) [63]. Given that final placement of the captured asteroid in the vicinity of the Earth may incur an impact risk, it is prudent to place the retrieved asteroid in an orbit from which it could only impact the Moon. Lunar orbits, or possibly regions near the Earth-Moon Lagrange points, would therefore be one of the preferred locations, although there is additional work required on this matter. Besides, the Earth-Moon L_2 point is also regarded as a candidate gateway for future space missions, since spacecraft on periodic orbits around the Earth-Moon L_2 point can easily achieve low-energy transfers to the vicinity of the Moon and the vicinity of the Sun–Earth L_1 and L_2 points [64–66]. Therefore, capturing asteroids and inserting them directly at the Earth-Moon L_1 and L_2 points may be of significant benefit for future space exploration by providing in-situ resources. In addition, due to the fact that the triangular points in the Earth-Moon system

are stable, the propellant required to maintain a captured NEA at such a location is modest [67]. For this reason, it may also be of interest to capture a NEA and place it on a periodic orbit around the triangular L_4 and L_5 points in the Earth-Moon system. Furthermore, due to fact that the Earth-Moon L_4 and L_5 points can be used as a parking orbits for travel to and from cis-lunar space, O'Neill [68] proposed to build space colonies at these points where captured NEAs could provide material for such large structures. Accordingly, DeFilippi Jr [69] studied station-keeping strategies at Earth-Moon L_4 point.

Mingotti, et al. [53] proposed the patched circular restricted three-body problem as a model, which consists of the Sun–Earth and the Earth–Moon circular restricted three-body problem (CRTBP) systems, to capture NEAs onto target periodic orbits around the Earth–Moon L_2 point. This would require a significant duration for the asteroid to be asymptotically captured onto periodic orbits around the Sun-Earth L_1 or L_2 points, compared to the traditional hyperbolic approach [43]. Tan, et al. [45] defined a direct capture strategy which is different from this indirect asteroid capture strategy. In this capture strategy, an initial impulse will modify the asteroid's orbit and a second impulse will insert it onto the stable manifold associated with an Earth-Moon L_2 periodic orbit directly. Moreover, both direct and indirect strategies were investigated to design the direct and indirect capture of asteroids to the triangular points in the Earth-Moon system [45].

1.1.3 Asteroid capture into bound orbits around the Earth

The material which can be extracted from NEAs has been regarded to be useful for future space missions by providing propellant, life support, water and metals [6, 7]. Among them, volatiles such as hydrogen and methane can be used to produce propellant for spacecraft parked in LEO, and therefore to transfer the spacecraft to some further destination, such as the moon or Mars [7]. Moreover, some in-situ materials have the potential for manufacture of solar energy systems, such as photovoltaic arrays [70]. These devices can be used to assemble solar power satellites in orbit around the Earth in order to provide electrical power for through microwave power-beaming to terrestrial receivers.

There exists two types of asteroid capture strategies around the Earth, corresponding to two different dynamical models. The first is to directly capture an asteroid into an elliptical orbit around the Earth which is modelled in the Earth-centred two-body problem. For example, in 2011, JPL and NASA investigated the feasibility of finding, capturing and then returning a NEA to the ISS [37, 38]. Moreover, Andrews, et al. [12] studied a commercial asteroid mining program and thus designed NEA capture and mining equipment such as a

LEO space operations centre for the asteroid material. Besides, Hasnain, et al. [16] investigated an asteroid capture strategy with a transfer trajectory designed by patching together the Sun-Earth CRTBP and Earth-centred two-body problem. In addition, Hills [71] proposed to capture a small asteroid into a bound orbit around the Earth in order to defend the Earth from future impact of a large asteroid.

In the other strategy, the motion of the captured asteroid is always modelled as a multi-body problem and there are then two types of capture, termed temporary and permanent capture. Tanikawa [72] proved that a retrograde satellite cannot be captured under gravitational interactions in the restricted three-body problem. However, permanent capture may occur when some non-gravitational forces such as gas drag are taken into account [73]. With regard to the capture conditions in the CRTBP, Cline [74] applied the patched conic method in a two-body problem to analyse the capture conditions in a planetary capture model. Villac and Scheeres [75], Paskowitz and Scheeres [76] used periapsis mapping to investigate the capture conditions in a Hill three-body problem. Besides, Verrier and McInnes [54] used the Kolmogorov–Arnold–Moser (KAM) method to capture an asteroid temporarily in the Earth’s Hill regions (although the capture duration is extremely long for practical purposes). Belbruno and Miller [77] firstly introduced the weak stability boundary (WSB) to design the low-energy transfer to the Moon and it can be also utilised to analyse temporary capture in CRTBP systems, such as the Sun-Jupiter system [78]. Furthermore, Belbruno [79] provided the satellite capture conditions for temporary and permanent capture in the Hill problem through defining the two-body Kepler energy of the satellite with respect to the central body. Moreover, to reduce the total capture cost, a lunar flyby can also be used to capture NEAs in the neighbourhood of the Earth in this multi-body environment [48]. Additionally, Tan, et al. [80] proposed to use aerobraking to achieve low energy capture of NEAs in bound orbits around the Earth.

Among the NEAs, the temporarily captured asteroids (TCAs) are a special class of the population of asteroids which can be naturally captured in the neighbourhood of the Earth for a limited duration [81]. Therefore, due to their relatively easy accessibility, they have been regarded as attractive candidates for the asteroid exploration and return missions [82–84]. Moreover, through analysis of the capture mechanism, Urrutxua, et al. studied extending the duration of their capture in order to provide extended opportunities for such missions [82, 85, 86]. In addition, observations using the Space Surveillance Telescope [87] and the Large Synoptic Survey Telescope [88] have been proposed to discover yet more TCAs. Moreover, NEAs which can be captured temporarily in the Earth-Moon system have been investigated to expand the population of TCAs [89, 90].

1.2 Low-energy strategies of capturing asteroids

In recent studies of asteroid capture, a range of new methods and techniques have been employed to lower the total cost of capturing NEAs, in terms of velocity increment or propellant consumption. These methods are summarized as follows.

1.2.1 Multi-body and invariant manifold theory

Low energy trajectory design in multi-body environments is a rich and active area of research which focuses on various classes of orbit design problems. Moreover, the utilisation of periodic orbits and their associated invariant manifolds, to design low-energy trajectories in multi-body systems, has been a topic of particular interest in recent years [91, 92]. Periodic orbits around collinear libration points have an unstable behaviour and will consequently diverge under small perturbations. The family of trajectories generated from a periodic orbit under such perturbations is the invariant manifold associated with that periodic orbit. Hence, such periodic orbits and their associated invariant manifolds can be employed to investigate low-cost transfer trajectories between different orbits [93-95]. After a spacecraft moves onto the stable manifold of a libration point orbit (LPO), it will transfer to the target periodic orbit without any further manoeuvres. Meanwhile, such dynamical characteristics have been widely used in various trajectory design problems, including transfers between LPOs within the CRTBP of the Sun-Earth system [66, 94, 95]. Furthermore, invariant manifolds have been utilised as the basic mathematical tool to design low-energy transfer trajectories between different multi-body systems, e.g., the Earth-Moon and Sun-Earth systems [96-98]. During such transfers, the spacecraft should first be inserted onto the stable manifold associated with the target periodic orbit around the libration point of interest. Once inserted onto the stable manifold, it will be asymptotically captured without further manoeuvres. A successful application of this method is the design of Hiten-like mission trajectories [99]. A further example of trajectory design includes transfer between LPOs within a restricted three-body system and transfer trajectories in multi-body dynamical systems [100]. Missions including Genesis, WMAP, Triana, ISEE-3 and WIND have utilised the circular restricted three-body problem to design transfers to and from LPOs in the Sun-Earth system. Moreover, the patched circular restricted three-body problem was introduced by Koon, et al. [96] and has been used to design low-energy transfer trajectories from the Earth to the Moon [96, 99, 101]. Usually a manoeuvre at or near the patching point is required to move the spacecraft from one

manifold tube to the other. Based on the patched restricted three-body approximation, the bi-circular restricted four-body model was proposed to design low-cost Earth-Moon transfer trajectories [97, 102].

To design transfer trajectories in multi-body environments, efficient mathematical tools are necessary, including the shooting method and Poincaré maps. Since the multiple shooting method can significantly reduce the dynamical sensitivities of trajectories associated with LPOs, it has been studied extensively to obtain solutions of boundary value problems (BVP) in the CRTBP [103, 104]. Moreover, the Poincaré map that employs a hyper-plane in a rotating reference frame can be used to transform a continuous time dynamical system to a discrete time system. A variety of map formulations are possible in the CRTBP and Hill's problem, including the periapsis map [75, 105].

Periodic orbits around the libration points, and the invariant manifolds associated with them, have generated significant interest for NEA exploration missions, including NEA flyby [59], NEA capture [50] and spacecraft reusability for NEA exploration [56]. Moreover, such periodic orbits with unstable characteristics can again be utilised to design low-energy ballistic transfers [93, 95]. These orbits can also serve as parking orbits for captured NEAs [43, 52]. Based on ballistic capture mechanics in the restricted three-body problem, transfers between NEAs and LPOs have also been recently investigated [50, 52, 55, 56, 58, 59]. For example, Mingotti, et al. [52] proposed the use of low thrust propulsion to capture NEAs to a target periodic orbit around the Sun-Earth L_1 and L_2 points by using the stable manifolds associated with the target periodic orbit. Farquhar, et al. [55] regarded the Sun-Earth L_2 libration point as a potential parking orbit and gateway station for missions to NEAs and Mars. Delivering NEA resources to a LPO at the L_2 point could therefore provide efficient logistic support. In order to lower the cost of future space exploration missions, Zimmer [56] studied reusability by stationing spacecraft on periodic orbits at the Sun-Earth L_1 and L_2 points between NEA missions. In related work, Wang, et al. [58] proposed to use a differential corrector method to design flyby trajectories from the Lissajous orbit of the CHANG'E 2 spacecraft to the asteroids Toutatis and 2010 JK1.

The stable manifolds associated with the Sun-Earth L_1 and L_2 points were employed to design transfer trajectories to enable the low energy capture of NEAs [17, 42, 50]. The utilisation of stable manifolds is also key to achieving low-cost capture, since flight along the stable manifold is ballistic and again no manoeuvre is required during this period. Based on these characteristics, Yáñez, et al. [50] obtained the list of EROs with a total capture cost of less than 500 m/s by patching the Lambert problem in the Sun-centred two-body problem and the stable manifolds of the L_1 and L_2 points in the Sun-Earth CRTBP. Moreover, to increase the number of potentially easily retrievable objects, Sánchez and

Yárnoz [18], Tang and Jiang [51] employed low thrust propulsion has to design the transfer between the asteroid's initial orbit and the appropriate stable manifold. Meanwhile, Mingotti, et al. [52] investigated other families of final periodic orbits (distant retrograde orbits) around the Sun-Earth L_1 and L_2 points for asteroid capture.

1.2.2 Gravity assist manoeuvres

Gravity assists have played a significant role in interplanetary mission design and deep space exploration. Such methods have been studied extensively and are regarded as a basic tool for the design of low-energy interplanetary transfer trajectories [106]. Between entering and leaving the gravitational field of a planet or moon, a spacecraft's heliocentric velocity can change significantly. The concept of the gravity assist was proposed by Minovitch, after he developed the patched conic method, and accordingly it was used to design a range of low-cost interplanetary trajectories [107]. Since then, gravity assists have been used for a series of interplanetary transfer missions. Some successful examples are listed as follows.

The Mariner 10 spacecraft was the first spacecraft to employ a gravity assist to transfer to Mercury by swinging by Venus in 1974 [108]. Launched in 1973, Pioneer 11 was configured to study the Jupiter, Saturn and the main asteroid belt using a gravity assist at Jupiter and Saturn [109]. In 1977, NASA began the Voyager missions which consisted of two spacecraft: Voyager 1 and Voyager 2. Voyager 2 flew by Jupiter, Saturn, Uranus and Neptune, sequentially while Voyage 1 flew by Jupiter, Saturn and Titan sequentially [110]. NASA's Galileo spacecraft was launched to transfer to Jupiter through flybys of Venus once and Earth twice [1]. In 1990, ESA's Ulysses spacecraft was launched by NASA to investigate the Sun's polar region after flying by Jupiter [111]. In 2004, the joint mission of NASA, ESA and the Italian Space Agency ASI, Cassini-Huygens reached Saturn after employing two gravity assists from Venus, one from the Earth, and one from Jupiter [112]. NASA's second Mercury spacecraft MESSENGER swung by the Earth once, Venus twice and Mercury three times to insert into orbit around Mercury [113]. Meanwhile, ESA launched the Rosetta spacecraft to explore comet 67P/Churyumov-Gerasimenko after it used a gravity assist of Mars and encountered three asteroids. [4]. Due to the significance of the gravity assist manoeuvre in interplanetary transfer missions design, a series of missions which will employ gravity assists are planned in coming years, such as NASA's Parker Solar Probe [114] and the joint mission of NASA, ESA and JAXA: Europa Jupiter System Mission [115].

Gravity assists can also provide extended opportunities for interplanetary exploration, including NEA exploration missions. Qiao, et al. [116] investigated Earth Gravity Assists (EGAs) to reduce the launch energy and the total cost of two-impulse transfer trajectories to NEAs. Eismont, et al. [117] also used EGA to reduce the total cost of transporting a small asteroid to impact a larger hazardous asteroid. Moreover, Casalino and Colasurdo [118] applied Mars gravity assists and solar electric propulsion to design low-cost transfer trajectories to the main belt asteroids and Chen, et al. [119] have proved that Mars is the most useful gravity-assist body for main-belt asteroid exploration through the utilisation of Tisserand graphs. Vasile and Pascale [120] applied multiple gravity assists (MGAs) based on a hybrid approach to design interplanetary transfers both to asteroids and comets. MGAs can be also used to design transfer trajectories between a NEA and a main-belt asteroid [47]. As for asteroid capture missions, a lunar flyby was considered to capture a NEA temporarily into the Earth's Hill region [48]. Bao, et al. [121] also investigate gravity assists to capture NEAs into bound orbits around the Earth. In addition, the strategy of coupling together a flyby of the Earth and stable manifolds to capture NEAs onto Sun–Earth L_1 and L_2 periodic orbits was proposed, and an additional manoeuvre imposed on the candidate NEA at the perigee of the flyby [44].

However, due to their weak gravitational field, small asteroids are not suitable for such manoeuvres. Nevertheless, Penzo and Mayer [122] proposed the use of a tether to temporarily connect a spacecraft with an asteroid for a tethered flyby manoeuvre. During the tethered flyby, the spacecraft is assumed to be attached to the asteroid with a tether, such that the spacecraft can swing around the asteroid through a large angle to yield a similar velocity change as a gravity assist from a planet or moon. Such tether dynamics were also utilised to study the possibility of tethering two asteroids, in order to capture one of them for resource extraction [123]. A similar idea of connecting a spacecraft to a moon in the CRTBP has been proposed to achieve subsequent capture of the spacecraft by the planet [124].

1.2.3 Aerobraking and aerocapture

On a grazing approach to a planetary body, the planet's atmosphere may provide an aerobraking manoeuvre, and thereby directly reduce the speed of the object through energy dissipation. Recently, technologies for such aerobraking manoeuvres have been studied extensively [125-128], with the Magellan [129] and MGS [130] spacecraft demonstrating the feasibility of multi-pass aerobraking for robotic missions. Besides, the benefit of

aerobraking and aerocapture in reducing total mission cost, it leads to many new scenarios for future interplanetary mission design. For example, aerocapture was investigated to significantly increase the spacecraft mass delivered to other planets or moons with atmospheres in the solar system, including Venus, Mars, Titan and Uranus [131]. In particular, detailed analyses of the aerocapture performance required in proposed missions to Titan [132], Neptune [133], Venus [134] and Mars [135] has been undertaken.

Moreover, Braun, et al. [136], Kumar and Tewari [137] proposed to use Earth aerobraking to design Earth-return trajectories from Mars or to transfer to a low Earth orbit from a generic hyperbolic trajectory. Moreover, Sonter [6] proposed the use of an “Earth-fabricated, LEO-fabricated, or asteroid-fabricated aerobrake” to return captured asteroid material to low Earth orbit. Manufacturing an engineered aerobrake directly from asteroid material offers interesting possibilities for the future. Baoyin, et al. [138] supposed that aerobraking would greatly reduce the velocity increment required to capture an asteroid into a bound orbit at the Earth. Based on a first order approximation of the aerobraking manoeuvre [139], Sanchez and McInnes [49] investigated the relationship between the mass loss of the captured asteroid due to ablation and the required compressive strength of the asteroid material during aerobraking. They then estimated the number of 10 m diameter asteroids which could in principle be captured by using an aerobraking strategy. In addition, Fast [38] proposed to use Earth aerobraking to deliver a captured asteroid with a diameter of less than 2 m to the ISS as a proof-of-concept mission. The combination of an Earth gravity assist and a small aerobraking manoeuvre with invariant manifolds was proposed to capture an asteroid onto a periodic orbit around the Sun-Earth libration points L_1 and L_2 [44]. Accordingly, Tan, et al. [80] provided a more general analysis of aerobraking strategies and used aerobraking to capture asteroids directly into bound orbits at the Earth.

The main problem of capturing asteroids using Earth aerobraking is clearly the potential for impact of the captured asteroid during the grazing flyby of the Earth in the event of manoeuvre errors. To address this problem, only small NEAs which in principle would ablate completely before reaching the Earth’s surface, and so would not represent a risk, should be considered as candidate asteroids for capture missions. The use of an engineered aerobrake manufactured from asteroid material also offers advantages for more precise aerocapture, and greater mass returned, rather than directly ablating the surface of the asteroid itself during the manoeuvre [140]. Clearly, an accurate and robust navigation and control strategy would also be required during the aerobraking and aerocapture. For example, the drag-modulation flight control method [126] and the blended control,

predictor-corrector guidance algorithm [128] may provide feasible solutions for an asteroid capture mission using aerobraking.

1.2.4 Momentum exchange theory

Momentum exchange theory can be used as a strategy to achieve manoeuvres or redirect target bodies by transporting the momentum from one object to the target [141, 142]. Generally speaking, this technique can be classified into instantaneous momentum exchange and slow momentum exchange techniques. Slow momentum exchange techniques can provide continuous manoeuvres and has been studied extensively for asteroid deflection using the gravity tractor or ion-beam shepherding [143-145]. On the other hand, instantaneous momentum exchange is usually considered to generate a single impulse and has also been widely applied to research on asteroids, including asteroid deflection by impactors and tether-assists [122, 123, 146-148].

Among the many deflection techniques, the kinetic impactor appears to be feasible with current technology. In this deflection strategy, a spacecraft with a kinetic impactor is first guided to directly impact a target asteroid at a sufficiently high velocity such that the momentum of the impactor is transferred to the target asteroid, causing a modification of the target asteroid's orbit with respect to its unperturbed orbit. In fact, only a modest perturbation to the target asteroid's original orbit is sufficient to achieve desired useful deflections, provided that the warning time is sufficiently long [147]. However, if the warning time is short, a large momentum transfer is required.

A means of improving momentum transfer through engineering a 'billiard shot' asteroid collision has been proposed by Canavan and Rather [149]. The key idea of this method is to use a small asteroid to impact a large asteroid for deflection. In this deflection strategy, a spacecraft is first guided to impact on a small asteroid, which is then delivered to approach a large target asteroid. The trajectory of the large target asteroid is then deflected through collision with the small asteroid. Furthermore, Nazirov and Eismont [150] proposed a way of improving the efficiency of this deflection strategy, through placing the small asteroid onto an Earth swing-by trajectory to modify the trajectory of the small asteroid, and hence enhance the resulting momentum transfer. Because the mass of the small asteroid is much larger than that of the spacecraft, this deflection method can in principle leverage more efficient asteroid deflection strategies. It should be noted that this method requires an accurate dynamical model of the orbits and properties of the relevant bodies, and there must be a small asteroid available with the appropriate orbital elements and size.

Moreover, momentum exchange theory has been used to attempt to lower the total cost of capturing asteroids at the Sun-Earth L_1 and L_2 points, including engineered impacts between asteroids and tethered assists [46].

1.2.5 Advanced propulsion technologies

For NEA capture and retrieval missions, the utilisation of a highly efficient spacecraft propulsion plays a key role in maximising the retrieved mass delivered to the final target orbit. At present, two types of spacecraft propulsion can be used to capture asteroids: high-thrust chemical propulsion and low-thrust propulsion (e.g. electric propulsion and solar sails).

In multi-body dynamical systems, the method of employing invariant manifolds to design transfer trajectories are often based on the application of propulsive manoeuvres, including trajectory design from, to and between libration points [151-154], low-energy transfers between different multi-body dynamical systems [155-157] and low-energy capture of asteroids into periodic orbits around the libration points [17, 43-46, 50]. These instantaneous velocity increments can be achieved using chemical propulsion, with high thrust but low specific impulse. It is clear that chemical propulsion can enable fast transfers. However, due to its low specific impulse, its efficiency in terms of propellant mass requirements is relatively low, compared with low-thrust propulsion. To solve this problem, advanced chemical propulsion technologies have been developed to increase performance, including the utilisation of cryocoolers and small turbopump engines for cryogenic propellants and space storable propellants (e.g. LOX-hydrazine) and advanced monopropellants [158, 159]. In this thesis, impulsive manoeuvres implemented by chemical propulsion are considered to capture NEAs.

If the flight time is long enough, low-thrust propulsion with a high specific impulse, such as the electric propulsion, can be used to increase the range of candidate NEAs for capture and the retrieved mass, since high specific impulse can enable better efficiency of propellant consumption, and thus the payload of the mission can be increased dramatically. With the development of such technology, low thrust propulsion has gradually become a primary propulsion technology for some missions, including Deep Space 1 [28] and the Small Missions for Advanced Research in Technology (SMART-1) [160]. In particular, Deep Space 1 is the first spacecraft to use low-thrust propulsion (i.e. electric propulsion) and flew by asteroid 9969 Braille and comet 19P/Borrelly. Nevertheless, low-thrust electric propulsion can only produce a low thrust and therefore the propulsion system has

to operate for a long duration in order to achieve the required velocity increment during transfer manoeuvres.

With such a long duration, the thrust magnitude and direction time history are unknown parameters, and thus it is difficult to design optimal low-thrust trajectories. Consequently, this optimisation problem has been studied extensively and the proposed methods for solving such problems can typically be classified as direct and indirect methods [161]. Indirect methods transcribe the optimisation problem into a two-point boundary value problem (TPBVP), in which some unknown costates and additional constraint equations are introduced. The TPBVP can usually be solved using the shooting method indirectly, where the shooting function is sensitive to the initial approximation of the costate variables which induces a very narrow convergence radius. Nevertheless, indirect methods often have rapid convergence compared to direct methods. The idea of the direct method is to convert the optimal control problem into a nonlinear programming (NLP) problem by parameterizing the control via explicit integration, and then to solve this problem by minimising the performance index. Sometimes additional design variables are added to increase the convergence domain, and thus the convergence domain of the direct method is usually larger than that of the indirect method. However, the results obtained from the direct methods are usually less optimal due to the parameterization in the conversion to NLP.

With respect to the application of low thrust propulsion to capturing NEAs, advanced solar electric propulsion (SEP) with a specific impulse of 3000 s was proposed to be used in the ARM mission [39]. Moreover, following the definition of EROs, low thrust was then considered to capture these asteroids onto periodic orbits around the Sun-Earth libration points using their stable manifolds [18, 51, 52]. Besides, Mingotti, et al. [53] proposed to combine low thrust propulsion and a patched three-body model to capture EROs into the Earth-Moon system. Again, to solve the problems caused by uncertainties in the target asteroid mass and injection manoeuvres, Ceriotti and Sanchez [57] proposed a control strategy using low thrust.

1.3 Objectives

The main objective of this thesis is to investigate asteroid capture strategies in order to achieve low energy capture of NEAs in the vicinity of the Earth, including the neighbourhood of the Moon, the Sun-Earth libration points L_1 and L_2 , and bound orbits

about the Earth itself. In order to achieve the main goal of this thesis, a series of secondary objectives are set as follows,

- When the NEA is captured in the vicinity of the Earth, it poses a potential impact risk. Therefore, asteroid hazard analysis should be undertaken to select appropriate candidate NEAs which would be disintegrated by the Earth's atmosphere for NEA capture and return missions;
- Considering the lower cost but longer transfer strategy of capturing NEAs in the Earth-Moon system by patching together the Sun-Earth CRTBP and Earth-Moon CRTBP, a relatively faster transfer of capturing NEAs in the vicinity of the Moon will be developed to balance the total cost in terms of velocity increment and flight time;
- The utilisation of the invariant manifolds can enable low energy transfers of capturing NEAs into periodic orbits around the Sun-Earth CRTBP. Accordingly, the combination of the invariant manifolds and other methodologies such as Earth flyby and momentum exchange will be investigated to further reduce the total cost of capturing NEAs into Sun-Earth periodic orbits;
- Aerobraking can enable NEAs to be captured around the Earth with extremely low energy. However, the mass loss of NEAs due to ablation when aerobraking and the mass of the transfer vehicle required should be taken into account. Therefore, optimisations using the ratio of the mass of the captured NEA to the mass of the spacecraft as the objective function will be carried out to maximize the yield of the asteroid capture mission.

1.4 Thesis outline

The main objective of this thesis is to investigate asteroid capture strategies in order to achieve low energy capture of NEAs in the vicinity of the Earth. The thesis is divided into 7 chapters which introduce different aspects of the research on these strategies. Each chapter discusses the method adopted and the detailed design procedure for capturing NEAs, and subsequently results are presented with the application of the theory. The thesis is organised as follows:

Chapter 2 summarises the dynamical models required for mission design for capturing NEAs. In this Chapter, the two-body problem, the model of the circular restricted three-body problem and the model of the Sun-Earth-Moon four-body problem are presented and their applications in the following sections are also described.

Chapter 3 introduces two types of lunar asteroid capture strategies, the direct and indirect capture. In the direct capture strategy, the target points on the stable manifolds associated with periodic orbits around the Earth-Moon L_2 point are filtered and the three-dimensional orbital element space is investigated to select candidate NEAs which have the potential to be captured with a total cost below 500 m/s. The single shooting differential correction method in the Sun-Earth-Moon restricted four-body problem is developed to generate the transfer trajectory from the asteroid's initial orbit to the stable manifold associated with Earth-Moon L_2 point, using a Lambert arc in the Sun-asteroid two-body problem as an initial guess. Accordingly, a global optimisation is carried out. On the other hand, the indirect capture strategy is accomplished by patching together invariant manifolds in the Sun-Earth CRTBP and Earth-Moon CRTBP systems. Finally, both capture strategies are also applied to consider the capture of asteroids at the triangular libration points in the Earth-Moon system. Results show that the direct asteroid capture strategy needs a shorter flight time compared to an indirect asteroid capture, while the indirect capture strategy can more easily achieve low energy capture of NEAs with a longer flight time.

Chapter 4 presents the concept of coupling together a flyby of the Earth and then capturing small NEAs onto Sun-Earth L_1 or L_2 periodic orbits. In this Chapter, the model of an aerobraking manoeuvre is firstly introduced and then the height threshold for aerobraking above the Earth's surface is determined. Then, according to the height of the flyby orbit at perigee, two types of the Earth flyby are determined, an Earth flyby with and without high altitude aerobraking. In particular, the aerobraking phase is investigated to calculate aerobraking opportunities and windows for capture to periodic orbits. After selecting appropriate candidate NEAs and calculating the NEA capture window, transfers for NEA capture with and without an Earth flyby are optimised. Results indicate that the NEA capture strategy using an Earth flyby with and without aerobraking both have the potential to be of lower cost than capture directly onto the stable manifold of the target orbit. Moreover, the NEA capture strategies using an Earth flyby also have the potential to save flight time.

Chapter 5 investigates the concept of capturing small NEAs onto bound orbits around the Earth (rather than Lagrange points) by using aerobraking. In this Chapter, the capture conditions in the CRTBP system are firstly analysed. Then, a Lambert arc in the Sun-

centred two-body problem is utilised to estimate the asteroid capture windows and two modes of aerobraking are determined, corresponding to retrograde orbits and prograde orbits. Then, two strategies to raise the perigee height of the asteroid orbit soon after aerobraking are considered. In the first case, an additional propulsive manoeuvre is required to raise the height of next perigee, and thus two manoeuvres are required to capture NEAs at the Earth. In the second case, the solar gravitational perturbation is used to raise the height of the asteroid perigee and an estimation of the change in perigee height under solar gravitational perturbations is used as a fundamental filter for the solution space in the following optimisation. Finally, a global optimisation is undertaken, and thus the list of the best candidate NEAs is obtained. It is found that aerobraking can enable candidate asteroids to be captured around the Earth with extremely low energy.

Chapter 6 describes a strategy for capturing small NEAs onto bound periodic orbits at the Sun-Earth L_1 and L_2 points using momentum exchange, such as kinetic impacts and the use of tethered assists. First, the minimum mass ratio of the large NEA and small NEA is defined to guarantee that the large NEA orbit is almost unchanged before and after momentum exchange. In the capture strategy using kinetic impacts, the optimal impact direction between the two asteroids is determined by analysing the collision geometry. Since the outcome of the impact depends on the material composition of the NEAs two types of NEAs are considered: basalt and metallic asteroids. In the capture strategy using the tethered assist, the maximum velocity increment provided by the tethered assist is firstly investigated by analysing the tether tension. Then, two different tether materials are considered to compare their performance. Finally, transfers for asteroid capture with and without using momentum exchange are optimised and results show that the capture strategy with momentum exchange can achieve more efficient capture for some NEAs. On the other hand, the flight time for NEA capture using momentum exchange is longer than that without momentum exchange.

Chapter 7 concludes the thesis and provides a summary of the thesis findings. Furthermore, current limitations of the work presented in the thesis are discussed, and proposed directions for future research are presented.

1.5 Publications

The contents of this thesis have been published, or submitted for publication in four journal papers, corresponding to the four technical Chapters of the thesis, respectively.

The study on direct and indirect strategies for capturing NEAs in the Earth-Moon system was published in *Celestial Mechanics and Dynamical Astronomy* [45]. It was demonstrated that a relatively fast transfer for capturing NEAs can be obtained in the direct capture strategy, while the indirect capture strategy can easily achieve low energy transfers. This work will be presented in Chapter 3.

Earth flyby and aerobraking strategies were investigated to reduce the total cost of capturing NEAs into periodic orbits around the Sun-Earth libration points and published in *Advances in Space Research* [44]. In this study, the height threshold for aerobraking was defined and therefore Earth flybys with and without aerobraking were developed to capture NEAs with low energy. This work will be presented in Chapter 4.

A general analysis of aerobraking was undertaken to design low energy capture of NEAs into bound orbit around the Earth and has been submitted to *Acta Astronautica* [80]. It was found that aerobraking can enable NEAs to be captured around the Earth with extremely low energy. Moreover, considering the considerable mass loss of the asteroid during aerobraking, the ratio of the mass of the captured NEA after aerobraking to the mass of the transfer vehicle is defined to measure the yield of the asteroid capture mission. This work will be presented in Chapter 5.

Finally, momentum exchange theory was investigated to capture NEAs around the Sun-Earth libration points. Due to the uncertain properties of NEAs, two different asteroid materials were investigated to study the outcome of collisions. Meanwhile, two different tether materials were also considered for momentum exchange. According to the geometry of collisions and the tether tension, optimisations were carried out. This work was published in the *Journal of Guidance, Control, and Dynamics* [46] and it will be presented in Chapter 6.

The list of the publications stated above is as follows:

- Tan, M., McInnes, C.R., and Ceriotti, M. "Direct and indirect capture of near-Earth asteroids in the Earth–Moon system," *Celestial Mechanics and Dynamical Astronomy*, Vol. 129, pp. 1-32, 2017.
- Tan, M., McInnes, C.R., and Ceriotti, M. "Low-Energy Near-Earth Asteroid Capture Using Momentum Exchange Strategies," *Journal of Guidance, Control, and Dynamics*, Vol. 41, pp. 632-643, 2017.

- Tan, M., McInnes, C.R., and Ceriotti, M. "Low-energy near Earth asteroid capture using Earth flybys and aerobraking," *Advances in Space Research*, Vol. 61, pp. 2099-2115, 2018.
- Tan, M., McInnes, C.R., and Ceriotti, M. "Capture of small near-Earth asteroids to Earth orbit using aerobraking", *Acta Astronautica (In press)*, 2018

CHAPTER 2

DYNAMICAL MODELS

This chapter introduces a number of dynamical models which are utilised to design the families of transfer trajectories for capturing NEAs in this thesis. The applications of these models in the thesis are summarized as follows:

- (1) *Two-body problem model*: In this thesis it is assumed that the motion of a candidate asteroid is modelled in the Sun-centred two-body problem before it is captured. The Lambert problem [162] in the two-body problem will therefore be applied to design the transfer trajectory between the asteroid orbit and the stable manifold in the Sun-Earth system in Chapter 3 and Chapter 6. Moreover, the Lambert arc can be used as an initial guess to design the direct transfer for a captured asteroid from its initial orbit to the stable manifold in the Earth-Moon system in Chapter 3. In addition, based on this model, the two-body orbital elements will be introduced to predict the motion of the captured asteroid after it has been captured around Earth using aerobraking in Chapter 5.
- (2) *Model of the circular restricted three-body problem*: This model will be introduced to calculate periodic orbits around the libration points and their associated stable manifolds. These periodic orbits are used as the final target orbit on which captured asteroids are placed, and their associated stable manifolds serve as a pathway which the captured asteroid will wind on to in Chapter 3, Chapter 4 and Chapter 6. Once inserted onto the stable manifold, the candidate asteroid will be asymptotically captured into the target periodic orbit without any further manoeuvres. Besides, this model will also be used to design transfer trajectories for capturing asteroids around the Earth using aerobraking in Chapter 5.
- (3) *Model of the Sun-Earth-Moon four-body problem*: This model will be used to design the direct transfer of capturing an asteroid from its initial orbit to the stable manifold in the Earth-Moon system in Chapter 3.

2.1 Two-body problem

In this thesis it is assumed that the motion of a candidate asteroid is modelled in the Sun-centred two-body problem before the first manoeuvre for capture is applied. Again, some transfer trajectories for capturing asteroids will be also designed in the two-body problem, e.g. transfer from a candidate asteroid's initial orbit to the stable manifold in the Sun-Earth system in Chapter 3, Chapter 4 and Chapter 6. In this model, it is assumed that a small body (e.g. an asteroid or spacecraft) moves around a large central body. In an inertial frame which is centred at the large central body, the motion of the small body can be written as [163]

$$\ddot{\mathbf{r}} = -\frac{G(m_1 + m_2)}{r^3} \mathbf{r} \quad (2.1)$$

where \mathbf{r} is the relative position vector of the small body with respect to the large central body; G is the gravitational constant; m_1 and m_2 are the mass of the central body and the small body respectively. The gravitational parameter μ_1 is then defined as

$$\mu_1 = G(m_1 + m_2) \quad (2.2)$$

It should be noted that if the mass of the small body is always negligible, compared to that of the central body, the gravitational parameter can be simplified as

$$\mu_1 \approx Gm_1 \quad (2.3)$$

Hence, Eq. (2.1) can be written as

$$\ddot{\mathbf{r}} = -\frac{\mu_1}{r^3} \mathbf{r} \quad (2.4)$$

In this thesis, the gravitational parameters assumed for the Sun-centred two-body problem and the Earth-centred two-body problem are $\mu_{Sun} = 1.3271244 \times 10^{11} \text{ km}^3/\text{s}^2$ and $\mu_{Earth} = 3.9860044 \times 10^5 \text{ km}^3/\text{s}^2$, respectively ².

Moreover, the magnitude of the relative position vector \mathbf{r} can be written as

$$r = \frac{h^2}{\mu_1} \frac{1}{1 + e \cos \theta} \quad (2.5)$$

² <https://ssd.jpl.nasa.gov/?constants>

where e is the orbit eccentricity and θ is the true anomaly of the small body around the central body, measured from the periapsis, as shown in Fig. 2.1. Moreover, \mathbf{h} is the relative angular momentum of the small body per unit mass and can be written as

$$\mathbf{h} = \mathbf{r} \times \mathbf{v}, \mathbf{v} = \dot{\mathbf{r}} \quad (2.6)$$

where \mathbf{v} is the velocity vector of the small body.

According to different values of the orbit eccentricity e , orbits in the two-body problem can be divided into four types: circular orbit, elliptical orbit, parabolic orbit and hyperbolic orbit, corresponding to $e = 0$, $e < 1$, $e = 1$, $e > 1$. The distance from the periapsis on these orbits to the central celestial body can be obtained when $\theta = 0$, as follows

$$r_p = \frac{h^2}{\mu_1} \frac{1}{1+e} = a(1-e) \quad (2.7)$$

where a is the semi-major axis of the orbit and thus can be computed by

$$a = \frac{h^2}{\mu_1} \frac{1}{1-e} \quad (2.8)$$

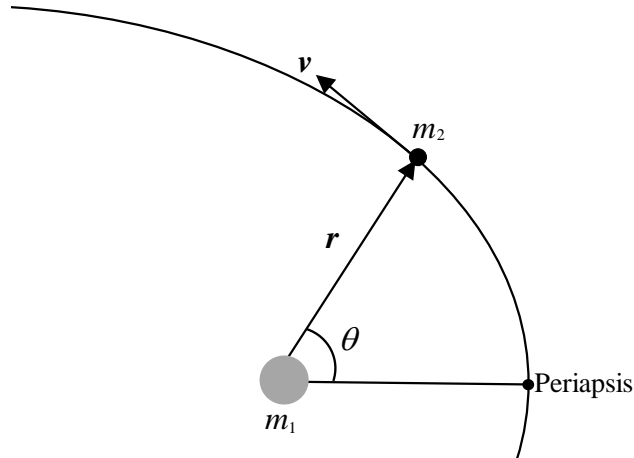


Fig. 2.1 Geometry of the two-body problem.

2.1.1 Orbital elements

The angular momentum \mathbf{h} can define the orbit plane. As shown in Eq. (2.8), the semi-major axis a of the orbit can be calculated from these two parameters. Besides, the true anomaly θ is required to locate a point on this orbit, as shown in Fig. 2.1. However, these parameter cannot describe the orientation of the orbit in three dimensions. Therefore, additional parameters must be used, as shown in Fig. 2.2. It should be noted that in Fig.

2.2, the X-axis points to the vernal equinox direction, the Y-axis is perpendicular to the X-axis in the equatorial plane of the central body and the Z-axis is perpendicular to the X-Y plane, measured according to the right-hand rule.

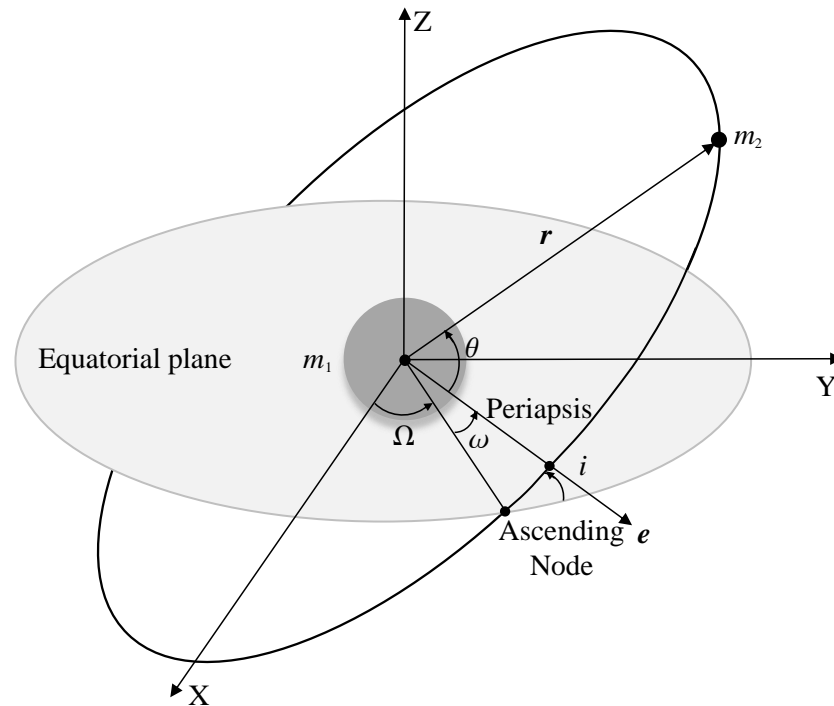


Fig. 2.2 Geometry of the orbital elements.

As shown in Fig. 2.2, the nodal line is the intersection of the orbital plane and the equatorial plane, and thus the ascending node is defined as the intersection point of the nodal line with the orbit. Therefore, the first angle, the right ascension of the ascending node Ω , is defined as the angle between the positive X-axis and the nodal line, with a range from 0 to 2π .

The second angle is the orbit inclination i , the angle between the orbit plane and the equatorial plane, measured according to the right-hand rule. The range of the inclination i is from 0 to π .

The eccentricity vector e is a line from the central body to the periapsis on the orbit and the third angle, the argument of perigee ω , is the angle between the nodal line and the eccentricity vector e , measured in the plane of the orbit. The range of the argument of perigee ω is from 0 to 2π .

In summary, the six orbital elements which are used in this thesis are listed as follows:

- a : semi-major axis.
- i : inclination.
- e : eccentricity.

- Ω : right ascension of the ascending node.
- ω : argument of perigee.
- θ : true anomaly.

The transformation between the position and velocity vector and the orbital elements can be obtained from [163].

2.1.2 Lambert arc

Lambert's problem is a key problem to determine the transfer trajectory which connects two position vectors \mathbf{r}_1 and \mathbf{r}_2 with respect to the central celestial body in space, with a given flight time Δt and number of orbit revolutions, as shown in Fig. 2.3. A Lambert arc is a coast arc which is obtained by solving Lambert's problem [162]. Once the two position vectors, the flight time and number of revolutions are given, the velocity vectors at the boundaries of the Lambert arc can be calculated, by using a multi-revolution Lambert solver which is based on the Battin's method [162]. In this method, the geometric orbital transformation for the Lambert's problem is first proposed to avoid the singularity when the transfer angle is π . Then the transfer time equation for the Lambert's problem is formulated in the transformed orbit and the solution of the Lambert's problem can be obtained by solving the transfer time equation. Consequently, the velocity increments required for the Lambert arc can be obtained. Denoting the velocity increments at the beginning and endpoint of the Lambert arc as $\delta\mathbf{v}_1$ and $\delta\mathbf{v}_2$, respectively, the total velocity increment required for the Lambert arc can be written as

$$\delta\mathbf{v} = \delta\mathbf{v}_1 + \delta\mathbf{v}_2 \quad (2.9)$$

The Lambert arc can be used to design transfer trajectories between different orbits for interplanetary transfer missions. In this thesis, the Lambert problem in the context of the two-body problem will be used to design the transfer trajectory between an asteroid orbit and stable manifolds in the Sun-Earth system in Chapter 3. Moreover, the Lambert arc can be used as an initial guess to design a direct transfer to capture asteroids from an initial orbit to stable manifolds in the Earth-Moon system in Chapter 3. In addition, the Lambert arc will act as an effective tool to design the transfer trajectory between the two asteroid orbits, along with the transfer trajectory which connects the asteroid orbit and stable manifolds in the Sun-Earth system in the asteroid capture strategy using momentum exchange in Chapter 6.

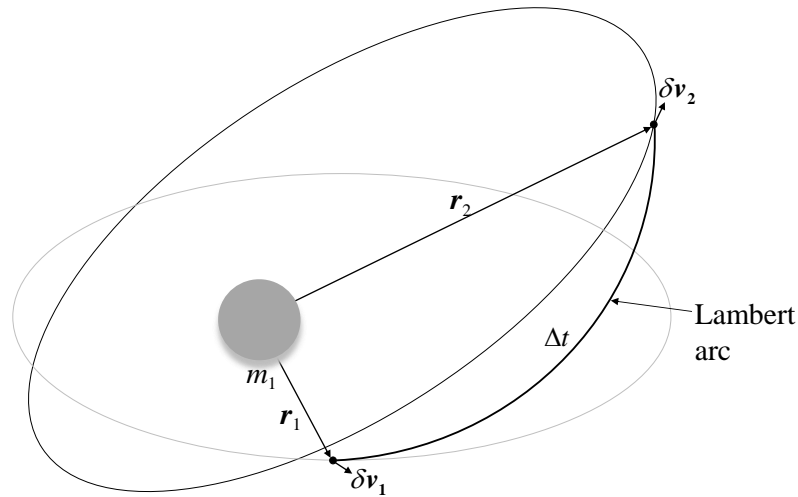


Fig. 2.3 Schematic diagram of the Lambert problem.

2.2 Circular restricted three-body problem

For some trajectories the motion of a small body under the gravitational attraction of more than one body, such as the Sun, planets or moons must be considered. In such cases, the problem can be simplified as a restricted problem, when the mass of the small body is negligible compared with that of the other bodies. Amongst these restricted problems, the circular restricted three-body problem (CRTBP) considers the motion of a small body (the third body), which moves under the gravitational attraction of two primary bodies, e.g. Sun and Earth or Earth and Moon, etc. Here we denote the masses of the larger primary body, the smaller primary body and the third body as m_1 , m_2 and m_3 respectively. In this model, it is assumed that the two primary bodies moves in circular orbits around their common centre-of-mass. Since these two primaries are only influenced by their mutual attraction, the motion of the two primaries can be modelled as a two-body problem which is centred at their common centre-of-mass. Therefore, the motion of the small body at position \mathbf{R} in an inertial frame (X, Y, Z) which is centred at this common centre-of-mass can be written as

$$\ddot{\mathbf{R}} = -\frac{\mu_1}{R_1^3} \mathbf{R}_1 - \frac{\mu_2}{R_2^3} \mathbf{R}_2 \quad (2.10)$$

where μ_1 and μ_2 are the gravitational parameters of the two primary bodies; \mathbf{R}_1 and \mathbf{R}_2 are the position vector of the third body with respect to the two primary bodies which can be written as

$$\mathbf{R}_1 = \mathbf{R} - \mathbf{R}_{p1}, \mathbf{R}_2 = \mathbf{R} - \mathbf{R}_{p2} \quad (2.11)$$

where \mathbf{R}_{p1} and \mathbf{R}_{p2} are the position vectors of the two primary bodies in a inertial frame, centred at their barycentre, which can be considered as a two-body problem.

It should be noted that in the CRTBP the two primaries move with a constant angular velocity around their barycentre and thus \mathbf{R} is a function of the angular velocity. To eliminate this angular velocity dependence, a coordinate frame (x, y, z) centred at the barycentre of the two primary bodies and rotating synchronously with them is introduced, termed the rotating frame. In this frame, the distance between the two primaries, the total mass and the angular velocity of two bodies are normalized to unity. Moreover, the x -axis of the rotating frame extends from the barycentre to the smaller primary body, the y -axis is perpendicular to the x -axis in the plane of the two primaries and the z -axis is perpendicular to the x - y plane, defined according to the right-hand rule. For a given CRTBP, there exists a mass parameter μ which can be defined as [164]

$$\mu = \frac{m_2}{m_1 + m_2} \quad (2.12)$$

After normalization, the orbital period of the two primaries is then equal to 2π . Besides, the masses of the larger and smaller primaries are equal to $1 - \mu$ and μ , respectively. The coordinates of the two primaries body in the rotating frame are then $[-\mu, 0, 0]$ and $[1 - \mu, 0, 0]$, respectively, as shown in Fig. 2.4, Therefore, the equations of the CRTBP can be written as [164]

$$\ddot{x} - 2\dot{y} = \frac{\partial \Omega}{\partial x}, \quad \ddot{y} + 2\dot{x} = \frac{\partial \Omega}{\partial y}, \quad \ddot{z} = \frac{\partial \Omega}{\partial z} \quad (2.13)$$

where the effective potential Ω is given by

$$\Omega(x, y, z, \mu) = \frac{1}{2}[(x^2 + y^2) + \mu(1 - \mu)] + \frac{1 - \mu}{r_1} + \frac{\mu}{r_2}$$

$$r_1 = [(x + \mu)^2 + y^2 + z^2]^{1/2}, \quad r_2 = [(x - 1 + \mu)^2 + y^2 + z^2]^{1/2}$$

and where r_1 and r_2 are the distances of the third body to the two primary bodies, scaled by the distance between the two primary bodies. It should be noted that different CRTBP systems have different values of μ . In this thesis, the focus is on the Sun-Earth CRTBP and Earth-Moon CRTBP systems. The mass parameters assumed for these two system are $\mu =$

$m_{Moon} / (m_{Earth} + m_{Moon}) = 1.215 \times 10^{-2}$ and $\mu = m_{Earth} / (m_{Sun} + m_{Earth}) = 3.0035 \times 10^{-6}$, respectively.

The position of the smaller primary body in an inertial frame, which is centred at the barycentre of the two primaries, can be described by the angle β , shown in Fig. 2.4. Here we denote the state of the CRTBP system in the rotating frame and in the inertial frame by \mathbf{X}^{ro} and \mathbf{X}^{in} respectively. Thus we have the transformation

$$\mathbf{X}^{in} = \mathbf{R}(\beta) \mathbf{X}^{ro}, \quad \beta \in [0, 2\pi] \quad (2.14)$$

$$\mathbf{X}^{ro} = \mathbf{R}^{-1}(\beta) \mathbf{X}^{in}, \quad \beta \in [0, 2\pi] \quad (2.15)$$

where $\mathbf{R}(\beta)$ the rotation matrix and it can be written as

$$\mathbf{R}(\beta) = \begin{bmatrix} \cos \beta & -\sin \beta & 0 & 0 & 0 & 0 \\ \sin \beta & \cos \beta & 0 & 0 & 0 & 0 \\ 0 & 0 & 1 & 0 & 0 & 0 \\ -\sin \beta & -\cos \beta & 0 & \cos \beta & -\sin \beta & 0 \\ \cos \beta & -\sin \beta & 0 & \sin \beta & \cos \beta & 0 \\ 0 & 0 & 0 & 0 & 0 & 1 \end{bmatrix}$$

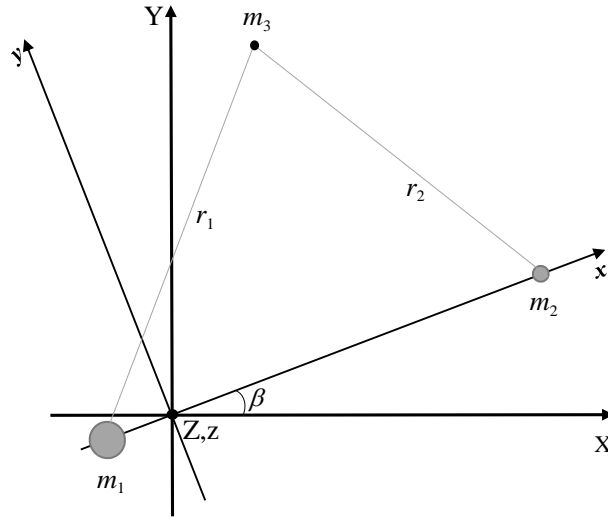


Fig. 2.4 Geometry of the CRTBP system in the frame xyz and in an inertial frame XYZ .

2.2.1 Libration points and Jacobi constant

For the CRTBP, there are five Lagrange equilibrium points, also known as the libration points, L_i , ($i = 1, 2 \dots 5$). The coordinates of the libration points can be computed such that

$$\begin{cases} \dot{x} = 0, & \dot{y} = 0, & \dot{z} = 0 \\ \ddot{x} = 0, & \ddot{y} = 0, & \ddot{z} = 0 \end{cases} \quad (2.16)$$

When substituting Eq. (2.16) into Eq. (2.13), the coordinates of the libration points can be obtained, with the coordinates of the libration points of the Sun-Earth CRTBP and Earth-Moon CRTBP system listed in Table 2.1. Figure 2.4 shows the geometry of the libration points in the Earth-Moon CRTBP. As shown in Fig. 2.5, L_1 - L_3 lie on the x -axis and thus they are termed the collinear libration points. Moreover, L_4 and L_5 are termed the triangular libration points, since the two primary bodies and these two libration points are located at the vertices of equilateral triangles. The third body will be stationary at these libration points if it has no initial velocity. However, the collinear libration points L_1 - L_3 are unstable. This dynamical characteristic is useful and accordingly invariant manifolds can be defined to achieve low-energy transfers [97, 157]. Furthermore, the triangular libration points are stable in the Earth-Moon CRTBP. For this reason, it may be of interest to capture an asteroid and place it on a periodic orbit around the triangular L_4 and L_5 points in the Earth-Moon system.

From Eq. (2.13), it can be shown that

$$\ddot{x} + \ddot{y} + \ddot{z} = \frac{\partial \Omega}{\partial x} \dot{x} + \frac{\partial \Omega}{\partial y} \dot{y} + \frac{\partial \Omega}{\partial z} \dot{z} \quad (2.17)$$

Thus, Eq. (2.17) becomes

$$\frac{1}{2} \frac{d}{dt} (\dot{x}^2 + \dot{y}^2 + \dot{z}^2) = \frac{d\Omega}{dt} \quad (2.18)$$

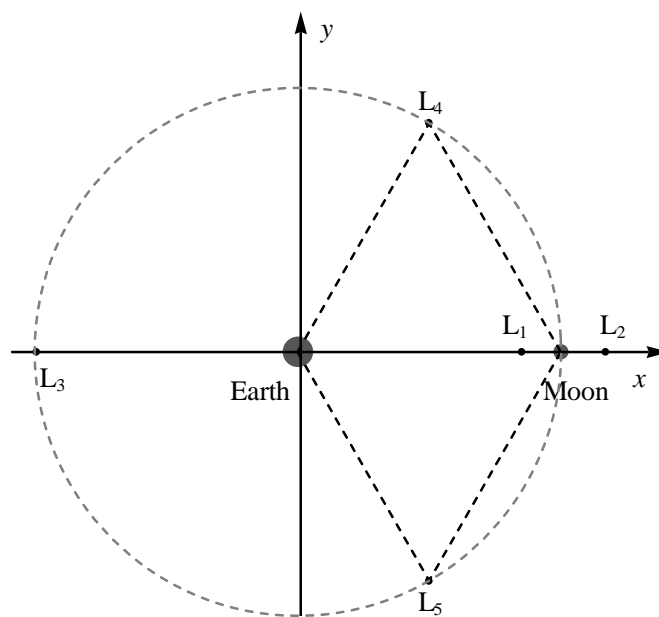
From Eq. (2.18), it can be seen that the dynamics of the CRTBP permit an integral of motion to exist in the rotating frame. In the CRTBP this is termed the Jacobi constant C , and can be obtained as follows [97]

$$2\Omega(x, y, z, \mu) - (\dot{x}^2 + \dot{y}^2 + \dot{z}^2) = C \quad (2.19)$$

From Eq. (2.19), it can be seen that the C will decrease when the third body (m_3) increases its velocity. Since the velocity of the third body (m_3) is always positive, C cannot exceed $2\Omega(x, y, z, \mu)$ at a given location and so it will define an allowed region of motion and a forbidden region, as discussed in the next section. Furthermore, the Jacobi constant of the third body is constant, unless a manoeuvre is required.

Table 2.1 Coordinates of the libration points in the Earth-Moon and Sun-Earth systems.

Libration point	Earth-Moon system		Sun-Earth system	
	x	y	x	y
L_1	0.836918	0	0.989991	0
L_2	1.155680	0	1.010070	0
L_3	-1.005062	0	-1.000001	0
L_4	$0.5 - \mu$	$\sqrt{3}/2$	$0.5 - \mu$	$\sqrt{3}/2$
L_5	$0.5 - \mu$	$-\sqrt{3}/2$	$0.5 - \mu$	$-\sqrt{3}/2$

**Fig. 2.5 Geometry of the libration points in the Earth-Moon CRTBP system.**

2.2.2 Zero-velocity surfaces

As noted in Section 2.2.1, the Jacobi constant C cannot exceed $2\Omega(x, y, z, \mu)$ at a given location and the threshold of this case defines the zero-velocity surface. The zero-velocity surface represents a boundary the third body with a given Jacobi constant cannot cross and can be computed when

$$\dot{x}^2 + \dot{y}^2 + \dot{z}^2 = 0 \quad (1.20)$$

An example of zero-velocity surfaces in the Earth-Moon CRTBP system is shown in Fig. 2.6. The zero-velocity surface can be utilised to analyse the possible region of the third body's motion near the primary bodies, especially the smaller primary.

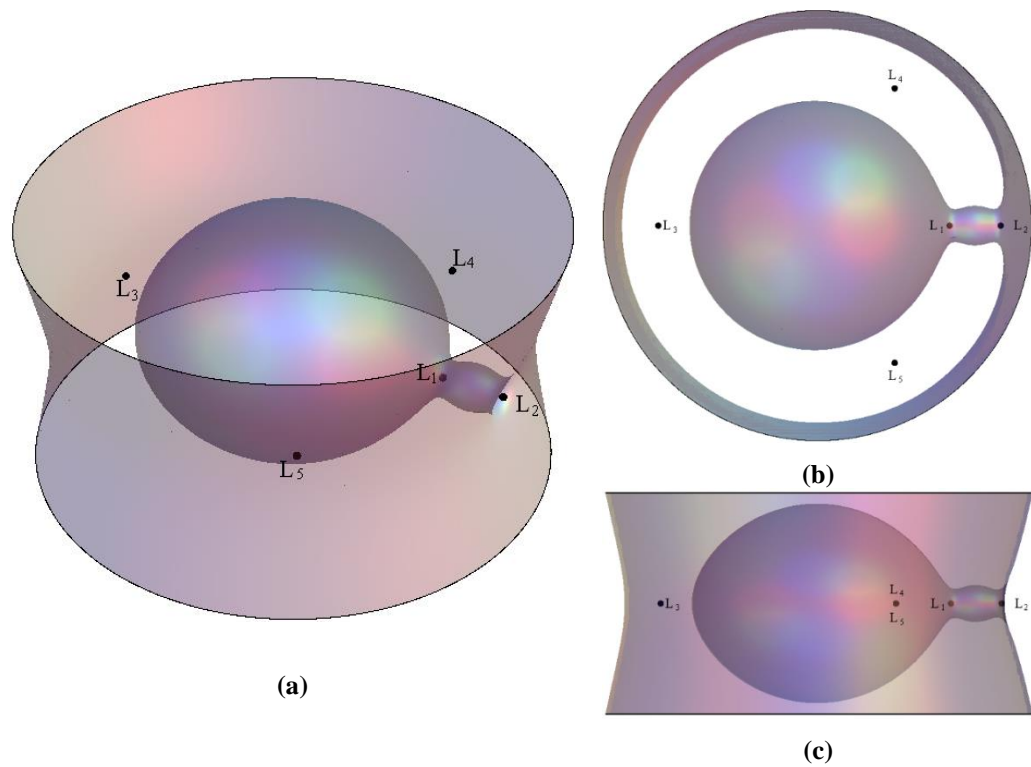


Fig. 2.6 Zero-velocity surface in the Earth-Moon CRTBP system with Jacobi constant $C = 3.16$: (a) 3D view; (b) x - y projection; (c) x - z projection.

The zero-velocity curve is the planar case of the zero-velocity surface, when $z = 0$. Since the zero-velocity curve is more intuitive than the zero-velocity surface, the zero-velocity curve is an alternative way to determine the possible region of the third body's motion in the CRTBP. Figure 2.6 shows the zero-velocity curve in the Earth-Moon system with different Jacobi constants C . For the CRTBP, there are five specific Jacobi constants, corresponding to the five libration points. Here we define the Jacobi constant at the libration point L_i ($i = 1 - 5$) as C_i ($i = 1 - 5$). Table 2.2 shows the Jacobi constants at five libration points in the Earth-Moon CRTBP and Sun-Earth CRTBP system and we can note that $C_1 > C_2 > C_3 > C_4 = C_5$. Figure 2.7 shows an example of the zero-velocity curves in the Earth-Moon CRTBP system with different Jacobi constants C .

Table 2.2 Jacobi constant at the libration points of the Earth-Moon and Sun-Earth systems.

Libration point	Jacobi constant C_i	Jacobi constant in the Earth-Moon CRTBP	Jacobi constant in the Sun-Earth CRTBP
L_1	C_1	3.188336	3.000897
L_2	C_2	3.172156	3.000893
L_3	C_3	3.012147	3.000003
L_4	C_4	2.987998	3.000106
L_5	C_5	2.987998	3.000106

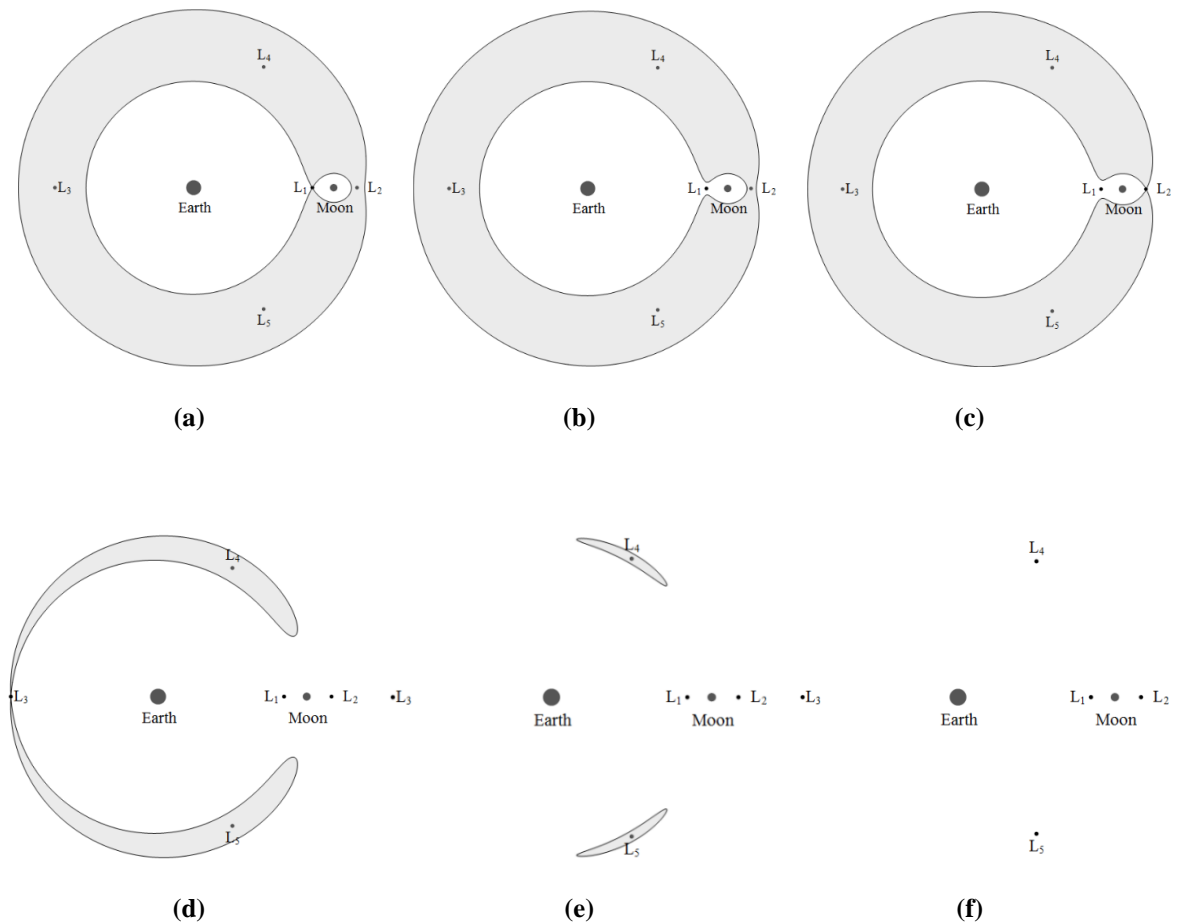


Fig. 2.7 Zero-velocity curve, possible region of motion (white) and forbidden region (grey) in the Earth-Moon CRTBP system with (a) $C = C_1$; (b) $C_2 < C < C_1$; (c) $C = C_2$; (d) $C = C_3$; (e) $C_4 = C_5 < C < C_3$; (f) $C = C_4 = C_5$.

As shown in Fig. 2.7, for $C > C_1$, the possible region of motion is composed of two separate oval regions centred at the two primary bodies (e.g. Earth and Moon) and an outer region beyond the outer zero-velocity curve. When $C = C_1$, the two inner oval regions merge at L_1 , as shown in Fig. 2.7(a). With a decrease of the Jacobi constant, the two inner regions connect and they become a single inner region (See Fig. 2.7(b)). When $C = C_2$, the

inner region and outer region merge at L_2 and then they connect with each other with the further decrease of C , as shown in Fig. 2.7(c). When $C = C_3$, the forbidden region separates into two parts at L_3 , as shown Fig. 2.7(d). When $C_4 = C_5 < C < C_3$ and C decreases, the two forbidden regions gradually reduce in size (See Fig. 2.7(e)) until these two separate regions disappear at L_4 and L_5 , respectively when $C = C_4 = C_5$, as shown in Fig. 2.7(f). In particular, for the Sun-Earth CRTBP system, C_1 and C_2 are critical since they can be used as capture conditions to determine whether a candidate asteroid can be captured nor not, when it approaches the vicinity of the Earth. This will be discussed further in Chapter 5.

2.2.3 State Transition and Monodromy Matrices

The state transition matrix reflects the linear influence of a small deviation to a reference trajectory in the CRTBP. It is particularly useful when calculating periodic orbits around the libration points and their associated invariant manifolds. Denoting the state of the CRTBP system as $\mathbf{X} = (x, y, z, \dot{x}, \dot{y}, \dot{z})$, its derivative can be written as

$$\dot{\mathbf{X}} = (\dot{x}, \dot{y}, \dot{z}, \ddot{x}, \ddot{y}, \ddot{z}) \quad (2.21)$$

Thus, the equations of the CRTBP in Eq. (2.13) can be simplified as

$$\dot{\mathbf{X}} = f(\mathbf{X}, t) \quad (2.22)$$

Let $\delta\mathbf{x}$ be a small deviation from the reference trajectory so that

$$\dot{\mathbf{X}} + \delta\dot{\mathbf{x}} = f(\mathbf{X} + \delta\mathbf{x}, t) \quad (2.23)$$

Then using a Taylor series expansion to expand $f(\mathbf{X} + \delta\mathbf{x}, t)$ and neglecting terms higher than the first order, the linear expansion can be obtained as follows

$$\delta\dot{\mathbf{x}} = \frac{\partial f(\mathbf{X}, t)}{\partial \mathbf{X}} \delta\mathbf{x} \quad (2.24)$$

The general solution to the equation above is

$$\delta\mathbf{X}(t) = \Phi(t, t_0)\delta\mathbf{X}(t_0) \quad (2.25)$$

where $\Phi(t, t_0)$ is the state transition matrix which can be calculated as [97]

$$\dot{\Phi}(t, t_0) = A(t)\Phi(t, t_0), \quad \Phi(t_0, t_0) = \mathbf{I}_{6 \times 6} \quad (2.26)$$

and where

$$\mathbf{A}(t) = \begin{bmatrix} \mathbf{0} & \mathbf{I}_{3 \times 3} \\ U_{xx} & \Psi \end{bmatrix}, \quad \Psi = \begin{bmatrix} 0 & 2 & 0 \\ -2 & 0 & 0 \\ 0 & 0 & 0 \end{bmatrix}, \quad U_{xx} = \begin{bmatrix} \frac{\partial \ddot{x}}{\partial x} & \frac{\partial \ddot{x}}{\partial y} & \frac{\partial \ddot{x}}{\partial z} \\ \frac{\partial \ddot{y}}{\partial x} & \frac{\partial \ddot{y}}{\partial y} & \frac{\partial \ddot{y}}{\partial z} \\ \frac{\partial \ddot{z}}{\partial x} & \frac{\partial \ddot{z}}{\partial y} & \frac{\partial \ddot{z}}{\partial z} \end{bmatrix}$$

For a periodic orbit around the libration points, if the state transition matrix is propagated for one full revolution, a specific state transition matrix, termed the monodromy matrix, Φ_T can be written as

$$\Phi_T = \Phi(t_0 + T_p, t_0) \quad (2.27)$$

where T_p is the period of the periodic orbit.

In this thesis, a standard Runge-Kutta fourth-order integration method with a tolerance 10^{-12} is used for the numerical simulations, including the calculation of the transformation matrix, periodic orbits, invariant manifolds and differential corrections. The state transition and monodromy matrices have widespread use in the calculation and correction of periodic orbits around the libration points and their associated invariant manifolds in the Earth-Moon CRTBP system and Sun-Earth CRTBP system.

2.2.4 Periodic orbits around L_1/L_2

Families of periodic orbits around the collinear libration points L_1 and L_2 in the CRTBP have been studied extensively [165-170]. There are two key classes of periodic orbits: halo orbits and Lyapunov orbits. For a periodic orbit around the L_1 or L_2 point, the third order Richardson expansion can be derived from the Lindstedt–Poincaré method as follows [165]

$$\begin{aligned} \xi &= a_{12}A_x^2 + a_{22}A_z^2 - A_x \cos(\lambda\tau + \phi) + (a_{23}A_x^2 - a_{24}A_z^2) \cos(2\lambda\tau + 2\phi) \\ &\quad + (a_{31}A_x^2 - a_{32}A_xA_z^2) \cos(3\lambda\tau + 3\phi) \\ \eta &= kA_x \sin(\lambda\tau + \phi) + (b_{21}A_x^2 - b_{22}A_z^2) \sin(2\lambda\tau + 2\phi) \\ &\quad + (b_{31}A_x^2 - b_{32}A_xA_z^2) \sin(3\lambda\tau + 3\phi) \\ \zeta &= \delta_n A_z \cos(\lambda\tau + \phi) + \delta_n d_{21} A_x A_z (\cos(2\lambda\tau + 2\phi) - 3) \\ &\quad + \delta_n (d_{33} A_z A_x^2 - d_{31} A_z^2) \cos(3\lambda\tau + 3\phi) \end{aligned} \quad (2.28)$$

where A_x and A_z are the amplitudes of the periodic orbit along the x -axis and z -axis, respectively; $\delta_n = \pm 1$ and the values of the remaining coefficients in Eq. (2.28) can be found in Ref. [165]. It should be noted that, the origin of the coordinate frame (ξ, η, ζ) is located at one of the collinear libration points and the ξ - η plane of this coordinate frame coincides with x - y plane in the Earth-Moon rotating frame. Moreover, the ξ -axis points from the larger primary body to the libration point, the η -axis is perpendicular to the ξ -axis in the plane of the two primaries and the ζ -axis is perpendicular to the ξ - η plane, defined according to the right-hand rule. The third order Richardson expansion in Eq. (2.28) can provide a good approximation of the initial state of a periodic orbit around the L_1 or L_2 points after which the accurate initial states of such periodic orbits can be computed by utilising the differential correction method [171]. Following this process, examples of a Lyapunov orbit and halo orbit around the Earth-Moon L_2 point are shown in Fig. 2.8 and Fig. 2.9, where the unit of length is the Earth-Moon distance (EM unit).

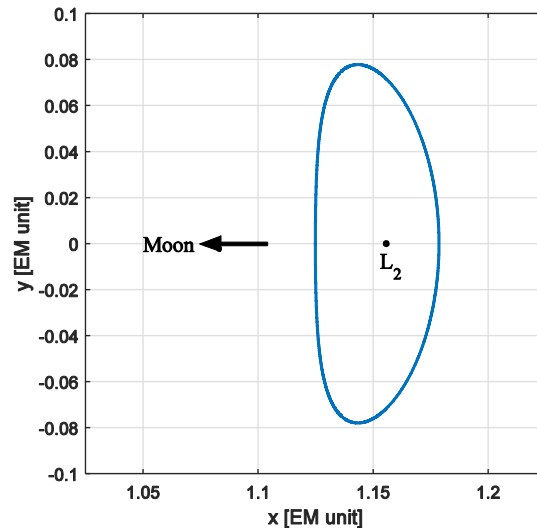


Fig. 2.8 A Lyapunov orbit with an initial guess when $A_x = 0.15$, $A_z = 0$ in Eq. (2.28).

It should be noted that the third order Richardson expansion can be used to compute families of Halo orbits. However, the family of planar Lyapunov orbits can be viewed as a special kind of halo orbit when the amplitude along the z -axis is zero. Therefore the analytical approximation in Eq. (2.28) is still valid to calculate Lyapunov orbits for small sizes. In practical computations, the analytical approximation is only used as an initial guess for a periodic orbit (both Lyapunov orbit and halo orbit) with small sizes. Then, the accurate initial state of the periodic orbit is again calculated using the differential correction method. Moreover, the families of periodic orbits can be calculated using the continuous method. In detail, this accurate initial state of the periodic orbit is the used as the initial guess to obtain the accurate initial state of a new periodic orbit with a slightly

larger displacement in amplitude along the x -axis (Lyapunov orbit) or z -axis (halo orbit). Repeating this process provides a series of periodic orbits with increasing energy, or decreasing Jacobi constant. This will be discussed further in Chapters 3, 4 and 6.

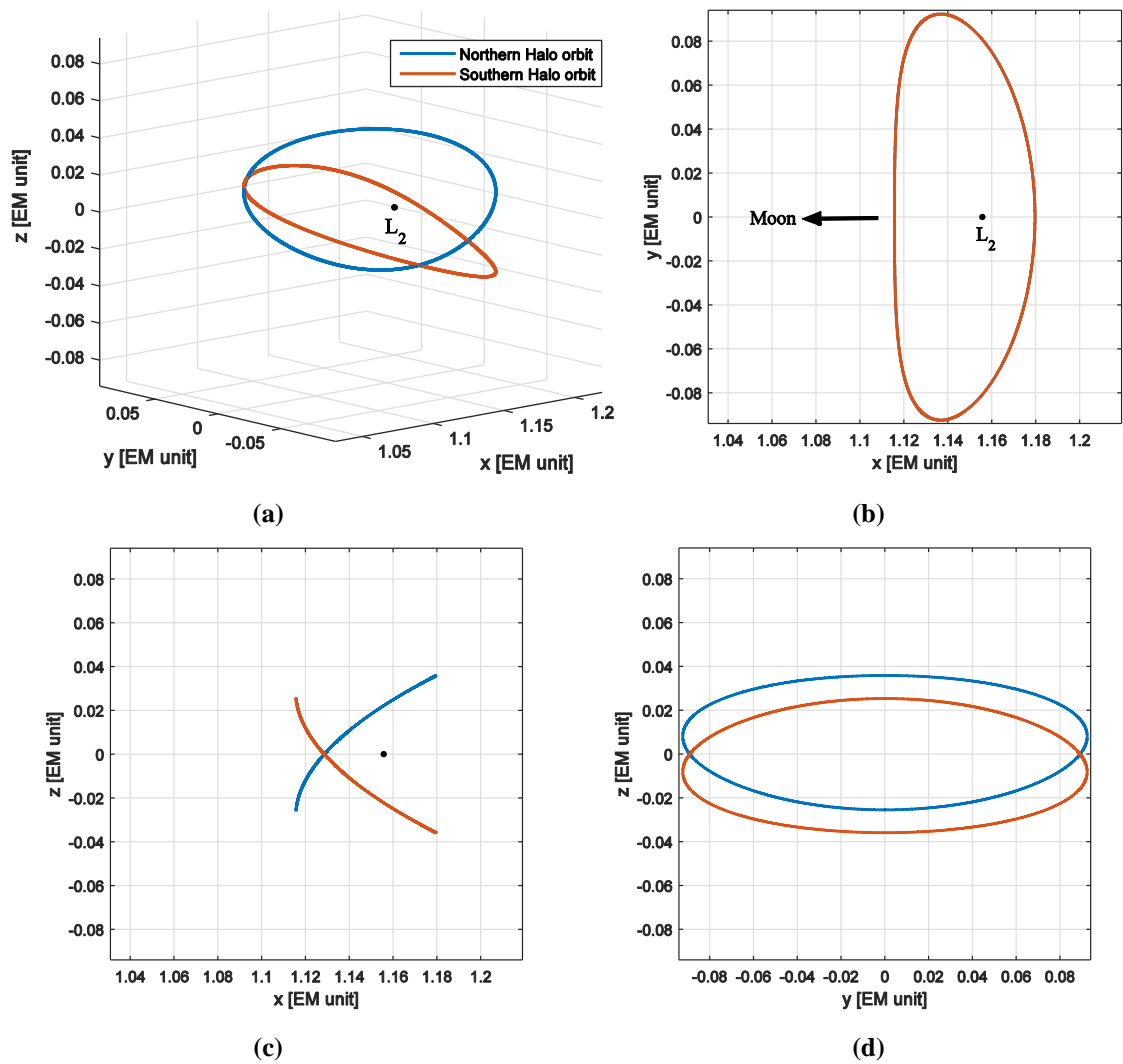


Fig. 2.9 Halo orbits with an initial guess when $A_x = 0.15$, $A_z = 0.38$ in Eq. (2.28): (a) 3D view; (b) x - y projection; (c) x - z projection; (d) y - z projection.

2.2.5 Periodic orbits around L₄/L₅

In the Earth-Moon CRTBP model, the triangular points L₄ and L₅ are stable. Even when the eccentricity of the lunar orbit and the influence of the solar radiation pressure are taken into account, the resulting instability of the triangular points is still much weaker than that of the collinear points [172]. This means that station-keeping does not require significant energy. Therefore, the vicinity of the triangular points in Earth-Moon system could be a preferred location for parking orbits for captured asteroids. However, the stability properties of the triangular points are also a disadvantage because there are no dynamical

structures such as the stable or unstable invariant manifolds which can be utilised to design low-cost transfer trajectories, as will be discussed further in Chapter 3.

In a rotating frame centred at one of the triangular points, the linearized solution for motion in the x - y plane around triangular points can be expressed as [164, 172]:

$$\begin{cases} \xi = \kappa_1 \cos \theta_1 + \kappa_2 \cos \theta_2 \\ \eta = w_1 \kappa_1 \cos \theta_1 + n_1 \kappa_1 \sin \theta_1 + w_2 \kappa_2 \cos \theta_2 + n_2 \kappa_2 \sin \theta_2 \end{cases} \quad (2.29)$$

where

$$w_i = -\Gamma_i \Omega_{xy}^0, \quad n_i = -2\omega_i \Gamma_i, \quad \Gamma_i = \frac{1}{\omega_i^2 + \Omega_{yy}^0}$$

$$\theta_i = \omega_i t + \varphi_i \quad (i=1, 2), \quad \Omega_{xy} = \frac{\partial}{\partial y} \left(\frac{\partial \Omega}{\partial x} \right)$$

$$\Omega_{yy} = \frac{\partial^2 \Omega}{\partial y^2}, \quad \omega_1 \cong \frac{27}{4} \mu, \quad \omega_2 \cong 1 - \frac{27}{8} \mu$$

and Ω_{xy}^0 , Ω_{yy}^0 are the values of Ω_{xy} , Ω_{yy} at the triangular points, respectively and the other parameters are defined in [3,10].

There are then two families of periodic orbits around the triangular points, long-period orbits and short-period orbits which are defined by the components ω_1 and ω_2 , respectively in Eq. (2.29) [164]. The coefficients κ_1 and κ_2 correspond to the amplitudes of the short periodic orbit and long periodic orbit, respectively. In addition φ_i ($i = 1, 2$) represents the initial phase angle. Generally speaking, the short-period orbits are much more stable than the long-period orbits, under given perturbations. Therefore, in this thesis, short-period orbits are chosen as the target orbit and an example of a short-period orbit around the L_4 and L_5 points in the Earth-Moon system is shown in Fig. 2.10. From Fig. 2.10, it can be seen that the short-period orbits around the L_4 and L_5 points are symmetric with respect to the x -axis.

2.2.6 Invariant manifolds

As stated in Section 2.2.1, the collinear libration points L_1 and L_2 are unstable and thus a particle which is placed at these points with zero relative velocity would deviate from them under a small perturbation. Moreover, such dynamical characteristics are also present for the unstable periodic orbits (Lyapunov orbits and halo orbits) around L_1 and L_2 . To

describe this dynamical characteristic, the invariant manifolds associated with periodic orbits around the collinear L_1 and L_2 libration points are defined as trajectories which asymptotically approach or depart from these target periodic orbits [97]. The stable manifold W^s associated with a periodic orbit consists of all trajectories that reach this target periodic orbit along the periodic orbit's stable eigenvector. The unstable manifold W^u associated with a periodic orbit includes all possible trajectories that depart from this target orbit along the target orbit's unstable eigenvector. Therefore, the stable manifold in the CRTBP can be calculated by propagating backwards from an initial condition as follows

$$\mathbf{X}_s = \mathbf{X}_0 \pm \varepsilon \mathbf{V}_s \quad (1.30)$$

and the unstable manifold can be computed by propagating forward from the following initial condition

$$\mathbf{X}_u = \mathbf{X}_0 \pm \varepsilon \mathbf{V}_u \quad (1.31)$$

where \mathbf{V}_s and \mathbf{V}_u are the stable and unstable eigenvectors of the monodromy matrix Φ_T evaluated at a point $\mathbf{X}_0 = [x_0, y_0, z_0, \dot{x}_0, \dot{y}_0, \dot{z}_0]^T$ on the periodic orbit. The parameter ε represents the magnitude of the perturbation, in the direction of the stable and unstable eigenvectors, between the periodic orbit and the initial condition of the stable and unstable manifolds. Gómez, et al. [173] suggested values of ε corresponding to non-dimensional position displacements of order 10^{-6} and a value on the order of 10^{-4} used for the Earth-Moon system [174]. In this thesis, values of ε are selected to be 2×10^{-4} and 2×10^{-6} for the Earth-Moon CRTBP and Sun-Earth CRTBP, respectively. An example of stable manifolds and unstable manifolds associated with a Lyapunov orbit around Earth-Moon L_2 point is shown in Fig. 2.11.

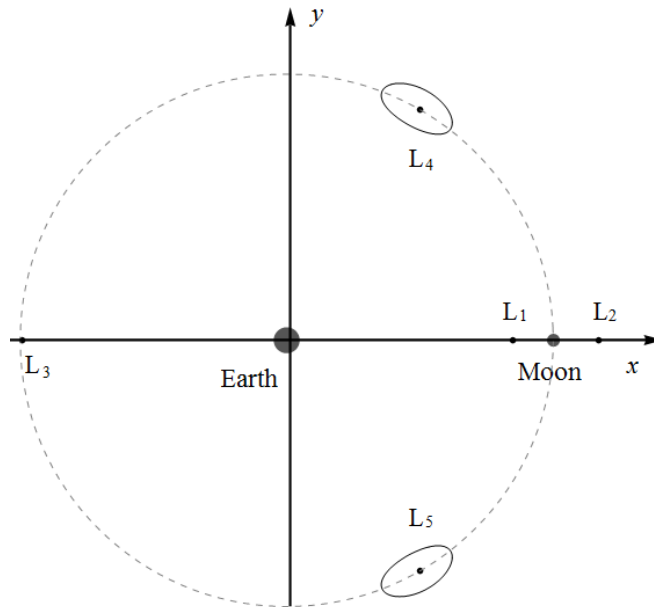


Fig. 2.10 Short-period orbits around the triangular points L_4 and L_5 points in the Earth-Moon system ($\kappa_1 = 0, \kappa_2 = 0.1$).

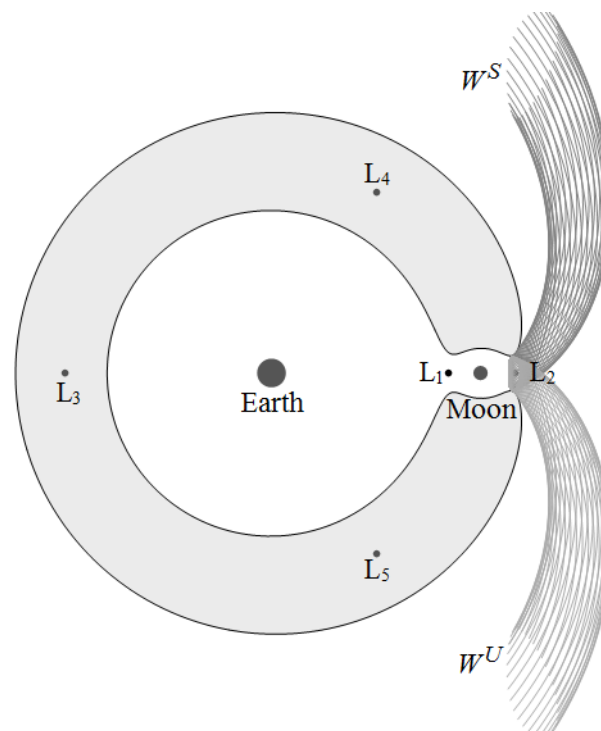


Fig. 2.11 Stable and unstable manifolds associated with a Lyapunov orbit around the Earth-Moon L_2 point in Fig. 2.8.

2.3 Sun-Earth-Moon four-body problem

In the asteroid capture strategy which will be proposed in Chapter 3, a candidate asteroid is assumed to be captured from its initial orbit directly into the Earth-Moon system. The

transfer trajectories from the asteroid's orbit to the Earth-Moon system are modelled by the Sun-Earth-Moon four-body problem. Therefore, the models of the Sun-Earth-Moon four-body problem are introduced here and will be applied to design the transfer trajectory of capturing asteroids in the Earth-Moon system in Chapter 3.

2.3.1 Patched three-body model

The patched three-body problem can provide an approximation of the Sun-Earth-Moon four-body problem and is decomposed into the Earth-Moon CRTBP and Sun-Earth CRTBP [97]. This model is used to design transfers from the Sun-Earth CRTBP system to the Earth-Moon system after the candidate asteroid is captured around the libration points L_1 or L_2 in the Sun-Earth system [53]. It is assumed that the Earth-Moon CRTBP system is coplanar with the Sun-Earth CRTBP system. Thus, asteroid capture trajectories can be accomplished by patching together the unstable manifolds in the Sun-Earth CRTBP system and the stable manifolds in the Earth-Moon CRTBP system. This model will be further discussed in Chapter 3.

2.3.2 Four-body problem in Sun-centred inertial frame

When designing direct transfer trajectories from the initial asteroid orbit to the Earth-Moon CRTBP system in Chapter 3, the Lambert arc in the Sun-centred two-body problem will be used as an initial estimate of the transfer in the Sun-Earth-Moon four-body problem.

Accordingly, the Sun-centred inertial frame is used as the reference frame in which the transfer trajectory for capturing an asteroid from its initial orbit into the Earth-Moon system is designed. In this frame, it is assumed that the motion of the asteroid is governed by the gravity of the Sun, Earth and Moon. Besides, the Earth and the Moon are assumed to be revolving in circular orbits around their barycentre, as shown in Fig. 2.12. In addition, the motion of the Earth-Moon barycentre with respect to the Sun is described by a Sun-centred two-body problem. Here the Sun-centred inertial frame is used to describe the Sun-Earth-Moon restricted four-body system such that

$$\begin{cases} \ddot{\mathbf{r}} = -\frac{\mu_{Sun}}{r^3}\mathbf{r} - \frac{\mu_{Earth}}{r_{ea}^3}(\mathbf{r} - \mathbf{r}_e) - \frac{\mu_{Moon}}{r_{ma}^3}(\mathbf{r} - \mathbf{r}_m) \\ \ddot{\mathbf{r}}_{em} = -\frac{\mu_{Sun}}{r_{es}^3}\mathbf{r}_{em} \end{cases} \quad (2.32)$$

where

$$r_{ea} = |\mathbf{r} - \mathbf{r}_e|, \quad r_{ma} = |\mathbf{r} - \mathbf{r}_m|$$

and where \mathbf{r} is the position vector of the asteroid with respect to the Sun; \mathbf{r}_{em} is the position vector of the Earth-Moon barycentre respect to the Sun in the two-body problem; \mathbf{r}_e and \mathbf{r}_m are the position vectors of the Earth and Moon, respectively, with respect to the Sun and can be calculated by using Eq. (2.14) as follows,

$$\mathbf{r}_e = \mathbf{r}_{em} + \mathbf{R}(\beta)\mathbf{X}_e^{ro} \quad (2.33)$$

$$\mathbf{r}_m = \mathbf{r}_{em} + \mathbf{R}(\beta)\mathbf{X}_m^{ro} \quad (2.34)$$

where $\mathbf{X}_e^{ro} = [-\mu, 0, 0, 0, 0, 0]^T$ and $\mathbf{X}_m^{ro} = [1-\mu, 0, 0, 0, 0, 0]^T$ are the non-dimensional states of the Earth and Moon in the Sun-Earth rotating frame, respectively. The motion of all four bodies are assumed to be in the same plane. In addition, μ_{Sun} , μ_{Earth} and μ_{Moon} are the gravitational parameters of the Sun, Earth and Moon, respectively. The gravitational parameters assumed for this model are $\mu_{Sun} = 1.3271244 \times 10^{11} \text{ km}^3/\text{s}^2$, $\mu_{Earth} = 3.9860044 \times 10^5 \text{ km}^3/\text{s}^2$ and $\mu_{Moon} = 4.9028002 \times 10^3 \text{ km}^3/\text{s}^2$.

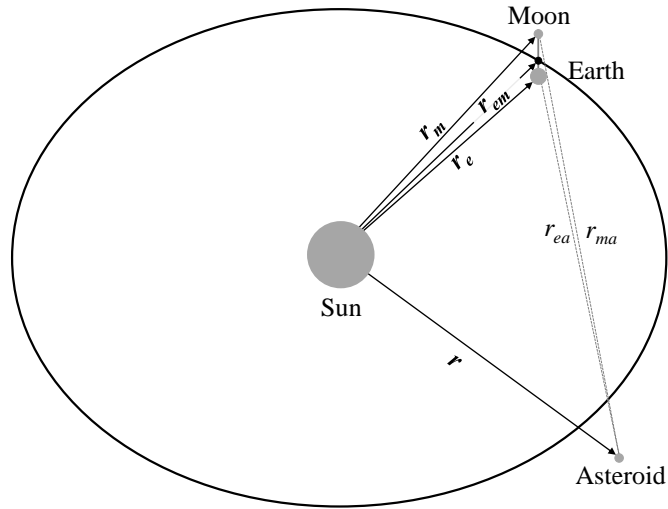


Fig. 2.12 Geometry of the Sun-Earth-Moon restricted four-body problem.

CHAPTER 3

CAPTURE OF SMALL NEAS IN THE VICINITY OF THE MOON

This Chapter introduces two different strategies for capturing asteroids in the Earth-Moon system, termed the direct and indirect asteroid capture strategies. Such capture strategies are of interest due to the possible future use of the Earth-Moon Lagrange points as staging points for future space exploration ventures. The capture of NEAs could then provide in-situ resources to support such exploration. The main contributions of this Chapter (which were presented in Ref [45]) are summarized as follows:

- (1) In the direct capture strategy, the candidate NEA leaves its heliocentric orbit after an initial impulse, with its dynamics modelled using the Sun-Earth-Moon restricted four-body problem until its insertion, with a second impulse, onto the L_2 stable manifold in the Earth-Moon CRTBP. A Lambert arc in the Sun-asteroid two-body problem is used as an initial guess and a differential corrector is then used to generate the transfer trajectory from the asteroid's initial orbit to the stable manifold associated with the Earth-Moon L_2 point;
- (2) In the indirect capture strategy, the candidate asteroid is firstly captured onto a periodic orbit around the Sun-Earth L_1 or L_2 libration point. Then the transfer trajectory from the Sun-Earth system to the Earth-Moon system can be accomplished by patching together the unstable manifolds in the Sun-Earth CRTBP system and the stable manifolds in the Earth-Moon CRTBP system;
- (3) The direct/indirect strategies are also applied to design the direct/indirect capture of asteroids to the triangular points in the Earth-Moon system. Transfer trajectories for direct asteroid capture can be designed from the candidate asteroid's orbit to the short-period orbits around the Earth-Moon L_4 or L_5 points directly, and the indirect capture is designed by patching the unstable manifolds of the Sun-Earth system with the short-period orbit around the Earth-Moon L_4 or L_5 points.

3.1 Direct capture of NEAs in the Earth-Moon system

3.1.1 Target periodic orbits in the Earth-Moon system

Following the process of numerical continuation to generate periodic orbits in Section 2.2.4, a series of periodic orbits (Lyapunov orbit and halo orbits) around the Earth-Moon L_2 point with increasing or decreasing Jacobi constant C can be calculated, as shown in Fig. 3.1, where the unit of length is the Earth-Moon distance (EM unit). In this chapter, those periodic orbits will serve as the final target orbits where the candidate asteroids are captured and placed.

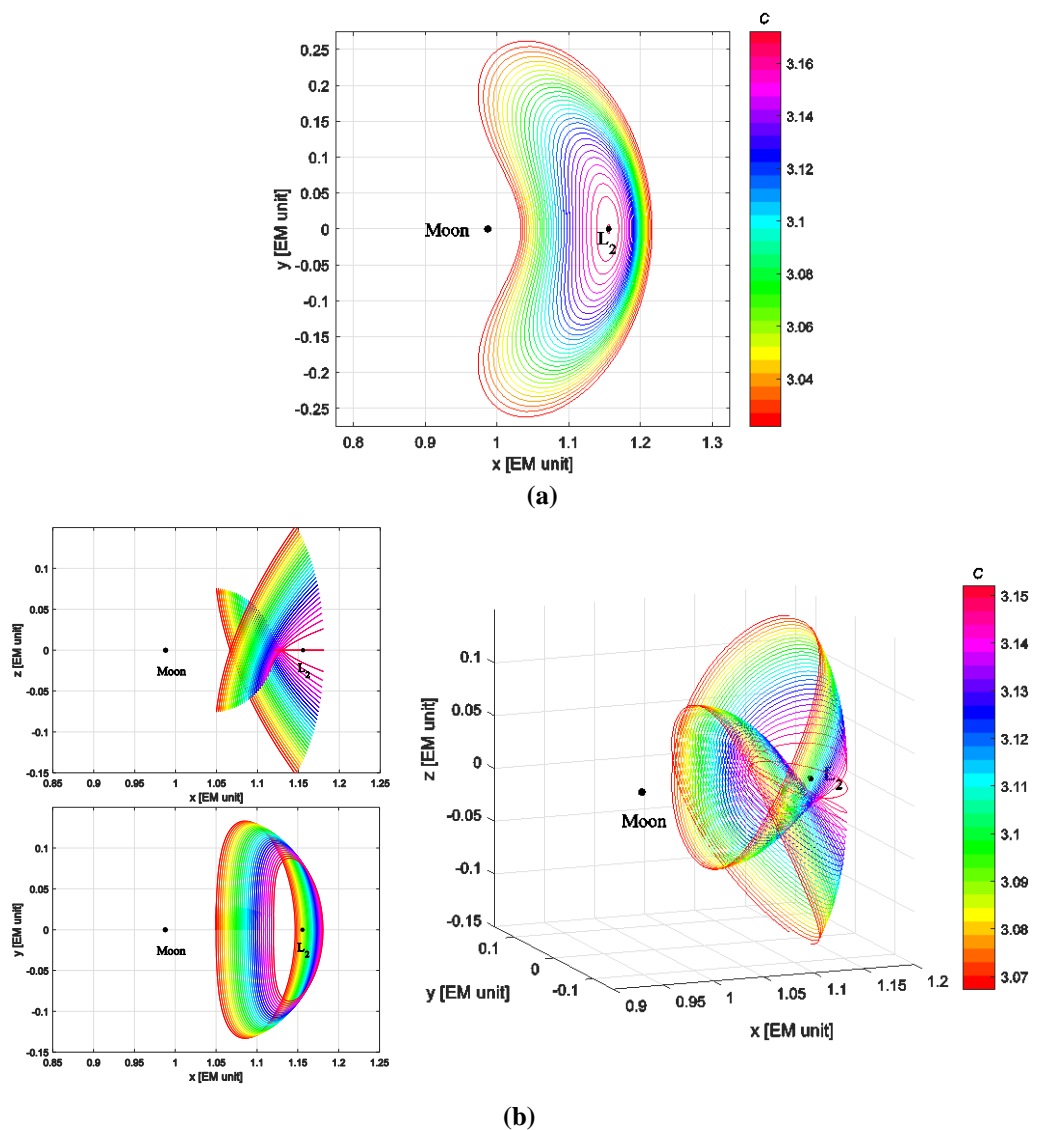


Fig. 3.1 Planar Lyapunov orbits with Jacobi constant [3.01017213, 3.17205221] and (b) halo orbits with Jacobi constant [3.06733209, 3.15211497] around L_2 point in the Earth-Moon system.

Then, the invariant manifolds associated with the periodic orbit around the Earth-Moon L_2 point can be calculated using Eq. (2.30) with the backward propagation time and the forward propagation times, defined as the stable manifold transfer time t_{sm} and the unstable manifold transfer time t_{um} , respectively. A Poincaré section can then be used to replace a continuous dynamical system with a discrete dynamical system [175], as used for the analysis of the Earth-Moon L_2 stable manifolds in the Section 3.1.5. Here, the Poincaré section is defined by the angle ϕ ($\phi > 0$), shown in Fig. 3.2. Then, the target points along stable manifolds on the Poincaré section in the Earth-Moon rotating system can be defined as

$$X_{EM}(C, \phi) = \left\{ (x, y, z, \dot{x}, \dot{y}, \dot{z}) \in W^s \mid y = (x + \mu) \tan \phi, 2\Omega(x, y, z, \mu) - (\dot{x}^2 + \dot{y}^2 + \dot{z}^2) = C \right\} \quad (3.1)$$

where the subscript “ EM ” in Eq. (3.1) denote the Earth-Moon system.

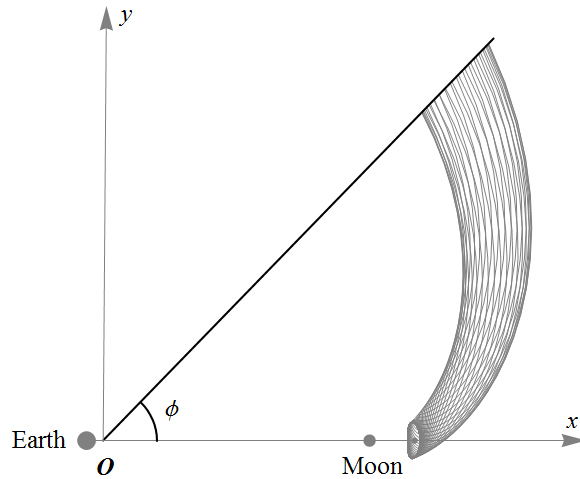


Fig. 3.2 Stable manifolds associated with a Lyapunov orbit ($C = 3.15415202$) around the Earth-Moon L_2 point.

3.1.2 Strategy for direct capture

The basic strategy for direct capture of asteroids is through the following steps:

(1) With an initial manoeuvre Δv_1 , the candidate asteroid leaves its orbit and is modelled in the Sun-Earth-Moon restricted four-body system (Eq. (2.32)), shown in Fig. 3.3(a);

(2) After a second manoeuvre Δv_2 , the candidate asteroid inserts onto the stable manifold associated with the periodic orbit around the Earth-Moon L_2 point and will be asymptotically captured onto it, shown in Fig. 3.3(b).

The total cost of capturing the asteroid onto the stable manifold associated with the periodic orbit around Earth-Moon L_2 point is therefore calculated as

$$\Delta v = \Delta v_1 + \Delta v_2 \quad (3.2)$$

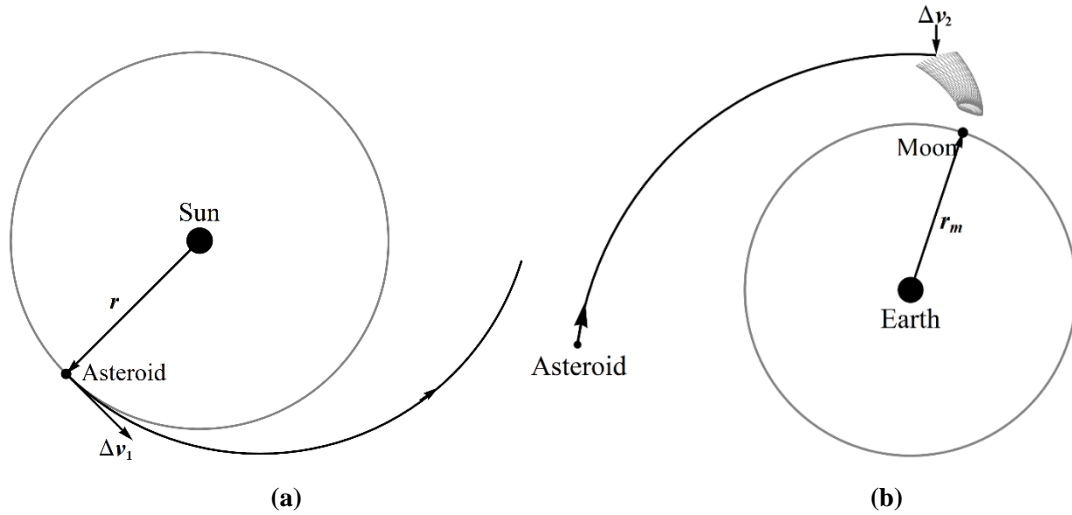


Fig. 3.3 Direct capture of a NEA: (a) initial impulse Δv_1 for the asteroid to leave its orbit; (b) second impulse Δv_2 to insert the asteroid onto the stable manifold associated with the periodic orbit around the Earth-Moon L_2 point.

Thus, for each candidate asteroid, there are 5 variables to describe the sequence of manoeuvres as follows:

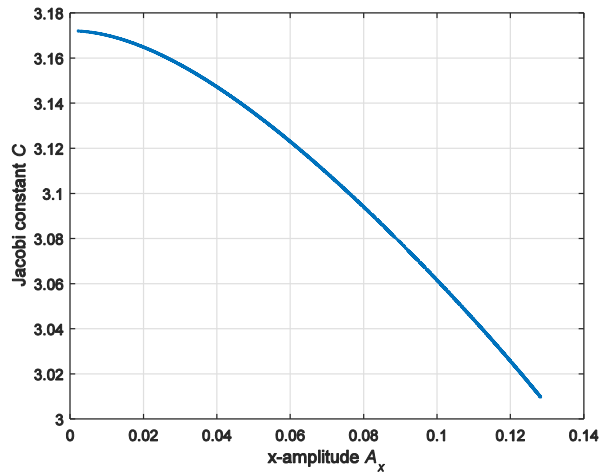
- T_0 : departure date when the first impulse Δv_1 is applied to the candidate asteroid and the asteroid leaves its initial orbit;
- T_f : approach date corresponding to the date when the candidate asteroid inserts onto the Earth-Moon L_2 stable manifold with the second impulse Δv_2 ;
- C : Jacobi constant of the final periodic orbit around the Earth-Moon L_2 point;
- t_p : time determining the state on the target periodic orbit around the Earth-Moon L_2 point where the Earth-Moon L_2 stable manifold is propagated backward from; $t_p \in [0, T_p]$ where T_p is the period of the final periodic orbit;
- t_{sm} : stable manifold transfer time determining the target point where the second impulse is applied.

For Lyapunov orbits, one value of the Jacobi constant C corresponds to only one Lyapunov orbit, as shown in Fig. 3.4(a). However, for halo orbits, one value of the Jacobi constant C corresponds to a northern halo orbit and a southern halo orbit, as shown Fig. 3.4(b). Hence, when optimising the transfers for capturing asteroids onto halo orbits in the

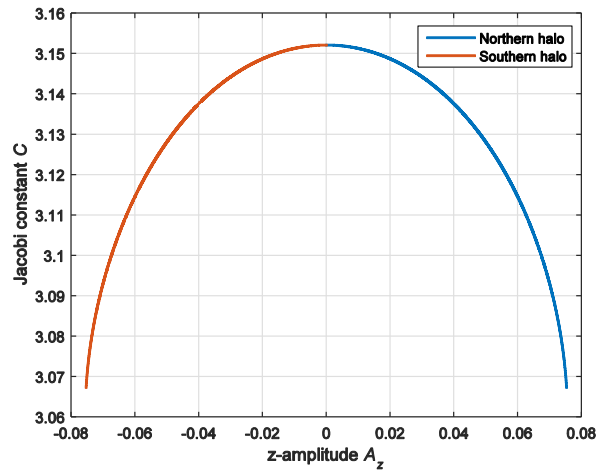
following section, capturing asteroids onto southern halo orbits and northern halo orbits should be considered separately. Otherwise, an alternative variable can be defined to unify them, termed the amplitude variable A_p which can be defined as

$$A_p = \begin{cases} A_x, & \text{for Lyapunov orbit} \\ \delta_n A_z, & \text{for Halo orbit} \end{cases} \quad (3.3)$$

where A_x is the amplitude of the Lyapunov orbit along the x -axis and A_z is the amplitude of the Halo orbit along the z -axis with respect to the Earth-Moon L_2 point in the Earth-Moon rotating frame (See Section 2.2.4).



(a)

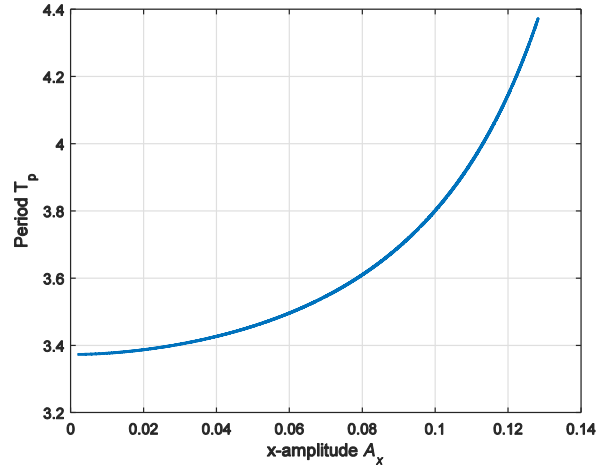


(b)

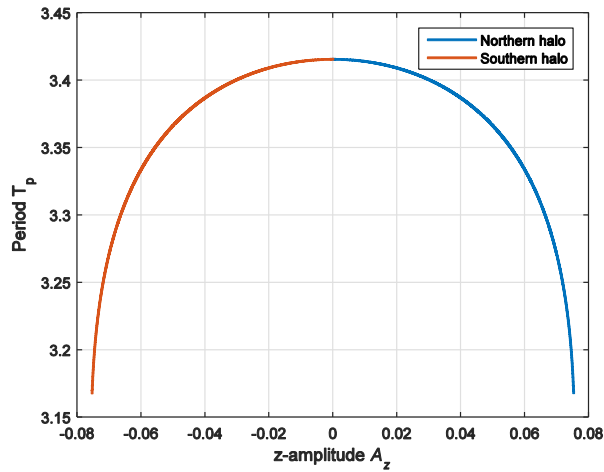
Fig. 3.4 (a) Jacobi constant of Lyapunov orbits with different x -amplitudes around the Earth-Moon L_2 point; (b) Jacobi constant of halo orbits with different z -amplitudes around the Earth-Moon L_2 point.

Therefore, as shown in Fig.3.4, it is found that A_p should be selected in the range $[0, 0.1282]$ for Lyapunov orbits, or $[-0.0753, 0.0753]$ for halo orbits. Therefore, for each candidate asteroid, the 5 variables $(T_0, T_f, A_p, t_p, t_{sm})$ can define the problem of capturing the asteroid in the Earth-Moon system. Figure 3.5 shows the period T_p of periodic orbits

with a different amplitude variable A_p . In general, for Lyapunov orbits and the southern halo orbits, T_p increases when the amplitude variable A_p increases. However, for the northern halo orbits, T_p decreases when the amplitude variable A_p increases. Since the amplitude variable A_p is unknown, a limited range of the time t_p should be chosen to fit all periodic orbits. Therefore, as shown in Fig. 3.5, it is found that t_p should be selected in the range $[0, 4.35]$ for Lyapunov orbits, or $[0, 3.42]$ for halo orbits.



(a)



(b)

Fig. 3.5 (a) Period T_p of Lyapunov orbits with different x -amplitudes around the Earth-Moon L_2 point; (b) Period T_p of halo orbits with different z -amplitudes around the Earth-Moon L_2 point.

3.1.3 Target point filter

After the first impulse, the asteroid leaves its orbit and is modelled using the Sun-Earth-Moon restricted four-body problem until the asteroid is captured onto the Earth-Moon L_2 stable manifold. When the asteroid inserts onto the invariant manifold, the asteroid's motion is modelled by the Earth-Moon CRTBP problem. Here, the patching of these two systems is defined within the Moon-Sun three-body sphere of influence (3BSOI) [174,

176]. Using an analytical approximation, the 3BSOI is a sphere centred at the Moon with a radius given by

$$R_{SOI} = r_e (\mu_{Moon} / \mu_{Sun})^{2/5} \approx 159200km \quad (3.4)$$

where r_e is the distance between the Sun and the Earth, equal to 1 AU. That is, once the asteroid is inserted onto the target point on the stable manifold inside the 3BSOI of radius R_{SOI} , the asteroid is regarded to be asymptotically captured into a bound orbit around the Earth-Moon L_2 point. Therefore, as shown in Fig. 3.6, the target points on the stable manifolds should be chosen such that

$$\sqrt{(x-1+\mu)^2 + y^2 + z^2} \leq R_{SOI} \quad (3.5)$$

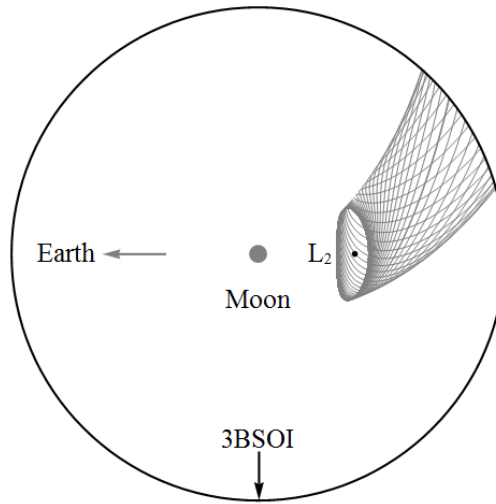


Fig. 3.6 Earth-Moon L_2 stable manifolds inside the 3BSOI.

It is assumed that \mathbf{r}_e and \mathbf{r}_m are the position vector of the Earth from the Sun and the position vector of the Moon from the Earth, respectively. Moreover, the radius vector defining the spacecraft or the captured asteroid position from the Moon is denoted as \mathbf{r}_s . Therefore, in the Moon-centred inertial frame, the position vectors of the Sun and the Moon can be written as

$$\mathbf{r}_{sm} = -\mathbf{r}_e - \mathbf{r}_m, \mathbf{r}_{em} = -\mathbf{r}_m \quad (3.6)$$

When the spacecraft or the captured asteroid is close to the Moon, the main acceleration is due to the Moon and thus in the Moon-centred inertial frame it can be written as

$$\mathbf{a}_m = -\frac{\mu_{Moon}}{r_m^3} \mathbf{r}_m \quad (3.7)$$

And the Sun and Earth accelerations on the spacecraft can be written as

$$\mathbf{a}_s = \mu_{Sun} \left(-\frac{\mathbf{r}_s + \mathbf{r}_e + \mathbf{r}_m}{|\mathbf{r}_s + \mathbf{r}_e + \mathbf{r}_m|^3} + \frac{\mathbf{r}_e + \mathbf{r}_m}{|\mathbf{r}_e + \mathbf{r}_m|^3} \right) \quad (3.8)$$

$$\mathbf{a}_e = \mu_{Earth} \left(-\frac{\mathbf{r}_s + \mathbf{r}_m}{|\mathbf{r}_s + \mathbf{r}_m|^3} + \frac{\mathbf{r}_m}{|\mathbf{r}_m|^3} \right) \quad (3.9)$$

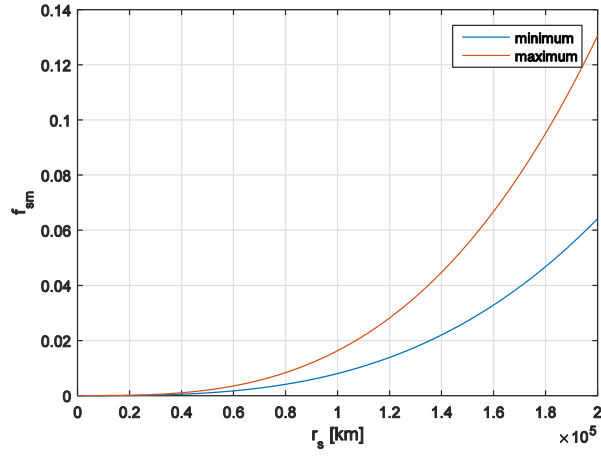
Then the ratio of the Sun acceleration and Moon acceleration is defined as

$$f_{sm} = |\mathbf{a}_s| / |\mathbf{a}_m| \quad (3.10)$$

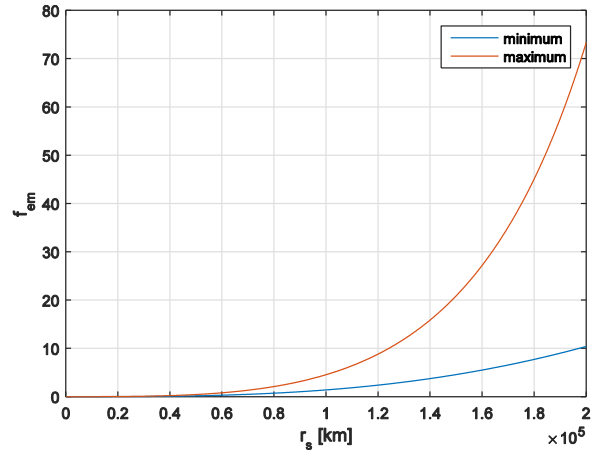
Similarly, the ratio of the Earth acceleration and Moon acceleration is written as

$$f_{em} = |\mathbf{a}_e| / |\mathbf{a}_m| \quad (3.11)$$

Figure 3.7 shows the maximum and minimum values of f_{sm} and f_{em} with different values of the radius r_s . As shown in Fig. 3.7, it can be seen that even inside the Moon-Sun 3BSOI ($r_s = 159200$ km), the Earth's gravity can still play a substantial role in the motion (acceleration) of the spacecraft or the captured asteroid. It keeps consistent with the model of Earth-Moon CRTBP. However, as for the Sun's gravitational influence, the acceleration due to the Sun on the Moon-Sun 3BSOI is only about 2.8% - 5.7 % of the acceleration due to the Moon. Thus, it is reasonable to assume that the Sun's gravitational influence can be ignored when the spacecraft or the captured asteroid is inside the Moon-Sun 3BSOI. In addition, the Moon-Sun 3BSOI is adopted to limit the target points on the stable manifolds of the Earth-Moon L_2 periodic orbits, the patching will occur at the target point which is very close to the Moon. Therefore, the gravity of the Moon can play a substantial role in the transfer trajectory especially when the candidate asteroid is close to the Moon. Hence, the model of the Sun-Earth-Moon restricted four-body problem would be required to describe the motion of the captured asteroid, especially when it is close to the Moon.



(a)



(b)

Fig. 3.7 Maximum and minimum values of (a) f_{sm} and (b) f_{em} with different values of r_s .

According to the definition of the Moon-Sun 3BSOI, the search domain of the stable manifold transfer time t_{sm} can be determined. Given one stable manifold which is determined by A_p and t_p , $t_{3BSOI}(A_p, t_p)$ is defined as the stable manifold transfer time t_{sm} when the stable manifold intersects the 3BSOI for the first time. Therefore, for the stable manifolds associated with a periodic orbit of amplitude variable A_p , the required set of t_{3BSOI} can be written as

$$\Gamma(A_p) = \bigcup_{t_p \in [0, T_p]} \{t_{3BSOI}(A_p, t_p)\} \quad (3.12)$$

and the maximum value of the set $\Gamma(A_p)$ is defined as

$$t_{threshold}(A_p) = \max_{t_p \in [0, T_p]} \{\Gamma(A_p)\} \quad (3.13)$$

Therefore, $t_{threshold}(A_p)$ is the maximum stable manifold transfer time of the stable manifolds associated with the periodic orbit with amplitude variable A_p . Therefore, it can

be utilised to determine the search domain of the stable manifold transfer time t_{sm} . Figure 3.8 shows $t_{threshold}$ with different amplitude variables A_p .

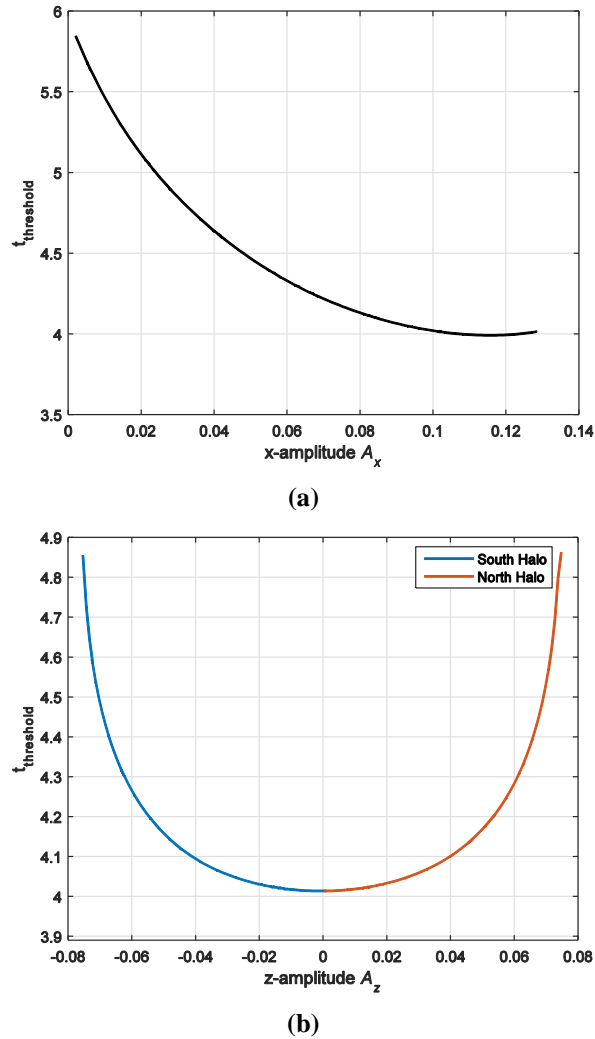


Fig. 3.8 $t_{threshold}$ with different amplitude variables A_p (a) stable manifold associated with Earth-Moon L_2 Lyapunov orbits; (a) stable manifold associated with Earth-Moon L_2 halo orbits.

As shown in Fig. 3.8, for Lyapunov orbits and southern halo orbits, $t_{threshold}$ decreases when the amplitude variable A_p increases and small values of A_p lead to large $t_{threshold}$. However, for the northern halo orbits, $t_{threshold}$ increases when the amplitude variable A_p increases. Since the amplitude variable A_p is unknown, a limited range of the stable manifold flight time t_{sm} should be selected to fit the stable manifolds of all periodic orbits. Therefore, it is found that t_{sm} should be selected in the range $[0, 5.8]$ for Lyapunov orbits, or $[0, 4.86]$ for Halo orbits.

3.1.4 Differential correction for the Sun-Earth-Moon four-body problem

A heliocentric two-body Lambert arc with two impulsive manoeuvres can be used to provide an initial guess, with the first impulse of the Lambert arc then applied to estimate the first manoeuvre of the asteroid transfer to the Earth-Moon system. It will be assumed that the initial state of the asteroid is $\mathbf{X}_i = [x_i, y_i, z_i, \dot{x}_i, \dot{y}_i, \dot{z}_i]^T$ after the first impulse, the state of the target point is $\mathbf{X}_f = [x_f, y_f, z_f, \dot{x}_f, \dot{y}_f, \dot{z}_f]^T$ and the final state of the Lambert arc is $\mathbf{X}'_f = [x'_f, y'_f, z'_f, \dot{x}'_f, \dot{y}'_f, \dot{z}'_f]^T$, before the second impulse, as shown Fig. 3.9. Then the final conditions for $\delta \mathbf{r}_f = [\delta x_f, \delta y_f, \delta z_f]^T = [x_f - x'_f, y_f - y'_f, z_f - z'_f]^T = \mathbf{0}$ can be sought by correcting the initial velocity vector $\delta \mathbf{v}_i = [\delta \dot{x}_i, \delta \dot{y}_i, \delta \dot{z}_i]^T$.

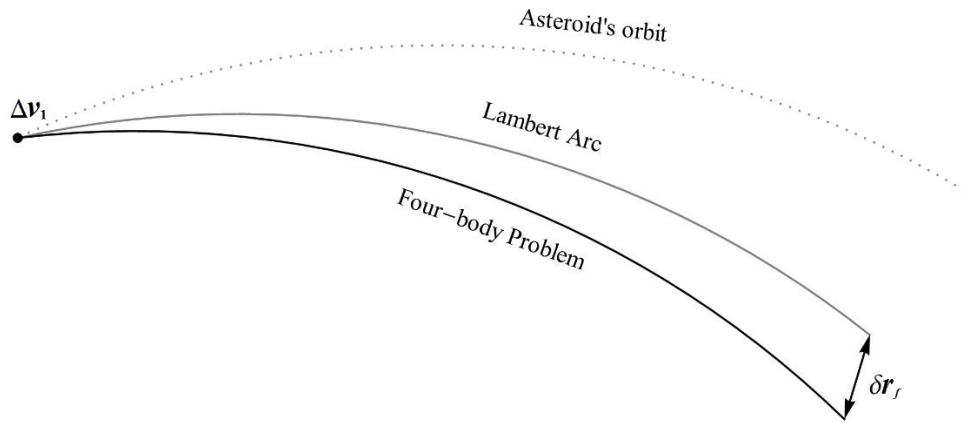


Fig. 3.9 Differential correction with an initial guess using a Lambert transfer.

It is assumed that the Sun-Earth-Moon restricted four-body system in Eq. (2.32) can be represented by a set of nonlinear equations of motion in the general form

$$\dot{\mathbf{X}} = \mathbf{F}(\mathbf{X}, t) \quad (3.14)$$

where $\mathbf{X} = [x, y, z, \dot{x}, \dot{y}, \dot{z}]^T$ is the state along the transfer trajectory for capturing the asteroid in the Sun-Earth-Moon restricted four-body problem.

Similar to Section 2.2.3, a solution $\mathbf{X}_0(t)$ is also referred to as the reference trajectory of Eq. (3.14). Defining the relationship between the reference trajectory $\mathbf{X}_0(t)$ and a nearby trajectory $\mathbf{X}(t)$, as

$$\mathbf{X}(t) = \mathbf{X}_0(t) + \delta \mathbf{X}(t) \quad (3.15)$$

and expanding about the reference solution in a Taylor series generates a set of linear equations such that

$$\delta \dot{\mathbf{X}} = \mathbf{A}_4(t) \delta \mathbf{X} \quad (3.16)$$

where $\mathbf{A}_4(t) = \left. \frac{\partial \mathbf{F}}{\partial \mathbf{X}} \right|_{\mathbf{X}_0}$. The general solution to the above equation is

$$\delta \mathbf{X}(t) = \Phi_4(t, t_0) \delta \mathbf{X}(t_0) \quad (3.17)$$

where the state transition matrix is again found from

$$\dot{\Phi}_4(t, t_0) = \mathbf{A}_4(t) \Phi_4(t, t_0), \Phi_4(t_0, t_0) = \mathbf{I}_{6 \times 6} \quad (3.18)$$

and

$$\mathbf{A}_4(t) = \frac{d\mathbf{F}(\mathbf{X}, t)}{d\mathbf{X}} = \begin{bmatrix} 0 & 0 & 0 & 1 & 0 & 0 \\ 0 & 0 & 0 & 0 & 1 & 0 \\ 0 & 0 & 0 & 0 & 0 & 1 \\ \frac{\partial \ddot{x}}{\partial x} & \frac{\partial \ddot{x}}{\partial y} & \frac{\partial \ddot{x}}{\partial z} & 0 & 2 & 0 \\ \frac{\partial \ddot{y}}{\partial x} & \frac{\partial \ddot{y}}{\partial y} & \frac{\partial \ddot{y}}{\partial z} & -2 & 0 & 0 \\ \frac{\partial \ddot{z}}{\partial x} & \frac{\partial \ddot{z}}{\partial y} & \frac{\partial \ddot{z}}{\partial z} & 0 & 0 & 0 \end{bmatrix} \quad (3.19)$$

The differential correction for the Sun-Earth-Moon restricted four-body problem can therefore be written as

$$\delta \mathbf{X}_i = \Phi(T_f, T_0)^{-1} \delta \mathbf{X}_f \quad (3.20)$$

where $\delta \mathbf{X}_i = [0, 0, 0, \delta \dot{x}_i, \delta \dot{y}_i, \delta \dot{z}_i]^T$, $\delta \mathbf{X}_f = [\delta x_f, \delta y_f, \delta z_f, 0, 0, 0]^T$.

The differential correction in Eq. (3.20) starts with the initial state \mathbf{X}_0 which is based on the Lambert arc and then the process is repeated until $\delta \mathbf{r}_f = [\delta x_f, \delta y_f, \delta z_f]^T$ is equal to $\mathbf{0}$ within some small tolerance.

3.1.5 Candidate asteroid selection

When the candidate asteroid is captured in the Earth-Moon system it poses a potential (if small) impact risk. Therefore, only those candidate asteroids which cannot in principle represent a threat should be considered. Since the Earth's atmosphere can disintegrate small bodies, and so acts as a shield, the candidate asteroids in this thesis should be those asteroids which would also be disintegrated by the Earth's atmosphere. Most asteroids with a diameter of less than 50 m are thought to break up in the atmosphere and cannot reach the surface [177, 178]. Besides, Vasile and Colombo [147] regarded 40 m as the critical threshold above which the Earth's atmosphere will no longer disintegrate an asteroid. Moreover, other authors have noted that the atmosphere can protect against asteroids with a diameter of less than 30 m [179, 180]. Therefore, to reduce the threat of impact with the Earth, only those small asteroids with $D < 30$ m are considered as candidates for the capture mission, although clearly a detailed risk assessment is required. The diameter D of the candidate asteroid can be estimated as [181]

$$D = 1329\text{km} \times 10^{-H/5} p_v^{-1/2} \quad (3.21)$$

where H is the absolute magnitude of the asteroid and p_v is its albedo. Here it is assumed that the asteroids have a typical albedo of $p_v = 0.154$ [181]. If $D \leq 30$ m then $H \geq 25.26$.

Moreover, it is necessary to immediately exclude asteroids with a semi-major axis or inclination much larger than the Earth's since the energy costs for capture would be prohibitive. With the target point filter, the target point on the stable manifold which is determined by the parameters A_p , t_p and t_{sm} can be written as

$$P_t(A_p, t_p, t_{sm}) = \left\{ (x, y, z, \dot{x}, \dot{y}, \dot{z}) \in W^s \mid \sqrt{(x-1+\mu)^2 + y^2 + z^2} \leq R_{SOI} \right\} \quad (3.22)$$

Then, the set of the target points on the stable manifolds can be obtained with varying A_p , t_p and t_{sm} . Let K be the set of the target points which can be written as

$$K = \left\{ P_t(A_p, t_p, t_{sm}) \mid A_{\min} \leq A_p \leq A_{\max}, 0 \leq t_p \leq T_p, 0 \leq t_{sm} \leq t_{\text{threshold}} \right\} \quad (3.23)$$

where $A_{\min} = 0$, $A_{\max} = 0.1282$ and $t_{\text{threshold}} = 5.8$ for the planar Lyapunov orbits while $A_{\min} = -0.0753$, $A_{\max} = 0.0753$ and $t_{\text{threshold}} = 4.86$ for the halo orbits.

Now that the set of target points is known, it is possible to calculate the three-dimensional orbital element space (the semi-major axis, eccentricity and inclination (a , e ,

i) of the candidate asteroids which can be captured onto Earth-Moon L_2 periodic orbits under a certain Δv threshold. The design procedure is presented as follows:

- (1) Given one approach date T_f , transform the set of target points K to the Sun-centred inertial frame by using Eq. (2.33) and Eq. (2.34) and then obtain the three-dimensional orbital element space of the target points in the Sun-centred inertial frame, shown in Fig. 3.10;

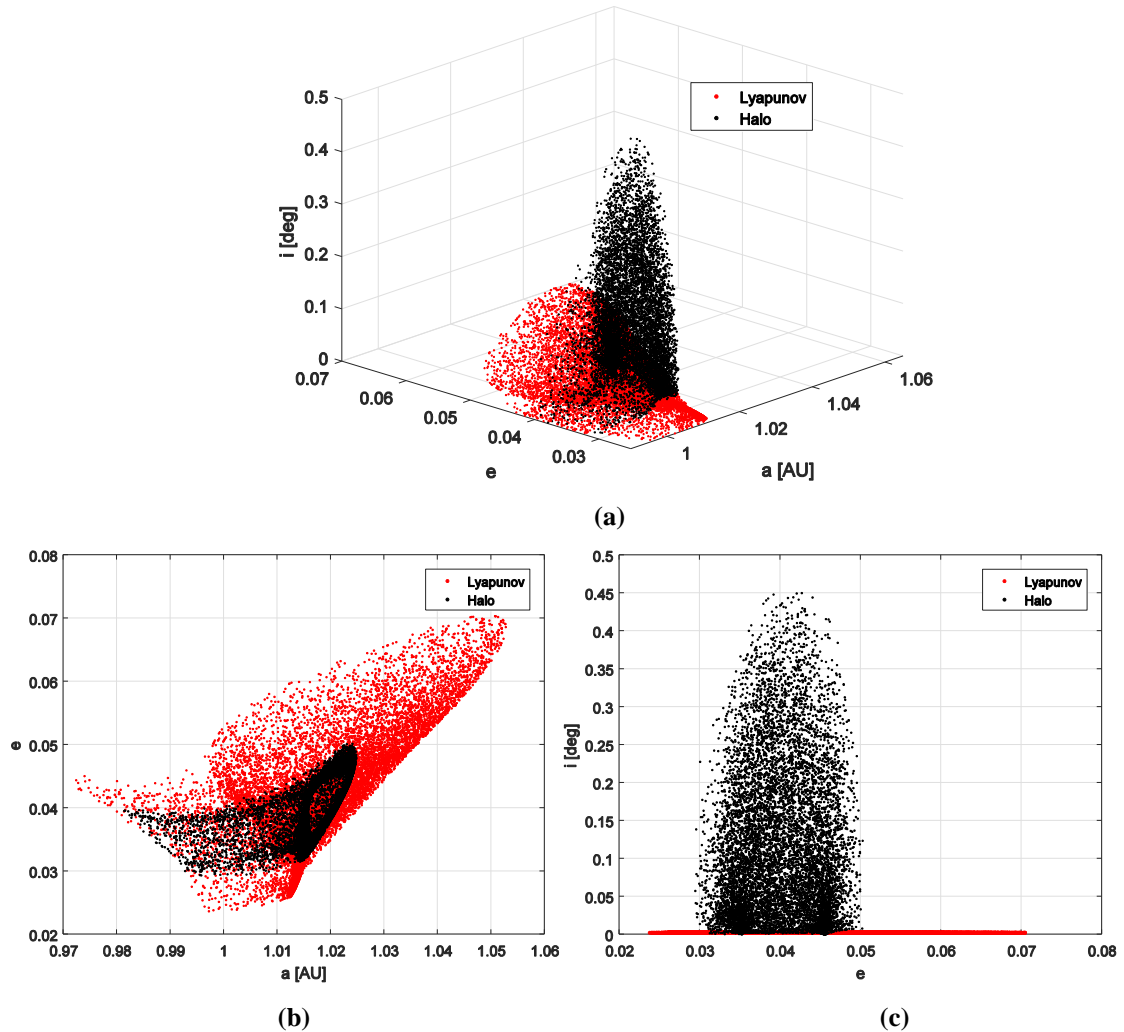


Fig. 3.10 Given $T_f=63000$ [MJD], the three-dimensional orbital element space of target points on the stable manifolds associated with Earth-Moon L_2 Lyapunov orbits (red) and halo orbits (black): (a) 3D view; (b) a - e projection; (c) e - i projection.

- (2) Add an impulse $\Delta v_2 = \Delta v_2 [\cos p_2 \cos q_2, \cos p_2 \sin q_2, \sin p_2]$ ($\Delta v_2 \leq \Delta v$, $p_2 \in [0, \pi]$, $q_2 \in [0, 2\pi]$) at these target points on the Earth-Moon L_2 stable manifolds and propagate these states backwards (with propagation time T (days)) in the Sun-Earth-Moon restricted four-problem model and then obtain the final states;

- (3) Add another impulse $\Delta \mathbf{v}_1 = \Delta v_1 [\cos p_1 \cos q_1, \cos p_1 \sin q_1, \sin p_1]$ ($\Delta v_1 \leq \Delta v - \Delta v_2$, $p_1 \in [0, \pi]$, $q_1 \in [0, 2\pi]$) at these final states and then calculate the three-dimensional orbital element space (a , e , i) of these states after Δv_1 is added;
- (4) Vary the approach date T_f , propagation time T ($T \in [0, 1000 \text{ days}]$), two impulses Δv_1 and Δv_2 and obtain the three-dimensional orbital element space (a , e , i) of the candidate asteroids that can potentially be captured under the Δv threshold.

According to the design procedure above, the three-dimensional orbital element space of candidate asteroids is plotted in Fig. 3.11 and Fig. 3.12 for transfers to the Earth-Moon L_2 stable manifolds with a Δv threshold of 500 m/s, as used by Yárnoz, et al. [50]. With a free phase, any asteroid with orbital elements inside these regions can be captured with a total Δv cost below 500 m/s. With this filter, the candidate asteroids are listed in Table 3.1.

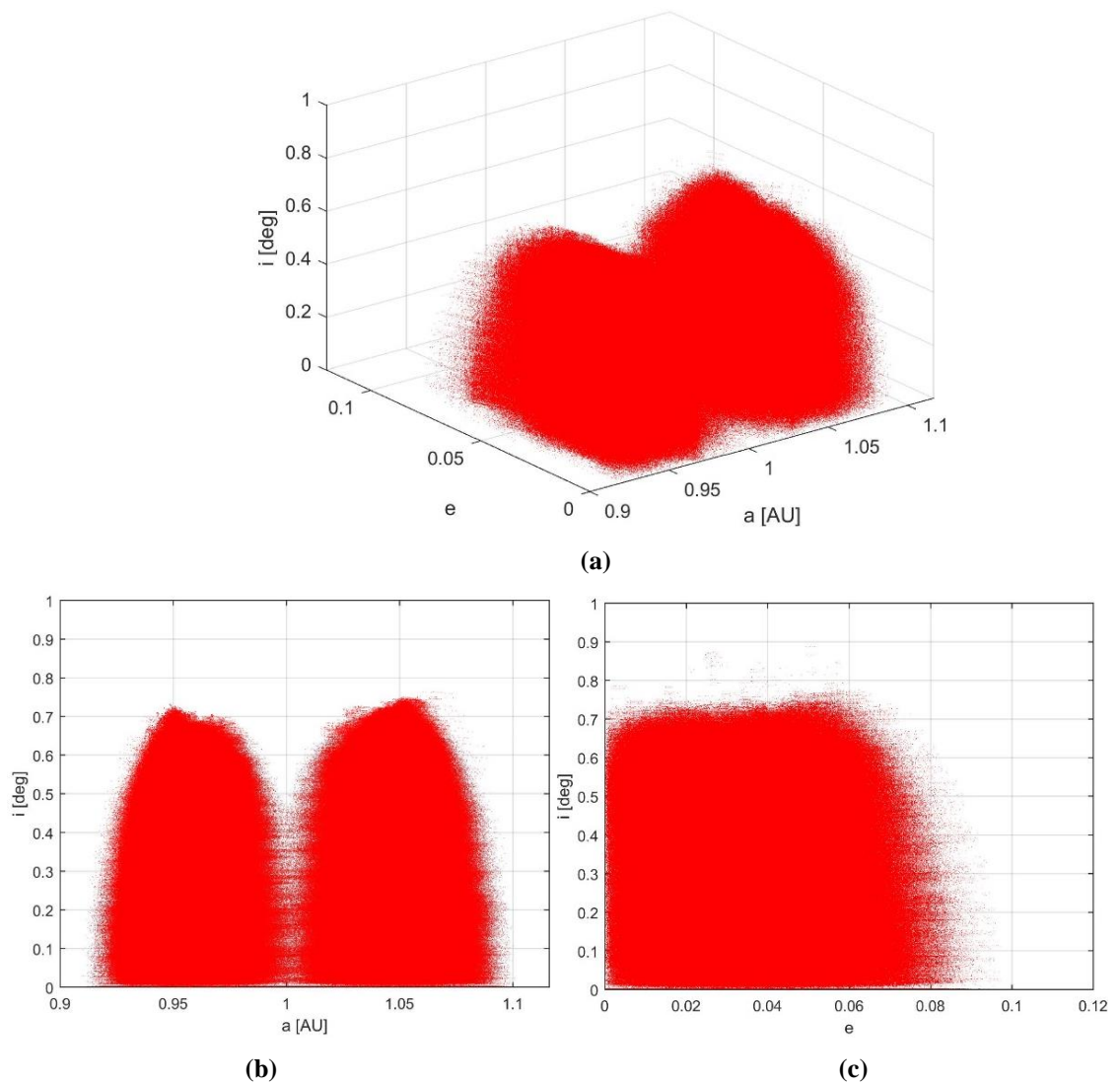


Fig. 3.11 Three-dimensional orbital element space of the stable manifold associated with Earth-Moon L_2 Lyapunov orbits with a Δv threshold of 500 m/s: (a) 3D view; (b) a - e projection; (c) e - i projection.

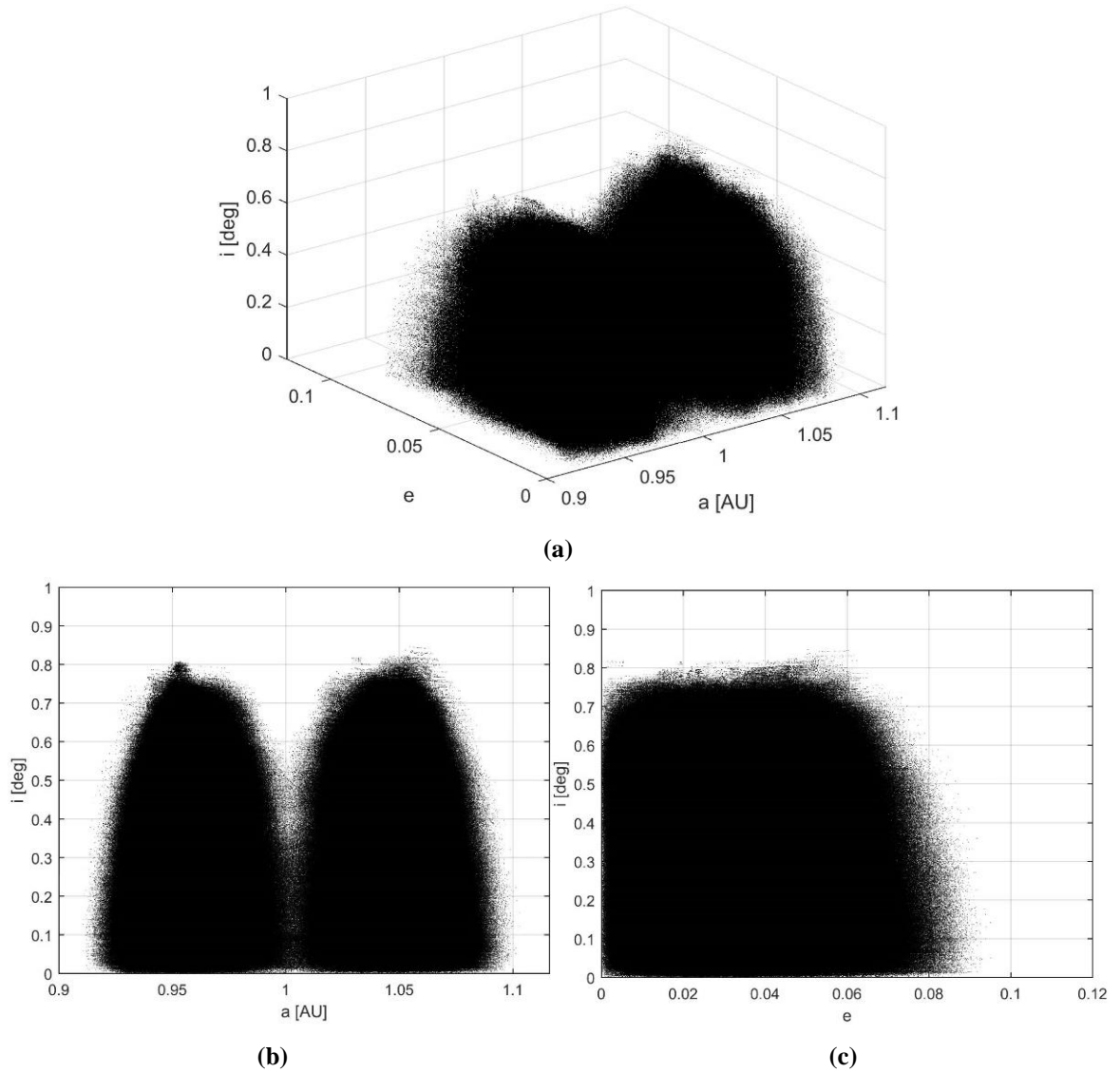


Fig. 3.12 Three-dimensional orbital element space of the stable manifold associated with Earth-Moon L_2 halo orbits with a Δv threshold of 500 m/s: (a) 3D view; (b) a - e projection; (c) e - i projection..

3.1.6 Approach date and departure date guess

For a candidate asteroid, there exists a date when the asteroid has its closest approach to the Earth. This date will be defined as the moment of minimum distance (MOMD) between the asteroid and the Moon. The distance between the candidate asteroid and the Moon can be calculated by propagating the candidate asteroid's initial state forward in the Sun-Earth-Moon restricted four-body problem and then the MOMD can be obtained, an example of which is shown in Fig. 3.13. Since low-cost transfers with a total Δv cost below 500 m/s is the objective of capturing asteroids in this chapter, the first impulse should be smaller than this value and then the asteroid's new orbit after the first impulse can be considered to be proximal to its former orbit. Therefore, the date of the asteroid's closest

approach to the Earth is considered to be nearby the MOMD. The approximate range of approach date can then be written as

$$[\text{MOMD} - T_{\text{period}}, \text{MOMD} + T_{\text{period}}] \quad (3.24)$$

where T_{period} is the asteroid's orbit period about the Sun.

Table 3.1 Orbital elements of the candidate NEAs

NEA	a , AU	e	i , deg	D , m
2006 RH120	1.03327	0.02449	0.59531	4.3
2007 UN12	1.05385	0.06046	0.23565	6.2
2008 EA9	1.05921	0.07982	0.42478	9.8
2008 UA202	1.03318	0.06855	0.26339	4.5
2009 BD	1.00976	0.04163	0.38448	8.1
2010 UE51	1.07102	0.07239	0.5886	7.4
2013 BS45	0.99184	0.08374	0.77251	22.4
2014 QN266	1.05269	0.0923	0.48822	18.6
2014 WX202	1.03567	0.05881	0.41258	4.1
2015 PS228	1.05679	0.08392	0.43892	5.9
2018 AV2	1.02961	0.03001	0.119	6.2

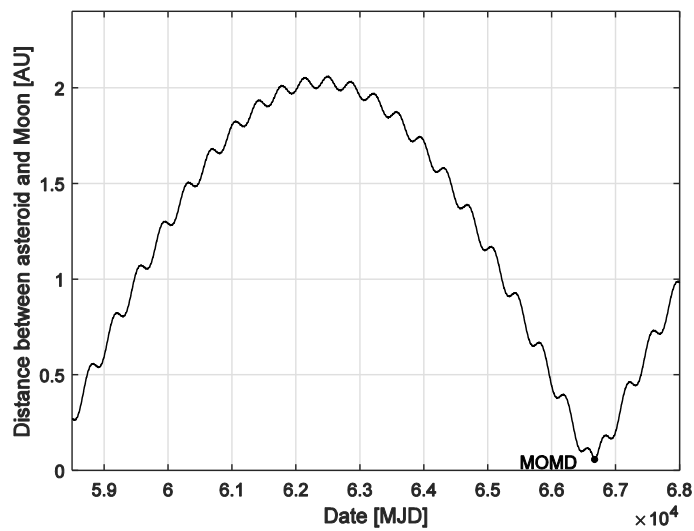


Fig. 3.13 Approach date guess by using MOMD (2018 AV2).

The Lambert arc in the two-body problem with two impulses can now be used as an initial guess of the departure date when the first impulse is applied and the asteroid transfers towards the target point in the Earth-Moon system. There are 2 variables in this problem: the departure date T_0 and the transfer time T_{fly} (or the approach date T_f). Then, the total cost of the Lambert transfer can be calculated using Eq. (2.9).

Since the influence of the Sun's gravity is only considered here, the total δv cost must be different from the result in the Sun-Earth-Moon restricted four-body problem model. However, the first Lambert impulse δv_1 can still be used to guess the first impulse Δv_1 in Sun-Earth-Moon restricted four-body model. Since an asteroid which can be captured directly with $\Delta v \leq 500$ m/s is expected to be found, here 500 m/s is set as a threshold for δv_1 and then the departure date T_0 is guessed. As shown in Fig. 3.6, the target points are defined in a limited region around the Moon (3BSOI). Thus, there should be only a marginal difference between the first impulse of the Lambert arc to the Moon and the first impulse of the Lambert arc to the target points. Therefore, for simplification, the target position for the Lambert arc is assumed to be the centre of the Moon, in order to provide a guess in the search domain of the departure date T_0 , shown in Fig. 3.14.

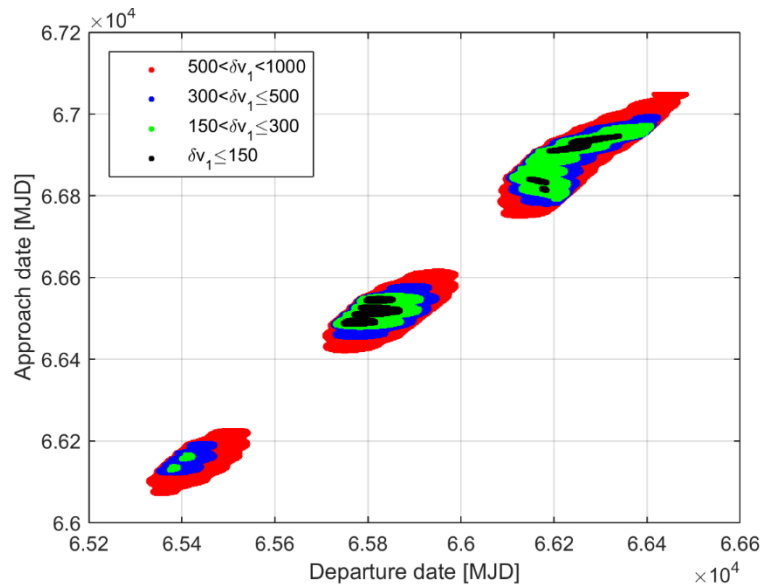


Fig. 3.14 The first impulse δv_1 (m/s) as a function of T_0 and T_f (2018 AV2).

3.1.7 Design procedure

The process of calculating the transfer trajectories from the candidate asteroid's orbit to the Earth-Moon L_2 stable manifold is as follows:

- (1) Select one target asteroid among the list of candidate asteroids (e.g., 2018 AV2) in Table 3.1;
- (2) Guess the range of the approach date using Eq. (3.24);
- (3) Assume that the Moon is the target position for the Lambert arc from the candidate asteroid's orbit and then guess the search domain of departure date T_0 and approach date T_f , corresponding to the first impulse $\delta v_1 \leq 500$ m/s, as shown in Fig. 3.14;
- (4) Given A_p , t_p and t_{sm} , the target point on the Earth-Moon L_2 stable manifolds is determined and then transformed to the Sun-centred inertial frame by using Eq.(2.33) and Eq. (2.34);
- (5) The Lambert arc in the Sun-centred two-body problem is utilised to design the transfer to the target points from the candidate asteroid's orbit and so the first impulse can be estimated;
- (6) Based on the initial guess of the first impulse, the differential correction in Eq. (3.20) is utilised to design the transfer trajectory to the target point from the candidate asteroid's orbit.

Then the capture trajectory can be obtained for a candidate asteroid to the Earth-Moon L_2 periodic orbit, as shown in Fig. 3.15.

3.1.8 Optimisation and discussion

For each candidate asteroid, feasible approach dates are assumed in the interval 2016–2050 (or 58484 MJD - 70171 MJD). The orbital elements of the candidate asteroids are assumed to be valid until their next close approach to the Earth. Thus, for each candidate asteroid, there are 5 variables: $(T_0, T_f, A_p, t_p, t_{sm})$. These transfer trajectories between the candidate asteroid initial orbit and the stable manifold can be searched using NSGA-II, a global optimisation method which is based on a multi-objective evolutionary algorithm [182], using the total Δv cost as the objective function. Then, transfers obtained with NSGA-II can be locally optimised with sequential quadratic programming (SQP), implemented in the function *fmincon* in MATLAB. Therefore, 6 asteroids that can be captured with a total Δv cost of less than 500 m/s are found, shown in Table 3.2. It can be seen that the optimal departure date for a given asteroid is almost the same for different target periodic orbits around the Earth-Moon L_2 point (i.e., halo orbits and Lyapunov orbits), as well as the approach date.

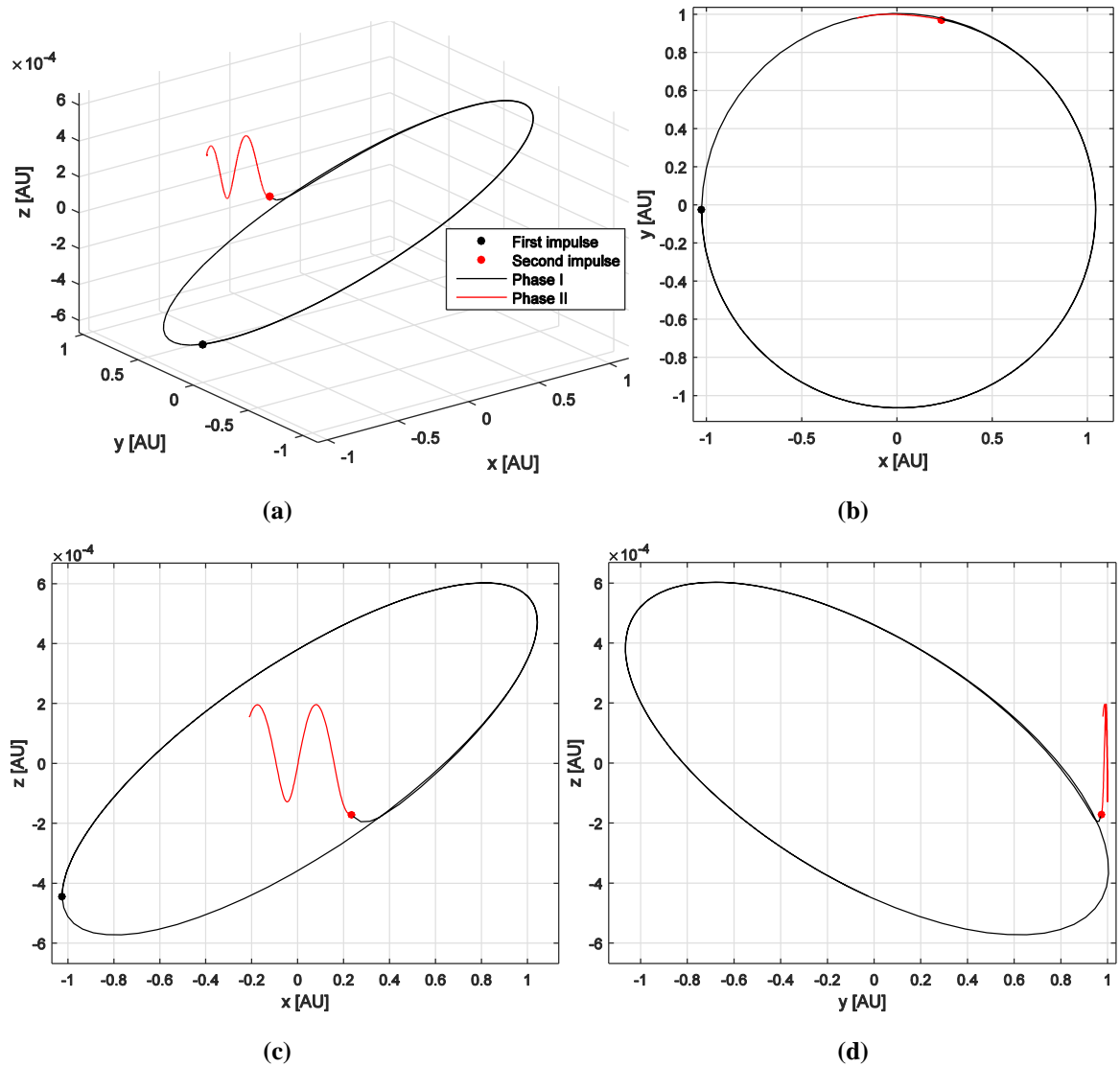


Fig. 3.15 Given $T_0 = 65833.1$ [MJD], $T_f = 66495.5$ [MJD], $A_p = -0.04994$, $t_p = 0.255$, $t_{sm} = 4.10$, direct capture trajectory (phase I) for 2018 AV2 to an Earth-Moon L₂ halo orbit and stable manifold (phase II) associated with the target halo orbit in the J2000 Sun-centred inertial frame: (a) 3D view; (b) x-y projection; (c) x-z projection; (d) y-z projection.

Comparing the direct capture strategy to Earth-Moon LPOs and the capture strategy into Sun-Earth LPOs in prior studies [18, 50], it is noted that one of the key differences between these two capture strategies is the flight time along the stable manifolds. That is, the direct capture of asteroids into the Earth-Moon LPOs needs a much shorter flight time along the stable manifolds associated with Earth-Moon LPOs, while the capture onto Sun-Earth LPOs requires a longer time for the asteroid to be asymptotically captured through utilising the stable manifolds associated with the Sun-Earth LPOs.

Without utilising the Earth-Moon L₂ stable manifolds, the transfer trajectory of the direct capture of the asteroid to the Earth-Moon L₂ target periodic orbit is also modelled in the Sun-Earth-Moon restricted four-body problem. The Lambert arc in the Sun-asteroid

two-body problem is used as an initial guess and then a differential corrector is used to calculate the transfer trajectory from the asteroid's initial orbit to the Earth-Moon L_2 target periodic orbit. The optimal results of the direct capture of the asteroids to the Earth-Moon L_2 target periodic orbit without utilising the Earth-Moon L_2 stable manifolds are shown in Table 3.3. Comparing the results in Table 3.2 and Table 3.3, it can be seen that direct capture using the stable manifolds is of lower cost than direct capture without utilising the stable manifolds. It can be concluded that the Earth-Moon L_2 stable manifolds can provide greater opportunities to achieve low cost asteroid capture.

Table 3.2 Results of optimal direct capture of asteroid to Earth-Moon L_2 periodic orbits using the stable manifolds

NEA	Δv_1 , m/s	Δv_2 , m/s	Δv , m/s	T_0 , MJD	T_{fly} , day	A_p , EM unit	Target (Earth-Moon)
2006 RH120	326.11	58.74	384.84	61471	652.7	0.08575	L_2 Lyapunov
	225.01	144.68	369.69	61262.1	840	0.06895	L_2 halo
2007 UN12	225.76	195.46	421.22	58822.1	320.1	0.12201	L_2 Lyapunov
	200.55	206.71	407.26	58834.3	295.3	-0.06719	L_2 halo
2008 EA9	324.27	167.68	491.95	58686.9	188.8	0.13763	L_2 Lyapunov
	312.38	376.31	607.17	58699.9	149.4	0.03695	L_2 halo
2010 UE51	314.36	162.53	476.89	63256.1	722	0.13261	L_2 Lyapunov
	295.7	285.11	580.81	63250.2	719.7	0.07214	L_2 halo
2014 WX202	376.45	103.76	480.22	63328.6	646.6	0.10408	L_2 Lyapunov
	497.98	2.57	500.55	63335.5	655.7	0.04317	L_2 halo
2018 AV2	102.23	134.74	236.96	65842.9	680	0.06876	L_2 Lyapunov
	107.02	177.17	284.19	65833.1	688.5	-0.04994	L_2 halo

Table 3.3 Results of optimal direct capture of asteroid to Earth-Moon L_2 periodic orbits without using the stable manifolds

NEA	Δv_1 , m/s	Δv_2 , m/s	Δv , m/s	T_0 , MJD	T_{fly} , day	A_p , EM unit	Target (Earth-Moon)
2006 RH120	319.97	151.84	471.81	61470.8	625.6	0.07357	L_2 Lyapunov
	403.15	153.05	556.2	61287.1	811.1	-0.02385	L_2 halo
2007 UN12	136.84	414.32	551.16	58816.4	310.2	0.09054	L_2 Lyapunov
	185.26	273.71	458.97	58838.5	264.8	-0.07429	L_2 halo
2008 EA9	323.64	230.59	554.23	58686.6	148.9	0.11513	L_2 Lyapunov
	311.15	338.68	649.84	58708.4	126.6	0.06511	L_2 halo
2010 UE51	323.46	309.44	632.9	63264.6	676.1	0.07878	L_2 Lyapunov
	301.47	330.71	632.18	63253	687.2	0.06163	L_2 halo
2014 WX202	393.67	194.44	588.11	63333	610.7	0.07250	L_2 Lyapunov
	368.92	235.32	604.24	63328.1	615.4	-0.06800	L_2 halo
2018 AV2	99	209.61	308.62	65835.7	662	0.08637	L_2 Lyapunov
	109.48	228.58	338.06	65844.3	653.6	-0.05687	L_2 halo

3.2 Indirect capture of NEAs to Earth-Moon L_2 periodic orbits

A further type of capture of asteroids in the Earth-Moon system will be termed indirect capture. In this capture strategy the asteroid capture trajectories are designed in a patched three-body model which consists of the Sun-Earth (SE) and Earth-Moon (EM) systems [53], based on the work of Sanchez and McInnes [42], Sanchez, et al. [43] and Yárnoz, et al. [50]. As an approximation of the Sun-Earth-Moon four-body problem, the patched three-body model can be decomposed into the Sun-Earth CRTBP system and the Earth-Moon CRTBP system. In this capture strategy, the candidate asteroids are firstly assumed to be captured onto periodic orbits around the Sun-Earth L_1 or L_2 libration points. Here a series of periodic orbits (Lyapunov orbit and halo orbits) around the Sun-Earth L_1 or L_2 points with different amplitude variables A_p can be calculated using the numerical procedure in Section 2.24, as shown in Fig. 3.16, where the unit of length is the Sun-Earth distance (AU).

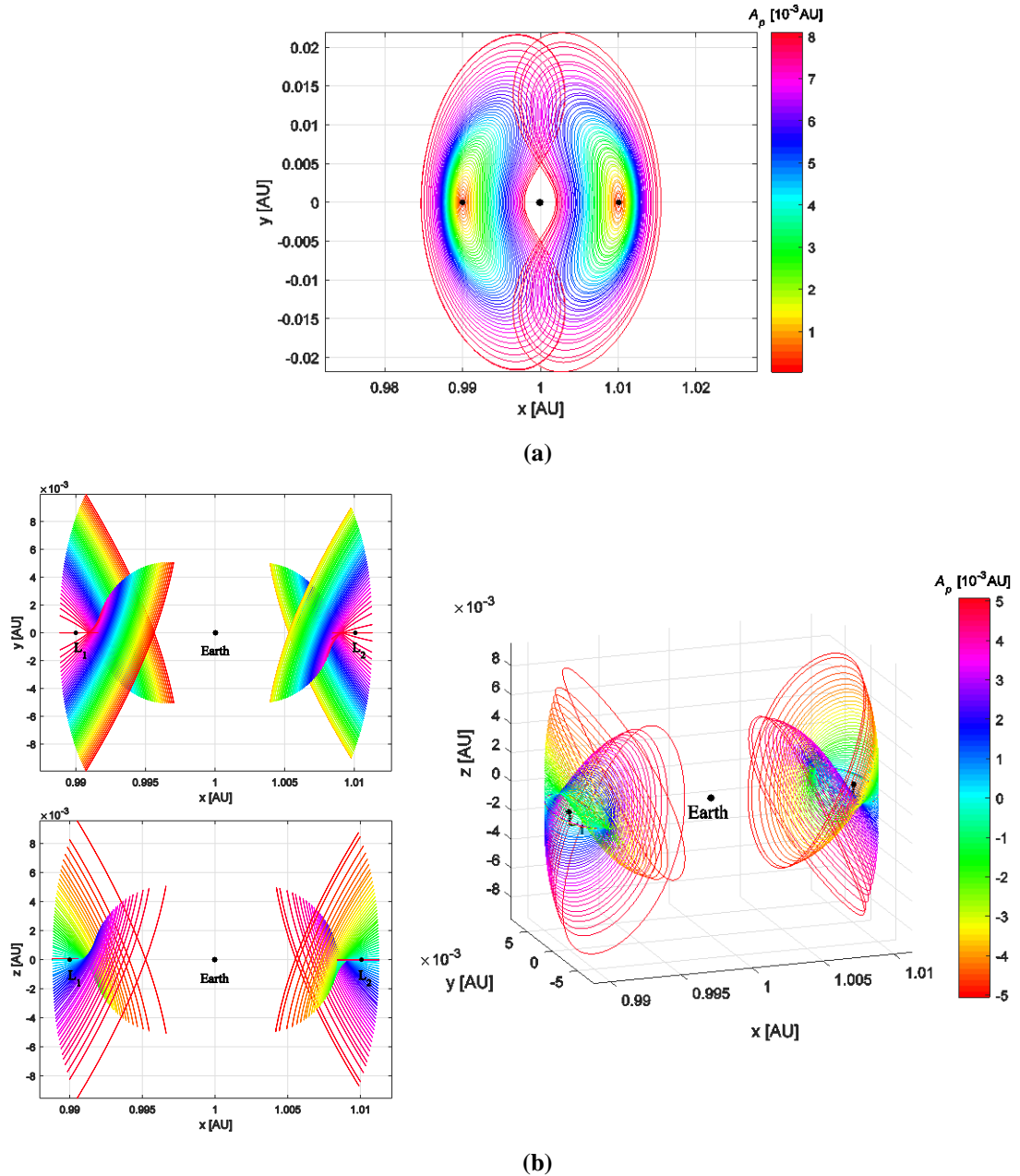


Fig. 3.16 (a) Planar Lyapunov orbits with x -amplitude $[0, 0.0080998]$ (corresponding to Jacobi constant $[2.99991065, 3.00089301]$) and (b) halo orbits with z -amplitude $[-0.0050595, 0.0050595]$ (corresponding to Jacobi constant $[3.00022207, 3.00083043]$) around L_1 and L_2 points in the Sun-Earth system.

As shown in Fig. 3.17, once the candidate asteroid is captured onto a periodic orbit around the Sun-Earth L_1 or L_2 points then the following capture trajectories can be accomplished by patching together the unstable manifolds in the Sun-Earth CRTBP system and the stable manifolds in the Earth-Moon CRTBP system. It should be noted that the patching points of the two invariant manifolds are defined by the chosen Poincaré section (angle γ), shown in Fig. 3.18. The design procedure for the indirect capture of asteroids by using these patched three-body problems can be divided into three parts as follows:

- (1) With the initial impulse Δv_1 , the asteroid leaves its orbit and is injected onto the stable manifolds associated with the Sun-Earth L_1 or L_2 points with the second impulse Δv_2 (See Fig. 3.17). These two impulsive burns can be estimated by using the Lambert arc in the Sun-asteroid two-body problem [50];

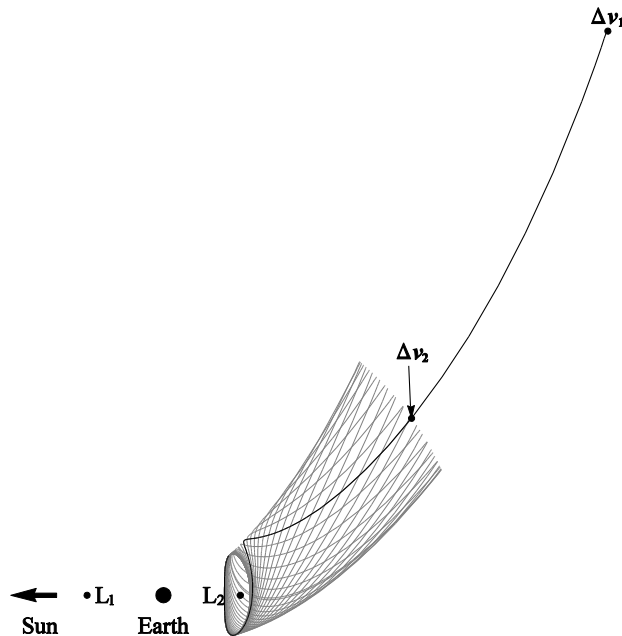


Fig. 3.17 Part of indirect asteroid capture by patching together the Lambert arc in the Sun-asteroid two-body problem and Sun-Earth stable manifolds.

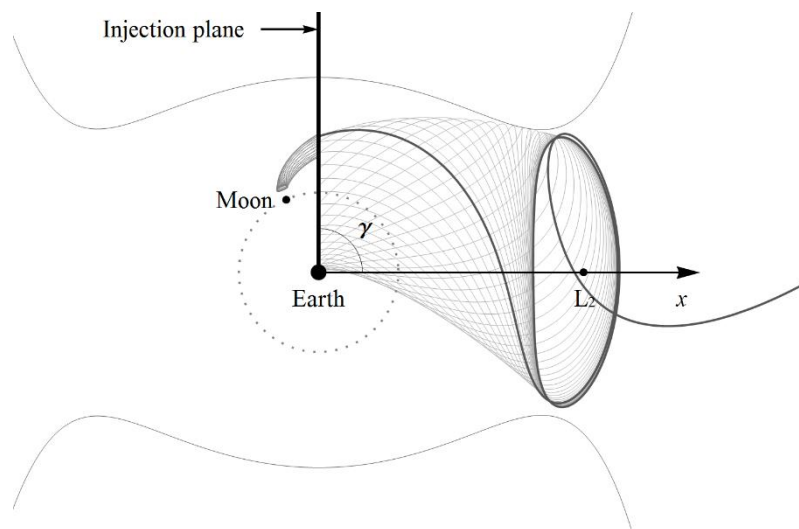


Fig. 3.18 Part of Indirect asteroid capture by patching together Sun-Earth unstable manifold and Earth-Moon stable manifold with the Poincaré section.

- (2) After the candidate asteroid inserts onto the stable manifold, it will be asymptotically captured onto a periodic orbit around the Sun-Earth L_1 or L_2 point;

the asteroid will be on the periodic orbit until it reaches the point where the Sun-Earth unstable manifold is propagated forward from; then the asteroid leaves the periodic orbit by utilising the unstable manifold and then approaches the injection plane between the Sun-Earth unstable manifold and the Earth-Moon L_2 stable manifolds;

- (3) With the third impulse Δv_3 , the asteroid inserts onto the Earth-Moon L_2 stable manifold and will be asymptotically captured onto a periodic orbit around the Earth-Moon L_2 point.

Therefore, in this problem, there are 9 variables as follows:

- T_0 : departure date when the first impulse Δv_1 is applied to the candidate asteroid and the asteroid leaves its orbit;
- T_f : approach date corresponding to the date when the candidate asteroid inserts into the Sun-Earth L_1 or L_2 stable manifolds with the second impulse Δv_2 ;
- t_{sm} : Sun-Earth L_1 or L_2 stable manifold transfer time;
- A_{SE} : amplitude variable of target periodic orbit around Sun-Earth L_1 or L_2 : x -amplitude A_x for Lyapunov orbits and z -amplitude A_z for halo orbits;
- t_{p1} : time determining the point on the target periodic orbit around Sun-Earth L_1 or L_2 where the Sun-Earth L_1 or L_2 stable manifold is propagated backward from;
- t_{p2} : time determining the point on the target periodic orbit around Sun-Earth L_1 or L_2 where the Sun-Earth L_1 or L_2 unstable manifolds is propagated forward from;
- γ : angle determining the injection plane where the Sun-Earth L_1 or L_2 unstable manifold and Earth-Moon L_2 stable manifolds are patched together with the third impulse Δv_3 ;
- A_{EM} : amplitude variable of target periodic orbit around Earth-Moon L_2 point: x -amplitude A_x for Lyapunov orbits and z -amplitude A_z for halo orbits;
- t_{p3} : time determining the point on the target periodic orbit around the Earth-Moon L_2 point where the Earth-Moon L_2 stable manifold is propagated backwards from.

These 9 variables can be divided into two parts: $(T_0, T_f, t_{sm}, A_{SE}, t_{p1})$ and $(A_{SE}, t_{p2}, \gamma, A_{EM}, t_{p3})$, corresponding to those associated with capturing the asteroid onto the Sun-Earth stable manifold (Part I) and those associated with patching together the Sun-Earth unstable manifold and Earth-Moon L_2 stable manifold (Part II), respectively. However, there exists a time constraint between the two parts. That is, once the variables $(T_0, T_f, t_{sm}, A_{SE}, t_{p1}, t_{p2}, \gamma)$ are given, the Sun-Earth unstable manifold is propagated forward until it reaches the

Poincaré section (angle γ) and then the Sun-Earth unstable transfer time t_{um} is determined; accordingly, the position of the Moon is then determined.

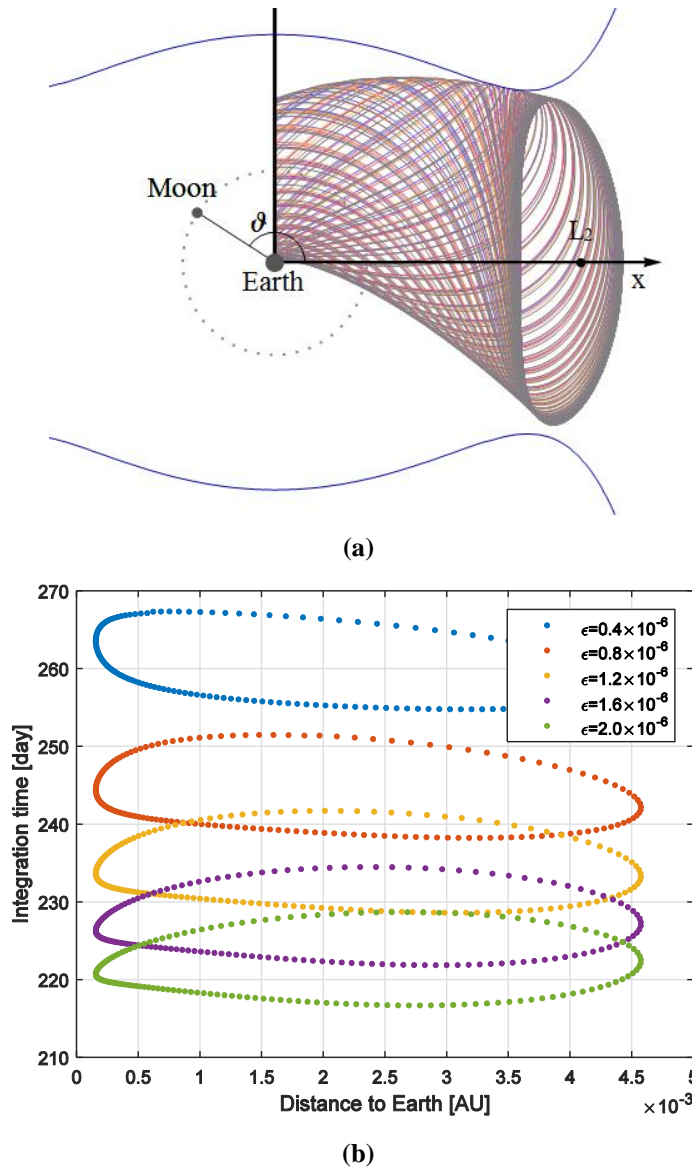
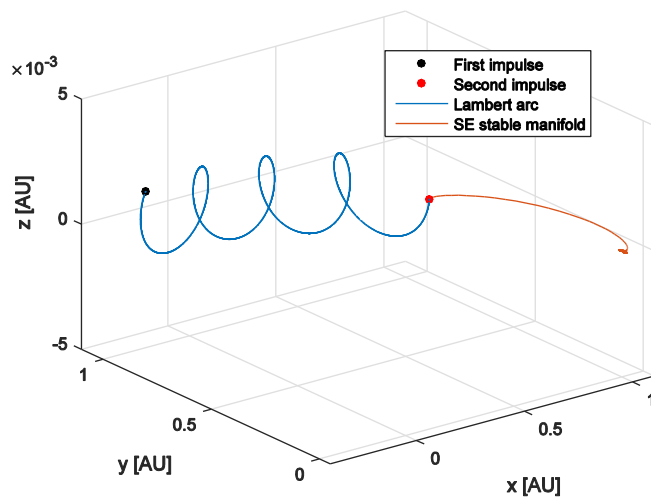


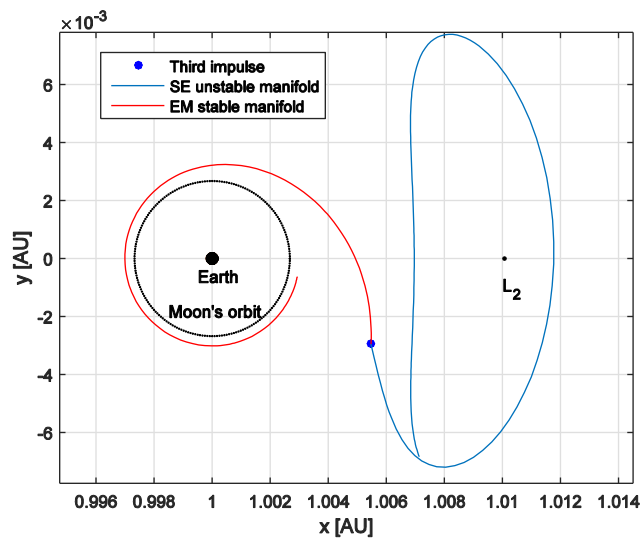
Fig. 3.19 (a) Unstable manifolds of Sun-Earth L_2 Lyapunov orbit ($A_{SE} = 0.0048497$ AU) and (b) their integration time to the same Poincaré section ($x = 1 - \mu$) with varying $\varepsilon \in [0.4 \times 10^{-6}, 2 \times 10^{-6}]$.

Figure 3.19(a) shows the unstable manifolds of a Lyapunov orbit around the Sun-Earth L_2 with different values of ε and it should be noted that small values of ε in Eq. (2.30) can result in large integration times when calculating the unstable manifolds. Figure 3.19(b) shows that the integration time of the Sun-Earth unstable manifolds to the same Poincaré section clearly changes when varying the value of ε . This means even given the values of $(t_0, t_f, t_{sm}, A_{SE}, t_{p1}, t_{p2}, \gamma)$, the position of the Moon can be anywhere along its orbit, as long as an appropriate value of ε is selected. Therefore, an additional variable ϑ ($0 \leq \vartheta < 2\pi$) is defined to determine the position of the Moon, shown in Fig. 3.19(a) and the variables of

Part II are extended to $(A_{SE}, t_{p2}, \gamma, A_{EM}, t_{p3}, \vartheta)$. The common parameter between the two parts is the amplitude variable A_{SE} of the target periodic orbit in the Sun-Earth system. Part II can then be optimised by using NSGA-II [182]. During each step in optimising Part II, there is a specific value of A_{SE} and given this value, Part I can be optimised by using the function *fmincon* in MATLAB. Therefore, this problem can be optimised with the total Δv cost as the objective function. The results of the indirect capture of the NEAs are listed in Table 3.4 and the optimal capture trajectory for 2018 AV2 to an Earth-Moon L_2 Lyapunov orbit is shown in Fig. 3.20. It should be noted that in Table 3.4 and Table 3.5, 2L, 2H, 1L, 1H denote the planar Lyapunov orbit around L_2 , the halo orbit around L_2 , the planar Lyapunov orbit around L_1 and the halo orbit around L_1 , respectively.



(a)



(b)

Fig. 3.20 Indirect capture trajectory for 2018 AV2 to Earth-Moon L_2 Lyapunov orbit in the Sun-Earth rotating frame: (a) the transfer trajectory of Part I (b) the transfer trajectory of Part II.

Table 3.4 Results of optimal indirect capture of asteroids to Earth-Moon L_2 periodic orbits

NEA	$\Delta v_1 + \Delta v_2$, m/s	Δv_3 , m/s	Δv , m/s	T_0 , MJD	T_{fly} , day	A_{EM} , EM unit	A_{SE} , $10^{-3}AU$	Target (SE+EM)
	333.18	4.26	337.44	58821	3352.2	0.00752	3.2761	1L+2L
2006	328.5	6.28	334.79	58785.9	3036.2	0.00011	2.5632	1L+2H
RH120	352.36	3.99	356.35	60481.5	1534.1	0.02913	-0.0024	1H+2L
	360.5	3.94	364.44	60504.2	1504.4	0.00004	-0.0074	1H+2H
	260.01	58.8	318.81	58562.5	1067.2	0.07606	7.0843	2L+2L
2007	342.73	29.28	372.01	58727.2	837.5	0.00042	5.4797	2L+2H
UN12	444.44	1.3	445.74	58524.7	1016.2	0.04448	0.0054	2H+2L
	458.21	11.02	469.23	58535.9	999.7	-0.00067	-0.0034	2H+2H
	420.13	14.39	434.51	61153.1	2585.3	0.06134	6.7931	2L+2L
2008	432.91	32.05	464.96	61294.6	2425.9	-0.0007	6.3944	2L+2H
EA9	662.78	0.64	663.42	62249.8	1368.8	0.01922	0.0016	2H+2L
	661.8	5.31	667.11	62245.3	1435.8	-0.00065	0.0058	2H+2H
	467.04	38.55	505.58	63244.6	1221.7	0.06286	7.029	2L+2L
2010	513.58	15.83	529.42	58599.8	2159	0.00613	6.0759	2L+2H
UE51	736.11	0.65	736.76	61746.2	2653.7	0.03853	0.0079	2H+2L
	731.68	2.27	733.95	61746	2651.4	0.00081	0.0217	2H+2H
	383.7	34.1	417.8	61495.1	2631.6	0.09149	7.127	2L+2L
2014	361.91	5.38	367.29	61504.4	2593	0.00098	6.4996	2L+2H
WX202	417.51	3.17	420.68	60286.8	3048.1	0.03801	-0.0081	2H+2L
	419.6	18.78	438.38	60271.8	3060.8	-0.0003	0.0009	2H+2H
	200.68	3.02	203.7	63329.7	2876.5	0.00944	2.654	2L+2L
2018	145.66	28.46	174.12	63643.4	2985.9	0.00021	6.2348	2L+2H
AV2	204.22	2.18	206.4	63301.4	2800.5	0.0193	-0.0065	2H+2L
	296.14	7.32	303.45	63201.3	2677.4	0.00042	0.0004	2H+2H

Comparing the results in the Table 3.2 and Table 3.4, it is found that the direct capture to the Earth-Moon L_2 point needs a shorter flight time and so chemical propulsion may be preferred for this capture strategy. On the other hand, the indirect asteroid capture always needs a much longer flight time. Moreover, this capture strategy can easily achieve a low energy transfer for capturing a NEA. Therefore, low-thrust propulsion can be more easily applied to the indirect capture strategy. For comparison, the optimal results of the indirect capture of asteroids to the Earth-Moon L_2 target periodic orbit without utilising the Earth-Moon L_2 stable manifolds are shown in Table 3.5. It is assumed that the transfer

trajectories for indirect asteroid capture can be designed by patching the Sun-Earth unstable manifolds and the Earth-Moon L_2 periodic orbits directly. Comparing the results in Table 3.4 and Table 3.5, it is shown that the indirect capture strategy using the Earth-Moon stable manifolds can easily achieve lower cost captures.

Table 3.5 Results of optimal indirect capture of asteroids to Earth-Moon L_2 periodic orbits without using the Earth-Moon stable manifolds

NEA	$\Delta v_1 + \Delta v_2$, m/s	Δv_3 , m/s	Δv , m/s	T_0 , MJD	T_{fly} , day	A_{EM} , EM unit	A_{SE} , $10^{-3}AU$	Target (SE+EM)
	365.01	18.03	383.04	58780.7	3021.9	0.05473	2.6947	1L+2L
2006	394.75	6.48	401.23	58798.2	2996.6	0.00195	2.4466	1L+2H
RH120	497.09	19.7	516.79	60391.9	1785.2	0.03964	-0.0131	1H+2L
	455.27	81.22	536.49	60527.3	1581.5	0.01784	-0.0143	1H+2H
	370.72	26.04	396.76	58526.4	1067.4	0.0501	7.1973	2L+2L
2007	339.38	137.66	477.05	58529.1	1068.5	-0.000120	7.1195	2L+2H
UN12	475.42	18.3	493.72	58523.7	1211.2	0.06394	-0.0119	2H+2L
	483.36	114.84	598.19	58511.8	1059.8	0.00398	0.00680	2H+2H
	423.14	89.03	512.17	61047.7	2351.7	0.13501	7.5718	2L+2L
2008	479.53	91.79	571.32	61046.3	2330	0.00110	7.1531	2L+2H
EA9	682.65	80.48	763.13	62227	1433.5	0.09171	-0.00120	2H+2L
	910.61	80.57	991.18	62194.4	1526.7	0.00488	-0.00850	2H+2H
	459.91	55.04	514.95	62253.5	2215.4	0.11002	7.4242	2L+2L
2010	477.15	102.24	579.39	62232.5	2227.7	0.00229	7.1293	2L+2H
UE51	767.58	45.26	812.83	61772.3	2718.4	0.1119	0.0135	2H+2L
	766.46	57.85	824.31	61757.9	2610.7	-0.00200	-0.00730	2H+2H
	423.16	26.54	449.7	61541.4	2485.2	0.07041	1.3148	2L+2L
2014	443.59	48.47	492.06	61540.5	2522	0.00328	2.5509	2L+2H
WX202	488.13	7.78	495.91	60265.8	3082	0.05891	0.00430	2H+2L
	476.24	93.19	569.43	60266.1	3082	0.00320	-0.00780	2H+2H
	358.48	95.35	453.83	63805.4	2715.9	0.09785	2.2355	2L+2L
2018	255.45	153.2	408.65	63521.1	3111.7	-0.000210	7.1101	2L+2H
AV2	305.72	21.26	326.98	63226	3000.5	0.08854	-0.0568	2H+2L
	285.95	67.45	353.4	63268	2953.4	0.000730	0.0279	2H+2H

From comparison of the results from Table 3.4 and Table 3.5, it can be seen that lower cost captures are available by patching together the Sun-Earth Lyapunov orbit unstable

manifold and Earth-Moon Lyapunov orbit stable manifold than to patch other combinations of the Sun-Earth unstable manifolds and Earth-Moon stable manifolds, e.g. the Sun-Earth halo orbit unstable manifold and Earth-Moon halo orbit stable manifold. This is because in the patched three-body problem it is assumed that the motion of all four bodies are in the same plane. Patching the Sun-Earth Lyapunov orbit unstable manifold and Earth-Moon Lyapunov orbit stable manifold together is a planar problem and the z -component of the manifolds is not considered. Therefore, there are more opportunities to patch the Sun-Earth Lyapunov orbit unstable manifold and Earth-Moon Lyapunov orbit stable manifold together, while there are only two intersection points between one Sun-Earth halo orbit unstable manifold and one Earth-Moon halo orbit stable manifold, as well as one Sun-Earth halo orbit unstable manifold and one Earth-Moon Lyapunov orbit stable manifold, one Sun-Earth Lyapunov orbit unstable manifold and one Earth-Moon halo orbit stable manifold, shown in Fig. 3.21.

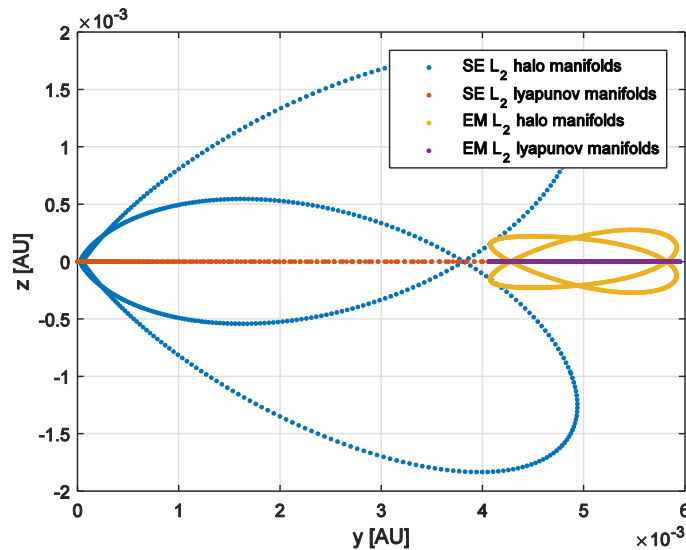


Fig. 3.21 Intersection of Sun-Earth L_2 manifolds and Earth-Moon L_2 manifolds ($\vartheta = 0.5\pi$) with Poincaré section ($x = 1 - \mu$) in the Sun-Earth rotating frame.

3.3 Direct and indirect capture of NEAs to Earth-Moon system triangular points

Due to their stability, the vicinity of the triangular points in Earth-Moon system could be a preferred location for captured asteroids. As discussed in Section 2.25, there are two families of periodic orbits around the triangular points, long-period orbits and short-period orbits. Generally speaking, the short-period orbits are much more stable than the long-

period orbits, under given perturbations. Therefore, short-period orbits with $C_1 = 0$ and $C_2 \leq 0.2$ are selected as the target orbit for the captured asteroids [172], as defined in Section 2.2.5. In this section, the amplitude variable A_p instead of the Jacobi constant is used to define a short-period orbit and so A_p can be written as

$$A_p = \kappa_2 \quad (3.25)$$

Then, a series of short-period orbits around the Earth-Moon triangular points with continuous amplitude variable A_p can be calculated, using the numerical procedure in Section 2.25, as shown in Fig. 3.22.

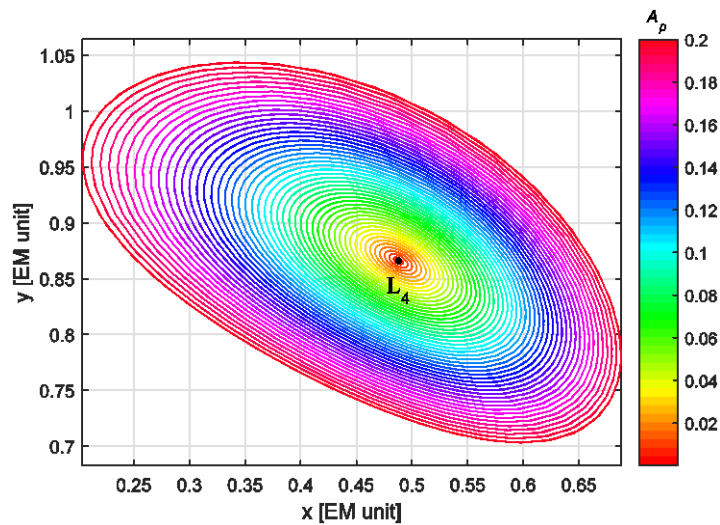


Fig. 3.22 Short-period orbits around the triangular points L_4 in the Earth-Moon system ($\kappa_1 = 0$, $A_p \leq 0.2$).

Similar to the direct/indirect asteroid capture to periodic orbits around the Earth-Moon L_2 point, there also exist two types of asteroid capture strategies and so the design procedures of Section 3.1-3.2 can still be applied to design the direct/indirect capture of asteroids to the triangular points. However, different to the transfers to the Earth-Moon L_2 periodic orbits, there are no dynamical structures such as invariant manifolds associated with periodic orbits around the triangular points in the Earth-Moon system. Therefore, transfer trajectories for direct asteroid capture can be designed from the candidate asteroid's orbit to the short-period orbits around the Earth-Moon L_4/L_5 points directly, shown in Fig. 3.23(a). For the indirect capture strategy, the unstable manifolds of the Sun-Earth system and the short-period orbit around the Earth-Moon L_4/L_5 points can be patched together, shown in Fig. 3.23(b).

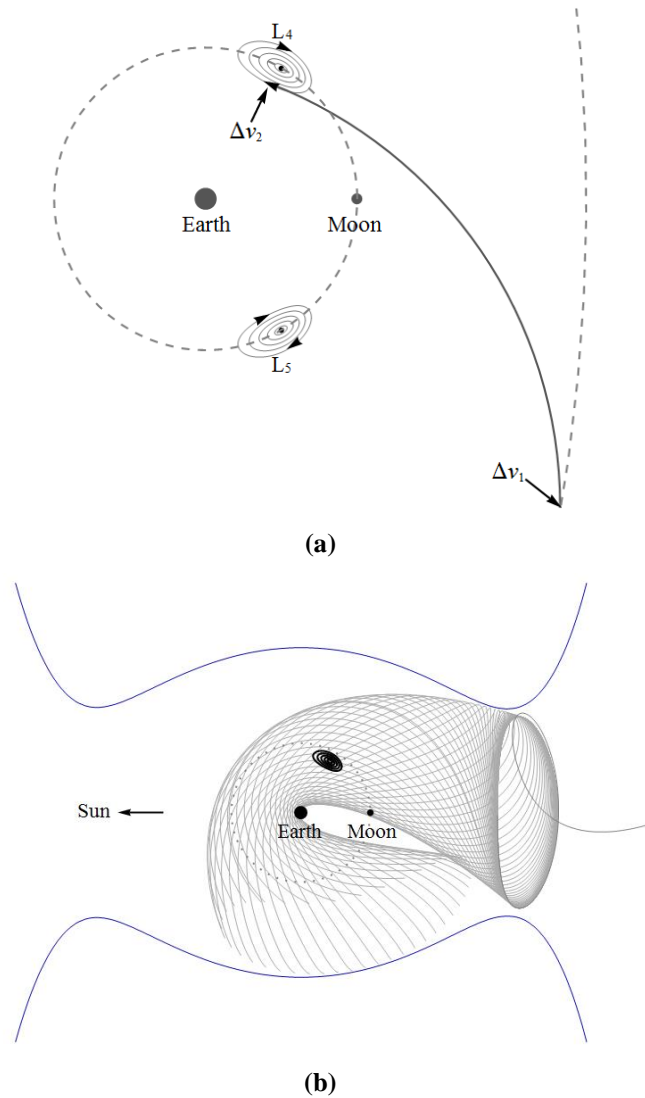


Fig. 3.23 Two types of asteroid capture strategies to the Earth-Moon triangular points: (a) direct capture strategy; (b) indirect capture strategy.

Similar to the optimisation of the direct/indirect capture trajectories to the Earth-Moon L_2 point, the direct/indirect capture trajectories to the Earth-Moon triangular points can again be optimised by using NSGA-II [182] followed by the function *fmincon* in MATLAB. The results of direct and indirect capture of asteroids to the triangular points in the Earth-Moon system is shown in Table 3.6 and Table 3.7. It can be seen that the direct asteroid capture strategy needs a shorter flight time, while the indirect asteroid capture strategy can achieve lower-cost capture. Compared to the results of Table 3.2 and Table 3.5, it can be seen that without invariant manifolds associated with the triangular points, much more energy (i.e., Δv_2) is required to insert the candidate asteroids into the short-period orbits around the Earth-Moon triangular points. The optimal direct and indirect capture trajectories for 2018 AV2 to the Earth-Moon L_4 point is shown in Fig. 3.24 and

Fig. 3.25 respectively. It should be noted that in Table 3.7, 2L denotes the planar Lyapunov orbit around L_2 .

Table 3.6 Results of optimal direct capture of asteroids to the Earth-Moon triangular point

NEA	Δv_1 , m/s	Δv_2 , m/s	Δv , m/s	T_0 , MJD	T_{fly} , day	A_p , EM unit	Target (EM)
2006 RH120	335.66	428.9	764.56	61095.1	996.8	0.19948	L_4
2007 UN12	174.65	584.73	759.38	58836	262.4	0.19992	L_4
2008 EA9	294.98	544.11	839.09	58678.4	178.7	0.19782	L_4
2010 UE51	293.09	643.74	936.82	63246.9	688.7	0.19921	L_4
2014 WX202	428.8	422.5	851.3	63342.8	621.2	0.19902	L_4
2018 AV2	171.98	374.64	546.62	65961.1	586.1	0.19957	L_4

Table 3.7 Results of optimal indirect capture of asteroids to the Earth-Moon triangular point

NEA	$\Delta v_1 + \Delta v_2$, m/s	Δv_3 , m/s	Δv , m/s	T_0 , MJD	T_{fly} , day	A_{EM} , EM unit	A_{SE} , $10^{-3} \times \text{AU}$	Target (SE+EM)
2006 RH120	326.84	234.45	561.29	58785.5	3013	0.58389	2.2935	1L+ L_4
	431.91	215.02	646.93	60427.2	1745.6	0.66505	-0.0076	1H+ L_4
2007 UN12	241.2	448.89	690.09	58571.5	1058.6	0.54696	7.441	2L+ L_4
	458.61	226.02	684.63	58529.2	1254.1	0.49543	-0.0185	1H+ L_4
2008 EA9	412.19	429.86	842.05	61059.7	2349.4	0.5169	7.7138	2L+ L_4
	723.66	206.78	930.44	62214.1	1449.4	0.6874	-0.0016	1H+ L_4
2010 UE51	409.06	423.39	832.45	62238.1	2266.6	0.46957	7.8272	2L+ L_4
	772.42	226.92	999.34	61771.6	2596.5	0.67423	-0.0188	1H+ L_4
2014 WX202	425.74	193.2	618.94	61542.9	2581	0.47584	1.0408	2L+ L_4
	481.29	223.13	704.42	60263.6	3088.2	0.61532	0.035	1H+ L_4
2018 AV2	267.19	245.12	512.31	64230.9	2676.4	0.53164	2.7445	2L+ L_4
	266.91	214.57	481.47	63273	2944.3	0.54619	-0.0216	1H+ L_4

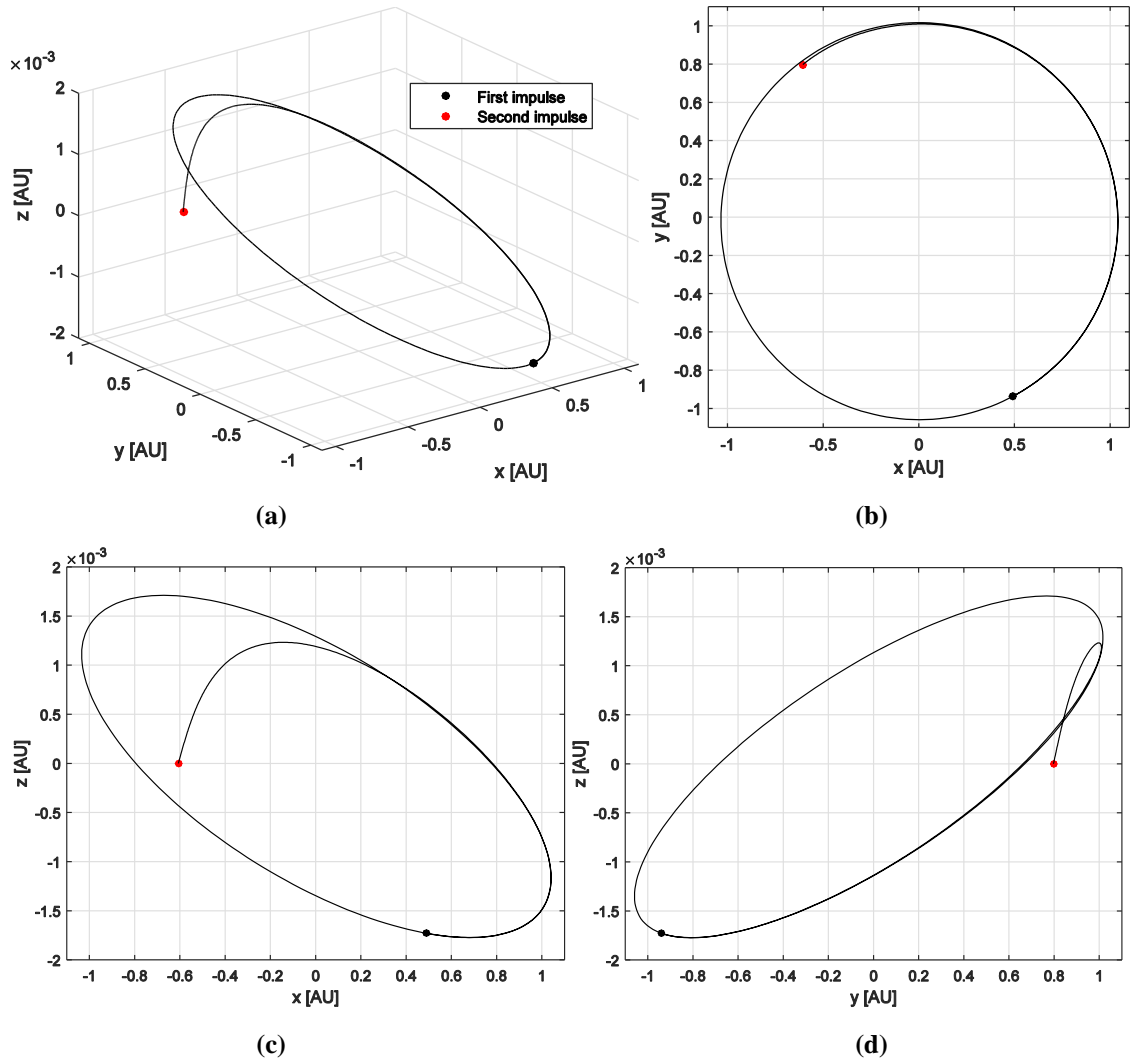


Fig. 3.24 Optimal direct capture trajectory for 2018 AV2 to the Earth-Moon L_4 periodic orbit in the J2000 Sun-centered inertial frame: (a) 3D view; (b) x - y projection; (c) x - z projection; (d) y - z projection.

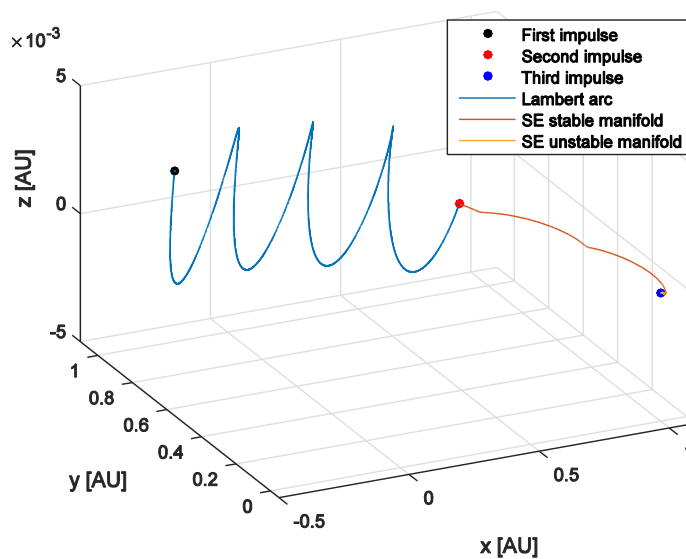


Fig. 3.25 Optimal indirect capture trajectory for 2018 AV2 to Earth-Moon L_4 periodic orbit in Sun-Earth rotating system.

3.4 Discussions

In this chapter, two different strategies for capturing asteroids in the Earth-Moon system have been presented, termed as the direct and indirect asteroid capture strategies.

As a candidate gateway station, and an ideal location for interplanetary transfers, the Earth-Moon L_2 libration point is of great importance for future deep space exploration. Capturing asteroids and inserting them onto periodic orbits around the Earth-Moon L_2 point offers in-situ resources to support such ventures. Therefore, the patched restricted three-body problem has been used to investigate the capture of asteroids into periodic orbits around the Earth-Moon L_2 point. However, using an indirect capture strategy via the Sun-Earth L_2 point the transfer duration is long due to the time required for the asteroid to move along the stable manifold in the Sun-Earth system.

Therefore, a direct asteroid capture strategy is proposed to capture asteroids into periodic orbits around the Earth-Moon L_2 point from the asteroid's heliocentric orbit directly. The CRTBP is firstly used to compute periodic orbits around the Earth-Moon L_2 point and their associated stable manifolds. The 3BSOI is then utilised as the boundary between the Sun-Earth-Moon restricted four-body problem and the Earth-Moon CRTBP. After the target points on the stable manifolds are transformed to the Sun-centred inertial frame, the three-dimensional orbital-element space of candidate NEAs is then obtained to select candidate NEAs which can be captured with a total cost under 500 m/s. After calculating the approximate approach date and departure date, a Lambert arc in the Sun-centred two-body problem is utilised to estimate the first impulse to the target points from the candidate asteroid's orbit. Based on the initial guess of the first impulse, a differential correction method is then used to design the transfer trajectory to the target points from the candidate asteroid's orbit in the Sun-Earth-Moon restricted four-body problem.

On the other hand, due to the stability of the triangular points in the CRTBP model, the vicinity of the triangular points in Earth-Moon system could be another preferred location for captured asteroids. The direct/indirect strategies are also applied to design the direct/indirect capture of asteroids to the triangular points. Since there are no invariant manifolds associated with periodic orbits around the triangular points, transfer trajectories for direct asteroid capture can be designed from the candidate asteroid's orbit to short-period orbits around the Earth-Moon L_4/L_5 points directly, and the indirect capture is designed by patching the unstable manifolds of the Sun-Earth system with short-period orbits around the Earth-Moon L_4/L_5 points.

Comparing the results of the two methods, it is noted that the direct asteroid capture strategy requires a shorter flight time while the indirect asteroid capture strategy can always achieve a lower cost capture in terms of energy requirements. Therefore, chemical propulsion may be preferred for the direct capture strategy. Moreover, low-thrust propulsion can be more easily applied to the indirect capture strategy.

CHAPTER 4

CAPTURE OF NEAS AROUND SUN-EARTH LIBRATION POINTS USING EARTH FLYBY AND AEROBRAKING

This Chapter introduces the concept of coupling together a flyby of the Earth and then capturing small NEAs onto Sun–Earth L_1/L_2 periodic orbits. Since the Sun-Earth L_1 and L_2 points represent potentially beneficial gateways for future interplanetary missions, capturing asteroids onto periodic orbits around the Sun-Earth L_1/L_2 points is of particular interest. The main contributions of this Chapter (which were presented in Ref [44]) are summarized as follows:

- (1) According to the height of the flyby orbit at perigee, two types of the Earth flyby are determined; an Earth flyby with and without high altitude aerobraking. In this capture strategy, the candidate asteroid leaves its orbit with an impulse manoeuvre and then flies by the Earth. At the perigee of the flyby, an aerobraking maneuverer or an additional propulsive manoeuvre is imposed on the asteroid. Accordingly, the asteroid is inserted onto the stable manifold of a target periodic orbit around the Sun-Earth L_1 or L_2 points;
- (2) In the NEA capture strategy using aerobraking, the aerobraking model is transformed from the Earth-centred inertial frame to the Sun-Earth rotating frame. The aerobraking phase is then investigated to calculate aerobraking opportunities and windows for capture to periodic orbits around the Sun-Earth libration point L_1 or L_2 .

4.1 Target periodic orbits and stable manifolds

As discussed in Section 3.3, the Lyapunov orbits and halo orbits around the Sun-Earth L_1 and L_2 points have been calculated using a numerical procedure in Section 2.2.4. In this Chapter, those periodic orbits will serve as the final target orbits where the candidate asteroids are captured and placed. The orbits are unstable periodic orbits which have associated stable manifolds. Once the candidate asteroid is captured onto the stable manifolds associated with the periodic orbits around the Sun-Earth L_1 and L_2 points, it will asymptotically approach and then be inserted onto the target orbit. The stable manifolds associated with a Sun-Earth L_2 Lyapunov orbit are shown in Fig. 3.15.

As discussed in Section 3.1.1, a Poincaré section can transform a continuous time dynamical system to a discrete time dynamical system. To obtain the state of the perigee of the Earth flyby orbit, the periapsis map can be used as a Poincaré map [75, 105, 183, 184]. The periapsis map is defined by the following condition

$$\dot{r}_2 = 0, \ddot{r}_2 > 0 \quad (4.1)$$

where r_2 is the distance between a third body (i.e. the asteroid) and the centre of the Earth (See Section 2.2).

The periapsis map of the stable manifolds associated with the Sun-Earth L_1 and L_2 periodic orbits can be obtained by propagating the stable manifolds backward until they cross the section defined by Eq. (4.1). An example of the periapsis map of the stable manifolds associated with a Sun-Earth L_2 Lyapunov orbit is shown in Fig. 4.1. In this Chapter, the aerobraking manoeuvre, or an additional propulsive manoeuvre, is assumed to occur at the perigee of the Earth flyby orbit where the state of the perigee of the flyby orbit can be determined by the periapsis condition defined by Eq. (4.1).

The states of the Sun-Earth L_1 and L_2 stable manifolds at the periapsis map in the Sun-centred inertial frame and in the Sun-Earth rotating frame are denoted by \mathbf{X}_S^{in} and \mathbf{X}_{SE}^{ro} respectively. Thus,

$$\mathbf{X}_S^{in} = \mathbf{R}(\beta)(\mathbf{X}_{SE}^{ro} - \mathbf{X}_{Sun}), \beta \in [0, 2\pi] \quad (4.2)$$

$$\mathbf{X}_{SE}^{ro} = \mathbf{R}^{-1}(\beta)\mathbf{X}_S^{in} + \mathbf{X}_{Sun}, \beta \in [0, 2\pi] \quad (4.3)$$

where $\mathbf{X}_{Sun} = [-\mu, 0, 0, 0, 0, 0]^T$ is the state of the Sun in the Sun-Earth rotating frame and $\mathbf{R}^{-1}(\beta)$ is a rotation matrix (See Section 2.2).

In the following sections, Eq. (4.2) will be used to transform the state of the candidate asteroid in the Sun-centred inertial frame to the Sun-Earth rotating frame. Moreover, Eq. (4.3) will be used to transform the state of the asteroid at the aerobraking manoeuvre in the Earth-centred inertial frame to the Sun-Earth rotating frame. Consequently, the dynamical model of the aerobraking manoeuvre in the Sun-Earth rotating frame can be obtained.

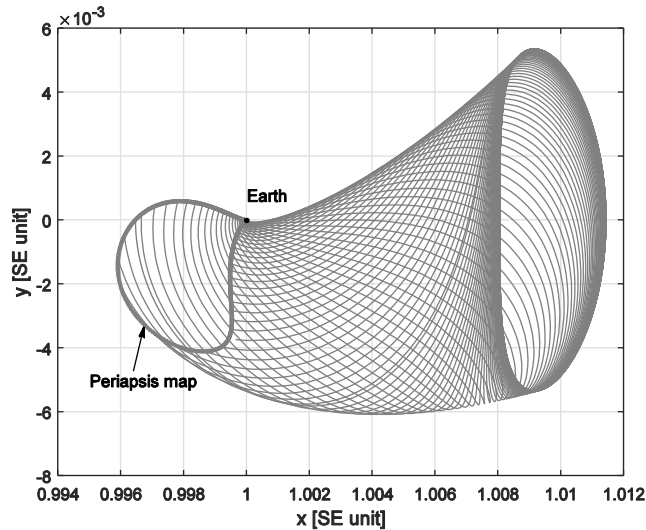


Fig. 4.1 Stable manifolds associated with a Sun-Earth L_2 periodic orbit ($A_p = 0.0020187$) and the periapsis map

4.2 Strategies for Earth flyby

During the flyby of the Earth, the Earth's atmosphere may provide opportunities for a grazing aerobraking manoeuvre to move the asteroid onto the stable manifold of the Sun-Earth L_1 or L_2 periodic orbits. Therefore, there will exist two types of Earth flyby, i.e. with and without the aerobraking manoeuvre, corresponding to a low or high altitude flyby orbit at perigee. In practice only small bodies would be considered to mitigate impact risks. Therefore, those asteroids which would completely ablate in the Earth's atmosphere at low altitude in the event of a failure prior to or during the aerobraking pass [147] are considered as candidate asteroids, as discussed in Section 3.1.5. Moreover, issues associated with the precision of the aerobraking manoeuvre required for subsequent injection onto the stable manifold are not considered here. However, for a small asteroid, the body may in principle be actively guided by a carrier spacecraft [39], with the carrier spacecraft remaining attached to, and shielded, by the asteroid during the aerobraking manoeuvre.

4.2.1 Aerobraking model

With a high relative velocity with respect to the Earth, a captured asteroid will pass through the Earth's atmosphere quickly and so would remain in the atmosphere for only a short duration, as shown in Fig. 4.2. The trajectory of the asteroid in the Earth's atmosphere can then be modelled by means of a Keplerian orbit.

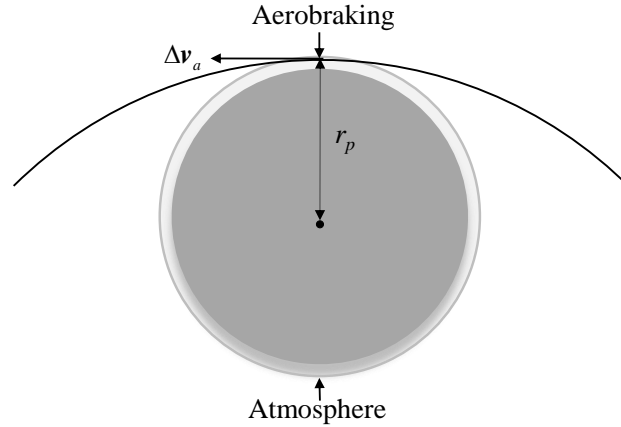


Fig. 4.2 Schematic diagram of an aerobraking

Thus, assuming that the asteroid remains in the Earth's atmosphere for a small arc of true anomaly close to pericentre, an approximate model can therefore be used where the aerobraking manoeuvre is modelled as a grazing hyperbolic flyby. During the flyby, a first order approximation of the velocity change (Δv_a) generated by the aerobraking manoeuvre can be written as [139]

$$\Delta \mathbf{v}_a = (1 - e^{-B\rho\sqrt{2\pi r_p H_s (e+1)/e}}) \mathbf{v}_{p-} \quad (4.4)$$

where \mathbf{v}_{p-} is the relative velocity of the asteroid at perigee with respect to the Earth and

$$B = C_d \frac{A}{2M} \quad (4.5)$$

is the asteroid ballistic coefficient, where C_d is the drag coefficient of a sphere, assumed to be 0.47 [49]; A/M is the area-to-mass ratio of the asteroid; r_p is the perigee radius of the flyby orbit from the centre of the Earth and e is the eccentricity of the flyby orbit; H_s is the atmosphere scale height. Assuming that the asteroid is a spherical with standard density $\rho_a = 2600 \text{ kg/m}^3$ [181], the asteroid ballistic coefficient can be written as

$$B = 0.75C_d \frac{1}{D\rho_a} \quad (4.6)$$

where D is the diameter of the asteroid (See Section 3.1.5).

Many density models of the Earth's atmosphere have been developed, including the Standard Atmosphere, USSA76 [185] and COSPAR International Reference Atmosphere [186]. However, one of the simplest models is the exponential atmospheric model [187]. In this model, it is assumed that the density of the atmosphere decreases exponentially from the Earth's surface and so can be written as

$$\rho = \rho_0 e^{-\frac{h}{H_s}} \quad (4.7)$$

where $\rho_0 = 1.225 \text{ kg/m}^3$ is the density of the Earth's atmosphere at the surface and $H_s = 7.249 \text{ km}$ is the scale height [187].

Moreover, during the aerobraking manoeuvre, the energy loss due to the grazing pass through the upper atmosphere will be converted to heat, and thus the aerobraking manoeuvre will lead to mass loss from the asteroid due to thermal ablation [188]. Therefore, it can be assumed that the mass loss of the asteroid should be a function of the change in the kinetic energy of the asteroid. Based on the approximate model for aerobraking in Eq. (4.4), the final mass m_+ of the candidate asteroid after aerobraking can be estimated as [49]

$$m_+ = m_- e^{\sigma(v_{p+}^2 - v_{p-}^2)/2} \quad (4.8)$$

where $\mathbf{v}_{p+} = \mathbf{v}_{p-} + \Delta\mathbf{v}_a$ is the relative velocity of the asteroid at perigee with respect to the Earth after aerobraking, m_- is the initial mass of the asteroid and σ is an ablation parameter, assumed to be $2.1 \times 10^{-8} \text{ s}^2/\text{m}^2$ [49]. In fact, the ablation parameter σ is not constant and can vary with the altitude of the aerobraking manoeuvre, the asteroid relative velocity and the size of the asteroid. Moreover, some large asteroids would suffer a lower level of ablation since the outer surface of the asteroid can act as an effective shield caused by a screening effect [189]. However, a constant value of the ablation parameter can provide an effective conservative estimate of the asteroid's final mass [49]. Meanwhile, the mass loss ratio is defined by

$$f = \frac{m_- - m_+}{m_-} = 1 - e^{\sigma(v_{p+}^2 - v_{p-}^2)/2} \quad (4.9)$$

The ablation model will be used later in Section 4.3.1 for hazard analysis to select candidate asteroids.

It should be noted that the aerobraking model in Eq. (4.4) is only valid when the mass loss of the captured asteroid is small, since the change in the momentum due to the mass loss is not taken into account in Eq. (4.4). To address this problem, a more accurate aerobraking model would be required. According to Newton's second law, one can get

$$F_d = -\frac{1}{2}\rho_a C_d A v^2 = \frac{d(mv)}{dt} \quad (4.10)$$

where F_d is the drag force; m and v are the mass and the velocity of the asteroid, respectively.

From Eq. (4.10), it can be shown that

$$\frac{1}{m} \frac{dm}{dt} v + \frac{dv}{dt} = -B \rho_a v^2 \quad (4.11)$$

Assuming that s is the distance along the aerobraking trajectory in the atmosphere [139], one can get

$$\frac{dv}{dt} = \frac{dv}{ds} \frac{ds}{dt} = \frac{dv}{ds} v, \quad \frac{dm}{dt} = \frac{dm}{ds} v \quad (4.12)$$

Therefore, Eq. (4.11) can be written as

$$\frac{1}{m} \frac{dm}{ds} v^2 + \frac{dv}{ds} v = -B \rho_a v^2 \quad (4.13)$$

$$\frac{1}{m} \frac{dm}{ds} + \frac{1}{v} \frac{dv}{ds} = -B \rho_a \quad (4.14)$$

From Eq. (4.6), it can be found that B is a function of the asteroid's diameter D and a small decrease in D can lead to a significant mass loss of the captured asteroid. For instance, for a captured asteroid with mass loss ratio f_m of about 50%, there is only a 20% decrease in its diameter D . Thus, for simplification, B is assumed to a constant during aerobraking. The general solution of Eq. (4.14) is

$$\int \frac{1}{m} dm ds + \int \frac{1}{v} dv ds = -\int B \rho_a ds \quad (4.15)$$

After some simple algebra, Eq. (4.15) reduces to

$$\ln \frac{m_+}{m_-} + \ln \frac{v_{p+}}{v_{p-}} = -B\rho\sqrt{2\pi r_p H_s(e+1)/e} \quad (4.16)$$

Substituting Eq. (4.8) in Eq. (4.16) yields

$$\frac{1}{2}\sigma(v_{p+}^2 - v_{p-}^2)/2 + \ln \frac{v_{p+}}{v_{p-}} = -B\rho\sqrt{2\pi r_p H_s(e+1)/e} \quad (4.17)$$

The accurate value of the velocity v_{p+} after aerobraking can then be obtained through Newton's method based on the initial guess in Eq. (4.4). With these assumptions and using Eq. (4.17), contour maps of the magnitude of the aerobraking manoeuvre imparted to the asteroid with respect to the asteroid's diameter D and the perigee height h above the Earth's surface are shown in Fig. 4.3 and Fig. 4.4.

From Fig. 4.3 and Fig. 4.4, it can be seen that once the height h at perigee above the Earth's surface is larger than approximately 100 km, the Earth's atmosphere can be assumed not to provide an aerobraking manoeuvre. Therefore, $h_{threshold} = 100$ km is defined as the height threshold for aerobraking, or $r_{threshold} = 6478$ km ($r_{Earth} + 100$ km) as the distance threshold for aerobraking, where $r_{Earth} = 6378$ km is the radius of the Earth.

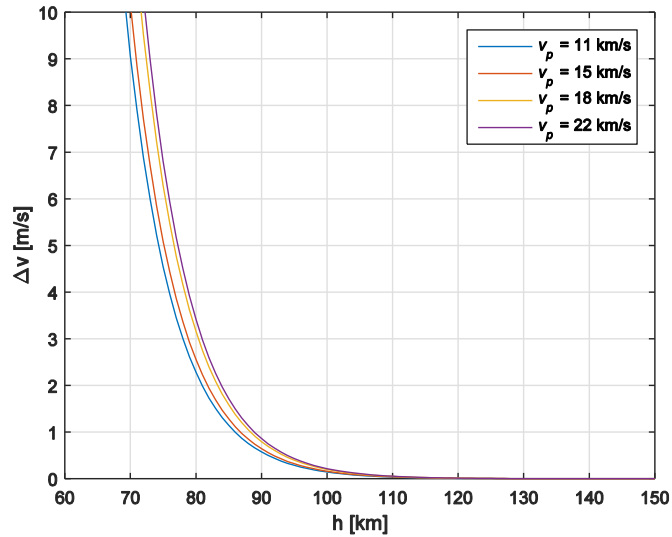


Fig. 4.3 Aerobraking Δv provided by the atmosphere as a function of height h and different relative velocities v_p of the asteroid, given an asteroid diameter of $D = 10$ m.

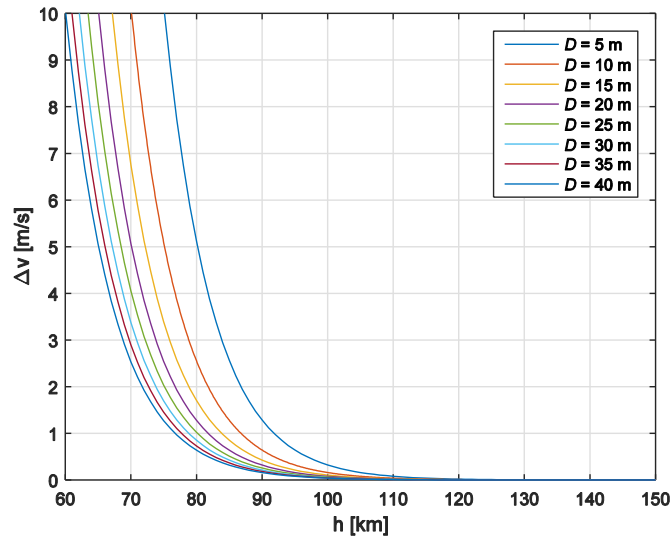


Fig. 4.4 Aerobraking Δv provided by the atmosphere as a function of height h and asteroid diameter D , given a perigee speed $v_p = 15$ km/s.

4.2.2 Earth flyby without aerobraking

When the candidate asteroid flies by the Earth at a high altitude above the Earth's surface ($h > 100$ km), the Earth's atmosphere cannot provide an aerobraking manoeuvre, as shown in Fig. 4.5. To be consistent with the asteroid capture strategy using aerobraking, an additional propulsive manoeuvre is assumed to be imposed on the candidate asteroid at the perigee of the flyby. This is because a manoeuvre at perigee can represent the most effective way to achieve the outgoing flyby orbit [190].

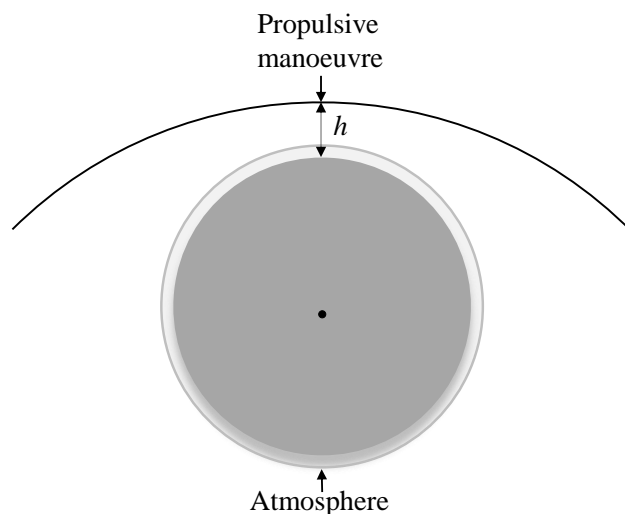


Fig. 4.5 Schematic diagram of an Earth flyby without aerobraking

4.3 Asteroid capture opportunities

4.3.1 Asteroid hazard analysis

When the candidate asteroid approaches the vicinity of the Earth, it again poses a potential (if small) impact risk. Undoubtedly, the grazing atmospheric pass for aerobraking will increase the possibility of impact. As discussed in Section 3.1.5, the Earth's atmosphere can protect against asteroids with a diameter of less than 30 m [179, 180]. Therefore, to reduce the threat of impact with the Earth, only those small asteroids with $D < 30$ m are considered as candidates for aerobraking, although again detailed risk assessment is required. In addition, if a mission to capture an asteroid with a diameter of 30 m fails and the asteroid's height at perigee with respect to the Earth is small enough to pose a threat of impact, the final mass of the asteroid after atmosphere entry and ablation can be estimated from Eq. (4.9). Figure 4.6 shows the mass loss ratio of a 30 m asteroid after aerobraking with a range of incident velocities relative to the Earth and a number of (low) perigee heights h with respect to the Earth's surface. As shown in Fig. 4.6, the aerobraking manoeuvre at low perigee heights (especially $h < 50$ km) can lead to significant mass loss, thereby potentially mitigating further risks of impact of the asteroid. However, the use of the analysis of Section 4.2 is clearly only approximate and it should be noted that complete ablation in the atmosphere may still lead to surface damage due to shock wave propagation [191].

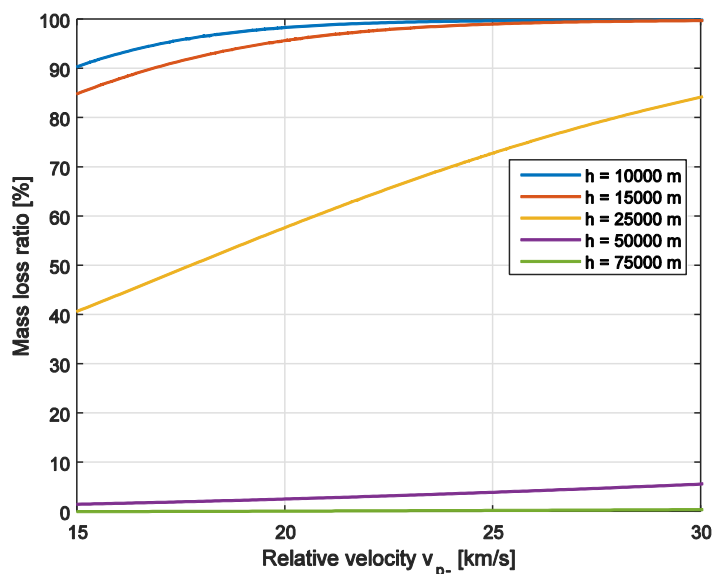


Fig. 4.6 Mass loss ratio of a 30 m asteroid after aerobraking with incident velocity with respect to the Earth

Furthermore, the natural average impact interval for asteroids can be estimated using an empirical scaling law [192]

$$T_{\text{impact}} = 3.71 \times 10^{-2} D^{2.377} \quad (4.18)$$

where the time interval is measured in years and the asteroid diameter is provided in meters. Figure 4.7 shows the corresponding natural average impact interval for asteroids with respect to the asteroid's diameter. As shown in the Fig. 4.7, the average impact interval for a 30 m asteroid is approximately 1 century. Therefore, the risk of capturing a similar body will add to the natural background risk, although again the risk is in principle small. It can also be considered that dis-assembling an asteroid prior to encounter, with a number of smaller fragments aerobraking individually, can reduce risks further. Considering $D < 30$ m, the candidate asteroids selected should again therefore be those asteroids with an absolute magnitude $H > 25.26$, as discussed in Section 3.1.5.

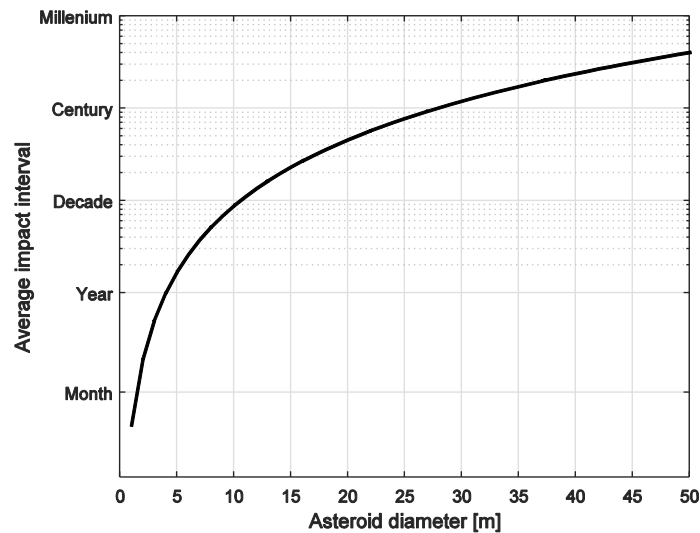


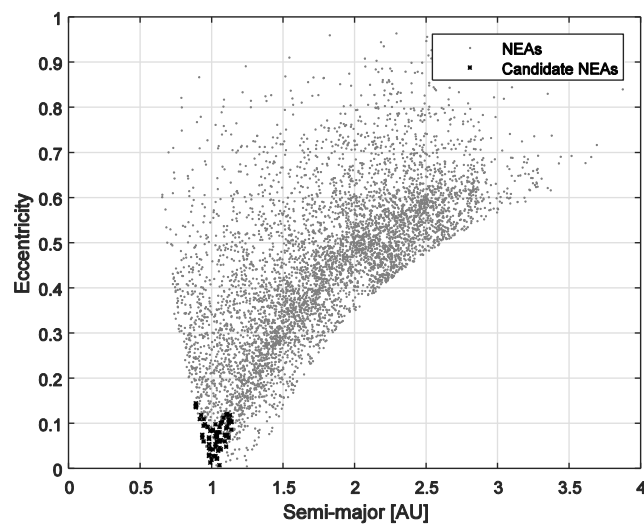
Fig. 4.7 Estimated average natural impact interval of asteroids versus asteroid diameter.

4.3.2 Candidate asteroids selection

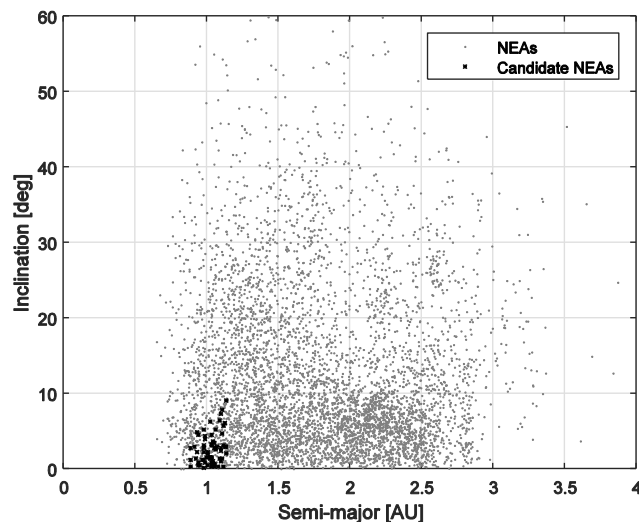
As discussed in Section 3.1.5, it is necessary to remove those asteroids with a high inclination and a semi-major axis far from that of the Earth's to capture NEAs with low energy. Therefore, those asteroids with a semi-major axis in the range 0.85-1.15 AU are considered to be candidates which can be captured into the vicinity of the Earth with a relatively low energy [43]. Furthermore, the Jacobi constant J of the asteroid can be approximated by the Tisserand parameter as follows [162]

$$J \approx 1/a + 2\sqrt{a(1-e^2)} \cos i \quad (4.19)$$

where a , e and i are the semi-major axis (in AU), eccentricity and inclination of the asteroid orbit. If an asteroid's Jacobi constant is significantly different from that of the final periodic orbit, it may have too high a total cost for capture [18]. It should therefore be possible to achieve low energy capture with a Jacobi constant close to the Jacobi constant of the target periodic orbit. As discussed in Section 3.2, it can be seen that the Jacobi constant of the target periodic orbits is in the range [2.999, 3.0009]. Therefore, here $J = 2.99$ is arbitrarily set as the critical value. Those asteroids with $J \geq 2.99$ are then considered to be candidate asteroids. Considering the filters stated above, the candidate asteroids should be those asteroids with $H \geq 25.26$, $J \geq 2.99$ and $a \in [0.85, 1.15]$, as shown in Fig. 4.8.



(a)



(b)

Fig. 4.8 Distribution of candidate asteroids: (a) semi-major and eccentricity and (b) semi-major and inclination.

4.3.3 Asteroid capture window

For each of these candidate NEAs, feasible capture dates are again assumed to be in the interval 2019–2050 (or 58484 MJD - 70171 MJD). As discussed in Section 3.1.5, the asteroid capture window is a time period during which the asteroid orbital elements are valid until it approaches the Earth. In this Chapter, it is assumed that the upper limit of the asteroid capture window is the date when the distance of the candidate asteroid from the Earth is 0.21 AU, where the gravitational attraction of the Earth is then considered small enough with respect to the gravity of the Sun (the ratio of Earth’s and Sun’s gravity is then less than 10^{-4}). Denoting the date when the asteroid has a distance from the Earth of 0.21 AU as $T_{threshold}$ ($T_{threshold} \leq 2050$), the capture window of a candidate asteroid is then $[2019, T_{threshold}]$, shown in Fig. 4.9.

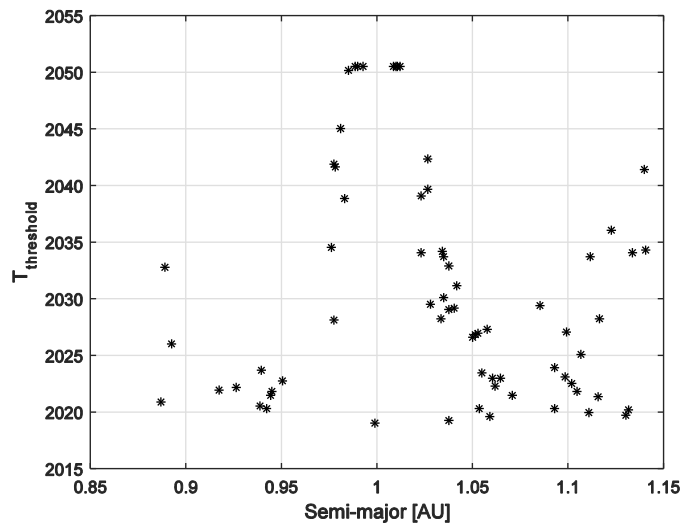


Fig. 4.9 $T_{threshold}$ of candidate asteroids

4.4 Asteroid capture using Earth flyby without aerobraking

4.4.1 Problem statement

In this capture strategy, a flyby of the Earth without aerobraking is used. The candidate asteroid leaves its orbit with an impulse manoeuvre and approaches the vicinity of the Earth for the flyby. At the perigee of the flyby, an additional manoeuvre is imposed on the candidate asteroid. This is because a manoeuvre at perigee can represent the most effective way to achieve the outgoing flyby orbit [190]. Finally, the asteroid moves onto the stable

manifold of a target periodic orbit around the Sun-Earth L_1 or L_2 points and will be asymptotically captured onto it. In this scenario, a manoeuvring spacecraft is first assumed to be attached to the target asteroid before the first manoeuvre and will then stay attached to the asteroid for the entire mission. All propulsive manoeuvres will be provided by the manoeuvring spacecraft. It should be noted that the entire transfer trajectory is modelled in the Sun-Earth CRTBP.

Figure 4.10 shows a schematic of the asteroid capture strategy using an Earth flyby without aerobraking. The basic concept of the asteroid capture strategy is through the following steps:

- (1) With an initial manoeuvre Δv_1 , the candidate asteroid leaves its initial orbit and its motion can then be described by the Sun-Earth CRTBP, shown in Fig. 4.10(a);
- (2) With a second manoeuvre Δv_2 , the asteroid approaches the vicinity of the Earth and then reaches perigee, shown in Fig. 4.10(b);
- (3) At the perigee, a third manoeuvre Δv_3 , which is parallel to the asteroid's current velocity vector, is applied to the asteroid and the asteroid then moves onto the stable manifold of a Sun-Earth L_1 or L_2 periodic orbit and so will asymptotically transfer onto it, shown in Fig. 10(b).

The total cost of capturing an asteroid onto the target periodic orbit around the Sun-Earth L_1 or L_2 points can then be written as

$$\Delta v = \Delta v_1 + \Delta v_2 + \Delta v_3 \quad (4.20)$$

Therefore, for each candidate asteroid, six parameters can determine the asteroid capture manoeuvre using an Earth flyby without aerobraking, as defined in Fig. 4.10 and described as follows:

- T_0 : epoch when the first manoeuvre is applied to the candidate asteroid;
- T_{fly1} : flight time between the first manoeuvre and the second manoeuvre;
- T_{fly2} : flight time between the second manoeuvre and the third manoeuvre;
- A_p : amplitude variable of the target Sun-Earth L_1 or L_2 periodic orbit;
- t_p : time t_p determining the point along the Lyapunov orbit where the stable manifold of the target Lyapunov orbit is propagated backward from and where $t_p \in [0 T_p]$ where T_p is the period of the final target orbit;
- Δv_3 : third manoeuvre that is parallel to the velocity vector of the asteroid at the perigee.

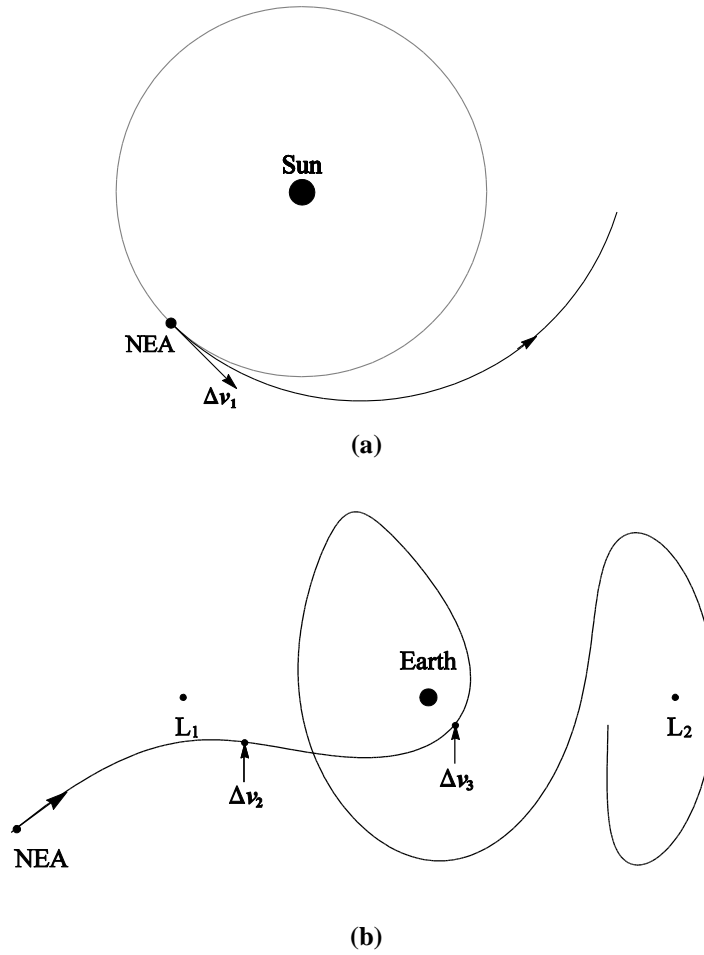


Fig. 4.10 Schematic strategy for asteroid capture using Earth flyby without aerobraking: (a) the candidate asteroid leaves its orbit with the first manoeuvre; (b) the candidate asteroid is inserted onto the stable manifold after the Earth flyby.

4.4.2 Initial guess and differential correction

A differential correction method will be utilised to design the transfer trajectory between the candidate asteroid's initial orbit and the target point where the second manoeuvre Δv_2 is applied to the asteroid in the following section. It is assumed that the asteroid initial state is $\mathbf{X}_i = [x_i, y_i, z_i, \dot{x}_i, \dot{y}_i, \dot{z}_i]^T$ and then the final state after flight time T is $\mathbf{X}_f' = [x_f', y_f', z_f', \dot{x}_f', \dot{y}_f', \dot{z}_f']^T$. Assuming that the state of the target point is $\mathbf{X}_f = [x_f, y_f, z_f, \dot{x}_f, \dot{y}_f, \dot{z}_f]^T$, the condition such that $\delta \mathbf{X}_f = [\delta x_f, \delta y_f, \delta z_f, 0, 0, 0]^T = \mathbf{0}$ (i.e. $[x_f - x_f', y_f - y_f', z_f - z_f', 0, 0, 0]^T = \mathbf{0}$) can be sought by correcting the initial velocity vector $\delta \mathbf{X}_i = [0, 0, 0, \delta \dot{x}_i, \delta \dot{y}_i, \delta \dot{z}_i]^T$ as follows

$$\delta \mathbf{X}_i = \Phi^{-1} \delta \mathbf{X}_f \quad (4.21)$$

where Φ is the 6×6 state transition matrix of the CRTBP (See Section 2.2.3).

A heliocentric Sun-centred two-body Lambert arc with two impulsive manoeuvres can be used to provide an initial guess, where the first impulse is applied and the asteroid transfers to the Sun-Earth stable manifold. The differential correction defined by Eq. (4.21) uses this initial guess and then the correction is repeated until $\delta \mathbf{r}_f = [\delta x_f, \delta y_f, \delta z_f]^T$ approaches $\mathbf{0}$, within some small tolerance.

4.4.3 Design Procedure

The process of designing the transfer trajectory to capture the candidate asteroid using an Earth flyby without aerobraking is as follows:

- (1) Select one target asteroid in the candidate catalogue (e.g. 2010 UJ) in Fig. 4.8;
- (2) Given the amplitude variable A_p of a periodic orbit and the parameter t_p , the stable manifold associated with the final periodic orbit is propagated backward within a given propagation time (e.g. 400 days); the perigee where the third manoeuvre Δv_3 is applied to the asteroid can then be determined, corresponding to the perigee along the stable manifold with the closest distance to the Earth and a height above the Earth's surface larger than 100 km. Then, the state $\mathbf{X}_{p^+} = [x_p, y_p, z_p, \dot{x}_p, \dot{y}_p, \dot{z}_p]^T$ at perigee is obtained, shown in Fig. 4.11;
- (3) Given the value of the third manoeuvre Δv_3 at perigee, the state before the third manoeuvre is $\mathbf{X}_{p^-} = [x_p, y_p, z_p, \lambda \dot{x}_p, \lambda \dot{y}_p, \lambda \dot{z}_p]^T$ where $\lambda = 1 + \Delta v_3 / (\dot{x}_p^2 + \dot{y}_p^2 + \dot{z}_p^2)^{1/2}$;
- (4) Given the flight time T_{fly2} , the state \mathbf{X}_{p^-} is propagated backward and then the target point \mathbf{X}_f is obtained, shown in Fig. 4.12;
- (5) Given a departure date T_0 , the transformation of the initial state of the candidate asteroid in the Sun-centred inertial frame to the Sun-Earth rotating frame \mathbf{X}_i is then obtained;
- (6) Given the flight time T_{fly1} , the Lambert arc in the Sun-centred two-body problem is utilised to design the transfer to the stable manifold from the candidate asteroid's orbit and so the first impulse can be estimated; based on the initial guess of the first impulse, the differential correction method in Eq. (4.21) is then applied to

design the transfer between the candidates asteroid's initial orbit X_i and the target point X_f . Thus, the manoeuvres Δv_1 and Δv_2 can be calculated.

The total cost of capturing the asteroid onto a Sun-Earth L_1 or L_2 periodic orbit using the Earth flyby can then be obtained, where the entire transfer trajectory is shown in Fig. 4.13 and Fig. 4.14.

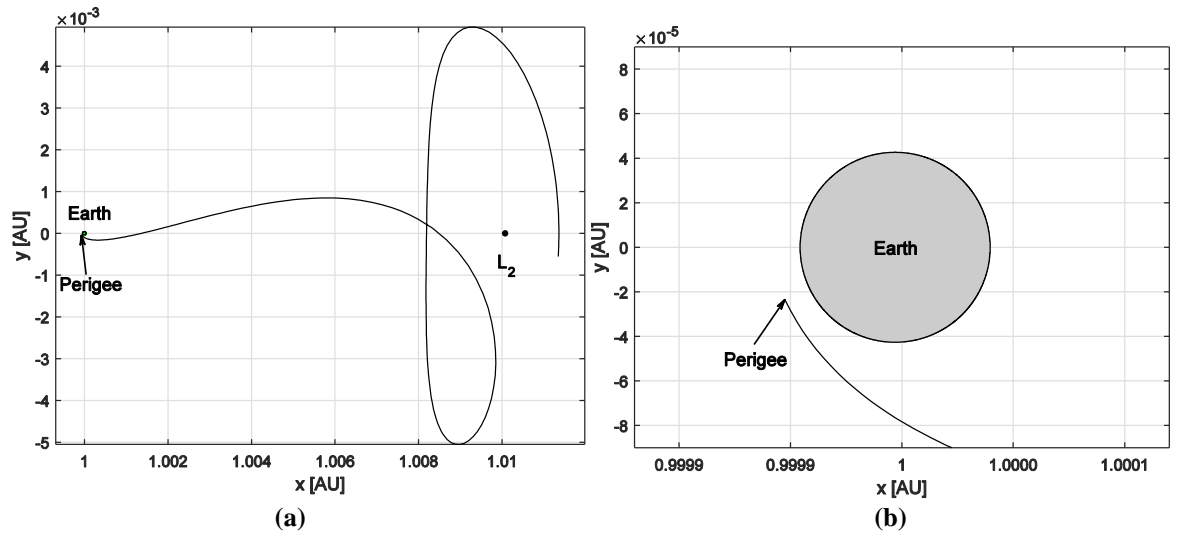


Fig. 4.11 Given $A_p = 0.0018878$, $t_p = 1.637679$, perigee of the stable manifold associated with the Sun-Earth L_2 Lyapunov orbit: (a) global view; (b) local view.

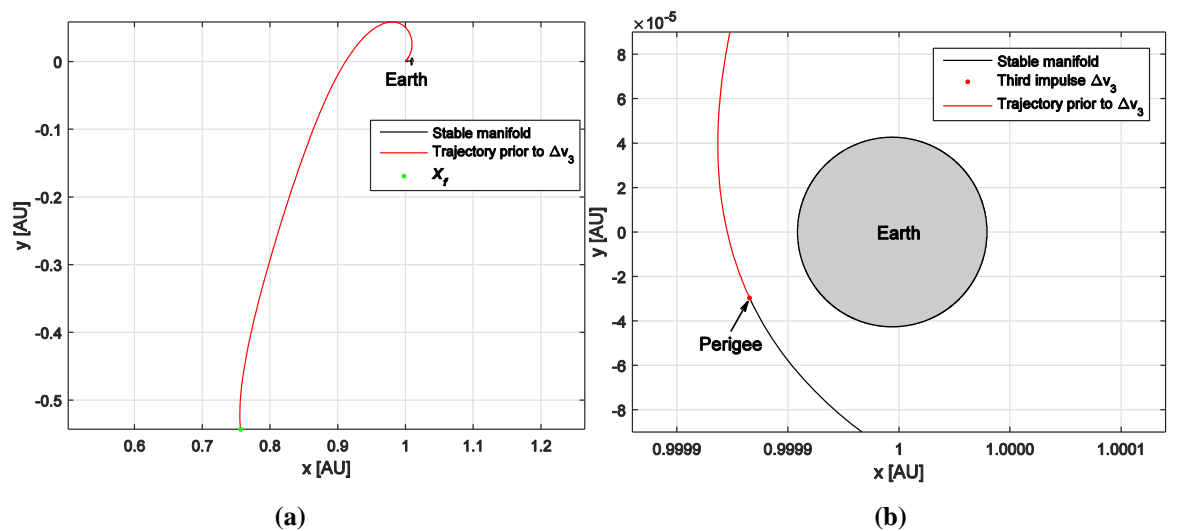


Fig. 4.12 Given $\Delta v_3 = 185.96$ m/s and $T_{fly2} = 270.58$ days, the trajectory prior to Δv_3 is obtained by propagating backward from the state at perigee: (a) global view; (b) local view.

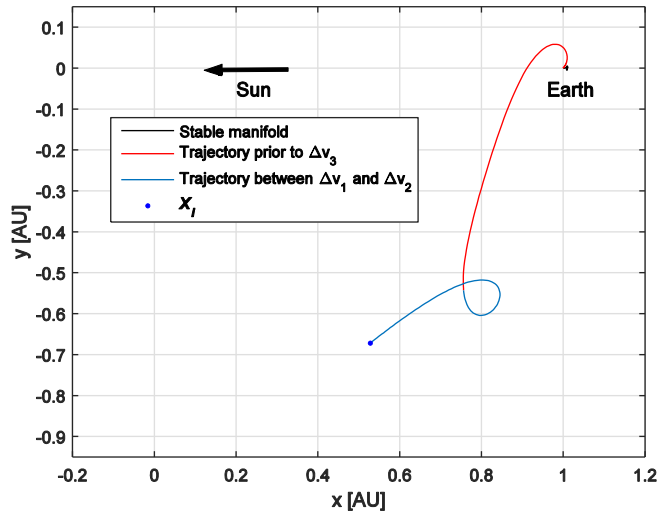


Fig. 4.13 Given $T_0 = 58977.85$ [MJD], $T_{fly1} = 285.87$ days, the transfer trajectory (x - y projection) to capture 2010 UJ onto a Sun-Earth L_2 Lyapunov orbit in the Sun-Earth rotating frame.

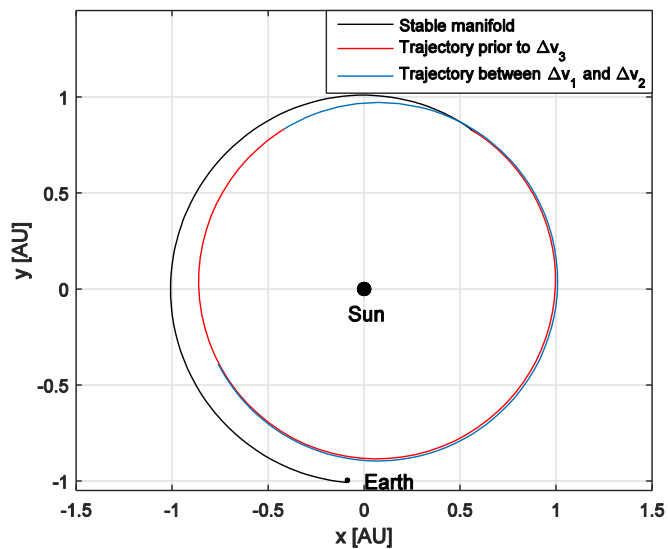


Fig. 4.14 Transfer trajectory (x - y projection) for capturing 2010 UJ onto the Sun-Earth L_2 Lyapunov orbit in the Sun-centred inertial frame.

4.4.4 Optimisation

For each of these candidate asteroids, there are 6 parameters, so the problem can be defined with the following variables: departure date T_0 , flight time T_{fly1} , flight time T_{fly2} , the amplitude variable A_p of the target periodic orbit, a variable t_p associated with the state on the target orbit where the stable manifold is integrated from and the value of the third manoeuvre Δv_3 that is parallel to the velocity vector of the asteroid at perigee of the flyby orbit. As the objective function for this optimisation problem, the total cost Δv can be minimised by optimising over these 6 parameters $(T_0, T_{fly1}, T_{fly2}, A_p, t_p, \Delta v_3)$ using NSGA-II

[182]. Then transfers obtained with NSGA-II can be locally optimised with the function *fmincon* in MATLAB. The optimal results of asteroid capture using the Earth flyby without aerobraking are shown in Table 4.1 and Table 4.2. From Table 4.1 and Table 4.2, it can be seen that some asteroids can be captured into Lyapunov orbits around the Sun-Earth libration points with lower cost than others, e.g. 2008 EL68 and 2010 UJ. However, the Earth flyby can achieve a lower-energy capture of asteroids into halo orbits, especially capturing 2008 JL24 and 2015 PS228.

Table 4.1 Results of capturing asteroids onto Sun-Earth L_1 or L_2 Lyapunov orbits using an Earth flyby without aerobraking

Asteroid	Total cost, m/s	Epoch, MJD	Total flight time, days	Amplitude variable A_p , 10^{-3} AU	Diameter D , m	Target point
2003 WT153	695.95	58585.2	425.5	1.8448	8.5	L_2
2006 UQ216	1391.82	58722.7	1328.6	6.4591	11.7	L_1
2007 UN12	218.86	58717.9	736.2	7.2695	6.2	L_1
2008 EL68	269.64	66206.9	776.3	7.4623	9.8	L_1
2008 JL24	786.29	59380.1	1372.2	7.6082	4.1	L_1
2009 YR	1155.95	58555.1	778	3.6533	8.5	L_1
2009 YR	1128.36	58569.3	474.4	3.8028	8.5	L_2
2010 UJ	505.97	59060.7	824.3	6.8335	19.5	L_1
2010 UJ	511.75	58977.8	769.3	1.8878	19.5	L_2
2010 UY7	713.92	61552.9	631.2	6.3898	6.8	L_2
2011 BQ50	611.51	58850.4	1580.3	7.9646	8.5	L_1
2011 CL50	558.04	58726.1	892.4	7.0928	10.2	L_2
2012 HG2	524.32	60396	693.9	6.6383	13.5	L_1
2012 WR10	466.24	61065.3	1677.6	6.6175	6.2	L_1
2014 JR24	1105.95	59577.5	1601.2	6.6969	4.7	L_1
2014 QN266	556.92	59719.6	1841.2	7.4758	18.6	L_1
2014 QN266	763.76	61272.8	390.9	9.0648	18.6	L_2
2015 PS228	713.31	61972.7	1653.6	6.2328	5.5	L_1

Table 4.2 Results of capturing asteroids onto Sun-Earth L₁ or L₂ Halo orbits using an Earth flyby without aerobraking

Asteroid	Total cost, m/s	Epoch, MJD	Total flight time, days	Amplitude variable A_p , 10^{-3} AU	Diameter D , m	Target point
2003 WT153	762.26	58614.6	392.2	0.6752	8.5	L ₂
2006 UQ216	1451.83	61491.9	886.3	1.5772	11.7	L ₁
2007 UN12	215.23	58486.8	845.2	-0.5260	6.2	L ₁
2008 EL68	421.35	65853.8	921.3	-0.2882	9.8	L ₁
2008 JL24	671.16	58617.2	1991.1	1.5423	4.1	L ₁
2009 YR	1205.26	58780.1	670.7	-1.5612	8.5	L ₁
2009 YR	1284.12	63604.5	1220.9	-1.2928	8.5	L ₂
2010 UJ	907.65	59289.6	759.6	0.5108	19.5	L ₁
2010 UJ	685.37	58630.5	1119.1	0.4842	19.5	L ₂
2010 UY7	774.02	61216.5	760.1	0.4272	6.8	L ₂
2011 BQ50	804.98	59444.4	822.1	0.4194	8.5	L ₁
2011 CL50	798.42	58731.3	723.2	-0.1338	10.2	L ₂
2012 HG2	524.42	60002.8	967.8	-0.06090	13.5	L ₁
2012 WR10	450.01	61328.1	1330.1	-1.2109	6.2	L ₁
2014 JR24	1036.19	60219.7	904.8	1.4263	4.7	L ₁
2014 QN266	590.94	61278.9	506	-0.3253	18.6	L ₁
2014 QN266	735.53	60634.9	1448.5	0.6632	18.6	L ₂
2015 PS228	421.37	62328.1	1287.1	1.5666	5.5	L ₁

4.4.5 Comparison of the results of asteroid capture with and without Earth flyby

According to the work of Yárnnoz, et al. [50] and Sánchez and Yárnnoz [18], a candidate asteroid can be captured directly from its orbit to the stable manifold of the target Sun-Earth L₁ or L₂ periodic orbit, where this asteroid capture strategy has been discussed in Section 3.2. In this Chapter, to avoid too long a flight time for capturing asteroids, Lambert arcs with up to 3 complete revolutions from the asteroid initial orbit to the stable manifold are considered. In this capture strategy, there are 5 parameters: $(T_0, T_f, t_{sm}, A_{SE}, t_{p1})$. Then

the total Δv can be minimised by optimising over these 5 parameters using NSGA-II. Transfers obtained with NSGA-II can again be locally optimised with the function *fmincon* in MATLAB. The optimal results of asteroid capture using the Earth flyby without aerobraking are shown in Table 1. The optimal results for asteroid capture without an Earth flyby are also listed in Table 4.3 and Table 4.4.

Table 4.3 Results of capturing asteroids onto Sun-Earth L_1 or L_2 Lyapunov orbits without using an Earth flyby

Asteroid	Total cost, m/s	Epoch, MJD	Total flight time, days	Amplitude variable A_p , 10^{-3} AU	Diameter D , m	Target point
2003 WT153	1973.55	58485.6	1049.7	7.6117	8.5	L_1
2006 UQ216	1714.17	61535.1	945.6	6.6708	11.7	L_2
2007 UN12	314.74	58543.7	827.7	5.883	6.2	L_2
2008 EL68	774.66	62767.9	1988.9	7.2019	9.8	L_2
2008 JL24	951.05	59445.3	1698	7.7028	4.1	L_2
2008 UA202	454.04	60329.7	1704.9	7.225	4.5	L_2
2009 YR	1378.33	58498.1	1392.1	6.7619	8.5	L_1
2010 JR34	1591.37	59349.7	1847.6	7.853	9.8	L_1
2010 UJ	824.19	58542.2	1790.2	7.6013	19.5	L_1
2010 UY7	1691.04	61130.6	2157.3	7.9587	6.8	L_1
2010 VQ	2386.46	59010.1	2954.5	4.1326	9.8	L_1
2011 BQ50	697.01	59439.5	852.5	6.8243	8.5	L_1
2011 CL50	1584.04	58931.9	1035.8	6.9948	10.2	L_2
2012 HG2	1921.56	60589.7	2629.7	5.7497	13.5	L_2
2012 WR10	921.84	60935.4	1754.2	5.8587	6.2	L_2
2014 AA	3420.17	58498.9	1416.6	2.9571	2.2	L_2
2014 JR24	1315.09	58817.3	2711.4	5.6231	4.7	L_2
2014 QN266	783.27	58571.3	2517.4	5.5207	18.6	L_2
2014 UV210	1753.41	58553.7	3005.3	2.9632	14.1	L_1
2014 WE6	1376.41	62097.6	1584.7	7.6019	2.8	L_2
2014 WX202	409.31	62264.2	1920.7	8.7576	4.1	L_2

Table 4.4 Results of capturing asteroids onto Sun-Earth L₁ or L₂ halo orbits without using an Earth flyby

Asteroid	Total cost, m/s	Epoch, MJD	Total flight time, days	Amplitude variable A_p , 10^{-3} AU	Diameter D , m	Target point
2003 WT153	2282.39	58484.4	1587.7	-3.2683	8.5	L ₁
2006 UQ216	1796.57	60195.9	1826.7	-4.5544	11.7	L ₂
2007 UN12	310.64	58673.9	655.7	3.3418	6.2	L ₂
2008 EL68	906.11	65704.8	1820.9	3.7911	9.8	L ₂
2008 JL24	1020.53	59586.7	2130.4	-4.836	4.1	L ₂
2008 UA202	415.96	59524.1	1959.2	-2.8832	4.5	L ₂
2009 YR	1311.25	58504.4	841.5	-0.7273	8.5	L ₁
2010 JR34	1620.25	59697.9	2050	4.9686	9.8	L ₁
2010 UJ	883.84	58484	1965	-3.4413	19.5	L ₁
2010 UY7	1776.82	58960.8	2293.4	4.747	6.8	L ₁
2010 VQ	2554.3	58565	1547	2.4473	9.8	L ₁
2011 BQ50	1009.23	59272.3	1267.7	-4.1162	8.5	L ₁
2011 CL50	1672.19	58635.7	1903	1.489	10.2	L ₂
2012 HG2	2050.83	58842.7	1376.1	1.058	13.5	L ₂
2012 WR10	1054.66	61347.3	1279.8	3.0741	6.2	L ₂
2014 AA	3364.1	58498.5	1450.5	4.7422	2.2	L ₂
2014 JR24	1308.21	59235.6	2621.2	-4.544	4.7	L ₂
2014 QN266	920.22	60697.7	1423.2	2.095	18.6	L ₂
2014 UV210	1947	58559.7	2986.8	-3.1312	14.1	L ₁
2014 WE6	1532.96	60388.4	1995.8	4.2308	2.8	L ₂
2014 WX202	323.58	61429.6	2032.4	-4.1198	4.1	L ₂

Comparing the results of Tables 4.1-4.4, it can be noted that the asteroid capture strategy using an Earth flyby has the potential to be cheaper in terms of Δv than the capture strategy without the Earth flyby, especially for 2011 CL50, 2012 HG2 and 2012 WR10. Moreover, since asteroid capture using an Earth flyby does not require significantly more time for the captured asteroid to travel along the stable manifold of the Sun-Earth L₁ or L₂ periodic orbit, this capture strategy also has the potential to achieve quicker transfers, e.g.

2003 WT153, 2010 UJ and 2011 CL50. Moreover, some candidate asteroids can be simultaneously captured with low energy onto periodic orbits both around the Sun-Earth L_1 and L_2 points, e.g. 2009 YR, 2010 UJ and 2014 QN266. Therefore, the Earth flyby can be regarded as a way of increasing asteroid capture opportunities. However, one drawback of the asteroid capture strategy using an Earth flyby is that the asteroid flies by the Earth at a relatively high velocity and thus we have limited time to apply the third manoeuvre to the asteroid at the perigee of the flyby orbit. Therefore, in principle a high thrust engine would be required to achieve the third manoeuvre in a realistic mission scenario.

4.5 Asteroid capture using aerobraking

In this capture strategy using aerobraking, the candidate asteroid is firstly assumed to leave its orbit with an impulse manoeuvre and approach the vicinity of the Earth for a single aerobraking pass. During the flyby of the Earth, the Earth's atmosphere provides drag to modify the asteroid orbit without the use of propellant. Again, after the flyby of the Earth, the candidate asteroid moves onto the stable manifold of a periodic orbit around the Sun-Earth L_1 or L_2 points.

4.5.1 Problem statement

Figure 4.15 shows the concept of asteroid capture using aerobraking as follows:

- (1) With a first manoeuvre Δv_1 , the candidate asteroid departs from its initial orbit and its motion can be described by the Sun-Earth CRTBP, shown in Fig. 4.15(a);
- (2) With a second manoeuvre Δv_2 , the asteroid approaches the vicinity of the Earth and accordingly it reaches perigee;
- (3) An aerobraking manoeuvre is applied to the candidate asteroid and then the asteroid moves onto the stable manifold of a periodic orbit around the Sun-Earth L_1 or L_2 points and will finally be captured, shown in Fig. 4.15(b).

The total cost of capturing the candidate asteroid onto the target periodic orbit around the Sun-Earth L_1 or L_2 points can then be written as

$$\Delta v = \Delta v_1 + \Delta v_2 \quad (4.22)$$

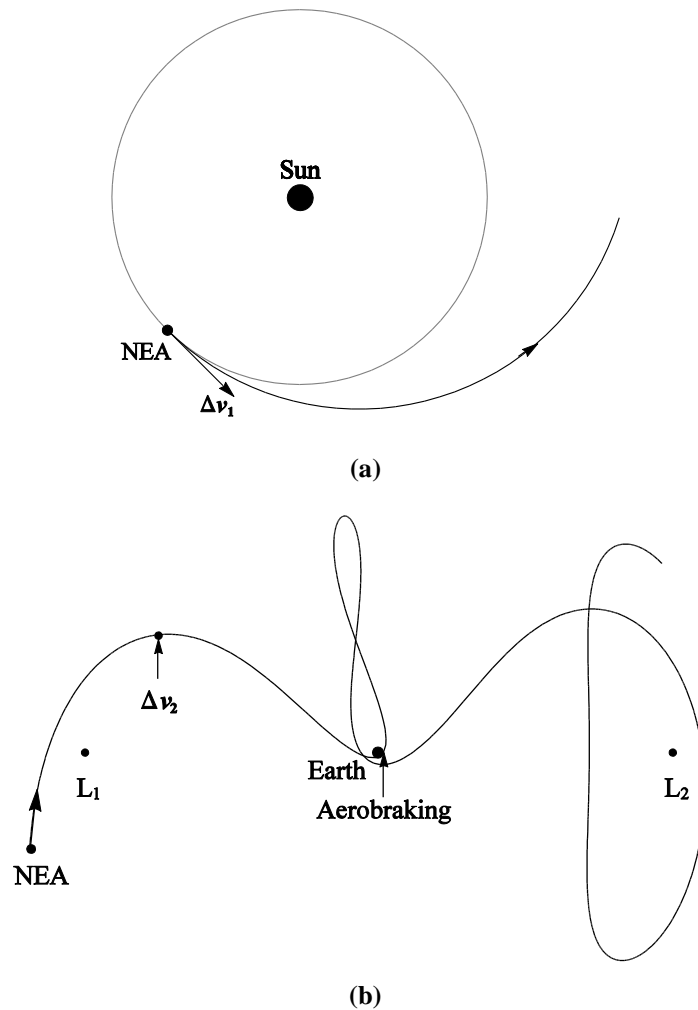


Fig. 4.15 Schematic strategy for asteroid capture using aerobraking: (a) the candidate asteroid leaves its orbit with the first manoeuvre; (b) the candidate asteroid is inserted onto the stable manifold after aerobraking.

Hence, for each candidate asteroid, there now are 5 parameters to describe the sequence of manoeuvres as follows:

- T_0 : epoch when the asteroid departs from its initial orbit;
- T_{fly1} : flight time between the first manoeuvre and the second manoeuvre;
- T_{fly2} : flight time between the second manoeuvre and the aerobraking phase;
- A_p : amplitude variable of the final periodic orbit around the Sun-Earth L_1 or L_2 points;
- t_p : time associated with the point on the periodic orbit where the stable manifold is integrated from where $t_p \in [0 T_p]$, where T_p is the period of the final periodic orbit.

4.5.2 Aerobraking phase

The aim of this Section is to transform the aerobraking model (Eq. (4.17)) from the Earth-centred inertial frame to the Sun-Earth rotating frame. Assuming that the states of the candidate asteroid before and after aerobraking in the Earth-centred inertial frame are given by $\mathbf{X}_{p^-}^E = [x_{p^-}^E, y_{p^-}^E, z_{p^-}^E, \dot{x}_{p^-}^E, \dot{y}_{p^-}^E, \dot{z}_{p^-}^E]^T$ and $\mathbf{X}_{p^+}^E = [x_{p^+}^E, y_{p^+}^E, z_{p^+}^E, \dot{x}_{p^+}^E, \dot{y}_{p^+}^E, \dot{z}_{p^+}^E]^T$, respectively, then

$$\frac{\mathbf{V}_{p^+}}{\mathbf{V}_{p^-}} = \frac{v_{p^+}}{v_{p^-}}, \mathbf{r}_{p^+} = \mathbf{r}_{p^-} \quad (4.23)$$

where $\mathbf{V}_{p^-} = [\dot{x}_{p^-}^E, \dot{y}_{p^-}^E, \dot{z}_{p^-}^E]^T$, $\mathbf{V}_{p^+} = [\dot{x}_{p^+}^E, \dot{y}_{p^+}^E, \dot{z}_{p^+}^E]^T$, $\mathbf{r}_{p^-} = [x_{p^-}^E, y_{p^-}^E, z_{p^-}^E]^T$, $\mathbf{r}_{p^+} = [x_{p^+}^E, y_{p^+}^E, z_{p^+}^E]^T$ and e is the eccentricity of the flyby orbit before aerobraking.

Here it is assumed that aerobraking only provides a limited manoeuvre and thus $e_- \approx e_+$ where e_+ is the eccentricity of the flyby orbit after aerobraking. Therefore, the velocity before aerobraking can be guessed as

$$\mathbf{V}_{p^-} \approx e^{B\rho\sqrt{2\pi r_p H_s (e_+ + 1)/e_+}} \mathbf{V}_{p^+} \quad (4.24)$$

The accurate value of the velocity \mathbf{V}_{p^-} before aerobraking can then be obtained in Eq. (4.17) through Newton's method based on the initial guess in Eq. (4.24).

It is assumed that the states of the candidate asteroid before and after aerobraking in the Sun-Earth rotating frame are then $\mathbf{X}_{p^-} = [x_{p^-}, y_{p^-}, z_{p^-}, \dot{x}_{p^-}, \dot{y}_{p^-}, \dot{z}_{p^-}]^T$ and $\mathbf{X}_{p^+} = [x_{p^+}, y_{p^+}, z_{p^+}, \dot{x}_{p^+}, \dot{y}_{p^+}, \dot{z}_{p^+}]^T$, respectively. Thus, it can be seen that

$$\mathbf{V}_{p^+} = \mathbf{KR}(\beta)(\mathbf{X}_{p^+} - \mathbf{X}_{Earth}) \quad (4.25)$$

$$\mathbf{V}_{p^-} = \mathbf{KR}(\beta)(\mathbf{X}_{p^-} - \mathbf{X}_{Earth}) \quad (4.26)$$

where $\mathbf{R}(\beta)$ is a coordinate transformation matrix from Eq. (2.14) in Section 2.2 and

$$\mathbf{S}_{Earth} = [1 - \mu_{se}, 0, 0, 0, 0, 0]^T, \mathbf{K} = \begin{bmatrix} 0 & 0 & 0 & 1 & 0 & 0 \\ 0 & 0 & 0 & 0 & 1 & 0 \\ 0 & 0 & 0 & 0 & 0 & 1 \end{bmatrix} \quad (4.27)$$

Defining $\gamma = v_{p^-} / v_{p^+}$, Eq. (4.23) can be written as

$$\mathbf{KR}(\beta)(\mathbf{X}_{p^-} - \mathbf{X}_{Earth}) = \gamma \mathbf{KR}(\beta)(\mathbf{X}_{p^+} - \mathbf{X}_{Earth}) \quad (4.28)$$

Then, after adding $\mathbf{R}^{-1}(\beta)\mathbf{K}^T$ to both sides of the Eq. (4.28), it can be seen that

$$\mathbf{R}^{-1}(\beta)\mathbf{K}^T\mathbf{KR}(\beta)(\mathbf{X}_{p^-} - \mathbf{X}_{Earth}) = \gamma \mathbf{R}^{-1}(\beta)\mathbf{K}^T\mathbf{KR}(\beta)(\mathbf{X}_{p^+} - \mathbf{X}_{Earth}) \quad (4.29)$$

Letting $\mathbf{M} = \mathbf{R}^{-1}(\beta)\mathbf{K}^T\mathbf{KR}(\beta)$, Eq. (4.29) can be simplified as

$$\mathbf{M}(\mathbf{X}_{p^-} - \mathbf{X}_{Earth}) = \gamma \mathbf{M}(\mathbf{X}_{p^+} - \mathbf{X}_{Earth}) \quad (4.30)$$

where

$$\mathbf{M} = \begin{bmatrix} 0 & 0 & 0 & 0 & 0 & 0 \\ 0 & 0 & 0 & 0 & 0 & 0 \\ 0 & 0 & 0 & 0 & 0 & 0 \\ 0 & -1 & 0 & 1 & 0 & 0 \\ 1 & 0 & 0 & 0 & 1 & 0 \\ 0 & 0 & 0 & 0 & 0 & 1 \end{bmatrix}$$

Equation (4.30) only contains information on the velocity vector when aerobraking. Hence, Eq. (4.30) and the position vector in Eq. (4.23) can be combined together as follows,

$$\mathbf{M}_1(\mathbf{X}_{p^-} - \mathbf{X}_{Earth}) = \mathbf{M}_2(\mathbf{X}_{p^+} - \mathbf{X}_{Earth}) \quad (4.31)$$

Thus,

$$\mathbf{X}_{p^-} = \mathbf{M}_1^{-1}\mathbf{M}_2(\mathbf{X}_{p^+} - \mathbf{X}_{Earth}) + \mathbf{X}_{Earth} \quad (4.32)$$

where

$$\mathbf{M}_1 = \begin{bmatrix} 1 & 0 & 0 & 0 & 0 & 0 \\ 0 & 1 & 0 & 0 & 0 & 0 \\ 0 & 0 & 1 & 0 & 0 & 0 \\ 0 & -1 & 0 & 1 & 0 & 0 \\ 1 & 0 & 0 & 0 & 1 & 0 \\ 0 & 0 & 0 & 0 & 0 & 1 \end{bmatrix}, \mathbf{M}_2 = \begin{bmatrix} 1 & 0 & 0 & 0 & 0 & 0 \\ 0 & 1 & 0 & 0 & 0 & 0 \\ 0 & 0 & 1 & 0 & 0 & 0 \\ 0 & -\gamma & 0 & \gamma & 0 & 0 \\ \gamma & 0 & 0 & 0 & \gamma & 0 \\ 0 & 0 & 0 & 0 & 0 & \gamma \end{bmatrix}$$

Therefore, the state of the captured asteroid at perigee before the aerobraking phase in the Sun-Earth rotating frame can be estimated by the state of the asteroid after aerobraking in the Sun-Earth rotating frame using the Eq. (4.32).

4.5.3 Aerobraking opportunities for periodic orbits

For some periodic orbits around the Sun-Earth L_1 or L_2 points, their associated stable manifolds may not pass through the Earth's atmosphere within a given stable manifold transfer time (t_{sm}) (see Section 3.3.1). An example is shown in Fig. 4.16. Therefore, it is necessary to exclude these periodic orbits which are not suitable for aerobraking from the solution space. Here it is assumed that the stable manifold transfer time (t_{sm}) is chosen from 0 to 400 days. The minimum distance between the stable manifolds associated with a periodic orbit (determined by the amplitude variable A_p) is denoted as r_{min} . As discussed in Section 4.2.1, once $r_{min} < r_{threshold} = 6478$ km, the periodic orbit can provide opportunities for aerobraking.

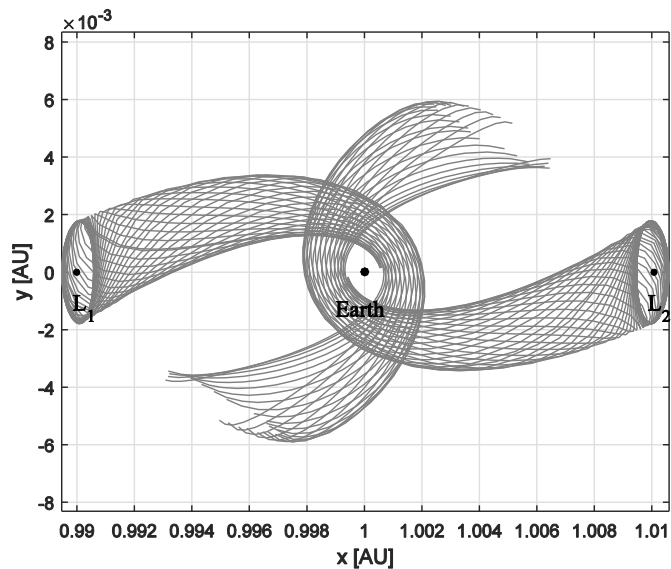


Fig. 4.16 Stable manifolds with Lyapunov orbits around the Sun-Earth L_1 and L_2 points.

Figures 4.17-4.20 show the relationship between r_{min} and the amplitude variable A_p of the periodic orbits. It should be noted that the grey parts correspond to $r_{min} < r_{threshold}$. Therefore, it is found that A_p should be selected in the range [0.0013452 AU, 0.0078331 AU] for Lyapunov orbits around the Sun-Earth L_1 point, [0.0013252 AU, 0.0079602 AU] for Lyapunov orbits around the Sun-Earth L_2 point, [0.00176583 AU, 0.00430523 AU] \cup [-0.0007607 AU, -0.0007607 AU] \cup [-0.0043052 AU, -0.00176582 AU] for Halo orbits around the Sun-Earth L_1 point or [0.004286 AU, 0.0017862 AU] \cup [0.0007863 AU, -

$0.0007863 \text{ AU}] \cup [-0.0017862 \text{ AU}, -0.004286 \text{ AU}]$ for Halo orbits around the Sun-Earth L_2 point.

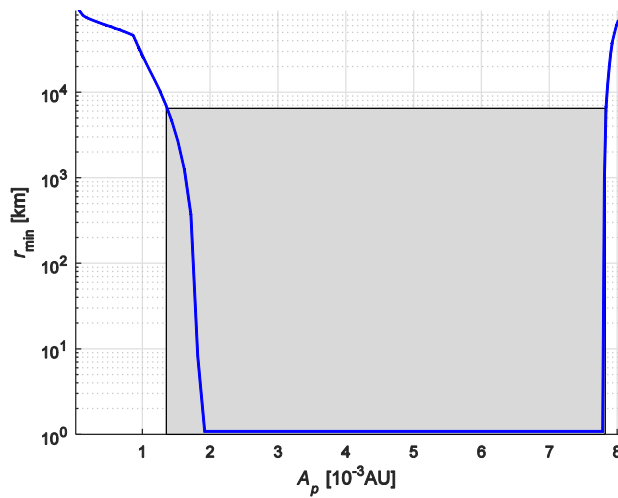


Fig. 4.17 Relationship between r_{\min} and the amplitude variable A_p of Lyapunov orbits around the Sun-Earth L_1 point within a given stable manifold flight time (400 days).

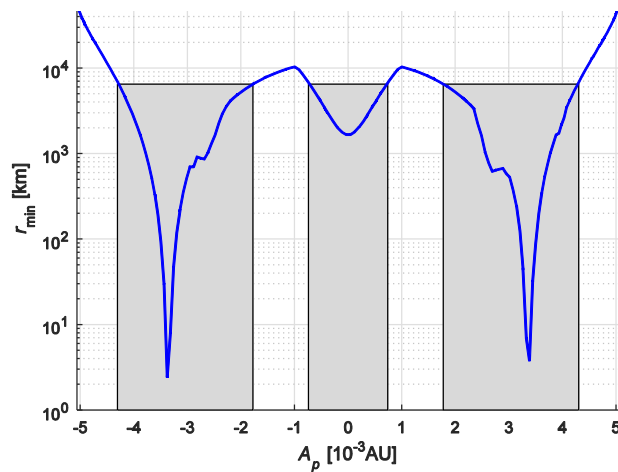


Fig. 4.18 Relationship between r_{\min} and the amplitude variable A_p of Sun-Earth L_1 halo orbits.

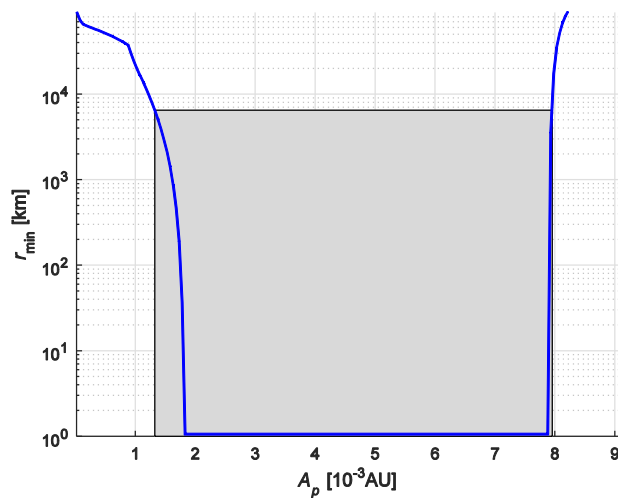


Fig. 4.19 Relationship between r_{\min} and the amplitude variable A_p of Sun-Earth L_2 Lyapunov orbits.

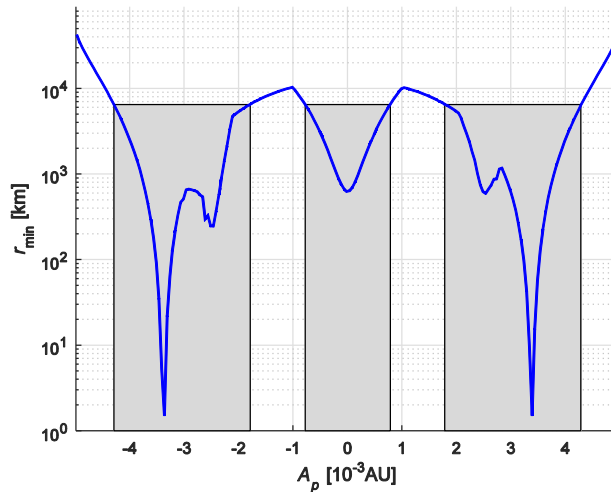


Fig. 4.20 Relationship between r_{\min} and the amplitude variable A_p of Sun-Earth L_2 halo orbits.

4.5.4 Aerobraking window

As noted earlier, the Earth's atmosphere can provide an aerobraking manoeuvre only when the height of the perigee of the flyby orbit is low enough ($h_{\text{threshold}} = 100$ km or $r_{\text{threshold}} = 6478$ km). However, for a periodic orbit which can provide opportunities for aerobraking in Section 4.5.3, only a few stable manifold trajectories can meet such a requirement, shown in Fig. 4.21.

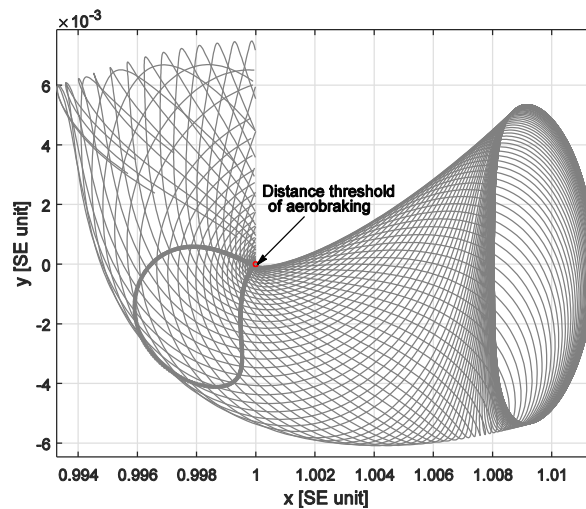


Fig. 4.21 Periapsis map of the stable manifolds of a Sun-Earth L_2 Lyapunov orbit with $A_p = 0.0020187$.

To determine the set of stable manifold trajectories whose perigee is lower than the distance threshold for aerobraking ($r_{\text{threshold}} = 6478$ km), the relationship between the distance of the perigee of the stable manifold and the parameter t_p is obtained, shown in Fig. 4.22. Therefore, the set of t_p which determines the perigee distance of the stable manifold to the centre of the Earth in the interval $[r_{\text{Earth}}, r_{\text{threshold}}]$ is defined as the

aerobraking window. As shown in Fig. 4.21, for a Lyapunov orbit with $A_p = 0.0020187$, the aerobraking window is defined by $\{t_p \mid t_p \in (1.6163, 1.6188] \cup t_p \in (2.0227, 2.0253]\}$.

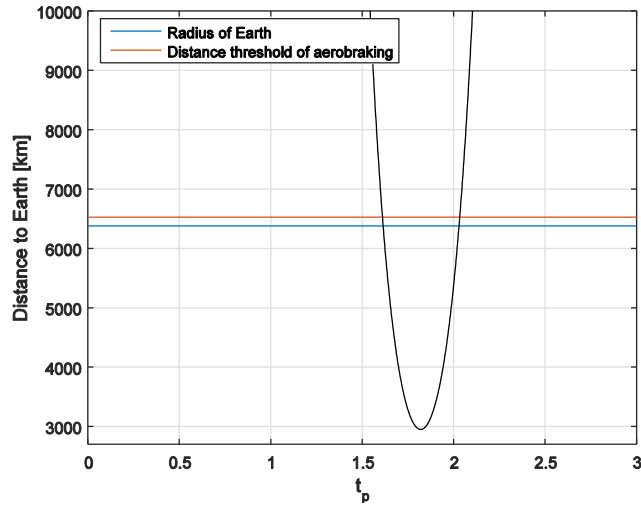


Fig. 4.22 Relationship between the distance of the perigee of the stable manifolds and the parameter t_p .

4.5.5 Design Procedure and Optimisation

The process of designing the transfer trajectory for asteroid capture using aerobraking is similar to Section 4.3 and is as follows:

- (1) Select one target asteroid in the candidate catalogue (e.g. 2009 UJ) in Fig. 4.8;
- (2) Given the amplitude variable A_p of a periodic orbit and t_p at the aerobraking window, which is obtained from Section 4.5.3 and 4.5.4, the stable manifold associated with the periodic orbit is propagated backwards until it reaches perigee and then the state $\mathbf{X}_{p+} = [x_p, y_p, z_p, \dot{x}_{p+}, \dot{y}_{p+}, \dot{z}_{p+}]^T$ at perigee in the Sun-Earth rotating frame is obtained, shown in Fig. 4.23;
- (3) The velocity \mathbf{V}_{p-} before aerobraking in the Earth-centred inertial frame can then be calculated and the state of the asteroid $\mathbf{X}_{p-} = [x_p, y_p, z_p, \dot{x}_{p-}, \dot{y}_{p-}, \dot{z}_{p-}]^T$ before aerobraking in the Sun-Earth rotating frame can be obtained using Eq. (4.32);
- (4) Given the flight time T_{fly2} , the state \mathbf{X}_{p-} is propagated backwards and then the target point \mathbf{X}_f is obtained, shown in Fig. 4.24;
- (5) Given a departure date T_0 , transform the initial state of the candidate asteroid in the Sun-centred inertial frame to the Sun-Earth rotating frame so that \mathbf{X}_i is then obtained;

(6) Given the flight time T_{fly1} , Eq. (4.21) is then applied to design the transfer between the candidate asteroid's initial orbit X_i and the target points X_f . Thus, the manoeuvres Δv_1 and Δv_2 can be calculated.

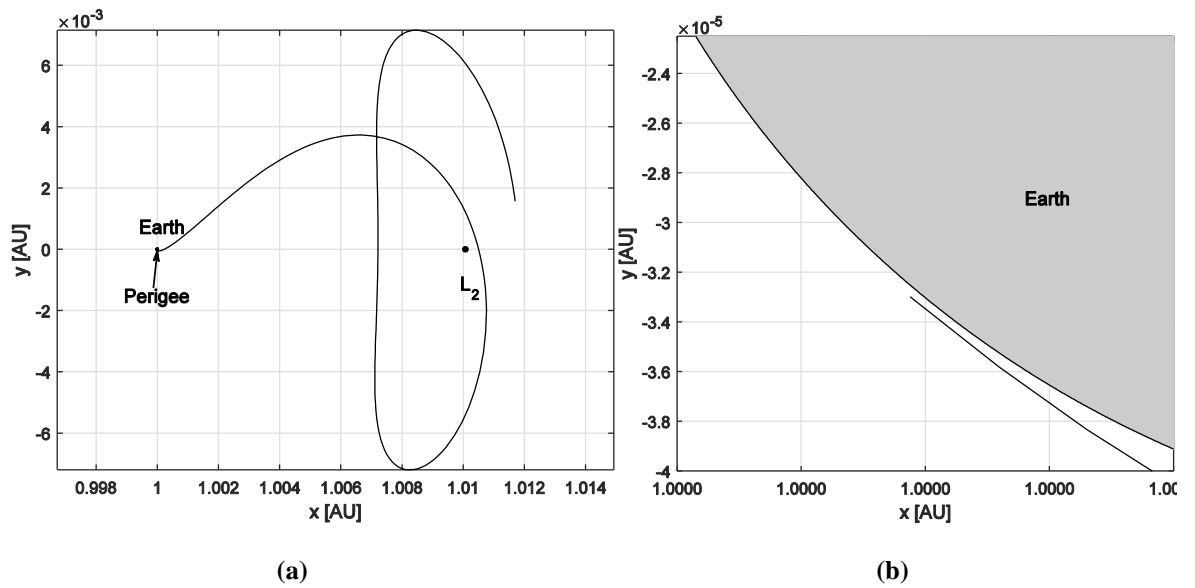


Fig. 4.23 Given $A_p = 0.0028288$ AU, $t_p = 1.478633$, the stable manifold associated with the Sun-Earth L_2 Lyapunov orbit and its perigee: (a) global view; (b) local view.

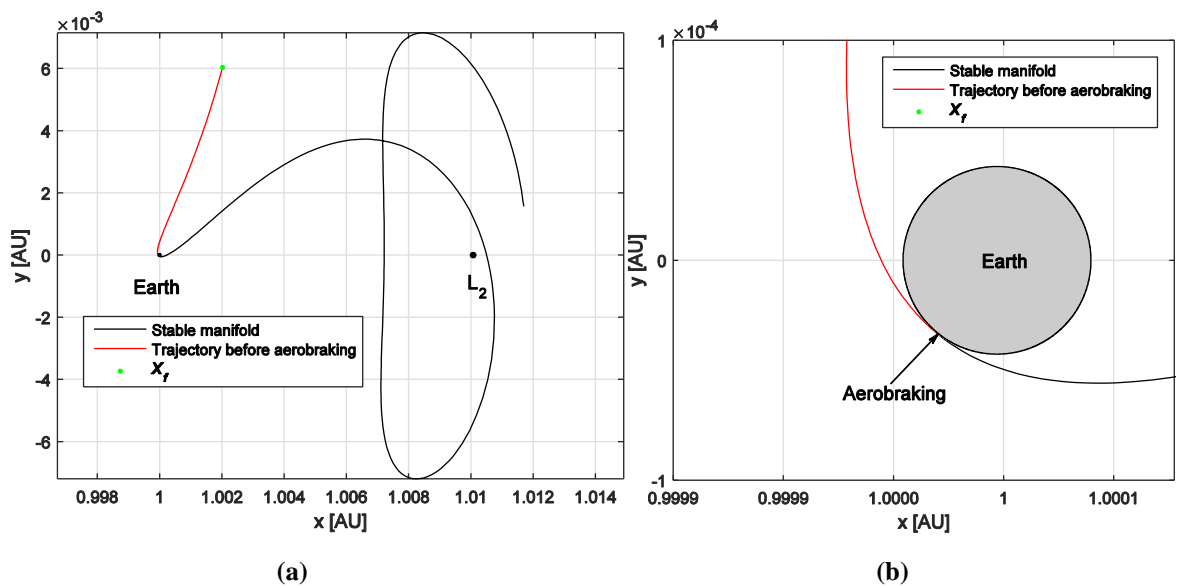


Fig. 4.24 Given $T_{fly2} = 5.64$ days, the trajectory before aerobraking is obtained by propagating backward from the state at perigee.

Then, the total cost of capturing the asteroid onto the target Sun-Earth L_1 or L_2 periodic orbit with aerobraking can be obtained by using Eq. (4.14). The transfer trajectory is shown in Fig. 4.25 and Fig. 4.26. The 5 parameters (T_0 , T_{fly1} , T_{fly2} , A_p , t_p) associated with the transfers from the candidate asteroid initial orbit to the stable manifold can again be

optimised using NSGA-II, using the total cost Δv as the objective function. The optimal results of capturing asteroids onto the Sun-Earth L_1 and L_2 periodic orbits are shown in Table 4.5 and Table 4.6.

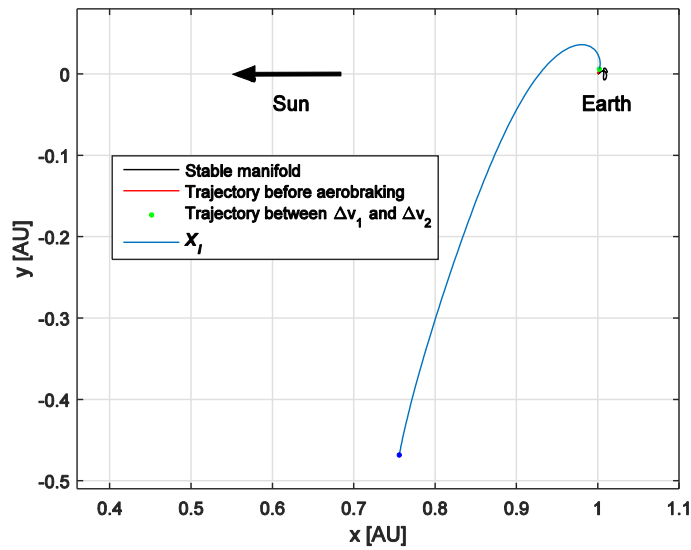


Fig. 4.25 Given $T_0 = 59298.19$ [MJD], $T_{fly1} = 216.31$ days, the transfer trajectory (x - y projection) for capturing 2010 UJ onto the Sun-Earth L_2 Lyapunov orbit in the Sun-Earth rotating frame.

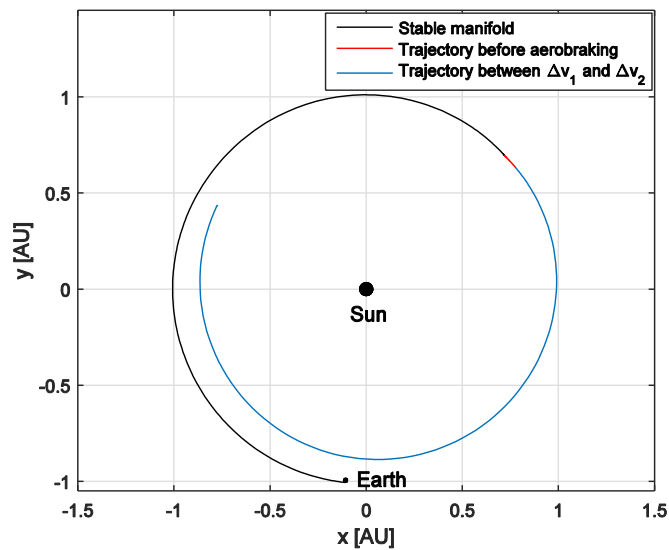


Fig. 4.26 Transfer trajectory (x - y projection) for capturing 2010 UJ onto the Sun-Earth L_2 Lyapunov orbit in the Sun-centred inertial frame.

It can be seen that the lowest cost capture transfers using aerobraking are below 200 m/s, corresponding to a capture of 2007 UN12 into a Lyapunov orbit and a halo orbit, and 2012 WR10 into a halo orbit. Moreover, aerobraking can achieve a lower-cost capture for capture into Lyapunov orbits, e.g. 2003 WT153, 2008 EL68 and 2009 YR. Besides, capturing some candidate asteroids onto halo orbits using aerobraking can be cheaper in

terms of Δv than a capture onto Lyapunov orbits, especially for capturing 2008 JL24, 2012 WR10 and 2015 PS228. Comparing the results of Tables 4.3-4.4 and Tables 4.5-4.6, it can be seen that aerobraking can save energy and so the capture strategy has the potential to be of lower cost than the asteroid capture strategy without a flyby. Moreover, the asteroid capture strategy using aerobraking also has the potential to require a shorter flight time, as does the capture strategy using the Earth flyby without aerobraking.

It should be noted that the method presented in this Chapter is used as a preliminary analysis of the asteroid capture strategy using aerobraking. The aerobraking model only provides an approximation of the aerobraking manoeuvre for the asteroid capture, without considering other perturbations such as the rotation of the Earth atmosphere. Here asteroid 2003 WT153 in Table 4.5 ($v_{p^-} = 11.919$ km/s and $v_{p^+} = 11.176$ km/s) will be taken as an example for a preliminary analysis of the effect of the rotation of the Earth atmosphere. The maximum rotational speed of the Earth atmosphere can be estimated by $v_a \approx 2\pi r_{Earth} / 24 / 3600 = 0.464$ km/s. Thus, the relative velocity of the asteroid to the atmosphere before aerobraking is $v_{p^-} + v_a = 12.383$ km/s. Therefore, the relative velocity of the asteroid to the atmosphere after aerobraking can be calculated using the Eq. (4.17) $v_{p^+}' = 11.545$ km/s. Then subtracting the rotational speed of the Earth atmosphere can yield the post-aerobraking velocity of the asteroid with respect the centre of the Earth $v_{p^+}' - v_a = 11.081$ km/s. Comparing v_{p^+} and $v_{p^+}' - v_a$, it can be seen that the rotation of the Earth atmosphere can lead to an error of about 95 m/s in the velocity of the asteroid after aerobraking. Accordingly, the candidate asteroid cannot insert onto the required stable manifold of the final target orbit and therefore the asteroid capture mission will fail. Moreover, according to mass loss model in Eq. (4.9), mass loss of this asteroid when considering the effect of the rotation of the atmosphere is about 2.5% more than that without considering the rotation of the atmosphere. Considering the sensitivity of the transfer trajectory in the Sun-Earth CRTBP, especially the aerobraking phase, a more accurate aerobraking model would be required to ensure that the captured asteroid is at the required altitude in order to insert into the final target orbit correctly. However, the transfers designed in this Chapter can provide good approximations to the asteroid capture missions using a more accurate aerobraking model.

Table 4.5 Results of capturing asteroids onto Sun-Earth Lyapunov orbits using aerobraking

Asteroid	Total cost, m/s	Epoch, MJD	Total flight time, days	Amplitude variable A_p , 10^{-3} AU	Mass loss, %	Diameter D , m	Target point
2003 WT153	271.81	58499.7	451.2	2.8334	16.5	8.5	L ₁
2006 UQ216	367.63	60551.7	1917.9	7.331	20.5	11.7	L ₁
2007 UN12	163.58	58550.4	833.3	5.5057	1.1	6.2	L ₁
2008 EL68	227.03	66008.1	875.8	7.051	4.7	9.8	L ₁
2008 JL24	548.07	59973.8	1024.7	3.5287	10.2	4.1	L ₁
2008 UA202	440.37	60673.3	1316.8	2.1888	0.7	4.5	L ₂
2009 YR	420.38	58527.5	889.4	2.1518	12.2	8.5	L ₂
2010 JR34	492.37	59890	1154.9	3.7658	21.3	9.8	L ₂
2010 UJ	459.68	59293.8	450.8	2.8288	3.8	19.5	L ₂
2010 UY7	435.68	61131.3	790.9	2.8413	14.3	6.8	L ₁
2011 BQ50	520.43	59796.5	702.8	3.959	7.9	8.5	L ₁
2011 BQ50	351.47	59332.8	1266.8	3.3558	8.9	8.5	L ₂
2011 CL50	947.31	58651.3	1128.9	2.844	9.7	10.2	L ₁
2012 HG2	984.21	60000.9	912.5	3.4038	47	13.5	L ₂
2012 WR10	571.8	61660.1	1393	3.2179	6.5	6.2	L ₁
2014 AA	2194.47	58511.8	822.5	1.7128	14.5	2.2	L ₂
2014 JR24	701.1	59773.4	1096	7.2507	5.6	4.7	L ₁
2014 UV210	573.1	58515.5	602	4.4857	9	14.1	L ₁
2014 UV210	1454.11	58638.4	517.4	2.9258	0.1	14.1	L ₂
2014 WE6	558.52	63926.3	1086.2	2.3748	13.4	2.8	L ₂
2014 WX202	254.86	63526.6	1066.3	1.9062	2.8	4.1	L ₁
2015 PS228	554.97	63012.1	1701.1	2.5912	5.2	5.5	L ₁

Table 4.6 Results of capturing asteroids onto Sun-Earth Halo orbits using aerobraking

Asteroid	Total cost, m/s	Epoch, MJD	Total flight time, days	Amplitude variable A_p , 10^{-3} AU	Mass loss, %	Diameter D , m	Target point
2003 WT153	606.41	58569.7	390.5	3.8368	33	8.5	L ₁
2006 UQ216	367.42	61507.2	919.3	2.7417	23.2	11.7	L ₁
2007 UN12	158.22	59068.6	571.6	2.2144	1.5	6.2	L ₁
2008 EL68	614.66	61246.8	822.3	1.9497	8.4	9.8	L ₁
2008 JL24	498.84	60131.2	839.8	1.9482	4.1	8.1	L ₁
2008 UA202	334.17	60410.7	1960.6	-0.4878	3.6	4.5	L ₂
2009 YR	583.63	58802.2	595.2	1.8132	8.5	8.1	L ₂
2010 JR34	745.79	745.79	745.79	745.79	9.8	12.8	L ₂
2010 UJ	341.96	58837.5	935.8	2.4632	12.3	19.5	L ₂
2010 UY7	863.8	59375.5	701.7	3.659	32.1	6.8	L ₁
2011 BQ50	977.81	59085.1	1584.9	1.6446	3.5	8.5	L ₂
2011 BQ50	338.87	59190.7	1392.6	-2.6228	11.7	8.5	L ₁
2011 CL50	1521.05	58780.5	794.5	3.7341	0.10	10.2	L ₂
2012 HG2	1415.72	58715.6	961.9	0.3992	32.4	13.5	L ₁
2012 WR10	168.06	61640.4	1031.8	2.2035	7.8	6.2	L ₂
2014 AA	2221.19	58517.8	818.4	-0.5398	9.4	2.2	L ₁
2014 JR24	989.57	60473.4	633.2	1.9516	4.9	4.7	L ₂
2014 UV210	651.43	58479.6	594.1	1.9649	8.9	14.1	L ₁
2014 UV210	1293.31	58556.6	601.8	-2.3488	0.10	14.1	L ₁
2014 WE6	843.27	63194.9	1026.8	2.0632	7.5	2.8	L ₂
2014 WX202	384.97	62852.3	1721.1	1.9879	2.9	4.1	L ₂
2015 PS228	299.31	62346.7	1267	1.9624	3.3	5.5	L ₁

Furthermore, comparing the results in Table 4.1-4.2 and Table 4.5-4.6, it can be seen that aerobraking can provide a manoeuvre which can help to achieve lower cost asteroid capture than the strategy using the Earth flyby without aerobraking, e.g. 2006 UQ216, 2011 BQ50 and 2010 UJ. However, for the practical implementation of the asteroid capture strategy using aerobraking, it is necessary to take into account the real ephemeris model and a more accurate atmosphere model. The preliminary results in this Chapter can

serve as an approximation for such real missions. Considering the sensitivity of the transfer trajectory in the Sun-Earth CRTBP, especially the aerobraking phase, an accurate navigation and control strategy would be required to guarantee that the flyby of the candidate asteroid is at the required altitude in order to obtain the necessary aerobraking manoeuvre. For example, the drag-modulation flight control method [126] and the blended control, predictor-corrector guidance algorithm [128] may provide feasible solutions for an asteroid capture mission using aerobraking. Again, the carrier spacecraft is envisaged as remaining attached to, and shielded by, the asteroid during the aerobraking manoeuvre to deliver active control.

4.6 Discussion

As an ideal location for space science, and a staging node for interplanetary missions in the future, the Sun-Earth L_1 and L_2 libration points are likely to play an important role for future space exploration. Therefore, capturing asteroids onto periodic orbits around the Sun-Earth L_1 and L_2 points would in principle be of significant scientific and commercial interest. A strategy to couple a flyby of the Earth to stable manifolds to capture asteroids onto Sun-Earth L_1/L_2 periodic orbits has been proposed. The dynamical model of the CRTBP is firstly introduced to calculate Lyapunov orbits around the Sun-Earth L_1 and L_2 points and their associated stable manifolds. Then, according to the height of the flyby orbit at perigee, two types of Earth flyby are determined, an Earth flyby with and without high altitude aerobraking. A grazing flyby is used, but it is assumed that only small bodies which would safely ablate in the Earth's atmosphere at lower altitudes are considered for aerobraking. After selecting appropriate candidate NEAs and calculating the NEA capture window, a detailed design procedure is presented and finally global optimisation is carried out. In this capture strategy the candidate asteroid is first assumed to leave its orbit with an impulse manoeuvre and will then approach the vicinity of the Earth for the flyby. During the flyby, the Earth's atmosphere may also provide an aerobraking manoeuvre. If not, a propulsive manoeuvre is required at the perigee of the flyby. After the flyby of the Earth, the candidate asteroid inserts onto the stable manifold associated with a periodic orbit around the Sun-Earth L_1 or L_2 points and will be asymptotically captured onto it.

Comparing the results of two methods, it is found that asteroid capture strategies using an Earth flyby with and without the aerobraking both have the potential to be lower cost (in terms of Δv) than direct stable manifold capture. Besides, due to the fact that direct capture without a flyby requires significant additional time to move along the stable manifolds of

the Sun–Earth L_1 or L_2 periodic orbits, asteroid capture strategies using Earth flyby also have the potential to save flight time.

CHAPTER 5

CAPTURE OF SMALL NEAS AT THE EARTH USING DIRECT AEROBRAKING

This Chapter introduces the concept of capturing NEAs onto bound orbits around the Earth by using direct aerobraking. In Chapter 4, a combination of an Earth gravity assist or a small aerobraking manoeuvre with invariant manifolds has been proposed to capture an asteroid into a periodic orbit around the Sun-Earth L_1 and L_2 libration points. This Chapter will provide a much more general analysis of aerobraking strategies and will use aerobraking to capture asteroids directly into bound orbits at the Earth.

- (1) Two strategies to capture asteroids into bound orbits at the Earth after aerobraking will be considered. In the first case, the motion of the captured asteroid after aerobraking is modelled in the Earth-centred two-body problem, and so a second impulse is required to raise the height of the perigee to avoid a second aerobraking pass. In the second case, the motion of the captured asteroid is still modelled in the Sun-Earth CRTBP and the solar gravitational perturbation used to passively raise the height of the asteroid perigee, again avoiding subsequent aerobraking passes. The boundary of these two cases is defined by the Earth's sphere of influence. Finally, the transfers are then optimised using a global optimisation algorithm and lists of candidate objects provided.
- (2) These two asteroid capture strategies are then investigated to maximize the yield of the retrieved mass of the asteroid with respect to the required spacecraft mass, taking account the mass loss due to ablation of the asteroid during the aerobraking manoeuvre.

5.1 Capture conditions

As discussed in Section 2.2.2, for the Sun-Earth CRTBP system, the Jacobi constant C_1 and C_2 at the Sun-Earth L_1 and L_2 points respectively are critical. They can be used as capture conditions to determine whether a candidate asteroid can be captured or not when it approaches the vicinity of the Earth. Figure 5.1 shows the x - y projection of the zero-velocity surface when $C = C_1$ and $C = C_2$ in the Sun-Earth CRTBP system. Generally speaking, for a captured asteroid in the vicinity of Earth with Jacobi constant $C \geq C_1$, its trajectory will be restricted in a space which is defined by the zero-velocity surface, as shown in Fig. 5.2 (a)-(b). However, if the Jacobi constant C of the asteroid is less than C_1 , it may orbit the Earth for some duration and then escape from the vicinity of the Earth, as shown in Fig. 5.2 (c)-(d).

The Jacobi constants of the captured asteroid before and after aerobraking are denoted as C_- and C_+ , respectively. Moreover, the two-body Kepler energy of the asteroid after aerobraking can be defined as [79]

$$H_2 = \frac{1}{2} v_{p+}^2 - \frac{\mu_{Earth}}{r_p} \quad (5.2)$$

where v_{p+} is the relative velocity of the asteroid at perigee with respect to the Earth after aerobraking and r_p is the perigee radius of the flyby orbit from the centre of the Earth (See 4.2.1). According to the capture condition [79], the candidate asteroid is assumed to be ballistically captured at the Earth if

$$H_2 < 0 \quad (5.1)$$

More specifically, the candidate asteroid is considered to be captured temporarily around the Earth if $v_{p+} < \sqrt{2\mu_{Earth}/r_p}$ and $C_+ < C_1$. Similarly, the asteroid can be captured permanently in the Earth's Hill region if $v_{p+} < \sqrt{2\mu_{Earth}/r_p}$ and $C_+ > C_1$ [48]. For the temporary capture case, the captured asteroid may orbit the Earth for a significant duration before it escapes from the vicinity of the Earth. Therefore, this capture strategy can still be practical. Thus, the asteroid capture strategy presented in this Chapter contains both temporary capture and permanent capture. That is, once $v_{p+} < \sqrt{2\mu_{Earth}/r_p}$, the candidate asteroid is considered to be captured at the Earth.

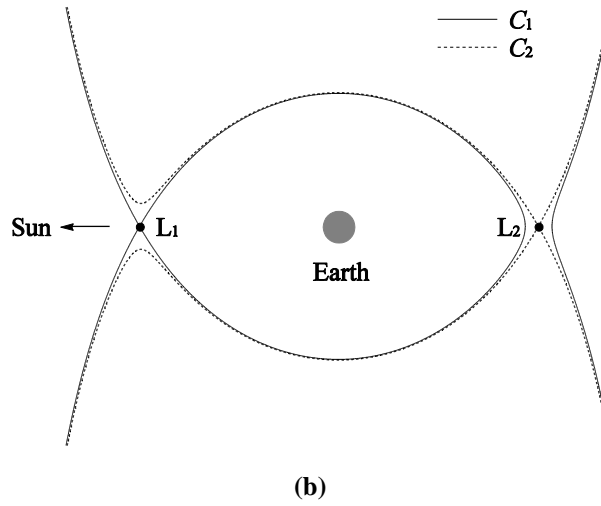


Fig. 5.1 x - y projection of the zero-velocity surface when $C = C_1$ and $C = C_2$.

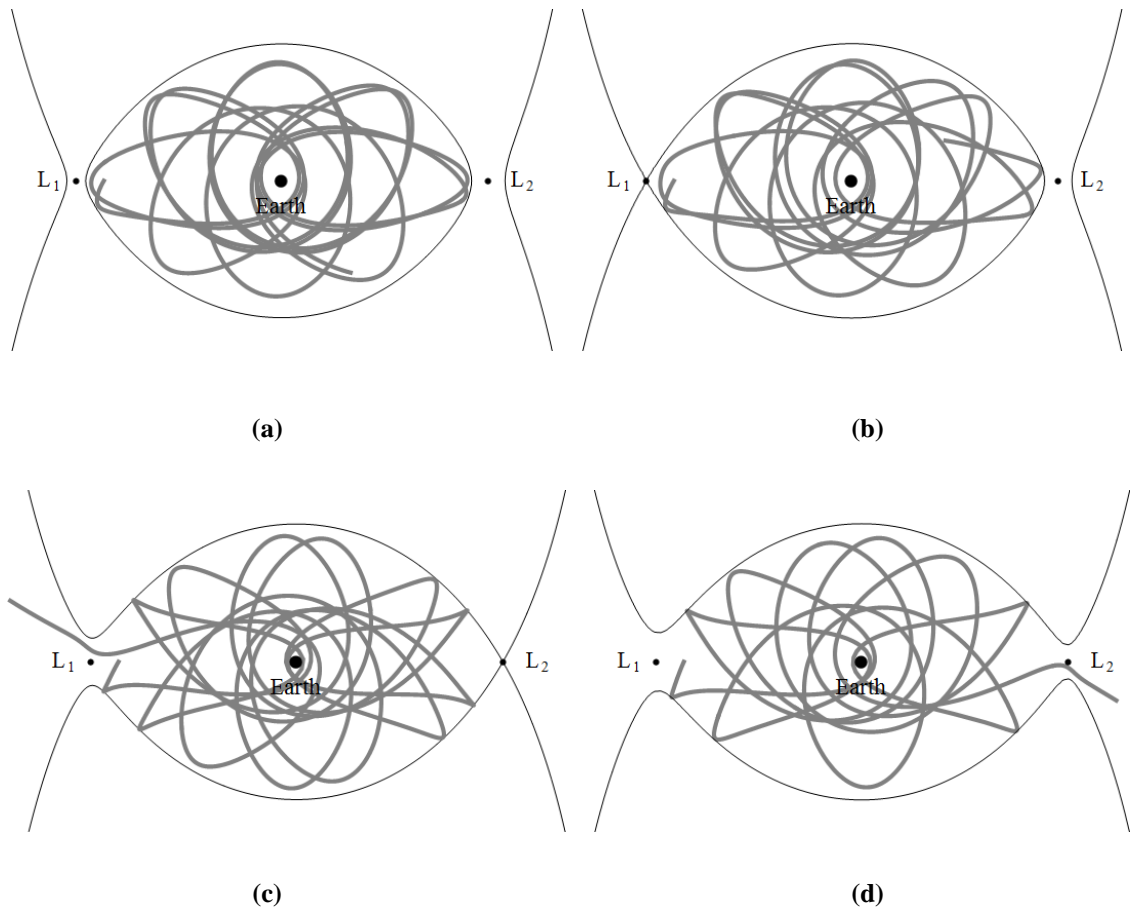


Fig. 5.2 Examples of trajectories of an asteroid with (a) $C > C_1$; (b) $C = C_1$; (c) $C = C_2 < C_1$; (d) $C < C_2$.

5.2 Asteroid capture around the Earth using aerobraking

The strategy for capturing an asteroid into a bound orbit at the Earth using a direct aerobraking manoeuvre is illustrated in Fig. 5.3. With an initial manoeuvre $\Delta \mathbf{v}_1 = \Delta v_1 [\sin \theta_1 \cos \theta_2, \sin \theta_1 \sin \theta_2, \cos \theta_1]^T$ with $\theta_1 \in [0, \pi]$ and $\theta_2 \in [0, 2\pi]$, referring to a local spherical reference frame along the asteroid's orbit where the x -axis is along the asteroid's velocity vector, the y -axis is perpendicular to the x -axis and in the plane of the asteroid orbit and the z -axis is normal to the plane of the asteroid's orbit, the candidate asteroid leaves its initial orbit and its motion can then be described by the Sun-Earth CRTBP, as detailed in Section 2.1. Subsequently, the candidate asteroid performs an aerobraking manoeuvre and is thus captured into a bound orbit about the Earth.

Thus, for each candidate asteroid, there are 4 variables to describe the sequence of manoeuvres as follows:

- T_0 : capture date when the first impulse $\Delta \mathbf{v}_1$ is applied to the candidate asteroid and the asteroid leaves its initial orbit;
- Δv_1 : magnitude of the initial manoeuvre $\Delta \mathbf{v}_1$;
- θ_1, θ_2 : angles which determine the direction of the initial manoeuvre $\Delta \mathbf{v}_1$.

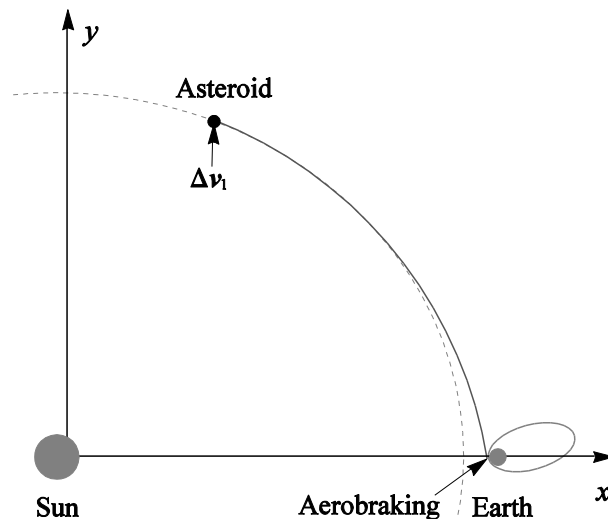


Fig. 5.3 Overview of capturing NEAs at the Earth using aerobraking

5.2.1 Asteroid capture opportunities and initial guess

As discussed in Section 3.1.5, those asteroids with a diameter D less than 30 m are considered as candidate asteroids for capture in order to reduce the threat of impact with

the Earth when aerobraking, Similarly, for each candidate asteroid, feasible capture dates are assumed to be in the interval 2019 - 2050 (or 58484 MJD - 70171 MJD).

The Lambert arc between the candidate asteroid's initial orbit and the Earth in the Sun-centred two-body problem can be used as an initial guess of the capture date T_0 and the first impulse Δv_1 . In addition, the first manoeuvre of this Lambert arc in the Sun-centred two-body problem is defined as δv_1 (see Section 2.1.2). Here a flight time $T_{fly} < 2000$ days is considered and then the first impulse δv_1 on the Lambert arc is utilised to guess the first impulse Δv_1 in the Sun-Earth CRTBP. Moreover, the relative velocity at the end of the Lambert arc at the Earth can be used as a preliminary analysis for candidate asteroid selection. When an asteroid is captured at the Earth using aerobraking at the threshold of the capture condition, i.e. $v_{p+} = \sqrt{2\mu_{Earth} / r_p}$, the mass loss ratio of the asteroid can be estimated from Eq. (4.10) in Section 4.2.1. Although the velocity of the captured asteroid relative to the Earth in the Sun-Earth CRTBP will be different from the relative velocity at the end of the Lambert arc at the Earth, it can still be utilised to guess the mass loss ratio due to aerobraking and thus can remove those asteroids with a large mass loss ratio. Figure 5.4 shows the mass loss ratio with different relative velocities and different perigee heights ($0 < h < 100$ km) of flyby orbit above the Earth's surface. It can be seen that once $v_p > 13.8$ km/s, the mass loss ratio is over 50 %. Therefore, $v_p < 13.8$ km/s can be set as a constraint at the end of the Lambert arc in the Sun-centred two-body problem, in order to exclude those asteroids which have potential for significant mass loss due to aerobraking.

The number of asteroids ($D < 30$ m, as discussed in Section 3.1.5) with a first manoeuvre δv_1 on the Lambert arc less than Δv ($\Delta v \in [0, 500]$ m/s) is shown in Fig. 5.5. This can be used as an estimate of the number of candidate asteroids which can be captured using aerobraking with total cost less than a given Δv . As shown in Fig. 5.5, it can be noted that the number of asteroids which can be captured at the Earth using aerobraking with a total Δv less than 10 m/s and 50 m/s are of the order of 10 and 100, respectively.

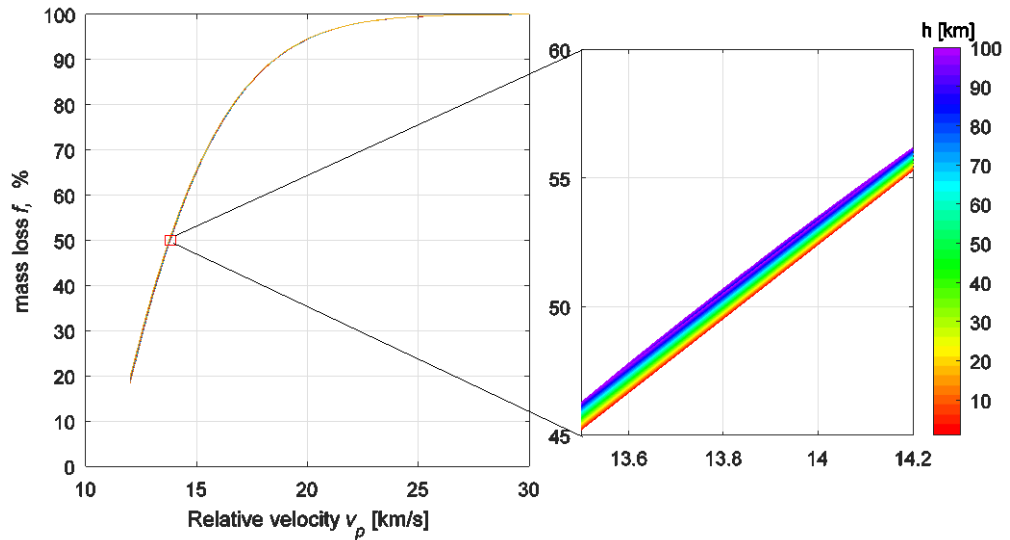


Fig. 5.4 Mass loss ratio of an asteroid caused by aerobraking, with different relative velocity and heights above the Earth's surface

Since we expect to find the candidate asteroids which can be captured with low cost, here we set 50 m/s as a threshold for Δv_1 . Therefore, those asteroids with $\delta v_1 \leq 50$ m/s and $D < 30$ m ($H > 25.26$) are then considered to be candidate asteroids, as shown in Fig. 5.6. For a suitable candidate asteroid, the departure date on the Lambert arc with $\delta v_1 \leq 50$ m/s can then be used as an approximation of the capture date T_0 when the first impulse Δv_1 is applied to the candidate asteroid, as shown for 2012 BK14 for illustration in Fig. 5.7.

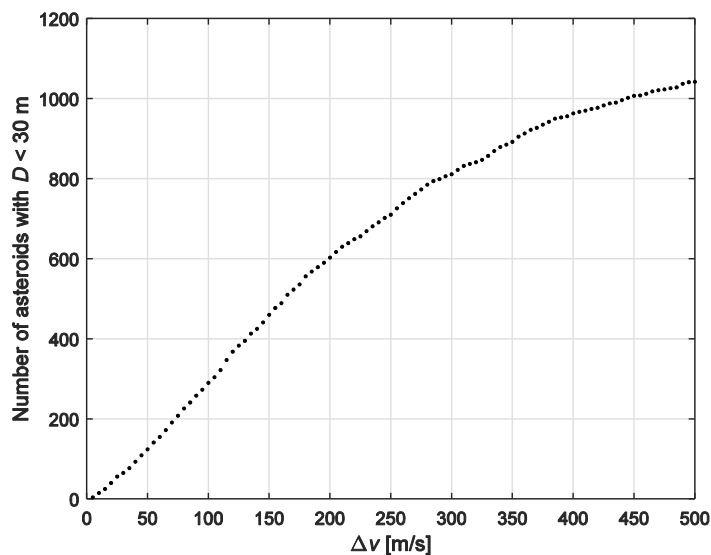
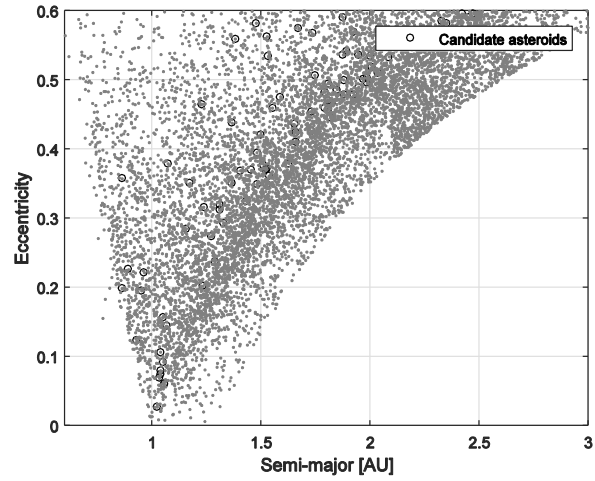
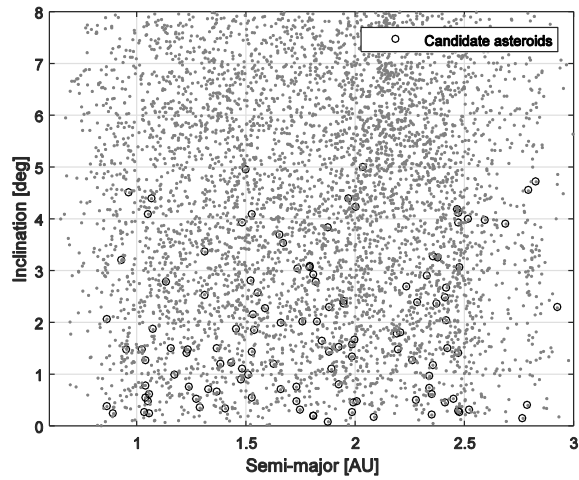


Fig. 5.5 Estimate of the number of asteroids as a function of Δv threshold.



(a)



(b)

Fig. 5.6 Distribution of candidate asteroids (circled) in the family of NEAs: (a) semi-major and eccentricity and (b) semi-major and inclination.

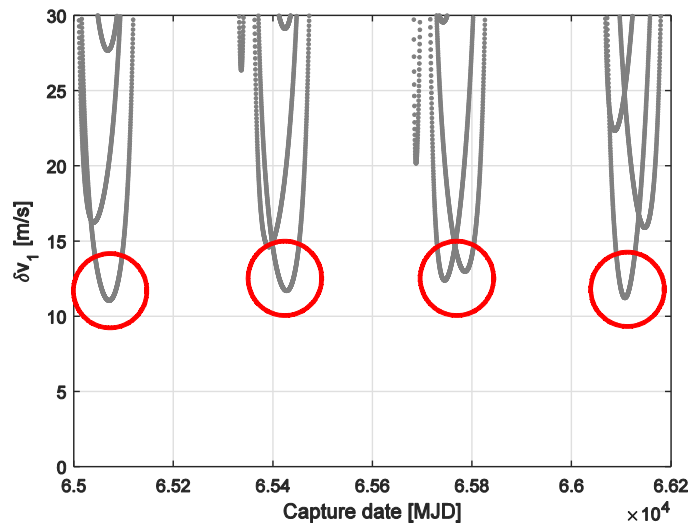


Fig. 5.7 Optimal capture date T_0 guess for capturing 2012 BK14 with potential capture dates highlighted.

5.2.2 Modes of aerobraking

Give one value of the first manoeuvre Δv_1 , a set of perigees of the asteroid orbit can be obtained by varying the angles θ_1 and θ_2 . Therefore, a whole set of perigees of the asteroid orbit can be obtained by varying Δv_1 , θ_1 and θ_2 . Based on the initial guess δv_1 of the first manoeuvre Δv_1 using the Lambert arc, a small modification from δv_1 can cause the perigee height of the asteroid orbit above the Earth surface to be low enough ($h < 100$ km) for aerobraking, as shown in Fig. 5.8. Figure 5.8 shows the perigee map of the asteroid orbit with different first manoeuvres Δv_1 , which varies slightly from the initial guess δv_1 . Accordingly, some asteroid orbits in the vicinity of the Earth generated from the Fig. 5.8 are shown in Fig. 5.9.

When an asteroid flies by the Earth, it may move in a retrograde orbit or prograde orbit with respect to the Earth, as shown in Fig. 5.9. Therefore, there are two types of aerobraking, corresponding to retrograde and prograde orbits. It should be noted that the black lines in Fig. 5.8 are the boundary of these two cases. In this Chapter, only aerobraking in a prograde orbit is considered and it can therefore be defined as,

$$x_p^E \dot{y}_{p-}^E - \dot{x}_{p-}^E y_p^E > 0 \quad (5.3)$$

where $\mathbf{r}_{p-} = [x_p^E, y_p^E, z_p^E]^T$ and $\mathbf{V}_{p-} = [\dot{x}_{p-}^E, \dot{y}_{p-}^E, \dot{z}_{p-}^E]^T$ are the position vector and velocity vector of the asteroid before aerobraking in the Earth-centred inertial frame.

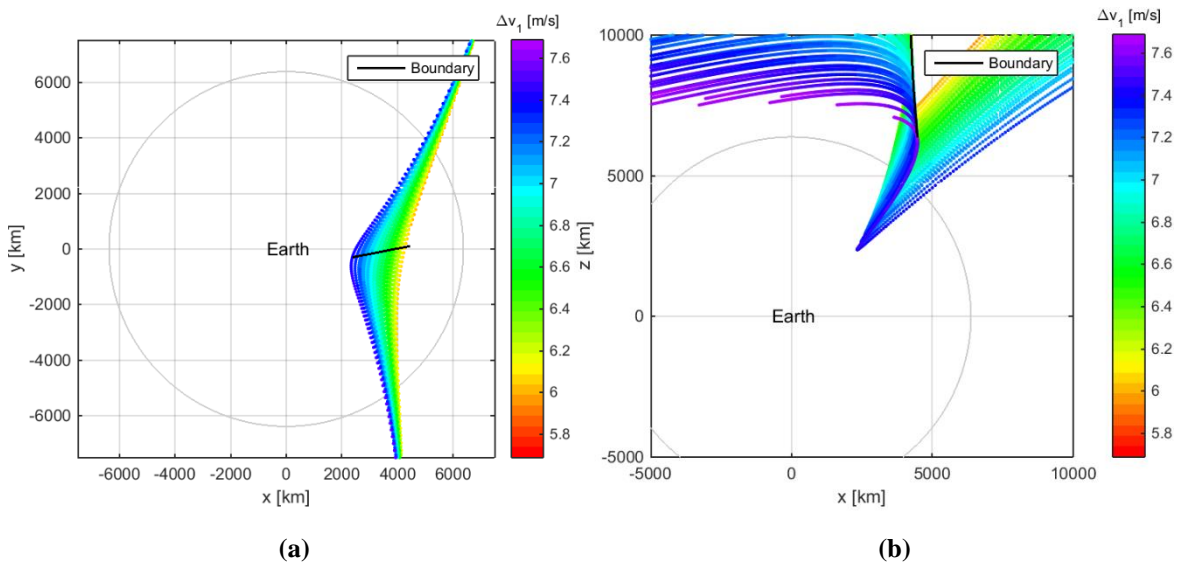


Fig. 5.8 Perigee map of the asteroid 2012 BK1 orbit with different initial manoeuvres: (a) x - y projection; (b) x - z projection.

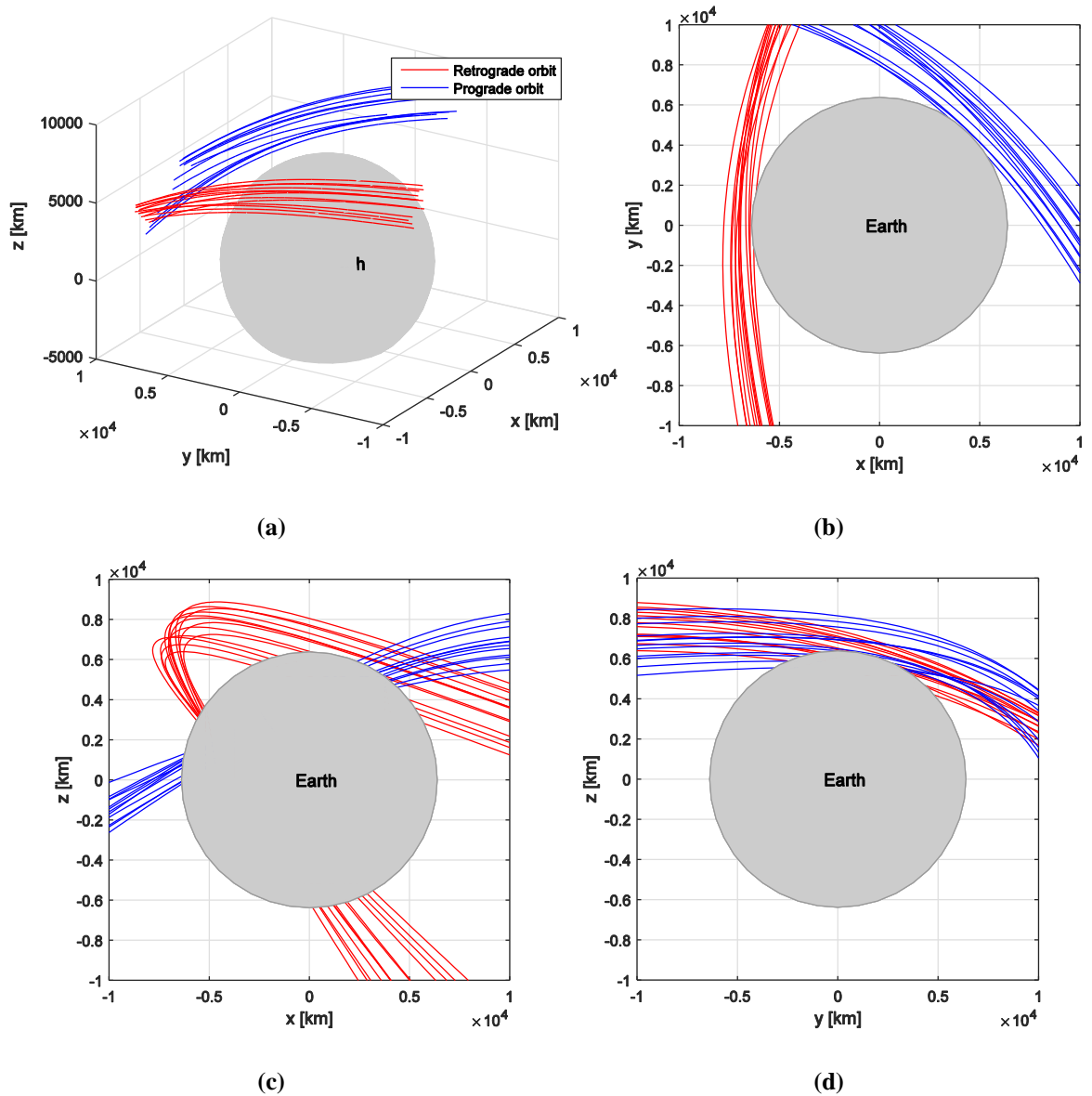


Fig. 5.9 Retrograde orbits and prograde orbits generated from Fig. 5.8: (a) 3D view; (b) x - y projection; (c) x - z projection; (d) y - z projection.

5.2.3 Two approaches to raise the perigee height after aerobraking

In order to simplify the capture strategy, only a single aerobraking manoeuvre is utilised to capture asteroids at the Earth in this Chapter. Therefore, strategies to raise the perigee height of the asteroid orbit soon after aerobraking are required, with the new perigee height (h) above the Earth's surface being more than 100 km. Here, two methods of raising the perigee height after aerobraking are proposed, corresponding to the two different dynamical models after the aerobraking manoeuvre, as show in Fig. 5.10.

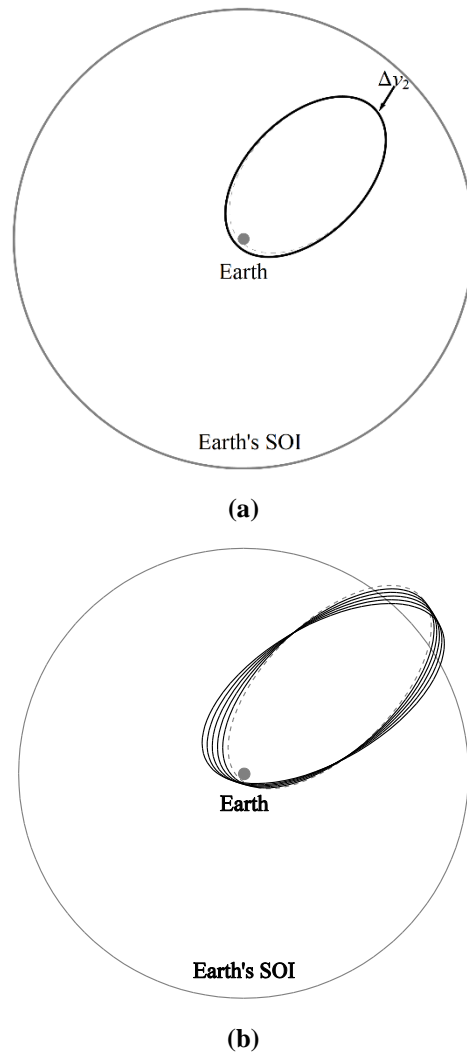


Fig. 5.10 Strategies to raise the perigee height after aerobraking: (a) additional manoeuvre at apogee; (b) three-body interaction.

After aerobraking, if the captured asteroid moves around the Earth inside the Earth's sphere of influence, it is assumed that the candidate asteroid is captured in a bound orbit at the Earth, and so an Earth-centred two-body analysis can be used. Hence, the state of the captured asteroid after aerobraking \mathbf{v}_{p+} should be propagated forward in the Earth-centred two-body problem until it reaches the apogee. At apogee, a second impulse $\Delta \mathbf{v}_2$ is applied to the asteroid in order to raise the next perigee ($h > 100$ km), as shown in Fig. 5.10(a). In this strategy, two manoeuvres are therefore required to capture the candidate asteroid into a suitable bound orbit at the Earth.

Instead, for orbits with a large post-aerobraking apogee the state of the captured asteroid after aerobraking should be propagated forward in the Sun-Earth CRTBP model and an alternative strategy can be devised. With the gravitational perturbation of the Sun, the orbit of the captured asteroid will deviate from a Keplerian ellipse [193], which in principle can be utilised to passively raise the perigee height after aerobraking. Therefore,

only one manoeuvre is in principle required to capture the candidate asteroid at the Earth, as shown in Fig. 5.10(b). In this strategy to raise the perigee height of the asteroid orbit, the Sun's gravity can be regarded as a disturbing perturbation to an Earth-centred two-body orbit and thus the short-term change of the perigee height of the asteroid orbit can be estimated by investigating the change in the asteroid's Earth-centred orbital elements using the Lagrange planetary equations [194]. Following Section 2.1.1, the eccentricity, inclination, right ascension of the ascending node, argument of perigee and true anomaly of the asteroid after aerobraking are denoted as e_+ , i , Ω , ω and θ respectively, shown in Fig. 5.11. When the asteroid is at the perigee of its orbit around the Earth, $\theta = 0$, the change in the height of next perigee (after 1 revolution) can be estimated using [194]:

$$\delta h = \frac{5\pi e_+}{n^2} \sqrt{\frac{1+e_+}{1-e_+}} K_p \quad (5.4)$$

$$K_p = \frac{3\mu_{Sun}}{r_{sp}^3} r_p (AB \cos(2\omega) - 0.5(A^2 - B^2) \sin(2\omega)) \quad (5.5)$$

where

$$A = \cos(\Omega - \theta_{SE}), B = -\cos i \sin(\Omega - \theta_{SE})$$

and r_{sa} is the distance between the candidate asteroid at perigee when aerobraking and the Sun; n is the mean angular motion of the captured asteroid around the Earth; θ_{SE} is the angle of the Sun with respect to the Earth, measured from the positive x axis in an Earth-centred inertial frame XYZ, shown in Fig. 5.11.

It should be noted that Eq. (5.4) provides an approximation to the change in the height of the next perigee after aerobraking and thus it will be different from the true change of the next perigee height in the Sun-Earth CRTBP model. However, we can still use the sign of the term K_p in Eq. (5.5) as a fundamental filter for the solution space in the following optimisations. That is, results with $K_p < 0$ will be discarded from the solution space before checking whether the height of new perigee above the Earth's surface is larger than 100 km or not in the following optimisation. This filter will discard capture orbits where the solar gravitational perturbation lowers the perigee further, rather than passively raising the perigee above 100 km.

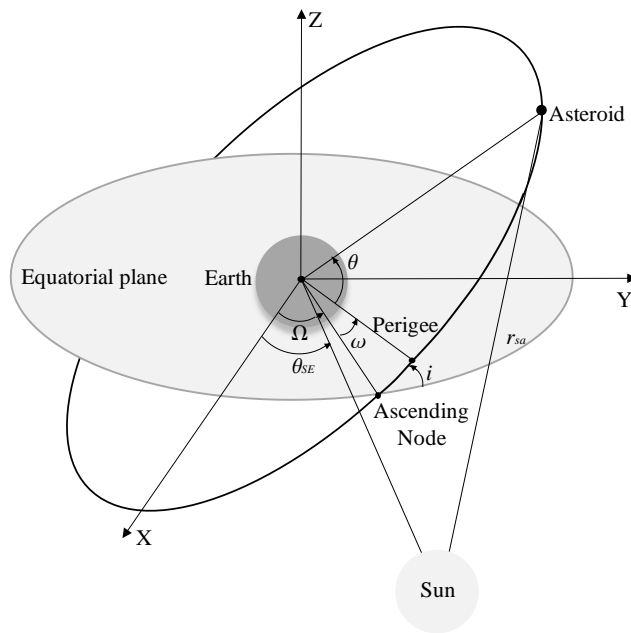


Fig. 5.11 Geometry of the captured asteroid and the Sun in the Earth-centred inertial frame XYZ.

5.2.4 Bi-impulse capture of asteroids at the Earth

As shown in Fig. 5.10(a), for the bi-impulse capture strategy, it is assumed that the captured asteroid moves in a bound orbit at the Earth inside the Earth's sphere of influence and so the state of the captured asteroid after aerobraking can be propagated forward in the Earth-centred two-body problem. Hence, capture of the asteroid at the Earth is defined here by

$$\begin{cases} v_{p+} < \sqrt{2\mu_{Earth} / r_p} \\ r_a < r_{SOI} \end{cases} \quad (5.6)$$

where r_a is the distance from the centre of the Earth to the apogee of the captured asteroid's orbit after aerobraking and $r_{SOI} = 925000$ km is the radius of the Earth's sphere of influence [195]. Then, a second impulse is required to raise the subsequent perigee of the trajectory after aerobraking out of the Earth's atmosphere so that the distance from the centre of the Earth to the new perigee of the asteroid's orbit should be

$$r_{np} \geq 6378 + 100 = 6478 \text{ km} \quad (5.7)$$

Therefore, the second impulse which is required to raise the orbit perigee can be written as

$$\Delta v_2 = \frac{h_a}{r_a} - \frac{\sqrt{r_a \mu_{Earth} (1 - e_n)}}{r_a} \quad (5.8)$$

where h_a is the magnitude of asteroid's angular momentum before aerobraking; e_+ is the eccentricity of post-aerobraking orbit; e_n is the eccentricity of the orbit with the perigee raised where

$$h_a = r_p |\mathbf{v}_{p+}|, \quad e_+ = \frac{h_a^2}{r_p \mu_{Earth}} - 1$$

$$r_a = \frac{h_a^2}{\mu_{Earth} (1 - e_+)}, \quad e_n = \frac{r_a - r_{np}}{r_a + r_{np}}$$

The minimum value of Δv_2 can be obtained when $r_{np} = 6478$ km. Therefore, the total cost of capturing an asteroid around the Earth using this capture strategy is given simply by

$$\Delta v = \Delta v_1 + \Delta v_2 \quad (5.9)$$

In this capture strategy, for one candidate asteroid, as shown in Fig. 5.6, there are 4 parameters: $(T_0, \Delta v_1, \theta_1, \theta_2)$. However, a uniform random sampling of θ_1 and θ_2 does not result in a uniform distribution of points in the solution space [190]. Therefore, a transformation of θ_1 and θ_2 is required such that [196]

$$\begin{cases} \theta_1 = 2\pi\alpha_1, & \alpha_1 \in [0,1] \\ \theta_2 = \cos^{-1}(2\alpha_2 - 1), & \alpha_2 \in [0,1] \end{cases} \quad (5.10)$$

This problem can then be transformed to a problem with 4 parameters: $(T_0, \Delta v_1, \alpha_1, \alpha_2)$. These transfer trajectories can again be searched using the global optimisation method NSGA-II [182], using the total Δv cost as the objective function and Eq. (5.6) as the constraints. Then, transfers obtained with NSGA-II can be locally optimised with the function *fmincon* in MATLAB. Therefore, a list of asteroids which can be captured with a total Δv cost of less than 50 m/s is shown in Table 5.1. An example of a transfer trajectory to capture 2012 BK14 is shown in Fig. 5.12.

As shown in Table 5.1, the asteroid capture strategy using aerobraking can achieve low-energy capture of asteroids, especially for 2005 VL1, 2012 GD and 2012 BK14. Amongst them, the lowest cost transfer is below 10 m/s, corresponding to the capture of 2012 BK14 into a bound orbit at the Earth. Comparing the results of the two manoeuvres

in Table 5.1, it is found that most of the second (perigee raising) manoeuvres are much smaller than the first manoeuvre. That is, for asteroid capture missions using aerobraking, most propellant will be consumed to manoeuvre the candidate asteroid from its initial orbit. Although aerobraking can enable low-energy capture of small asteroids, the accompanying mass loss of the captured asteroid due to atmospheric ablation may be high, as determined from Eq. (4.10). For example, over half of 2012 GD's mass would be lost during the aerobraking when the total Δv cost alone is used as the objective function for the optimisation problem. Therefore, an asteroid capture mission with minimum total Δv cost may not be economically optimal, as will be discussed later in Section 5.3.

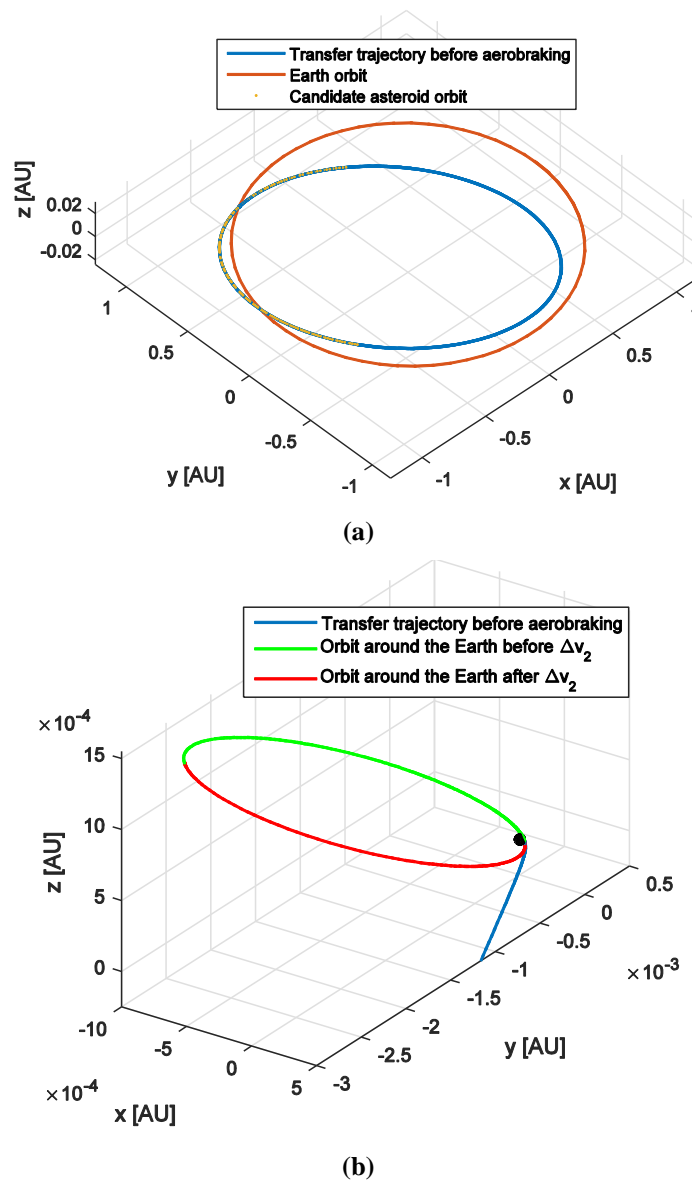


Fig. 5.12 Transfer trajectory capturing 2012 BK14 including: a) transfer trajectory before aerobraking in the Sun-centred inertial frame; b) orbit around the Earth after aerobraking in the Earth-centred inertial frame.

Table 5.1 Optimal results of capturing asteroids around the Earth in the Earth two-body problem

Asteroid	Diameter D , m	Capture date T_0 , MJD	Flight time, day	Total cost, m/s	Δv_1 , m/s	Δv_2 , m/s	Mass loss f , %	r_a/r_{SOI}
2000 AG6	29.5	64741	1417.2	27.08	25.89	1.19	31.5	0.419
2005 VL1	17	58514.2	1003.3	11.9	10.99	0.91	31.3	0.524
2007 UD6	7.4	62998.6	888.1	37.36	36.45	0.91	28.7	0.481
2008 HJ	23.4	62099.6	1623.6	35.24	34.37	0.88	40.8	0.578
2009 SN103	4.3	58938.6	1289.1	27.96	27.25	0.72	44.4	0.615
2009 VT1	4.3	58936	1291.7	28.13	27.35	0.78	44.5	0.564
2009 XR1	4.9	63457.8	1578.3	16.6	15.84	0.76	41.2	0.582
2010 UY7	6.8	60206.8	1498.3	28.98	28.32	0.66	12.2	0.594
2010 VL65	7.1	59369.2	153.1	24.76	24.05	0.72	22	0.591
2012 BK14	11.2	65196.1	1708.3	7.36	6.50	0.86	28.3	0.531
2012 GD	14.1	67440.4	1797.4	7.02	6.18	0.85	52.2	0.593
2012 TC4	15.5	58734.7	1126.9	17.06	15.73	1.33	41.8	0.367
2012 VJ38	6.8	61517.7	1660	29.04	28.31	0.72	25.6	0.593
2012 XB112	3.5	63373.9	1663.5	31.7	30.95	0.75	19.1	0.517
2012 XN134	9.8	58557.5	1736.5	15.85	15.26	0.59	44.7	0.815
2013 FU13	11.2	64006	1496.6	14.83	13.9	0.92	33.1	0.503
2014 JR24	4.7	59306.2	1500.7	20.14	19.51	0.63	11.6	0.594
2014 QN266	18.6	59964.6	1513.2	34.68	33.8	0.88	8.10	0.473
2014 WE6	2.8	63074	1572	28.07	27.44	0.63	16.5	0.588
2015 EZ6	6.50	66236.2	1450.7	28.01	27.33	0.68	12.2	0.574
2016 FY2	26.9	62275.2	1371.6	25.24	24.47	0.78	14.6	0.591
2016 FZ13	7.4	59943.7	1547.3	15.42	14.69	0.72	21.7	0.588
2016 YR	12.3	65792.3	1808.2	27.4	26.73	0.68	8.20	0.590
2017 FU102	6.2	63067.6	1720.5	16.46	15.68	0.78	39.3	0.573
2017 RV2	19.5	65609	1522.7	17.57	16.66	0.91	31.1	0.533
2017 SA20	7.8	58855.4	1569	16.07	15.33	0.74	27.1	0.593
2017 UQ6	12.3	60390.5	1613.9	28.53	27.84	0.69	9.50	0.594
2018 EM4	29.5	61249.5	1706.8	31.61	29.89	1.72	35	0.292

It should be noted that in this capture strategy, for some asteroids such as 2009 SN103 and 2012 XN134, their apogees have a considerable distance to the centre of the Earth. This means, the Sun's gravity still has a considerable influence on the captured asteroid at apogee. Therefore, with the gravitational perturbation due to the Sun, the orbit of the captured asteroid may deviate from a Keplerian ellipse. This is one drawback of the bi-impulse capture strategy using aerobraking and thus the station-keeping strategies would then be required. To address this problem, a smaller apogee distance of the captured asteroid orbit to the centre of Earth would be required. In addition, as shown in Table 5.1, it can be seen that the apogee distance of the captured asteroid orbit to the centre of the Earth is often much smaller than the Earth's SOI, for example 2000 AG6, 2012 TC4 and 2018 EM4. Therefore, for these asteroids, the assumption of their motions in the Earth-centred two-body problem is still valid.

5.2.5 Single impulsive capture of asteroids around the Earth

As shown in Fig. 5.10(b), in this capture strategy, the state of the captured asteroid after aerobraking should be propagated forward in the Sun-Earth CRTBP. Here we assume that the captured asteroid moves away from the vicinity of the Earth such that the perigee of the captured asteroid is outside the Earth's sphere of influence. Therefore, capture of the asteroid can be defined here by

$$\begin{cases} v_{p+} \leq \sqrt{2\mu_{Earth} / r_p} \\ \min(r_{p+}) > 6478 \text{ km} \\ \max(r_{p+}) < r_{SOI} \end{cases} \quad (5.11)$$

where $\min(r_{p+})$ is the minimum perigee distance to the centre of the Earth after aerobraking and $\max(r_{p+})$ is the maximum perigee distance after aerobraking within a given post-aerobraking duration (1000 days). It should be noted that even although the new perigee height above the Earth's surface can be raised to be more than 100 km, the Earth's atmosphere can still provide a small drag force at subsequent perigee passages and thus would act as a perturbation to the asteroid orbit. Considering the sensitivity of orbit in the Sun-Earth CRTBP, we should take this perturbation into account within a given post-aerobraking duration (1000 days) which can be estimated using Eq. (4.4). Here, the total cost of capturing the asteroid about the Earth is given simply as

$$\Delta v = \Delta v_1 \quad (5.12)$$

In this capture strategy, for one candidate asteroid in Fig. 5.6, there are also 4 parameters: $(T_0, \Delta v_1, \alpha_1, \alpha_2)$. These transfer trajectories can again be searched using NSGA-II, using the total Δv cost as the objective function and Eq. (5.12) as the constraints. Then, transfers obtained with NSGA-II can be locally optimised with the function *fmincon* in MATLAB. Therefore, the list of asteroids that can be captured with a total Δv cost below 50 m/s is shown in Table 5.2. An example of a transfer trajectory is shown in Fig. 5.13-5.14 and the time history of the perigee height of the captured asteroid's orbit above the Earth's surface with respect to flight time is shown in Fig. 5.15.

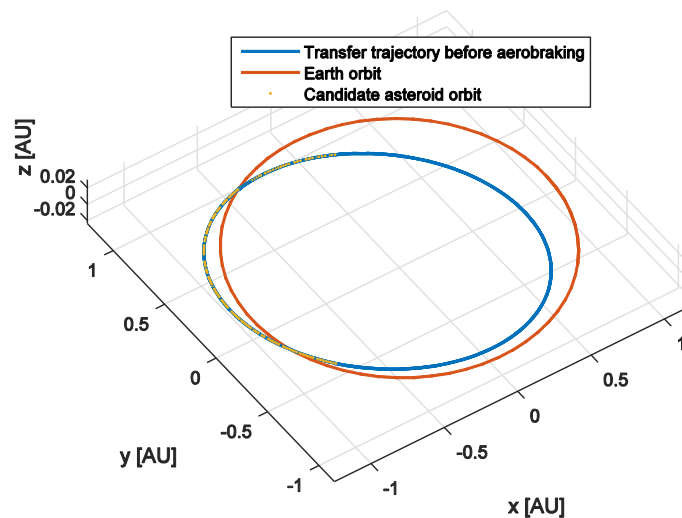


Fig. 5.13 Transfer trajectory of capturing 2012 BK14 before aerobraking in the Sun-centred inertial frame.

Similar to the bi-impulse capture strategy, aerobraking can again save significant energy and thus can enable the low-cost capture of a number of asteroids in the Sun-Earth CRTBP. Since no further manoeuvre is required to raise the perigee height after aerobraking, the total cost of this capture strategy is slightly smaller than the bi-impulse capture strategy in the Earth-centred two-body problem. For example, the cheapest transfer in this capture strategy also corresponds to the capture of 2012 BK14, and its total cost is only 1.64 m/s smaller than that of the bi-impulse capture strategy. Due to the gravitational perturbation of the Sun, the captured asteroid is strongly perturbed with the perigee height passively raised, as shown in Fig. 5.15. However, as shown in Fig. 5.14, with the long-term influence of the Sun's gravity, the perigee height of the captured asteroid orbit around the Earth may be lowered gradually after a significant duration (about 2900 days). Consequently, a second aerobraking phase may occur 5800 days after aerobraking for

asteroid capture. Nevertheless, before the second aerobraking phase, there is in principle sufficient time to explore and exploit the captured asteroid and its resources.

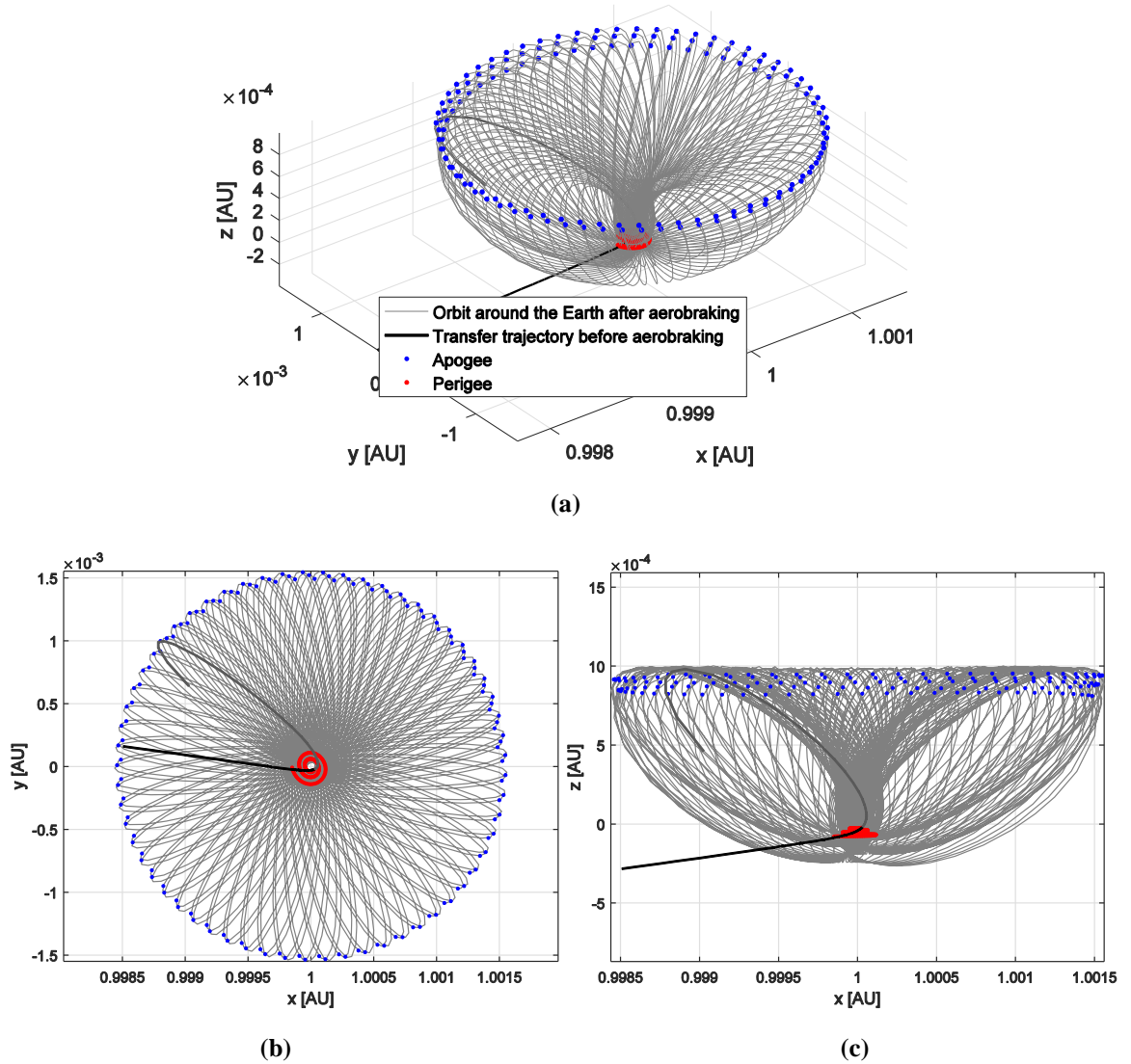


Fig. 5.14 Capture orbit of 2012 BK14 around the Earth after aerobraking for 1000 days in the Sun-Earth rotating frame: (a) 3D view; (b) x - y projection; (c) x - z projection.

To further illustrate this dynamical behaviour, the change in the height between one perigee and the previous perigee along the asteroid orbit around the Earth is defined as the following:

$$\Delta h_j = h_j - h_{j-1}, \quad j = 1, 2, 3, \dots \quad (5.13)$$

where h_j is the height of j^{th} perigee with respect to the centre of the Earth after aerobraking and h_0 is the perigee height when aerobraking. Moreover, using the approximation in Eq. (5.4), the estimated change in the height between one perigee and the previous perigee can be written as

$$\delta h_j = (h_{j-1} + \delta h) - h_{j-1}, \quad j = 1, 2, 3 \dots \quad (5.14)$$

where δh is the estimated change in height between the j^{th} perigee and the $(j-1)^{\text{th}}$ perigee using Eq. (5.4), based on the true orbital elements at the $(j-1)^{\text{th}}$ perigee. A comparison of the true change and estimated change in the perigee height is shown in Fig. 5.15. The slight differences between the true change and estimated change demonstrates the validity of the approximation in Eq. (5.4). Furthermore, the change in the perigee height has clear periodicity and it exhibits a long-period variation, as discussed earlier.

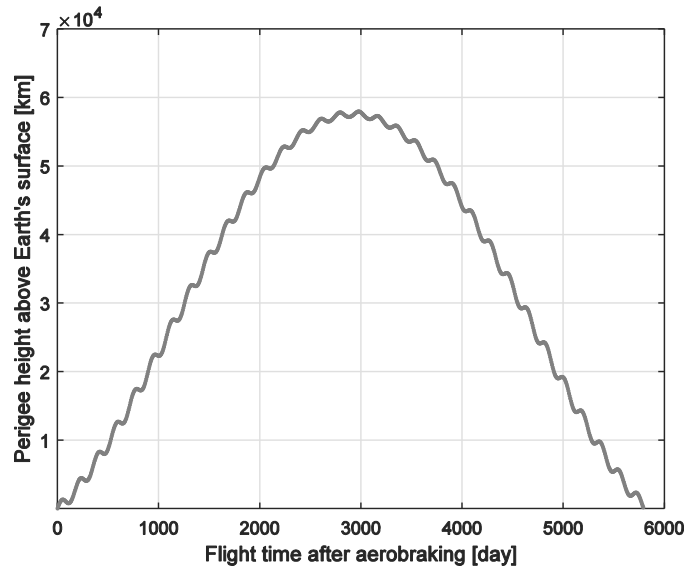


Fig. 5.15 Perigee height of the captured asteroid's orbit around the Earth after aerobraking

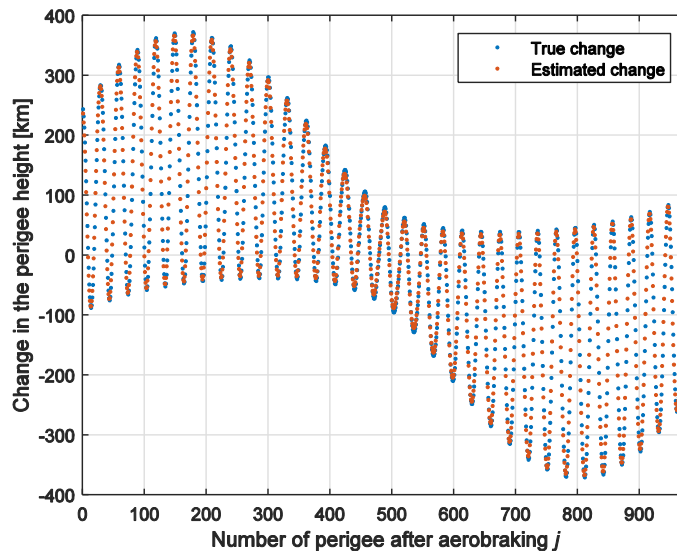


Fig. 5.16 Comparison of the true change and estimated change in the perigee height.

Table 5.2 Results of capturing asteroids around the Earth in the Sun-Earth CRTBP

Asteroid	Diameter D , m	Capture date T_0 , MJD	Flight time, day	Total cost, m/s	Mass loss f , %	r_a/r_{SOI}
2000 AG6	29.5	64749.2	1409	23.8	31.2	0.521
2005 VL1	17	58499.6	1017.8	10.61	30.8	0.976
2007 UD6	7.40	62967.2	919.8	33.31	28.8	0.510
2008 HJ	23.4	62099.9	1623.4	31.91	41	0.470
2009 SN103	10.2	67634	981.3	34.4	30.4	0.446
2009 VT1	4.30	58973.3	1254.5	29.13	44.4	0.562
2009 XR1	4.90	63428	1608.1	15.92	41.4	0.490
2010 UY7	6.80	60226.7	1478.2	27.09	12.5	0.490
2010 VL65	7.10	59364.4	157.8	23.91	21.8	0.701
2012 BK14	11.2	65262	1642.4	8.81	27.6	1.374
2012 GD	14.1	67446.8	1791.1	6.19	52.2	0.638
2012 TC4	15.5	58748.6	1113.1	15.16	41.4	0.478
2012 VJ38	6.80	61501.7	1676.2	30.62	25.9	0.474
2012 XB112	3.50	63380.1	1657.3	30.32	18.9	0.603
2012 XN134	9.8	58544.9	1749.2	15.59	44.7	0.840
2013 FU13	11.2	63989.4	1513.7	12.5	33.3	0.481
2014 JR24	4.70	59269.6	1538	20.13	11	1.05
2014 QN266	18.6	59940.6	1536.7	33.23	8.50	0.404
2014 WE6	2.80	63112.3	1533.8	26.37	17	0.487
2015 EZ6	6.50	66229.6	1457.1	26.68	11.2	1.856
2016 FY2	26.9	62295.6	1351.4	24.12	14.7	0.509
2016 FZ13	7.40	59927.5	1563.4	14.71	21.3	0.993
2016 YR	12.3	65810.2	1790	25.32	7.90	0.797
2017 FU102	6.20	63092.4	1695.7	21.01	39.7	0.408
2017 RV2	19.5	65605.1	1526.5	16.68	30.6	0.937
2017 SA20	7.80	58829.7	1594.4	13.73	27.3	0.513
2017 UQ6	12.3	60390.7	1613.8	27.82	8.80	1.263
2018 EM4	29.5	61226.6	1729.8	30.61	34.2	0.497

Another challenge is the uncertainty of the properties of the candidate asteroid. Aerobraking can cause mass loss of the asteroid due to ablation which depends on the asteroid's geometry, material properties and composition. A suitable heat shield, potentially an inflatable structure, or manufactured from the asteroid material itself [140], could provide protection of the candidate asteroid and thereby reduce ablative mass loss during aerobraking, while improving the predictability of the aerobraking manoeuvre.

5.3 Maximum mass ratio of the captured asteroid and spacecraft

From an economic point of view, the mass of the spacecraft required to capture the candidate asteroid should be taken into account. Moreover, to measure the yield of the asteroid capture mission, the ratio of the mass of the captured asteroid after aerobraking to the mass of the transfer vehicle is defined as

$$f_m = m_+ / m_0 \quad (5.14)$$

where m_0 is the (wet) mass of the transfer vehicle at rendezvous with the candidate asteroid, and again m_+ is the final mass of the asteroid after aerobraking. It is assumed that a minimum of 20% of the mass of the transfer vehicle is allocated to structure and subsystems and that its specific impulse is $I_{sp} = 300$ s (bi-propellant engine).

For the bi-impulse capture strategy, after the first impulse Δv_1 , the spacecraft mass is then

$$m_1 = (m_- + m_0)e^{-\Delta v_1/(gI_{sp})} - m_- \quad (5.15)$$

and then after second impulse Δv_2 , the spacecraft's mass becomes

$$m_2 = ((m_- + m_0)e^{-\Delta v_1/(gI_{sp})} - m_- + m_+)e^{-\Delta v_2/(gI_{sp})} - m_+ \quad (5.16)$$

again where m_- is the initial mass of the asteroid prior to aerocapture. Thus, we have

$$((m_- + m_0)e^{\frac{-\Delta v_1}{gI_{sp}}} - m_- + m_+)e^{\frac{-\Delta v_2}{gI_{sp}}} - m_+ \geq 0.2m_0 \quad (5.17)$$

Hence, the minimum (wet) mass of the spacecraft required to capture the target asteroid can be written as

$$m_0 = \frac{(m_- - m_+)e^{-\Delta v_2/(gI_{sp})} + m_+ - m_- e^{-\Delta v/(gI_{sp})}}{e^{-\Delta v/(gI_{sp})} - 0.2} \quad (5.18)$$

Therefore, after substituting Eq. (4.9) into Eq. (5.18), the mass ratio of the captured asteroid after aerobraking and the required spacecraft mass can be written as

$$f_m = \frac{e^{-\Delta v/(gI_{sp})} - 0.2}{(e^{-\sigma(v_{p+}^2 - v_{p-}^2)/2} - 1)e^{-\Delta v_2/(gI_{sp})} + 1 - e^{-\Delta v/(gI_{sp}) - \sigma(v_{p+}^2 - v_{p-}^2)/2}} \quad (5.19)$$

where the ablative mass loss of the asteroid has been accounted for. On the other hand, for the single impulsive asteroid capture strategy, the mass ratio of the captured asteroid after aerobraking and the required spacecraft mass is given by

$$f_m = \frac{e^{-\Delta v/(gI_{sp})} - 0.2}{1 - e^{-\Delta v/(gI_{sp}) - \sigma(v_{p+}^2 - v_{p-}^2)/2}} \quad (5.20)$$

In these two capture strategies, for each candidate asteroid, there are again 4 variables: $(T_0, \Delta v_1, \alpha_1, \alpha_2)$. The same list of asteroids in Table 5.1 and Table 5.2 is investigated and the optimal transfers for capturing those asteroids around the Earth using aerobraking can again be obtained with NSGA-II using Eq. (5.19) or Eq. (5.20) as the objective function. Therefore, the new optimal results are shown in Table 5.3 and Table 5.4.

From Table 5.3 and Table 5.4, it can be seen that the retrieved masses of the captured asteroids using aerobraking are tens of times more than that of the spacecraft that is required to execute the mission, particularly for 2005 VL1, 2012 GD and 2012 BK14. Comparing the results of Table 5.1-5.4, the asteroids with smaller total Δv cost in Table 5.1 and Tables 5.2 can potentially be captured with a larger ratio of the retrieved mass to the required spacecraft mass. However, the minimum total Δv cost does not always imply the maximum yield of a retrieval mission. For example, the mass ratio f_m for capturing 2008 HJ is larger than that of capturing 2009 SN103, as shown in Table 5.4, while the total Δv cost of capturing 2009 SN103 is smaller than that of capturing 2008 HJ, as shown in Table 5.2. Furthermore, capturing 2012 BK14 is the most attractive target, with the retrieved mass of the asteroid 236 and 285 times more than that of the spacecraft itself at the start of the capture manoeuvre, corresponding to the bi-impulse capture and single impulse asteroid capture strategies, respectively. Therefore, asteroid 2012 BK14 can be considered to be the best candidate asteroid, when minimising the total Δv cost or maximizing the fraction of retrieved mass to the required spacecraft mass.

Table 5.3 Results of bi-impulsive capture of asteroids at the Earth when optimising f_m

Asteroid	Diameter, D	Capture date T_0 , MJD	Flight time, day	Mass ratio f_m	Total cost, m/s	Mass loss f , %
2000 AG6	29.5	64742.6	1415.5	61	26.67	31.2
2005 VL1	17	58512.5	1005	139.6	11.82	31.3
2007 UD6	7.4	62991	895.8	45.5	36.71	28.9
2008 HJ	23.4	62098.2	1625.1	40.7	34.08	42
2009 SN103	10.2	67611.2	1004.3	45.1	36.39	30
2009 VT1	4.3	58948.1	1279.5	46.7	28.11	44.6
2009 XR1	4.9	63452.7	1583.4	87.1	16.13	41.2
2010 UY7	6.8	60220.1	1485	72	28.55	12.2
2010 VL65	7.1	59366.9	155.2	73.4	24.92	22.3
2012 BK14	11.2	65196.7	1707.6	236.8	7.36	28.4
2012 GD	14.1	67473	1764.9	161.9	7.56	52.6
2012 TC4	15.5	58739	1122.7	87.4	16.12	41.5
2012 VJ38	6.8	61532.7	1645	60.1	29.01	25.8
2012 XB112	3.5	63381.5	1655.8	61.4	30.95	18.9
2012 XN134	9.8	58537.4	1756.7	79.2	16.71	45.4
2013 FU13	11.2	64029	1473.3	104.6	15.31	32.8
2014 JR24	4.7	59317.5	1489.4	106.1	19.57	11.6
2014 QN266	18.6	59959.7	1518.1	62.3	34.53	7.8
2014 WE6	2.8	63087.3	1558.7	70.5	27.73	16.6
2015 EZ6	6.5	66227.6	1459.2	76	27.06	12.2
2016 FY2	26.9	62281.9	1364.9	80.1	25.04	14.5
2016 FZ13	7.4	59965.7	1525.3	124.2	14.94	21.7
2016 YR	12.3	65798.7	1801.7	82.4	26.06	8.3
2017 FU102	6.2	63035	1753.1	85.9	16.87	39.2
2017 RV2	19.5	65598	1533.7	93.7	17.5	31
2017 SA20	7.8	58849.6	1574.7	104.3	16.57	27.7
2017 UQ6	12.3	60407.3	1597	72.4	29.24	9.6
2018 EM4	29.5	61250.7	1705.6	50.2	30.91	34.3

Table 5.4 Results of single impulse capture of asteroids at the Earth when optimising f_m

Asteroid	Diameter, D	Capture date T_0 , MJD	Flight time, day	Mass ratio f_m	Total cost, m/s	Mass loss f , %
2000 AG6	29.5	64743.3	1414.9	72.6	22.32	30.7
2005 VL1	17	58503.6	1013.9	151.1	10.72	30.9
2007 UD6	7.4	62993.5	893.2	47.4	35.39	28
2008 HJ	23.4	62077.6	1645.4	42.3	32.77	40.6
2009 SN103	10.2	67637.3	978	46.4	34.72	30.8
2009 VT1	4.3	59026.1	1201.4	47.4	27.26	44.7
2009 XR1	4.9	63454.3	1581.9	86.5	16.02	40.9
2010 UY7	6.8	60229.9	1475	75.1	27.43	11.8
2010 VL65	7.1	59374.8	147.4	76.3	24.03	21.6
2012 BK14	11.2	65213.2	1691.1	285.3	5.77	27.1
2012 GD	14.1	67459.6	1778.3	186.5	6.05	51.9
2012 TC4	15.5	58767.2	1094.4	83.4	16.57	41
2012 VJ38	6.8	61508.5	1669.4	61.3	28.53	25.1
2012 XB112	3.5	63395.8	1641.5	63.1	30.18	18.4
2012 XN134	9.8	58556.6	1737.4	83.6	15.39	45.1
2013 FU13	11.2	64010.4	1492.5	120.5	13.12	32.6
2014 JR24	4.7	59272.2	1535.3	105.4	19.76	11
2014 QN266	18.6	59958.3	1519.3	63.7	33.77	7.7
2014 WE6	2.8	63107.2	1538.8	72.8	26.91	16.2
2015 EZ6	6.5	66237.5	1449.6	74.5	27.74	11.5
2016 FY2	26.9	62289.1	1357.9	85.3	23.52	14.2
2016 FZ13	7.4	59933.9	1557	125.2	14.66	21.6
2016 YR	12.3	65800.7	1799.5	86	25.06	7.8
2017 FU102	6.2	63096.2	1691.8	85.7	16.69	38.9
2017 RV2	19.5	65584	1547.6	93.3	17.37	30.8
2017 SA20	7.8	58829.2	1595	123.6	13.89	26.7
2017 UQ6	12.3	60386.5	1618	76.5	27.82	8.9
2018 EM4	29.5	61229.1	1727.3	49.7	30.88	34.2

In addition, the semi-major axis of the target asteroid 2012 BK14 is not close to that of the Earth. This indicates that although only a small manoeuvre is required to move the asteroid from its initial orbit to intersect the Earth's orbit, the relative velocity of the asteroid with respect to the Earth should be considerable and thus it would need a large impulse to insert onto a stable manifold associated with a periodic orbit around the Sun-Earth libration points at L_1 or L_2 . Therefore, this asteroid is not in the list of EROs [9].

5.4 Discussion

This chapter provides a general analysis of aerobraking strategies and uses aerobraking to capture asteroids directly onto bound orbits about the Earth. In detail, two strategies have been proposed for capturing NEAs at the Earth by using a single-pass aerobraking manoeuvre. Although aerobraking can increase risk during capture manoeuvres due to the requirement for a grazing flyby, a selection criterion for candidate asteroids was investigated to minimise such risks. Then, single impulse and bi-impulse capture of asteroids was discussed, using the total impulse and the yield of the retrieved mass of the asteroid with respect to the required spacecraft mass as objective functions. Comparing the results of these two capture strategies, aerobraking can greatly reduce the energy required to capture small NEAs. Optimisation then finds the best candidate asteroids which can be captured using aerobraking. This indicates that 2012 BK14 is one of the best targets which can be captured with a total cost below 10 m/s. Moreover, considering mass loss during aerobraking, capturing 2014 BK14 is also the most economical and the retrieved mass can be over 200 times more than that of the spacecraft which is required to execute the mission.

The strategies proposed are intended to be used for the preliminary analysis of aerobraking for asteroid capture. For the practical implementation of this concept, a real ephemeris model must be taken into account, along with robust navigation and control. Moreover, the structural integrity of the asteroids also needs to be ensured and thus active protection for the captured asteroids may be required. However, since the model of the Sun-Earth CRTBP can provide a good approximation of the real Sun-Earth system, the list of the NEAs that can be captured with low energy are not expected to change significantly.

CHAPTER 6

CAPTURE OF NEAS USING MOMENTUM EXCHANGE STRATEGIES

This Chapter investigates the concept of capturing small NEAs into bound periodic orbits at the Sun-Earth L_1 and L_2 points using momentum exchange theory, including both kinetic impacts and the use of tethered assist. The key contribution of the Chapter is in coupling momentum exchange strategies to invariant manifolds in the Sun-Earth CRTBP system through the use of dynamical models of the kinetic impact and tether-assisted flyby. The analysis undertaken in this Chapter (which was presented in Ref [46]) is summarized as follows:

- (1) A selection strategy for candidate asteroids is proposed by considering both the deflection windows for capturing asteroids and the size of the candidate asteroids.
- (2) In the capture strategy using kinetic impacts, the small asteroid leaves its initial orbit through an impulse delivered from a spacecraft and then approaches a large target asteroid. Accordingly, the small asteroid then collides with the large asteroid with an impact geometry such that the small asteroid will be captured onto the stable manifold associated with the Sun-Earth L_1 or L_2 points, thus leveraging the orbit energy of the large asteroid by investigating the outcome of the impact on the small asteroid;
- (3) In the capture strategy using the tethered assist, after a targeting impulse, the small asteroid approaches the large asteroid and then connects with the large asteroid through a tether; the tether is then released after the flyby manoeuvre. As a result, the small asteroid will again be transferred onto the stable manifold associated with the Sun-Earth L_1 or L_2 points, based on the maximum velocity increment available which can be obtained by analysing the tension of the tether.

6.1 Target periodic orbits and invariant manifolds

In both asteroid capture strategies using momentum exchange, the small asteroid leaves its orbit and will be inserted onto the stable manifold associated with the periodic orbits of the Sun-Earth L_1 or L_2 points after the momentum exchange encounter. During the transfer from the asteroid orbit to the stable manifold, the motion of the asteroid is considered in the Sun-asteroid two-body problem. When the small asteroid is captured onto the stable manifold, it will then be modelled by the Sun-Earth CRTBP.

As discussed in Section 3.3, the Lyapunov orbits and halo orbits around the Sun-Earth L_1 and L_2 points have been calculated using a numerical procedure in Section 2.2.4. In this Chapter, these periodic orbits will again serve as the final target orbits where the candidate asteroids are captured and parked. Invariant manifolds associated with periodic orbits around the libration points are again key to the design of low-energy transfer trajectories.

As discussed in Section 3.1.1, the Poincaré surface of section is now defined by a plane in position space $y = (x + \mu) \tan \beta$ where β is the angle of the section with respect to the Sun in the rotating frame, as shown in Fig. 6.1. Transfer trajectories from the initial asteroid orbit to the stable manifolds associated with the Sun-Earth L_1 and L_2 periodic orbits can then be designed by solving for a Lambert arc in the two-body Sun-asteroid model. Here $\beta = \pm\pi/8$ is set as the threshold of the boundary of the Sun-asteroid two-body problem and the Sun-Earth CRTBP ($\pi/8$ for the L_2 stable manifold and $-\pi/8$ for the L_1 stable manifold) [18, 50].

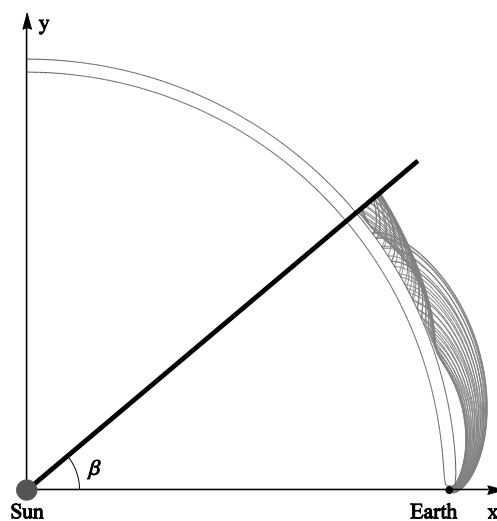


Fig. 6.1 Stable manifolds associated with the Lyapunov orbit ($A_p = 0.0020101$ AU) around Sun-Earth L_2 .

6.2 Candidate asteroid selection

6.2.1 Capture windows

As discussed in Section 4.3.3, the date when the distance between the Earth and the asteroid is 0.21 AU is defined as a threshold date of the capture window. Given one small asteroid and one large asteroid, the threshold dates of the small asteroid and the large asteroid are denoted as T_s and T_l , respectively. Therefore, the domain of the impulse date (T_0) to deflect the small asteroid from its natural orbit and the flight time (T_{fly1}) from the impulse to the interception of the large asteroid should be

$$\begin{cases} T_0 \in [2019, T_s], & T_s \leq 2050 \\ T_0 + T_{fly1} \in [2019, T_l], & T_l \leq 2050 \end{cases} \quad (6.1)$$

6.2.2 Candidate asteroid filter

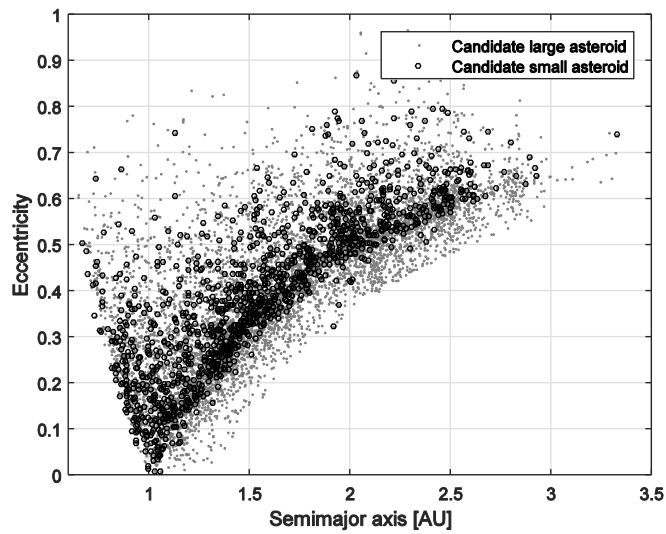
Potentially Hazardous Asteroids (PHAs) are those asteroids with an Earth Minimum Orbit Intersection Distance (MOID) of 0.05 AU or less and an absolute magnitude (H) of 22.0 or less [197]. PHAs can be considered to pose a potential threat to the Earth when they have a close approach. A momentum exchange encounter with an asteroid with H smaller than 22.0 but MOID larger than 0.05 AU may decrease the MOID and thus the asteroid may become a PHA. Therefore, asteroids with H smaller than 22.0 are unsuitable targets for momentum exchange. This is used as a filter criteria for the large asteroid so that candidate large asteroids should have $H > 22.0$.

Furthermore, $D \leq 30$ m ($H \geq 25.26$) is again set as a threshold on asteroid size since captured asteroids may also be a potential impact threat to Earth, as discussed in Section 3.1.5. Objects of 30 m in diameter can be considered as the critical threshold above which the Earth's atmosphere will no longer disintegrate the object [147]. Considering this filter criteria, the candidate small asteroids should therefore have $H \geq 25.26$.

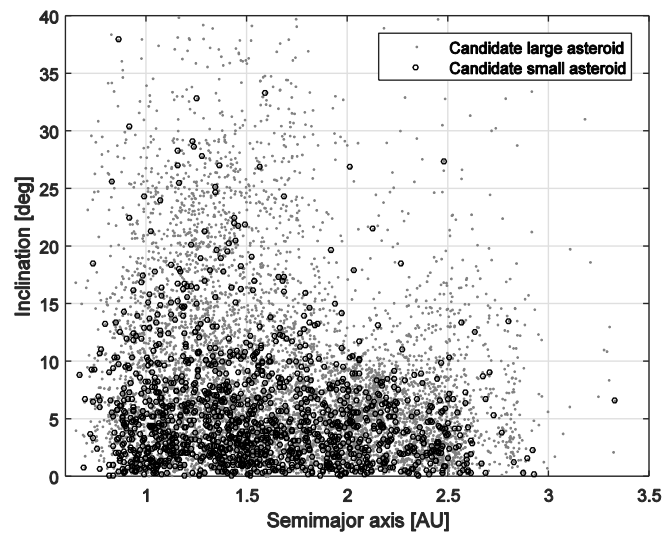
In order to minimise the influence of the impact on the large asteroid, and so guarantee that the large asteroid orbit is almost unchanged before and after the encounter, it is expected that the mass of the large asteroid (m_l) should be at least two orders of magnitude greater than that of the small asteroid (m_s) such that

$$\frac{m_l}{m_s} \geq 100 \quad (6.2)$$

Considering a large asteroid with $H > 22$ and a mass ratio of the two asteroids as defined in Eq. (6.2), the small asteroid should be selected such that $H > 25.33$. All candidate large asteroids and small asteroids are shown in Fig. 6.2.



(a)



(b)

Fig. 6.2 Distribution of candidate large and small asteroids: (a) semi-major and eccentricity and (b) semi-major and inclination.

6.3 Small asteroid capture through impact of a large asteroid

In this Section, kinetic impact theory is applied to the capture of asteroids. In this capture strategy, the small asteroid leaves its initial orbit through an impulse from a spacecraft and then approaches a large target asteroid. At interception, the small asteroid collides with the large asteroid with a suitable impact geometry such that the small asteroid is deflected, and subsequently captured onto the stable manifold associated with the Sun-Earth L_1 or L_2

points, thus transferring some of the orbit energy from the large asteroid to the small asteroid.

6.3.1 Problem statement

Figure 6.3 shows an overview of the strategy for capturing a small asteroid by the impact of a large asteroid. The mission scenario consists of the following steps: with the first impulse Δv_1 , the small asteroid leaves its orbit and will approach the vicinity of the target large asteroid; then the small asteroid collides with the large asteroid delivering a second impulse Δv_2 for a Lambert arc to intersect the stable manifold associated with the Sun-Earth L_1 or L_2 point; with the third impulse Δv_3 , the small asteroid is captured onto the stable manifold associated with the Sun-Earth L_1 or L_2 point.

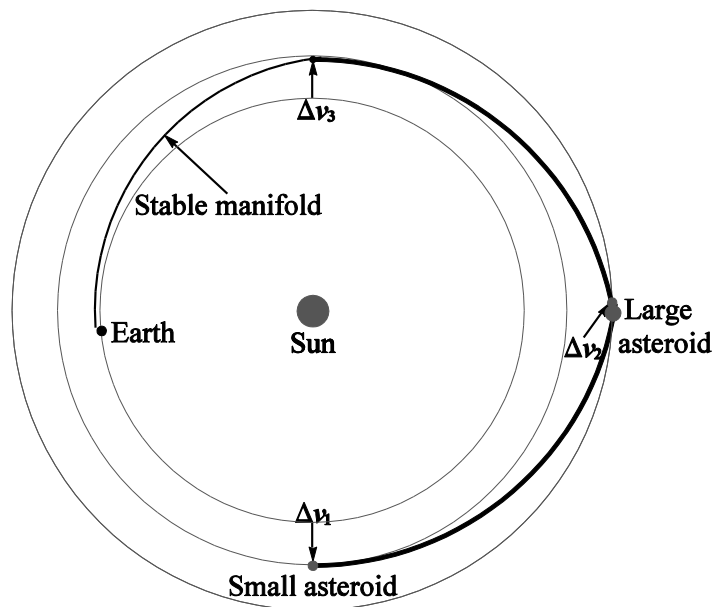


Fig. 6.3 Overview of small asteroid capture through impact of a large asteroid.

Given one small asteroid and one large asteroid, there are six variables in the solution space:

- T_0 : the date of the first impulse Δv_1 ;
- T_{fly1} : the flight time of the small asteroid between the first impulse and the impact;
- T_{fly2} : the flight time of the small asteroid between the collision and the impulse Δv_3 for insertion onto the stable manifold;

- A_p : amplitude variable of the target periodic orbit around the Sun-Earth L_1 or L_2 point (see Section 3.1.2);
- t_p : the parameter determining the point on the periodic orbit where the stable manifold is calculated from;
- t_m : the stable manifold transfer time determining the point on the stable manifold where the small asteroid inserts onto it.

6.3.2 Collision geometry

In practice, the small asteroid needs to accurately target an impact point on the large asteroid. Moreover, the masses of the two asteroids and the momentum exchange parameter between the asteroids are both major uncertainties. Therefore, high-precision navigation and pre-launch characterization and identification of the asteroid properties are necessary. It can be noted that such uncertainties are clearly important, but they are not considered in this Chapter whose aim is to define the overall capture strategy.

The collision geometry of a small asteroid with a large asteroid is shown schematically in Fig. 6.4. The centre-of-mass of the large asteroid and small asteroid are denoted as O_1 and O_2 respectively. Let \mathbf{v}_{s-} and \mathbf{v}_{s+} be the velocity vector of the small asteroid before and after the collision with the large asteroid, and let \mathbf{v}_{l-} and \mathbf{v}_{l+} be the velocity vector of the large asteroid before and after the collision. The unit normal vector \mathbf{n} is along the centre-of-mass of the two asteroids and the unit tangent vector $\boldsymbol{\tau}$ is perpendicular to \mathbf{n} . It will be assumed that the collision point is on the line \mathbf{n} along the mass centres of the two asteroids and the dynamics of the two asteroids is considered in the direction of \mathbf{n} only. According to the conservation of linear momentum, the velocity of the small asteroid after collision is given by [198]

$$\begin{cases} \mathbf{v}_{s\tau+} = \mathbf{v}_{s\tau-} \\ \mathbf{v}_{sn+} = \mathbf{v}_{sn-} - (1+k) \frac{m_l}{m_l + m_s} (\mathbf{v}_{sn-} - \mathbf{v}_{ln-}) \end{cases} \quad (6.3)$$

where $\mathbf{v}_{s\tau+} = (\mathbf{v}_{s+}^T \boldsymbol{\tau}) \boldsymbol{\tau}$, $\mathbf{v}_{s\tau-} = (\mathbf{v}_{s-}^T \boldsymbol{\tau}) \boldsymbol{\tau}$, $\mathbf{v}_{sn+} = (\mathbf{v}_{s+}^T \mathbf{n}) \mathbf{n}$ and $\mathbf{v}_{sn-} = (\mathbf{v}_{s-}^T \mathbf{n}) \mathbf{n}$.

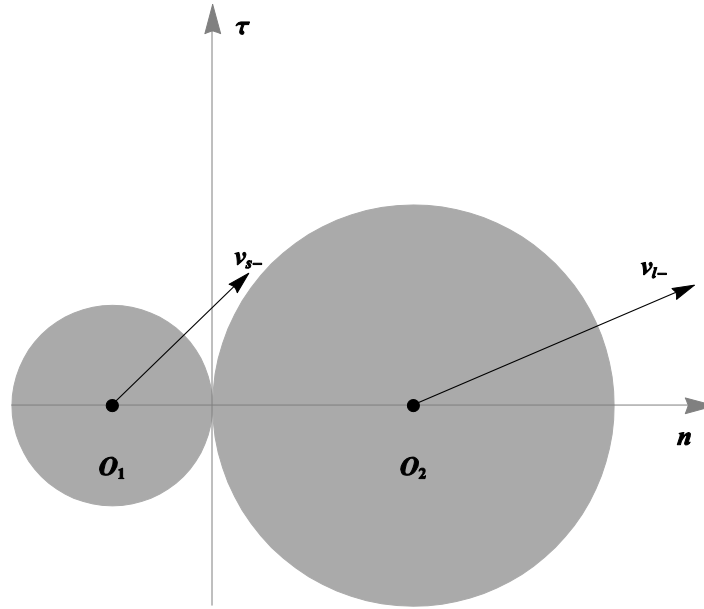


Fig. 6.4 Collision geometry of the two asteroids.

Therefore, Eq. (6.3) can be written as

$$\mathbf{v}_{s+} = \mathbf{v}_{s-} - (1+k) \frac{m_l}{m_l + m_s} ((\mathbf{v}_{s-} - \mathbf{v}_{l-})^T \mathbf{n}) \mathbf{n} \quad (6.4)$$

where the coefficient of restitution k is assumed to be 1 for a perfectly elastic collision. The relative velocity between the two asteroids in direction \mathbf{n} can then be written as

$$\Delta v_n = |\Delta \mathbf{v}_n| = |(\mathbf{v}_{s-} - \mathbf{v}_{l-})^T \mathbf{n}| \quad (6.5)$$

This relative velocity is key to estimating whether the small asteroid will remain intact or not after the collision. Here $\Delta v_{threshold}$ is denoted as the threshold such that once $\Delta v_n > \Delta v_{threshold}$, disruption of the asteroid will occur, as will be discussed later. Assuming \mathbf{v}_{Lam} is the required post-collision velocity vector of the small asteroid obtained by solving the Lambert arc from the large asteroid orbit to the stable manifold associated with Sun-Earth L_1 and L_2 periodic orbits, the second impulse $\Delta \mathbf{v}_2$ can therefore be written as

$$\Delta \mathbf{v}_2 = \mathbf{v}_{Lam} - \mathbf{v}_{s+} = \Delta \mathbf{v}_- - \lambda (\Delta \mathbf{v}_{ls}^T \mathbf{n}) \mathbf{n} \quad (6.6)$$

where

$$\Delta \mathbf{v}_- = \mathbf{v}_{Lam} - \mathbf{v}_{s-}, \lambda = (1+k) \frac{m_l}{m_l + m_s}, \Delta \mathbf{v}_{ls} = \mathbf{v}_{l-} - \mathbf{v}_{s-}$$

Once the six variables (T_0 , T_{fly1} , T_{fly2} , A_p , t_p , t_m) have been selected, the first impulse $\Delta\mathbf{v}_1$ and the third impulse $\Delta\mathbf{v}_3$ can then be determined by solving two Lambert arc problems, where the second impulse $\Delta\mathbf{v}_2$ is a function of the unit vector \mathbf{n} . The optimisation problem can therefore be written as,

$$\min |\Delta\mathbf{v}_2| \text{ subject to } |\Delta\mathbf{v}_{ls}^T \mathbf{n}| < \Delta v_{threshold} \quad (6.7)$$

It should be noted that the set $(\lambda\Delta\mathbf{v}_{ls}^T \mathbf{n})\mathbf{n}$ is a sphere with diameter $|\lambda\Delta\mathbf{v}_{ls}|$ which is centred at $\frac{1}{2}\lambda\Delta\mathbf{v}_{ls}$. According to the geometric relationship between the vectors in Eq.

(6.6), shown in Fig. 6.5, there exists a critical value of \mathbf{n} , $\mathbf{n}_c = \frac{2\Delta\mathbf{v}_- + (1-\gamma)\lambda\Delta\mathbf{v}_{ls}}{|2\Delta\mathbf{v}_- + (1-\gamma)\lambda\Delta\mathbf{v}_{ls}|}$ where

$\gamma = \frac{|\lambda\Delta\mathbf{v}_{ls}|}{|2\Delta\mathbf{v}_- - \lambda\Delta\mathbf{v}_{ls}|}$. When $|\Delta\mathbf{v}_{ls}^T \mathbf{n}_c| \leq \Delta v_{threshold}$, shown in Fig. 6.5(a), the second impulse is

minimised by choosing $\mathbf{n} = \mathbf{n}_c$ and this minimum value is found to be

$$\Delta v_{2min} = \min(|\Delta\mathbf{v}_2|) = \frac{1}{2} \left\| |2\Delta\mathbf{v}_- - \lambda\Delta\mathbf{v}_{ls}| - |\lambda\Delta\mathbf{v}_{ls}| \right\| \quad (6.8)$$

On the other hand, if $|\Delta\mathbf{v}_{ls}^T \mathbf{n}_c| > \Delta v_{threshold}$, shown in Fig. 6.5(b), the second impulse is minimised when $|\Delta\mathbf{v}_{ls}^T \mathbf{n}| = \Delta v_{threshold}$ and the minimum value is then found to be

$$\Delta v_{2min} = \min(|\Delta\mathbf{v}_2|) = \sqrt{p_2^2 + (\sqrt{p_1^2 - p_2^2} - p_3)^2} \quad (6.9)$$

where

$$\mathbf{X} = \frac{\lambda\Delta v_{threshold}^2}{|\Delta\mathbf{v}_{ls}|^2} \Delta\mathbf{v}_{ls}, p_1 = |\Delta\mathbf{v}_- - \mathbf{X}|, p_2 = \left| \frac{\Delta\mathbf{v}_-^T \cdot \mathbf{X}}{|\mathbf{X}|} - |\mathbf{X}| \right|, p_3 = \sqrt{\Delta v_{threshold}^2 - |\mathbf{X}|^2}$$

Therefore, the total cost of the capture strategy can be written as

$$\Delta v = \Delta v_1 + \Delta v_{2min} + \Delta v_3 \quad (6.10)$$

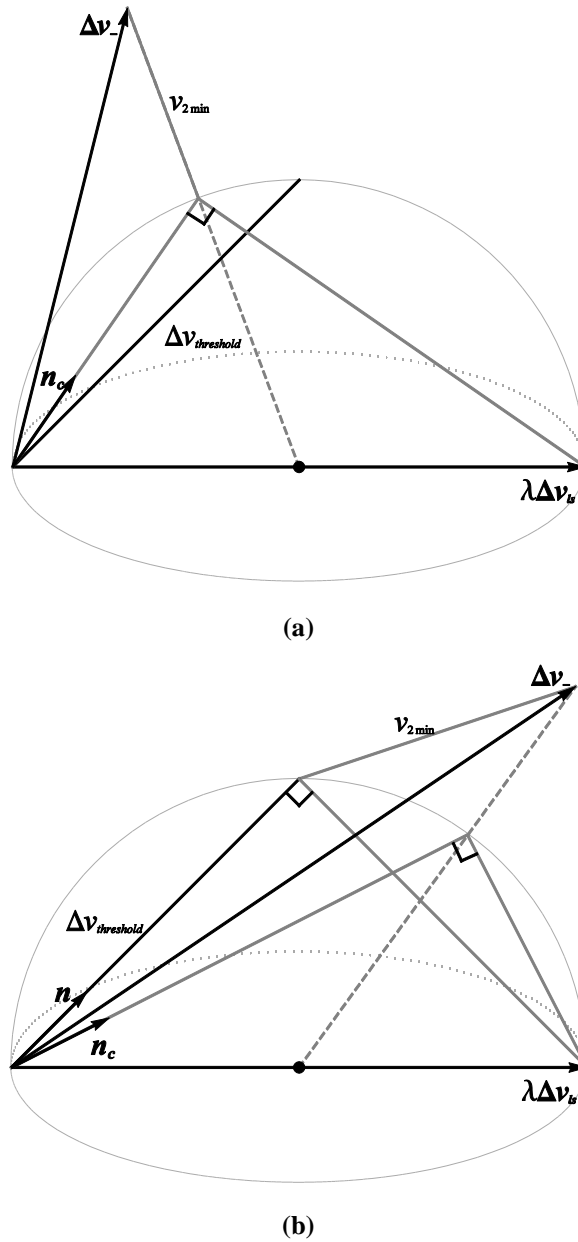


Fig. 6.5 Geometric relationship of the vectors in Eq. (6.6) (a) when $|\Delta v_{ls}^T n_c| \leq \Delta v_{threshold}$ (b) when

$$|\Delta v_{ls}^T n_c| > \Delta v_{threshold}.$$

6.3.3 Analysis of impact mechanics

The relative kinetic energy E of the large asteroid and the small asteroid at collision can be written as [199]

$$E = \frac{m_l m_s}{2(m_l + m_s)} \Delta v_n^2 \quad (6.11)$$

Assuming that the large and small asteroid have the same composition, the relative kinetic energy is partitioned in equal parts between the two asteroids [200]. If the small

asteroid is shattered, the size of the largest fragment as a fraction of the original mass is given by [201, 202]

$$f_l = \frac{1}{2} \left(\frac{S_s m_s}{\rho_a E / 2} \right)^{1.24} \quad (6.12)$$

where S_s is the effective impact strength of the small asteroid and ρ_a is the density of the small asteroid.

The effective impact strength of the small asteroid S_s can be written as [199, 203, 204]

$$S_s = S_{s0} + \frac{\pi k_p G \rho_a D^2}{15} \quad (6.13)$$

where S_{s0} is the material impact strength; G is the gravitational constant; k_p is a proportionality constant and D is the diameter of the small asteroid.

The model of the impact strength in Eq. (6.13) consists of two components: the first part is related to the material properties of the small asteroid and the second part is due to its self-compressional strength. For asteroids with diameters less than approximately 10 km, the compressive strength can be ignored compared to the material strength so that $S_s \approx S_{s0}$ [204].

If the small asteroid remains intact after collision, $f_l = 1$ and thus the threshold of Δv_n can be estimated as

$$\Delta v_{threshold} = 2 \sqrt{\frac{S_s (m_l + m_s)}{\kappa \rho_a m_l}} \approx 2 \sqrt{\frac{S_s}{\kappa \rho_a}} \quad (6.14)$$

where $\kappa = 2^{1/1.24}$. However, there are a range of experimental studies using small projectiles impacting on large targets with results for the ratio of the mass of the largest fragment to the initial target mass, as a function of impact strength or the impact energy [71, 205-208]. Figure 6.6 shows the contour map of $\Delta v_{threshold}$ as a function of S_{s0} and ρ_a .

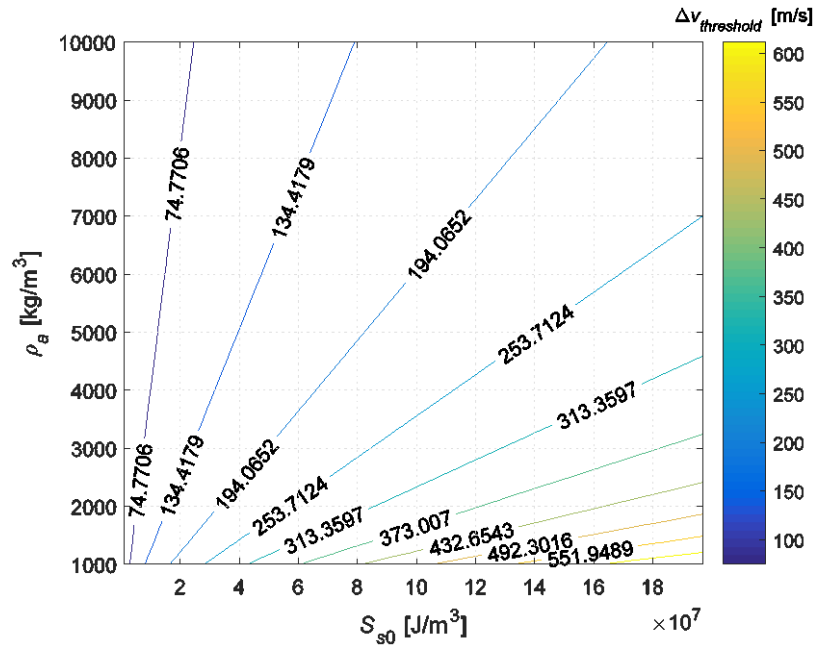


Fig. 6.6 Contour map of $\Delta v_{threshold}$ as a function of S_{s0} and ρ_a .

Since the material properties of the target asteroids are largely unknown, two special cases are considered: metallic asteroids and the basalt asteroids. From [203], it can be shown that $S_{s0} = 1 \times 10^8 \text{ J/m}^3$ and $\rho_a = 6000 \text{ kg/m}^3$ for metallic asteroids and $S_{s0} = 3 \times 10^6 \text{ J/m}^3$ and $\rho_a = 3000 \text{ kg/m}^3$ for basalt asteroids. Therefore, $\Delta v_{threshold} \approx 196 \text{ m/s}$ can be obtained for metallic asteroids and $\Delta v_{threshold} \approx 48 \text{ m/s}$ for basalt asteroids. In fact, capturing a fragment of an asteroid is also of interest and so the value of $\Delta v_{threshold}$ would in principle be much larger than that stated above if $f_i < 1$. In practice however, due to the assumptions and uncertainties stated, active protection (e.g. an ablative layer or air-bags) for the target small asteroid could in principle be required, as noted below. Although clearly speculative, the use of active protection would have the potential to increase $\Delta v_{threshold}$. For example, the spacecraft could be assumed to carry an ablative coating or air-bags. After it deflects the target small asteroid from its initial orbit to transfer to the large asteroid, the ablative materials or air-bags could be installed by the spacecraft on the surface of the small asteroid where the collision of the two asteroids will occur. Once such active protection is installed, the ablative material or airbags could sacrificially protect the small asteroid from disruption. Clearly this would incur significant technical challenges which are not addressed here.

6.3.4 Selection of candidate large asteroids

In previous work [40, 50], it is shown that a small asteroid can be captured onto periodic orbits at the Sun-Earth L_1 or L_2 points in a direct capture strategy by solving the Lambert arc problem between the small asteroid's initial orbit and the stable manifold associated with the periodic orbits at the Sun-Earth L_1 or L_2 points. In the direct capture strategy, the candidate asteroid is first assumed to leave its orbit with an initial manoeuvre and will then transfer to the stable manifold of the Sun-Earth L_1 or L_2 periodic orbits with a second manoeuvre. These two manoeuvres can be calculated by solving a Lambert arc between the asteroid orbit and the stable manifold in the Sun-centred two-body problem. Finally, once the asteroid moves onto the stable manifold, it will then transfer to the target periodic orbit without any further manoeuvres.

In this prior direct capture problem, there are five variables and so optimal strategies for direct capture can be obtained by varying these variables. The optimal total cost of the direct capture strategy is denoted as ΔV . Here it is expected that capture of the small asteroid by impacting the large asteroid will be possible with the total cost being lower than ΔV . In order to find low energy capture trajectories for the small asteroid, $\Delta V/2$ is set as the threshold of the first impulse Δv_1 and thus this critical value can be utilised as a selection criterion for the large asteroid. For the small asteroid, the Lambert transfer between the small asteroid and the large asteroid can then be optimised using MATLAB's function *fmincon*. Single objective optimisations with the first impulse Δv_1 as a cost function can then be undertaken. For one given target small asteroid, there are two variables in the solution vector of this optimisation problem: T_0 and T_{fly1} . Their bounds can be obtained through the procedure in Section 6.2.1. An example of large asteroids as selected when considering the capture of the small asteroid 2008 JL24 is shown in Fig. 6.7 for illustration.

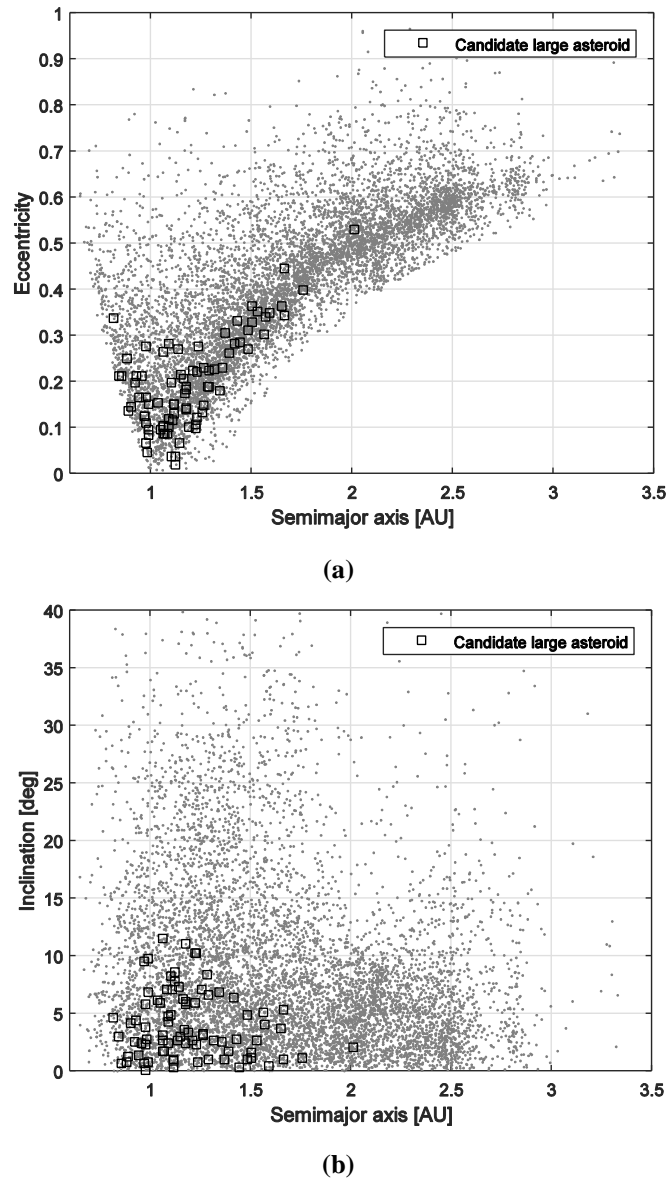
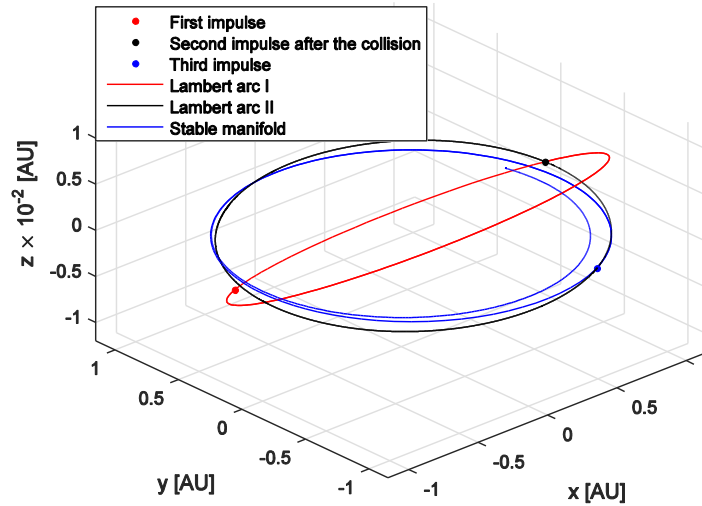


Fig. 6.7 Candidate large asteroids when capturing 2008 JL24 into a Lyapunov orbit with $\Delta V/2 = 441.19$ m/s.

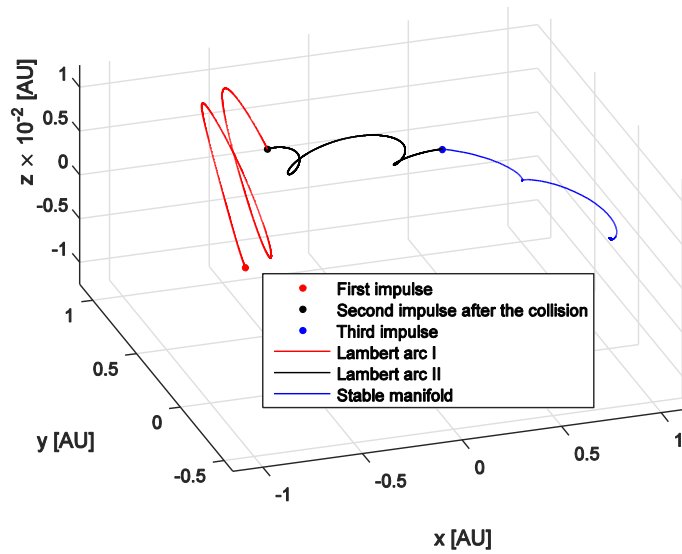
6.3.5 Design procedure and optimisation

The design procedure is now as follows: one candidate small asteroid with $H > 25.33$ (e.g. 2008 JL24) is first selected and then the corresponding candidate large asteroids can be found using the selection criteria in Section 6.2.2, as shown in Fig. 6.7. Thus, one target large asteroid in Fig. 6.7 (e.g. 2001 QJ142) is selected. Then given the deflection date T_0 and the first flight time T_{fly1} ($T_0 \in [2019, T_s], T_0 + T_{fly1} \in [2019, T_l]$), the trajectory from the candidate small asteroid orbit to the large asteroid can be calculated as the heliocentric Lambert arc of a two-body problem. Thus, the first impulse Δv_1 can then be obtained. Given the amplitude variable A_p , t_p and t_m , the stable manifold associated with the target periodic orbit can then be calculated. Given the second flight time T_{fly2} , the transfer

trajectory from the vicinity of the large asteroid to the stable manifold is designed by solving the Lambert arc and so the third impulse Δv_3 can be obtained. The second impulse Δv_2 can then be optimised by using Eq. (6.8) and Eq. (6.9) and the entire transfer trajectory from the small asteroid orbit to the stable manifold can be designed, as shown in Fig. 6.8.



(a)



(b)

Fig. 6.8 Transfer trajectory for capturing 2008 JL24 into a Lyapunov orbit by impacting 2001 QJ142 (a) in the Sun-centred inertial frame; (b) in the Sun-Earth rotating frame, assuming that they are metallic asteroids.

Table 6.1 Results for the capture of metallic asteroids into Lyapunov orbits with and without impacting large metallic asteroids

Small NEA	Large NEA	Capture date, MJD	Δv using impact, m/s	T_{tot} using impact, day	Δv without impact, m/s	T_{tot} without impact, day	Final target orbit
2006 JY26	2002 VX91	62238.2	1038.91	2948.4	1203.48	2715.1	L ₁
2008 KT	2002 VX91	62223.9	1286.65	2792.6	1435.89	2612.3	L ₁
2009 BD	2000 SG344	59446.1	241.12	2694.2	488.67	2717.2	L ₁
2009 BD	2007 CS5	62350.3	395.37	2491.9	488.67	2717.2	L ₁
2011 UD21	2002 VX91	63420.5	365.01	2688.3	618.16	1758	L ₁
2013 RZ53	2016 FZ12	58944.7	993.17	2318.1	1129.76	2498.3	L ₁
2014 HN2	2010 VC72	59117.7	1019.67	1193.1	1231.64	2215.7	L ₁
2008 HU4	2012 DK4	59543.4	716.93	1835.3	753.37	2680.2	L ₂
2008 HU4	2003 LN6	58484.3	404.12	2934.9	753.37	2680.2	L ₂
2008 HU4	2010 JK1	58865.7	566.33	2579.8	753.37	2680.2	L ₂
2008 JL24	2001 QJ142	58743.4	703.92	2308.9	882.38	2025.2	L ₂
2008 JL24	2011 MW1	58662.3	729.35	1649.5	882.38	2025.2	L ₂
2008 JL24	2016 CF137	59023.5	665.42	1630.2	882.38	2025.2	L ₂
2010 VQ98	2016 TP11	61985.7	675.41	2506.4	759.4	1995.3	L ₂
2011 MD	2015 XP128	58710.8	1049.86	1655.1	1248.74	1210.7	L ₂
2012 EP10	1999 SF10	58723.2	1071.39	2601.4	1282.51	1967.4	L ₂
2012 EP10	2004 XK3	59050.6	1182.7	2273.4	1282.51	1967.4	L ₂
2012 TF79	2012 DK4	59621.4	371.89	1985.1	540.07	2555.3	L ₂
2012 WR10	2014 KF39	60479.1	739.68	2188.6	834.53	2418.6	L ₂
2012 WR10	2015 VO105	60498.4	852.46	2129.7	834.53	2418.6	L ₂
2013 RZ53	2013 BS45	66088.1	956.01	2786.5	1129.76	2498.3	L ₂
2014 WX202	2012 FC71	61499	301.22	2190	380.76	1837.6	L ₂
2014 WX202	2011 BP40	61218.2	268.83	2363.3	380.76	1837.6	L ₂
2015 JD3	2015 XA352	60325.6	1207.66	1650.6	1406.6	1829.9	L ₂
2015 KK57	2012 MD7	58587.6	530.39	2147	614.28	2223.9	L ₂
2015 VC2	2009 TP	59778.6	408.35	2618.5	621.34	2621	L ₂

Table 6.2 Results for the capture of basalt asteroids into Lyapunov orbits with and without impacting large basalt asteroids

Small NEA	Large NEA	Capture date, MJD	Δv using impact, m/s	T_{tot} using impact, day	Δv without impact, m/s	T_{tot} without impact, day	Final target orbit
2006 JY26	2002 VX91	62277.6	1333.07	2831	1203.48	2715.1	L ₁
2008 KT	2002 VX91	62946	1555.34	2621.1	1435.89	2612.3	L ₁
2009 BD	2000S G344	59440.8	559.39	2688.8	488.67	2717.2	L ₁
2009 BD	2007 CS5	62736	650.53	2815.3	488.67	2717.2	L ₁
2011 UD21	2002 VX91	63787.9	641.83	2334	618.16	1758	L ₁
2013 RZ53	2016 FZ12	58953.9	1256.12	2260	1129.76	2498.3	L ₁
2014 HN2	2010 VC72	59079.9	1312.83	1446	1231.64	2215.7	L ₁
2008 HU4	2012 DK4	59552.3	855.11	1873.2	753.37	2680.2	L ₂
2008 HU4	2003 LN6	58892.9	658.9	2689.8	753.37	2680.2	L ₂
2008 HU4	2010 JK1	58500.5	853.51	2940.6	753.37	2680.2	L ₂
2008 JL24	2001 QJ142	58745.9	1028.29	2213.5	882.38	2025.2	L ₂
2008 JL24	2011 MW1	58641	1034.47	1662.6	882.38	2025.2	L ₂
2008 JL24	2016 CF137	59014.3	870.83	1835.9	882.38	2025.2	L ₂
2010 VQ98	2016TP11	61940.7	822.4	2509.8	759.4	1995.3	L ₂
2011 MD	2015 XP128	58707	1297.21	1652.6	1248.74	1210.7	L ₂
2012 EP10	1999 SF10	58738.7	1278.31	2560.8	1282.51	1967.4	L ₂
2012 EP10	2004 XK3	59042.4	1500.05	2240	1282.51	1967.4	L ₂
2012 TF79	2012 DK4	59558.2	520.52	2066.7	540.07	2555.3	L ₂
2012 WR10	2014 KF39	61328.2	908.31	1538.3	834.53	2418.6	L ₂
2012 WR10	2015 VO105	61013.8	962.76	1942.5	834.53	2418.6	L ₂
2013 RZ53	2013 BS45	65699.8	1103.38	2860.6	1129.76	2498.3	L ₂
2014 WX202	2012 FC71	61473.4	493.6	2365	380.76	1837.6	L ₂
2014 WX202	2011 BP40	61236.7	394.4	2216.4	380.76	1837.6	L ₂
2015 JD3	2015 XA352	60321	1415.94	1623.8	1406.6	1829.9	L ₂
2015 KK57	2012 MD7	58957.9	700.33	1769.5	614.28	2223.9	L ₂
2015 VC2	2009 TP	59717.1	650.46	2705.3	621.34	2621	L ₂

Table 6.3 Results for the capture of metallic asteroids into halo orbits with and without impacting large metallic asteroids

Small NEA	Large NEA	Capture date, MJD	Δv using impact, m/s	T_{tot} using impact, day	Δv without impact, m/s	T_{tot} without impact, day	Final target orbit
2006 JY26	2002 VX91	62246.7	897.72	2689.3	1105.24	2854.8	L ₁
2008 KT	2002 VX91	62246.3	1101.16	2402.8	1309.22	1175.2	L ₁
2009 BD	2000 SG344	59437.3	345.8	2397.6	413.38	2669.2	L ₁
2009 BD	2007 CS5	62358.3	391.03	2472.1	413.38	2669.2	L ₁
2011 UD21	2002 VX91	62705.7	335.81	2155.5	373.71	2119	L ₁
2013 RZ53	2016 FZ12	58931.7	725.16	2312.7	1003.01	1783.3	L ₁
2014 HN2	2010 VC72	58769	1158.33	1923.3	1284.08	2049.4	L ₁
2008 HU4	2012 DK4	59549.1	669.56	2268.2	664.51	1413.6	L ₂
2008 HU4	2003 LN6	58676.1	747.45	2683.4	664.51	1413.6	L ₂
2008 HU4	2010 JK1	58897.2	765.11	2502.4	664.51	1413.6	L ₂
2008 JL24	2001 QJ142	59342.5	805.51	1249.8	974.51	1881.5	L ₂
2008 JL24	2011 MW1	58616.5	840.74	1618.4	974.51	1881.5	L ₂
2008 JL24	2016 CF137	59014.1	754.38	1563.5	974.51	1881.5	L ₂
2010 VQ98	2016 TP11	61629.8	512.42	2503.8	571.24	2762.4	L ₂
2011 MD	2015 XP128	58700.5	945.83	2004.9	1101.39	857.7	L ₂
2012 EP10	1999 SF10	58722.2	1084.38	2528.7	1301.62	1331.2	L ₂
2012 EP10	2004 XK3	59036.9	1101.74	2255.7	1301.62	1331.2	L ₂
2012 TF79	2012 DK4	59976.1	310.4	2060.6	427.55	1768.9	L ₂
2012 WR10	2014 KF39	61336.7	955.88	1687.3	1057.32	2540.9	L ₂
2012 WR10	2015 VO105	61320.8	934.04	1329.2	1057.32	2540.9	L ₂
2013 RZ53	2013 BS45	65717.3	896.25	2829.6	1003.01	1783.3	L ₂
2014 WX202	2012 FC71	61867.3	398.48	1596.7	345.1	1876	L ₂
2014 WX202	2011 BP40	61210.9	144.24	2230	345.1	1876	L ₂
2015 JD3	2015 XA352	60323.8	1006.79	1686.3	1165.48	2414	L ₂
2015 KK57	2012 MD7	58955.3	402.92	1791.1	555.56	1955.4	L ₂
2015 VC2	2009 TP	60173.8	486.58	2534.9	642.32	1363	L ₂

Table 6.4 Results for the capture of basalt asteroids into halo orbits with and without impacting large basalt asteroids

Small NEA	Large NEA	Capture date, MJD	Δv using impact, m/s	T_{tot} using impact, day	Δv without impact, m/s	T_{tot} without impact, day	Final target orbit
2006 JY26	2002 VX91	62815.8	1143.21	2220	1105.24	2854.8	L ₁
2008 KT	2002 VX91	62246.2	1392.41	2388	1309.22	1175.2	L ₁
2009 BD	2000 SG344	59442.4	639.36	2840.3	413.38	2669.2	L ₁
2009 BD	2007 CS5	62703.8	663.47	2464.7	413.38	2669.2	L ₁
2011 UD21	2002 VX91	63421.7	517.11	2200.7	373.71	2119	L ₁
2013 RZ53	2016 FZ12	58929.9	1023.2	2178.3	1003.01	1783.3	L ₁
2014 HN2	2010 VC72	58792.6	1323.04	1905.5	1284.08	2049.4	L ₁
2008 HU4	2012 DK4	59545.6	915.4	2244.4	664.51	1413.6	L ₂
2008 HU4	2003 LN6	58686.7	884.67	2680.7	664.51	1413.6	L ₂
2008 HU4	2010 JK1	58895.3	1014.86	2474.9	664.51	1413.6	L ₂
2008 JL24	2001 QJ142	58769.8	1038.21	2162.2	974.51	1881.5	L ₂
2008 JL24	2011 MW1	58964.3	1141.85	1675.5	974.51	1881.5	L ₂
2008 JL24	2016 CF137	59031.1	1017.43	1537.2	974.51	1881.5	L ₂
2010 VQ98	2016 TP11	61608.5	711.55	2929.7	571.24	2762.4	L ₂
2011 MD	2015 XP128	58715.8	1157.77	2030.3	1101.39	857.7	L ₂
2012 EP10	1999 SF10	58735.4	1298.49	2548.1	1301.62	1331.2	L ₂
2012 EP10	2004 XK3	59058.8	1398.94	2214.3	1301.62	1331.2	L ₂
2012 TF79	2012 DK4	59609.9	500.55	2001.3	427.55	1768.9	L ₂
2012 WR10	2014 KF39	61327.2	1089.64	1321.6	1057.32	2540.9	L ₂
2012 WR10	2015 VO105	60938.6	1189.08	1690.8	1057.32	2540.9	L ₂
2013 RZ53	2013 BS45	65328.5	967.68	2562.7	1003.01	1783.3	L ₂
2014 WX202	2012 FC71	61470.8	626.52	2010.8	345.1	1876	L ₂
2014 WX202	2011 BP40	60992.5	245.99	2458.7	345.1	1876	L ₂
2015 JD3	2015 XA352	60315.4	1224.66	1693.7	1165.48	2414	L ₂
2015 KK57	2012 MD7	58585.6	553.51	2180	555.56	1955.4	L ₂
2015 VC2	2009 TP	60202.6	603.37	2169.1	642.32	1363	L ₂

According to the design procedure stated above, the transfer trajectory from the small asteroid's initial orbit to the stable manifold can be designed, and then the six variables can be optimised using NSGA-II [182]. In order to limit the total duration of the transfers (T_{tot}), the Lambert arcs required for designing the transfer from the small asteroid's orbit to the large asteroid, and the transfer from the large asteroid's orbit to the stable manifolds are assumed to be up to two complete revolutions. The optimal results of small asteroid capture by impacting large asteroids are shown in Tables 6.1-6.4, corresponding to metallic asteroids and basalt asteroids, respectively. For comparison, the direct capture of small asteroids onto bound periodic orbits around the Sun-Earth L_1 and L_2 points without impact can be designed directly from the asteroid orbit to the stable manifolds. The optimal results are also shown in Tables 6.1-6.4.

By comparison of the results with and without impacting the large asteroid in Table 6.1, it can be seen that the capture of small asteroids by impacting large asteroids has the potential to reduce capture energy, especially for cases such as 2009 BD, 2011 UD21 and 2015 VC2. Moreover, a range of large asteroids may be available when capturing the same small asteroid, e.g. when capturing 2008 JL24. Furthermore, one small asteroid can be captured onto periodic orbits around either the Sun-Earth L_1 or L_2 points by impacting different large asteroids, e.g. 2013 RZ53. This implies that the impact can increase the range of capture opportunities. However, due to the additional transfer time from the small asteroid orbit to the large asteroid orbit, the capture of the small asteroid using a large impacting asteroid always needs a greater flight time than a direct capture.

In this capture strategy, the collision of the small asteroid and large asteroid provides an impulsive manoeuvre for the small asteroid, and it is the mechanics of this interaction that reduces the energy required for the capture strategy. Therefore, the total cost of the capture strategy greatly depends on the threshold of the manoeuvre which is provided by the collision, while avoiding fragmentation of the asteroid. Furthermore, comparing the results in Tables 6.1-6.4, it can be seen that a smaller value of $\Delta v_{threshold}$ can lead to an increase of the total capture cost. Moreover, with a smaller value of $\Delta v_{threshold}$, the total cost of capturing some asteroids by impacting large asteroids can be even greater than the direct capture strategy, e.g. 2008 KT, 2012 EP10 and 2015 KK57. This is one drawback of the capture strategy of using a small asteroid to impact a large asteroid, since many small asteroids are thought to be rubble piles, and thus the collision between these asteroids can only provide a limited manoeuvre. However, through the analysis in Section 6.3.3, if capturing one segment of an asteroid, not the entire asteroid, the collision can in principle

deliver a much larger impulse. Moreover, the use of active protection (e.g. air bags) could in principle increase the value of $\Delta v_{threshold}$.

One of the challenges of this capture strategy is also the uncertainty of the properties of the candidate asteroids, including their shape, mass and material properties. Therefore, pre-launch observations using radar and optical/infrared telescopes would again be required to provide good estimates of these parameters [21, 23]. Moreover, in-situ asteroid exploration missions, including the flyby and rendezvous, can also be viewed as an effective way to address these uncertainties [59]. An accurate navigation and control strategy would clearly be required to guarantee that the candidate small asteroid impacts the large asteroid with the correct collision geometry to achieve the required manoeuvre for asteroid capture.

6.4 Small asteroid capture by tether-assisted flyby of large asteroids

Another momentum exchange strategy to transfer small asteroids onto the stable manifold associated with the Sun-Earth L_1 or L_2 points is to use a tethered assist. In this capture strategy, the small asteroid approaches the large asteroid and then connects to the large asteroid through a tether, such that the tether is released after the flyby. Again, the small asteroid will be transferred onto the stable manifold associated with the Sun-Earth L_1 or L_2 points.

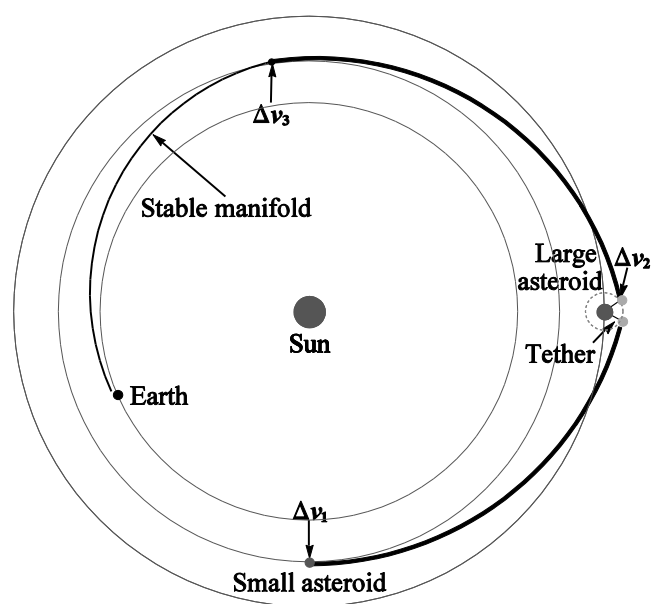


Fig. 6.9 Overview of small asteroid capture using tether-assisted flyby.

6.4.1 Statement of the problem

A schematic of the tether-assist strategy is shown in Fig. 6.9. The mission scenario consists of the following steps: with the first impulse Δv_1 , the small asteroid leaves its initial orbit and will then approach the target large asteroid; the small asteroid connects to the large asteroid by a tether until it is released so that a second impulse Δv_2 is added; with the third impulse Δv_3 , the small asteroid is captured onto the stable manifold associated with the Sun-Earth L_1 or L_2 points.

For this strategy, given one small asteroid and one large asteroid, there are now seven variables in the problem:

- T_0 : the date of the first impulse Δv_1 ;
- T_{fly1} : the flight time of the small asteroid to reach the vicinity of the large asteroid,
- T_{tether} : the tether connection time;
- T_{fly2} : the flight time of the small asteroid between the moment when the small asteroid is released and the moment when the small asteroid injects onto the stable manifold;
- A_p : the amplitude variable of the target periodic orbit around the Sun-Earth L_1 or L_2 point;
- t_p : the parameter determining the point on the periodic orbit where the stable manifold is calculated from;
- t_m : the stable manifold transfer time which determines the point on the stable manifold where the small asteroid inserts onto it.

It should be noted that if the connection of the two asteroids is instantaneous and thus $T_{tether} \approx 0$, then there are only six variables required to define the problem.

6.4.2 Dynamical model during tether-assisted flyby

In this problem, it is assumed that a spacecraft is first launched and then achieves a rendezvous with each asteroid to prepare an anchor point using a penetrator or a net or bag [122]. Alternatively, an anchor point could be delivered by a penetrator from the small asteroid to the large asteroid during the close approach. As the small asteroid approaches the vicinity of the large asteroid, the two anchor points are assumed to be connected by a tether. The spacecraft-to-asteroid tether attachment is assumed to occur when the velocity

vector is exactly perpendicular to the radius vector between the two asteroids. Therefore, high-precision navigation is clearly required, but again will not be considered here.

Since the mass ratio of the two asteroids is large (Eq. (6.2)), it is assumed that the large asteroid's orbit during the small asteroid flyby is unchanged. Here the velocity vector of the small asteroid before and after the flyby are denoted as \mathbf{v}_{s+} and \mathbf{v}_{s-} respectively, where \mathbf{v}_{l-} is the velocity vector of the large asteroid before the flyby and \mathbf{v}_{l+} is the velocity vector of the large asteroid after the flyby. Before the flyby, the relative velocity of the small asteroid with respect to the large asteroid can therefore be written as

$$\Delta\mathbf{v}_{sl} = \mathbf{v}_{s-} - \mathbf{v}_{l-} \quad (6.15)$$

Considering the relative velocity $\Delta\mathbf{v}_{release}$ of the small asteroid with respect to the large asteroid when released, one can obtain

$$|\Delta\mathbf{v}_{sl}| = |\Delta\mathbf{v}_{release}| \quad (6.16)$$

and so the velocity vector of the small asteroid after the flyby can be written as

$$\mathbf{v}_{s+} = \mathbf{v}_{l-} + \Delta\mathbf{v}_{release} \quad (6.17)$$

Moreover, \mathbf{v}_{Lam} is again the velocity vector of the small asteroid required for the Lambert arc to the stable manifold after the flyby, so that the second impulse can therefore be written as

$$\Delta\mathbf{v}_2 = \mathbf{v}_{Lam} - \mathbf{v}_{s+} = \Delta\mathbf{v}_- - \Delta\mathbf{v}_{release} \quad (6.18)$$

where

$$\Delta\mathbf{v}_- = \mathbf{v}_{Lam} - \mathbf{v}_{l-} \quad (6.19)$$

The minimum value of the second impulse is then found to be

$$\Delta v_{2\min} = \min(|\Delta\mathbf{v}_2|) = \min(|\Delta\mathbf{v}_- - \Delta\mathbf{v}_{release}|) = \left| |\Delta\mathbf{v}_-| - |\Delta\mathbf{v}_{release}| \right| \quad (6.20)$$

when $\Delta\mathbf{v}_{release}$ has the same direction as $\Delta\mathbf{v}_-$. Therefore, the total cost of the capture strategy can be written as

$$\Delta v = \Delta v_1 + \Delta v_{2\min} + \Delta v_3 \quad (6.21)$$

6.4.3 Analysis of the tether forces

When the small asteroid connects to the large asteroid via the tether, the small asteroid has a relative velocity of $\Delta \mathbf{v}_{sl} = \mathbf{v}_s - \mathbf{v}_l$ with respect to the large asteroid. Then, after the tether is connected, the small asteroid moves in a circle around the large asteroid with radius L , and so the tether tension at the small asteroid is $T_L = m_s \omega^2 L$, where $\omega = |\Delta \mathbf{v}_{sl}| / L$. Thus, the tension T can be written as [122]

$$\frac{dT}{dr} = -A \rho_{tether} \omega^2 r \quad (6.22)$$

where r is the distance along the tether with respect to the large asteroid and $r \in [0, L]$; ρ_{tether} is tether density and A is the constant cross-sectional area. Considering the boundary condition $T_L = m_s \omega^2 L$ ($r = L$), the solution of Eq. (6.22) is given by

$$T = m_s \omega^2 L + \frac{1}{2} \rho_{tether} \omega^2 (L^2 - r^2) \quad (6.23)$$

Considering that the tether mass is $m_{tether} = \rho_{tether} AL$, the stress on the tether is given by

$$S = \frac{T}{A} = \left(\frac{m_s}{m_{tether}} + \frac{L^2 - r^2}{2L^2} \right) \rho_{tether} (|\Delta \mathbf{v}_{sl}|)^2 \quad (6.24)$$

Therefore, the maximum tether stress is $S_{\max} = (m_s / m_{tether} + 1/2) \rho_{tether} (|\Delta \mathbf{v}_{sl}|)^2$ when $r = 0$. If the maximum safe working stress of the tether is defined as S_0 , the small asteroid-to-tether mass ratio can then be written as [122]

$$\frac{m_s}{m_{tether}} = \left(\frac{v_c}{|\Delta \mathbf{v}_{sl}|} \right)^2 - \frac{1}{2} \quad (6.25)$$

where $v_c = \sqrt{S_0 / \rho_{tether}}$ is the characteristic velocity of the tether material. According to Eq. (6.25), the contour map of $|\Delta \mathbf{v}_{sl}|$ as a function of the small asteroid-to-tether mass ratio and the characteristic velocity of the tether is shown in Fig. 6.10.

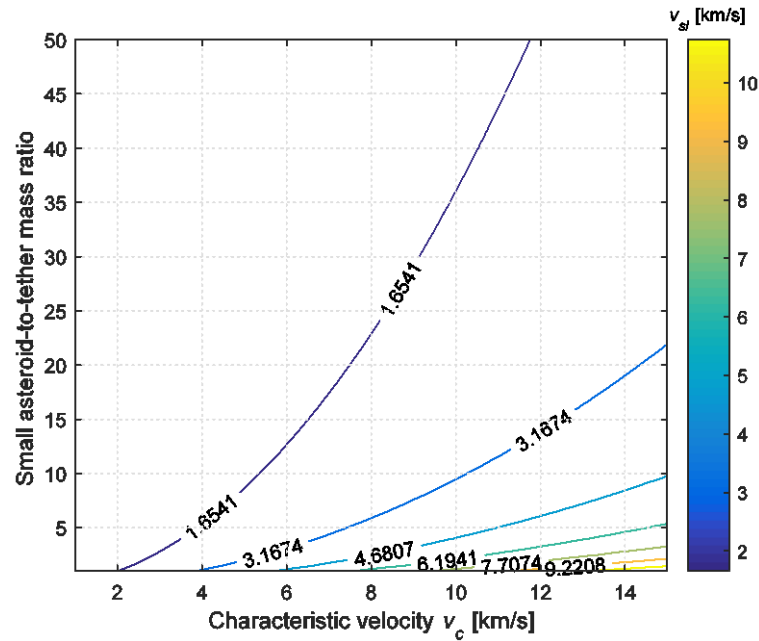


Fig. 6.10 Contour map of the Δv_{sl} as a function of the small asteroid-to-tether mass ratio and the characteristic velocity of the tether.

It is assumed now that small asteroid-to-tether mass ratio is 20-to-1, i.e., the mass of the smaller asteroid is at least twenty times larger than that of the tether [123]. From Eq. (6.25), it can be noted that the characteristic velocity of the tether has a substantial effect on the threshold of $|\Delta v_{sl}|$ and thus two different tether materials will be considered to compare their performance. One is a hypothetical carbon nanotube tether (CNT) with a density of 1300 kg/m^2 , a maximum safe working stress of 130 GPa and a characteristic velocity of 10 km/s. This material is chosen from the example of Van Zandt [123]. From Eq. (6.25), the threshold of the relative velocity of the small asteroid with respect to the large asteroid is then approximately 2200 m/s. The other material considered is a more conventional Zylon tether with a characteristic velocity of 2.7 km/s [209] and so the threshold of the relative velocity of the small asteroid with respect to the large asteroid is then approximately 600 m/s.

In this asteroid capture strategy, it is assumed that the tether with a constant cross-section is utilised to connect the large asteroid with the small asteroid. Considering that small asteroid-to-tether mass ratio is assumed to be 20-to-1, the tether mass will be significant when capturing an asteroid with a large mass. To reduce the tether mass for asteroid capture, one of the most efficient ways is to use the variable cross-section tethers. From Eq. (6.23), it can be seen that the tension distribution is uneven along the tether. Therefore, the utilisation of a variable cross-section tether on which every cross-section can experience the same maximum safe working stress would lead to a significant saving

in the tether mass. Accordingly, using variable cross-section tethers will produce more attractive results for this asteroid capture strategy.

6.4.4 Selection strategy for candidate asteroids

Here it is again supposed that $\Delta V/2$ is the threshold of the magnitude of the first impulse Δv_1 . Therefore, the threshold of the first impulse Δv_1 and the threshold of the relative velocity $|\Delta \mathbf{v}_{st}|$ between the two asteroids when they approach can be utilised as the selection criteria for the large asteroid. For the small asteroid, the Lambert transfer to the large asteroid can again be optimised using MATLAB's function *fmincon*. Single objective optimisations with the first impulse Δv_1 as a cost function can then be undertaken. There are again two variables in the optimisation problem: T_0 and T_{fly1} . Their search domains are assumed to be $T_0 \in [2019, T_s]$ and $T_0 + T_{fly1} \in [2019, T_l]$.

6.4.5 Design procedure and optimisation

The design procedure is as follows: one candidate small asteroid with $H > 25.33$ (e.g. 2008 JL24) is first selected. Then, the set of the candidate large asteroids can be obtained using the selection criteria in Section 6.2.2, and thus one target large asteroid is selected. Given the deflection date T_0 and the first flight time T_{fly1} ($T_0 \in [2019, T_s], T_0 + T_{fly1} \in [2019, T_l]$), the trajectory from the candidate small asteroid orbit to the large asteroid can again be calculated as the heliocentric Lambert arc of a two-body problem (Lambert arc I), and thus the first impulse can then be obtained. Then, the small asteroid connects to the large asteroid via the tether until it is released. Given the amplitude variable A_p , t_p and t_m , the stable manifold associated with the target periodic orbit can be calculated. Given the flight time T_{fly2} , the transfer trajectory from the vicinity of large asteroid to the stable manifold is designed by solving a Lambert arc (Lambert arc II) and so the third impulse can be obtained. The second impulse can then be optimised by using the Eq. (6.21) and so the entire transfer trajectory can be designed, as shown in Fig. 6.11.

According to the design procedure detailed above, the transfer trajectory from the small asteroid's initial orbit to the stable manifold is again optimised using NSGA-II. Similarly, it is also assumed that the Lambert arcs required for designing the transfer from the small asteroid's orbit to the large asteroid, and the transfer from the large asteroid's orbit to the stable manifolds are assumed to be up to two complete revolutions. The comparison of the results of asteroid capture with and without the tether-assist is shown in Tables 6.5-6.8, corresponding to the carbon nanotube tether and the Zylon tether. As can

be seen from Table 6.5 and Table 6.7, the use of the carbon nanotube tether assist can lead to a substantial saving in total cost, compared with capture without the tether-assist. Four small asteroids appear to be particularly suited to the benefits from this strategy; 2008 WO2, 2010 TE55, 2012 HN1 and 2015 ON22. The results for capturing these four asteroids with the carbon nanotube tether assist show cost savings of order 60%-80%, compared with capture without it. On the other hand, asteroid capture with the Zylon tether assist also has the potential to reduce the total capture cost, as shown in Table 6.6 and Table 6.8. However, this saving in total cost incurs a longer flight time. This is mainly due to the extra flight time required for the transfer from the small asteroid orbit to the large asteroid orbit.

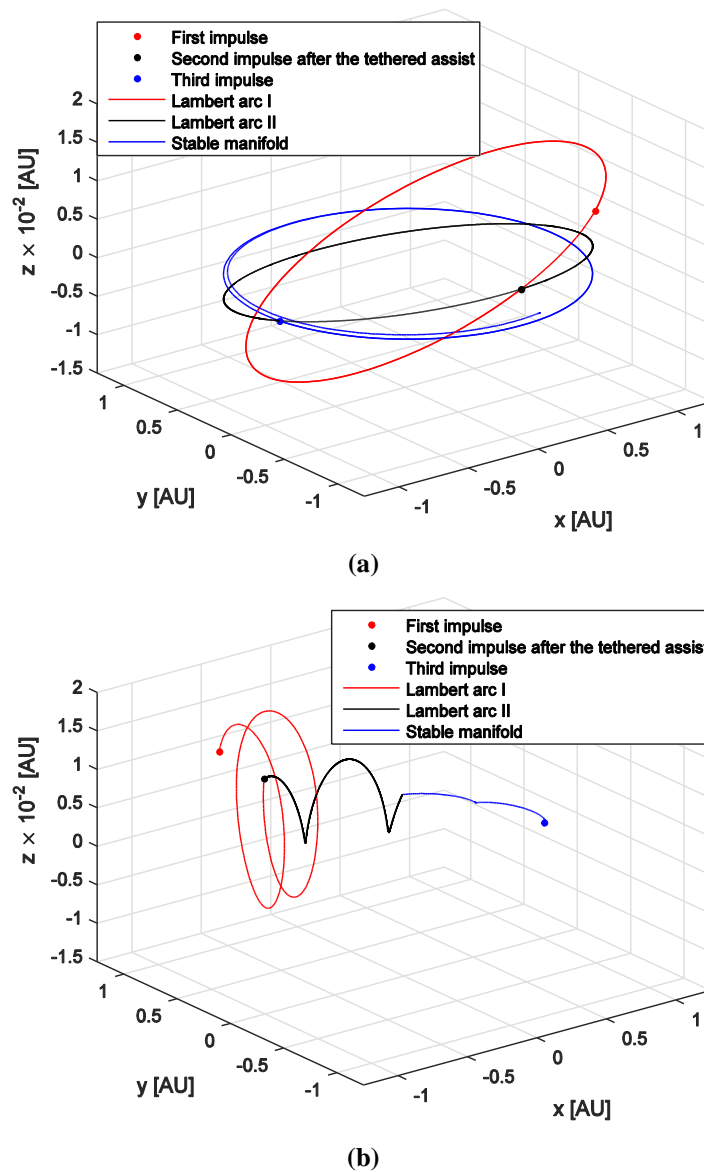


Fig. 6.11 Transfer trajectory for capturing 2008 JL24 into a Lyapunov orbit using the carbon nanotube tethered flyby of 2015 KE (a) in the Sun-centered inertial frame; (b) in the Sun-Earth rotating frame.

Table 6.5 Results for asteroid capture into Lyapunov orbits with and without the carbon nanotube tether assist

Small NEA	Large NEA	Capture date, MJD	Δv with tether assist, m/s	T_{tot} with tether assist, day	Δv without tether assist, m/s	T_{tot} without tether assist, day	Final target orbit
2008 JL24	2000 SG344	60889.3	531.37	2645.1	882.38	2025.2	L ₁
2008 WO2	2010 JK1	58604.6	998.44	2357.6	2786.45	1223.6	L ₁
2009 BD	2000 SG344	59082.3	198.98	1914.8	488.67	2717.2	L ₁
2009 SH1	2016 FP12	58580.6	1840.96	2623.6	3965.38	3058.4	L ₁
2010 TE55	2000 SG344	58513	908.09	2152	1541.23	2124	L ₁
2012 EP10	2000 SG344	60695.1	781.71	2199.3	1282.51	1967.4	L ₁
2014 HJ197	2000 SG344	59318	694.83	2178.6	2011.61	2212.2	L ₁
2014 HJ197	2015 KE	61289.8	652.25	2559.5	2011.61	2212.2	L ₁
2014 HY198	2006 HE2	59341.2	2249.03	3103.6	3016.25	1254.8	L ₁
2014 WU200	2000 SG344	59065.6	706.08	2267.7	876.76	2150	L ₁
2015 VU64	2007 VU6	58609.6	798.62	2945.4	1787.12	2164.6	L ₁
2015 VU64	2015 BM510	58560.5	1065.65	2516.6	1787.12	2164.6	L ₁
2015 TC25	2000 SG344	59308.6	449.92	2655.8	2478.95	2709.7	L ₁
2016 ES85	2007 VU6	63101.3	1081.93	2146.3	1501.15	1871.8	L ₁
2008 JL24	2015 KE	58951.2	306.73	2352.8	882.38	2025.2	L ₂
2012 EP10	2016 CF137	58583.4	569.36	2301.1	1282.51	1967.4	L ₂
2012 HN1	2003 SM84	59909.8	969.86	3091.9	2362.22	2872.4	L ₂
2012 XB112	2014 YD	63071.5	964.14	1588.6	1806.93	1636.2	L ₂
2013 RZ53	2016 RD34	66343.1	399.23	2541.2	1129.76	2498.3	L ₂
2013 PG10	2009 CV	59917.6	1431.25	3215	2585.67	2739.7	L ₂
2014 HJ197	2015 KE	67134.2	844.22	1975.1	2011.61	2212.2	L ₂
2014 HJ197	2016 UE	59688	1052.7	2586.8	2011.61	2212.2	L ₂
2014 HY198	2003 SM84	59599.1	1872.42	3253.3	3016.25	1254.8	L ₂
2015 HM182	2016 TB18	58609.7	1388.83	3198.3	3241.03	2285.9	L ₂
2015 ON22	2012 EC	64275.8	1067.81	2268.6	2142.49	1838.5	L ₂
2015 VU64	2007 VU6	58485.4	1145.19	2979.1	1787.12	2164.6	L ₂
2016 ES85	2014 QN266	59265.5	238.27	2488.8	1501.15	1871.8	L ₂
2016 GC134	2003 SM84	64986	840.87	2119.8	3212.69	1883.7	L ₂

Table 6.6 Results for asteroid capture into Lyapunov orbits with and without the Zylon tether assist

Small NEA	Large NEA	Capture date, MJD	Δv with tether assist, m/s	T_{tot} with tether assist, day	Δv without tether assist, m/s	T_{tot} without tether assist, day	Final target orbit
2008 WO2	2010 JK1	62965	2660.65	2188.3	2786.45	1052.7	L ₁
2009 SH1	2016 FP12	59426.8	3710.85	3163.6	3986.13	1120.1	L ₁
2010 TE55	2000 SG344	58807.8	1231.37	2127	1541.23	2124	L ₁
2012 EP10	2000 SG344	60923.9	2759.4	2083.3	1282.51	1967.4	L ₁
2014 HJ197	2000 SG344	59665.1	1891.29	2005.1	2011.61	2212.2	L ₁
2014 HJ197	2015 KE	61596.2	1187.22	2637.4	2011.61	2212.2	L ₁
2014 WU200	2000 SG344	59073.2	737.2	2093.2	876.76	2150	L ₁
2015 VU64	2015 BM510	59755.7	1652.46	2053.1	1777.05	2225.1	L ₁
2015 VU64	2007 VU6	58731.6	1864.3	2904	1777.05	2225.1	L ₁
2015 TC25	2000 SG344	59376.2	2472.47	1892.7	2499.64	1239.7	L ₁
2016 ES85	2007 VU6	62460.3	1583.64	1595.2	1501.15	1871.8	L ₁
2008 WO2	2010 JK1	60718.4	2023.52	2218.2	2786.45	1052.7	L ₂
2012 XB112	2014 YD	63760	2974.87	2544.6	1806.93	1465.3	L ₂
2013 RZ53	2016 RD34	66289.2	723.22	2505.4	1141.75	1842.6	L ₂
2013 PG10	2009 CV	60737.2	2206.72	2103.7	2611.13	2555.8	L ₂
2014 HJ197	2015 KE	66877.6	1533.35	2325.5	2011.61	2212.2	L ₂
2014 HJ197	2016 UE	66257.2	2218.76	1675.2	2011.61	2212.2	L ₂
2015 HM182	2016 TB18	59419.9	2412.78	2237.3	3241.03	2285.9	L ₂
2015 ON22	2012 EC	59648.1	1774.82	2937.4	2142.49	1838.5	L ₂
2015 VU64	2007 VU6	58797.6	1390.97	3037.4	1777.05	2225.1	L ₂
2016 GC134	2003 SM84	58863.5	3833.99	3299.2	3239.73	1925.9	L ₂

Table 6.7 Results for asteroid capture into halo orbits with and without the carbon nanotube tether assist

Small NEA	Large NEA	Capture date, MJD	Δv with tether assist, m/s	T_{tot} with tether assist, day	Δv without tether assist, m/s	T_{tot} without tether assist, day	Final target orbit
2008 JL24	2000 SG344	60430.6	651.97	1810.2	974.51	1881.5	L ₁
2008 WO2	2010 JK1	58985.8	1183.58	2644.9	2748.8	1365.4	L ₁
2009 BD	2000 SG344	59450.5	199.68	1959.1	413.38	2669.2	L ₁
2009 SH1	2016 FP12	58597	1832.67	2501.5	3934.56	1828	L ₁
2010 TE55	2000 SG344	58510	963.66	2153.5	1535.23	1989.3	L ₁
2012 EP10	2000 SG344	60706.9	851.43	1420.5	1301.62	1331.2	L ₁
2014 HJ197	2000 SG344	59309.8	744.39	2551.6	2071.24	1722.8	L ₁
2014 HJ197	2015 KE	61273.6	757.11	2775.3	2071.24	1722.8	L ₁
2014 HY198	2006 HE2	59343.1	2316.35	3091	3087.8	1498.8	L ₁
2014 WU200	2000 SG344	59064.4	602.03	1682.4	738.27	1913.7	L ₁
2015 VU64	2007 VU6	58913.1	527.26	2990.9	1794.96	2067.7	L ₁
2015 VU64	2015 BM510	60053.2	1329.16	1659.6	1794.96	2067.7	L ₁
2015 TC25	2000 SG344	59300.3	489.32	2298.8	2513.25	2331.9	L ₁
2016 ES85	2007 VU6	62056.7	936.24	2198.6	1462.61	1662.8	L ₁
2008 JL24	2015 KE	58980	282.94	2230.8	974.51	1881.5	L ₂
2012 EP10	2016 CF137	58613.8	432.14	2304.9	1301.62	1331.2	L ₂
2012 HN1	2003 SM84	62942.5	828.18	1790.4	2434.92	2062.3	L ₂
2012 XB112	2014 YD	63083.5	847.24	1580.9	1873.46	2666.4	L ₂
2013 RZ53	2016 RD34	66365.3	274.47	2827	1003.01	1783.3	L ₂
2013 PG10	2009 CV	59972	1648.05	3134.1	2731.68	1439.9	L ₂
2014 HJ197	2015 KE	67130.9	836.16	1789.5	2071.24	1722.8	L ₂
2014 HJ197	2016 UE	58878.7	1482.16	3122.6	2071.24	1722.8	L ₂
2014 HY198	2003 SM84	59593.6	1975.86	3259.2	3087.8	1498.8	L ₂
2015 HM182	2016 TB18	58984.2	1239.41	3048	3245.73	1686	L ₂
2015 ON22	2012 EC	64278.7	885.93	2326.8	2128.6	1789.9	L ₂
2015 VU64	2007 VU6	58486	1102.34	2981.9	1794.96	2067.7	L ₂
2016 ES85	2014 QN266	59284.3	193.69	2453.6	1462.61	1662.8	L ₂
2016 GC134	2003 SM84	64994.2	678.28	2016.7	3271.69	1807.3	L ₂

Table 6.8 Results for asteroid capture into halo orbits with and without the Zylon tether assist

Small NEA	Large NEA	Capture date, MJD	Δv with tether assist, m/s	T_{tot} with tether assist, day	Δv without tether assist, m/s	T_{tot} without tether assist, day	Final target orbit
2008 WO2	2010 JK1	62959.4	2726.8	2108.4	2748.8	1365.4	L ₁
2009 SH1	2016 FP12	59427.7	3874.41	2213	3934.56	1443.9	L ₁
2010 TE55	2000 SG344	58808.7	1382.1	2613.9	1535.23	1989.3	L ₁
2012 EP10	2000 SG344	60923.9	2899.3	2002.9	1313.92	1256.5	L ₁
2014 HJ197	2000 SG344	59670.1	1875.71	1790	2071.24	1722.8	L ₁
2014 HJ197	2015 KE	61602.3	1232.82	2453.8	2071.24	1722.8	L ₁
2014 WU200	2000 SG344	59072.4	742.05	2080.1	738.27	1913.7	L ₁
2015 VU64	2015 BM510	60095.9	1762.86	1537.2	1794.96	2067.7	L ₁
2015 VU64	2007 VU6	58676.8	2499.58	2892.1	1794.96	2067.7	L ₁
2015 TC25	2000 SG344	59372.7	2162.81	1723.3	2514.07	1862.7	L ₁
2016 ES85	2007 VU6	62458.4	1926.57	1344.3	1462.61	1662.8	L ₁
2008 WO2	2010 JK1	61461.5	2223.39	1864	2748.8	1365.4	L ₂
2012 XB112	2014 YD	63379.8	2842.46	1598.9	1941.23	2535.6	L ₂
2013 RZ53	2016 RD34	66321.2	379.84	2961.6	1003.01	1783.3	L ₂
2013 PG10	2009 CV	60741.9	2377.89	2105	2731.68	1055.8	L ₂
2014 HJ197	2015 KE	66882.7	1507.21	2065.4	2071.24	1722.8	L ₂
2014 HJ197	2016 UE	66253.6	2034.1	1655.1	2071.24	1722.8	L ₂
2015 HM182	2016 TB18	59418.7	2531.24	2224.8	3245.73	1686	L ₂
2015 ON22	2012 EC	64155.3	1820.27	2387.6	2128.6	1789.9	L ₂
2015 VU64	2007 VU6	58797.3	1365.64	3047.5	1794.96	2067.7	L ₂
2016 GC134	2003 SM84	58868.5	4474.25	3214.3	3288.63	2520.1	L ₂

Comparing the results of Tables 6.5-6.8, it can be concluded that the tether material plays a crucial role in this asteroid capture strategy. A higher characteristic velocity means a larger threshold of the relative velocity between the two asteroids and thus larger savings in the total cost of capturing candidate small asteroids.

Moreover, since the threshold of the velocity between the two asteroids is utilised as a filter, a higher tether characteristic velocity allows more candidate large asteroids to be considered when capturing the same small asteroid. Consequently, with a tether assist of

higher tether characteristic velocity, more small asteroids can be captured with a total cost which is less than that for direct capture, as shown in Tables 6.5-6.8. This is the main limitation of the small asteroid capture strategy using the tether-assist: the carbon nanotube tether cannot yet be applied to practical engineering problems, however improvements in the characteristic velocity of current tether materials can be foreseen [210, 211]. Therefore, with the improvement of advanced tether materials, the capture of asteroids using tether assist can in principle save energy compared to more direct strategies.

Tables 6.1-6.8 show the results of the two asteroid capture strategies investigated in this Chapter. Comparing the results of the two strategies, it can be seen that the capture strategy using a tethered-assist flyby has the potential to achieve much lower energy captures than the capture strategy using kinetic impacts, e.g. 2008 JL24, 2009 BD, 2012 EP10 and 2013 RZ53. Nevertheless, due to the additional filter criteria in the asteroid capture strategy using the tether assist, the capture strategy using kinetic impact in principle enables a wider range of candidate large asteroids to capture the same small asteroid, e.g. 2008 JL24, 2009 BD and 2012 EP10.

In this capture strategy, the main challenge is the limitation of the tether material since the efficiency and feasibility of the capture strategy is strongly dependent on the tether material properties. The ratio of tether material strength to weight is of key importance to the performance of the tether. A number of materials have been developed to increase the ratio of material strength to weight and some tether materials, including Spectra and Zylon, with a high strength-to-weight ratio have been proposed for other tether missions, e.g. Mars missions with tether assists [209, 212]. Current research on carbon nanotubes suggests remarkable potential for tether materials in the future [123, 213]. The shape of the tether also has an influence its performance and it has been demonstrated that a tapered tether can improve performance for tether missions [214]. Moreover, an accurate navigation and control strategy is again required to ensure that the candidate small asteroid connects reliably to the large asteroid via the tether.

6.5 Conclusions

Momentum exchange has been proposed to efficiently capture small asteroids into periodic orbits around the Sun-Earth L_1 and L_2 points. A small asteroid is first manoeuvred to engineer a flyby with a larger asteroid. Two strategies are then considered: when the small asteroid approaches the vicinity of the large asteroid, it will either impact the large asteroid or connect to it with a tether. In both strategies, momentum exchange can be used to effect

the capture of one of the small asteroids. Then, a two-impulse Lambert arc is utilised to design a post-encounter transfer trajectory to the stable manifolds of the Sun-Earth L_1 or L_2 points. A selection strategy for candidate asteroids has been proposed by considering both the deflection windows for capturing asteroids and the size of the asteroids. By investigating the outcome of the impact on the small asteroid, or the tension of the tether, the maximum velocity increment available using these momentum exchange strategies has been investigated. Finally, a detailed design procedure is presented which is then optimised using a global optimisation strategy. Results show that momentum exchange can achieve more efficient capture of some asteroids relative to direct manifold capture strategies. On the other hand, the flight time for asteroid capture using momentum exchange is longer than that for direct capture. By comparing the asteroid capture strategy using kinetic impacts and asteroid capture strategy using a tether assist, the kinetic impact strategy offers more candidate large asteroids when capturing the same small asteroid. However, the use of a high-stress tether assists can lead to a substantial saving in total cost, compared with small asteroid capture using kinetic impacts. Future improvements in tether materials will produce more attractive results for this strategy.

The methods proposed are intended to be used as a preliminary analysis of these asteroid capture strategies. The shape, mass and material properties of the candidate asteroids are the major source of uncertainty. Therefore, pre-launch characterization and observation would again be required to identify the geometry and composition of the target asteroids, while high precision navigation and orbit control would be required to ensure the correct geometry for momentum exchange, either through an impact or coupling via a tether.

CHAPTER 7

CONCLUSIONS

This thesis has presented methods to design low energy transfer trajectories for capturing NEAs in the neighbourhood of the Earth. In this Chapter, an overview and summary of the thesis are provided. According to the current limitations of the work, an outline of future work is presented.

7.1 Summary of thesis

In this thesis, tools and methods for achieving low energy capture of NEAs have been investigated and discussed. Since NEAs can provide valuable opportunities to exploit in-situ resources for future space exploration, capturing and returning NEAs to the neighbourhood of the Earth has generated significant interest. However, one of the key barriers for asteroid capture missions is the limitation on the returned NEA mass using current propulsion technologies. Hence, the utilisation of new methods and techniques which can reduce the total energy cost of capturing NEAs is the main objectives of this thesis.

According to a preliminary asteroid risk analysis, small asteroids with a diameter of less than 30 m have been considered as candidate asteroids in this thesis. In principle these are unlikely to represent an impact hazard to the Earth. This is constraint has been used to filter candidate asteroids before the tools and methods for low energy asteroid capture have been developed.

First, as a candidate gateway for future space missions, the Earth-Moon L_2 point is regarded as one of preferred locations where captured NEAs can be delivered. Developing capture strategies to this point has been a key contribution. Following prior work on asteroid capture onto periodic orbits around the Sun-Earth L_1 and L_2 points, an indirect asteroid capture strategy was introduced by patching together unstable manifolds in the Sun-Earth CRTBP and stable manifolds in Earth-Moon CRTBP system. The total flight

time of this capture strategy is always of the order of several years. In addition, a faster asteroid capture strategy was developed, termed the direct asteroid capture strategy. In this capture strategy, the Moon-Sun 3-body sphere of influence was utilised as the boundary between the Sun-Earth-Moon restricted four-body problem and the Earth-Moon CRTBP. Then, target points on the stable manifolds were transformed to a Sun-centred inertial frame. The three-dimensional orbital-element space of candidate NEAs was then obtained to select candidate NEAs which can be captured with a total cost less than 500 m/s. After calculating the approximate approach date and departure date, a Lambert arc in the Sun-centred two-body problem was utilised to estimate the first impulse to the target point on the stable manifold from the candidate asteroid's initial orbit. Based on the initial guess of the first impulse, a differential correction method was then used to design the transfer trajectory to the target point from the candidate asteroid's orbit in the Sun-Earth-Moon restricted four-body problem.

Since the direct capture strategy needs a shorter flight time, chemical propulsion may be more suitable, provided that the retrieved mass of the candidate NEA is within the capability of the propulsion system. On the other hand, low-thrust propulsion may be more easily applied to the indirect capture strategy. Moreover, by investigating the direct and indirect asteroid capture strategies without using stable manifolds in the Earth-Moon system, it was shown that the use of stable manifolds can enable low energy capture of NEAs, as expected.

Other targets for asteroid capture missions are orbits at the Sun-Earth L_1 and L_2 points. The strategy of coupling together a flyby of the Earth and capturing NEAs onto Sun-Earth L_1 or L_2 periodic orbits was then proposed. An aerobraking manoeuvre was firstly introduced and then the height threshold for aerobraking above the Earth's surface was determined. In this capture strategy the candidate NEA is first assumed to leave its orbit with an impulse manoeuvre and will then approach the vicinity of the Earth for the flyby. During the flyby, the Earth's upper atmosphere may also provide an aerobraking manoeuvre. If not, a propulsive manoeuvre is required at the perigee of the flyby. After the flyby of the Earth, the candidate NEA inserts onto the stable manifold associated with a periodic orbit around the Sun-Earth L_1 or L_2 point, and will be asymptotically captured onto it. Based on the detailed design procedure presented, a final global optimisation was carried out. Comparing the results of NEA capture strategies with and without the Earth flyby, the NEA capture strategy using an Earth flyby, with and without aerobraking, both have the potential to be of lower cost. Moreover, these NEA capture strategies using an Earth flyby also have the potential to deliver shorter flight times.

Momentum exchange theory was also applied to the capture of small NEAs into periodic orbits around the Sun-Earth L_1 and L_2 points. In the capture strategy using kinetic impacts, the small NEA leaves its initial orbit through an impulse from a spacecraft and then approaches a large target NEA. Accordingly, the small NEA then collides with the large NEA, with an impact geometry such that the small NEA will be captured onto the stable manifold associated with the Sun-Earth L_1 and L_2 points, thus leveraging the orbit energy of the large NEA. In the capture strategy using the tethered assist, after a targeting impulse, the small NEA approaches the large NEA and then connects with the large asteroid through a tether; the tether is then released after the assisted flyby manoeuvre. As a result, the small NEA will be transferred onto the stable manifold associated with the Sun-Earth L_1 and L_2 points. The key contributions are in coupling momentum exchange strategies to invariant manifolds, dynamical models of the kinetic impact itself and the tether-assisted flyby, and then optimising the strategies to achieve the low-energy capture of the small NEA onto periodic orbits around the Sun-Earth L_1 and L_2 points. It can be noted that the capture strategy with momentum exchange can achieve more efficient capture of some NEAs than the capture strategy without momentum exchange. Moreover, the efficiency of this method was strongly dependent on the materials of the two NEAs and tether material properties.

Another key contribution has been demonstrating that aerobraking can enable lower cost capture of asteroids onto periodic orbits around the Sun-Earth L_1 and L_2 points. Furthermore, a more general analysis of aerobraking was carried out, when aerobraking was used to capture asteroids directly onto bound orbits at the Earth. A Lambert arc in the Sun-centred two-body problem was utilised to estimate the asteroid capture window and the first impulse used to manoeuvre the candidate asteroid from its initial orbit. Based on the initial guess from the first impulse, the transfer trajectory for the captured asteroid was propagated in the Sun-Earth CRTBP system. Then, two strategies to capture asteroids into bound orbits at the Earth after aerobraking were considered. In the first case, the motion of the captured asteroid after aerobraking was modelled in the Earth-centred two-body problem, and so a second impulse was required to raise the height of the perigee to avoid a second aerobraking pass. In the second case, the motion of the captured asteroid is still modelled in the Sun-Earth CRTBP and solar gravitational perturbations used to passively raise the height of the asteroid perigee, again avoiding subsequent aerobraking passes. It was shown that aerobraking can in principle enable candidate asteroids to be captured around the Earth with extremely low energy requirements. It can be found that 2012 BK14 is one of the best targets which can be captured with a total capture cost below 10 m/s. Moreover, considering mass loss during aerobraking, capturing 2014 BK14 is also the

most economical such that the retrieved mass can be over 200 times that of the spacecraft which is required to execute the mission during the capture phase.

7.2 Current limitations

One of the limitations of the work in this thesis is the simplified dynamical models which are initialized from the real ephemeris on 1 January 2019. For example, in the CRTBP model, it is assumed that small primary body and the large primary body move on circular orbits around the barycentre, without considering orbit eccentricity and inclination or other perturbations. Therefore, the final target orbits for the captured asteroids are no longer simply periodic when perturbations are taken into account. An active control strategy is therefore required to maintain a captured asteroid in orbit around a libration point. In particular, for the Earth-Moon CRTBP system, the influence of the CRTBP assumption will be important in practice, due to the considerable eccentricity and inclination of the lunar orbit. However, although the results of asteroid capture in the full ephemeris will be different from those in the CRTBP model, the family of candidate asteroids which can be captured at low cost in the CRTBP model are not expected to change significantly, and thus they can serve as candidate asteroids. The transfers obtained in the CRTBP can serve as an initial guess for the real ephemeris.

Another limitation is the uncertainty on the properties of the candidate asteroids, including their shape, mass and material properties. In this thesis, the NEAs are assumed to be a spherical. To address the uncertainty on material properties, asteroids with standard density are assumed, so that basalt and metallic asteroids are considered. For future asteroid capture missions, pre-launch observations using radar and optical/infrared telescopes would again be required to provide good estimates of these parameters. Moreover, in-situ asteroid exploration missions, including flyby and rendezvous can also be viewed as an effective way to address these uncertainties.

7.3 Remarks on future work

Considering the limitations of the current work discussed in Section 7.2, future work should focus on addressing such issues, along with other extensions of the thesis.

7.3.1 Trajectory refinement

In a real mission for capturing NEAs, refinements to the model, including the eccentricity, inclination and the gravitational perturbations from other bodies should be considered. A Sun-centred J2000 inertial frame can be utilised to describe the motion of captured asteroids in the full ephemeris dynamical model. Then, the state in the CRTBP models can be mapped to the Sun-centred J2000 inertial system through the transformation in [215]. Transfers in the CRTBP models developed in this thesis then serve as initial guesses, and so trajectories in the full ephemeris model can be corrected and refined.

In general, Lyapunov orbits and halo orbits around the libration points are unstable and the final target orbits for the captured asteroids are no longer simply periodic in the full ephemeris model. Accordingly, station-keeping manoeuvres are required to maintain the orbit of the captured asteroids. Both chemical propulsion and low thrust propulsion can be employed for station-keeping, and some control strategies such as the Baseline Orbit Control-Point Targeting Strategy [60] can be investigated.

7.3.2 Optimisation for maximum economic return

In the strategy of capturing NEAs at the Earth using aerobraking, the mass loss of the asteroid due to ablation during aerobraking is considerable and thus an index, the ratio of the mass of the captured asteroid after aerobraking to the mass of the transfer vehicle is defined to measure the yield of the asteroid capture mission. Furthermore, this index can be extended to other NEA capture strategies in order to investigate the maximum economic return for NEA resource missions [6].

In this thesis, chemical propulsion is assumed to provide impulsive manoeuvres to capture NEAs in the neighbourhood of the Earth. The low efficiency, in terms of propellant mass consumption, of chemical propulsion, thus limits the retrieved mass of the NEA. Therefore, low-thrust propulsion with a high specific impulse, such as electric propulsion, can be used to increase the candidate NEA's retrieved mass, and thereby improve the feasibility of capturing and returning entire NEAs. Optimal control strategies including direct transcription and multiple shooting [52] and particle swarm optimisation [51], are then required to design low thrust optimal trajectories for capturing asteroids in multi-body problems, including CRTBP models and with a full ephemeris.

Moreover, reducing the mass loss of the candidate NEA during capture can further maximize the economic return from NEA resource missions. For example, in the NEA capture strategy using aerobraking, a suitable heat shield, potentially an inflatable

structure, or manufactured from the asteroid material itself [140], could provide protection of the candidate asteroid and thereby reduce ablative mass losses during aerobraking, while improving the predictability of the aerobraking manoeuvre. Moreover, active protection (e.g. ablative layer [216] or air-bags [217]) for the target small NEA could be required in the NEA capture strategy using momentum exchange. Therefore, the NEA transfer vehicle could deliver these devices: an ablative coating, shield or air-bags and thus they should be taken into account when sizing and designing the NEA transfer vehicle. After the transfer vehicle moves the target NEA from its initial orbit, the ablative materials or air-bags could then be installed on the surface of the candidate NEA where momentum exchange or ablation due to aerobraking will occur. Once such protection systems are installed, the ablative material or airbags could sacrificially protect the candidate NEA from disruption and thereby reduce mass loss.

7.3.3 NEA transfer vehicle design and mission operations

As noted above, the NEA transfer vehicle should be designed to carry ablative materials or air-bags to reduce the mass loss of the NEAs for the aerocapture, and potentially momentum exchange strategies.

One of the main challenges of these capture strategies is the sensitivity of the transfer trajectory of the candidate NEA in multi-body environments, since small perturbations or impulse manoeuvre errors would result in the failure of the NEA capture and return mission. Therefore, an accurate and robust navigation and control strategy (e.g. Precise One-Way Radio Metric Tracking, Autonomous Navigation [218], drag-modulation flight control methods [126] or blended control, predictor-corrector guidance algorithms [128]) would be required to guarantee that the candidate NEA approaches the large NEA for momentum exchange, or encounters the Earth with the correct perigee height to achieve the required aerobraking manoeuvre for capture. It is envisaged that the transfer vehicle would remain attached to candidate NEA through an asteroid surface attachment device [219] or a flexible bagging device [39], thereby allowing mid-course corrections. In particular, depending on the size of the asteroid and transfer vehicle, the vehicle could remain attached during aerobraking, with the asteroid body protecting the vehicle.

In addition, unknown properties of the candidate NEAs, including their shape, mass and material properties should be addressed in advance of the NEA return mission. Therefore, pre-launch observations would again be required, e.g. by using radar and optical/infrared telescopes [21, 23]. Besides, flyby and rendezvous during the asteroid exploration missions would provide more accurate observations, measure and

determination of the candidate NEA properties [59]. For the capture strategy using momentum exchange, an additional spacecraft may also be required to achieve a rendezvous with each asteroid to prepare an anchor point using a penetrator or a surrounding net or bag [122]. As the small NEA approaches the vicinity of the large NEA, the two anchor points are assumed to be connected by a tether. The design and sizing of such vehicles, and their inclusion in a globally optimised mission design, represent future work to build on the findings of this thesis.

REFERENCES

- [1] J. Lieske, "Galilean satellites and the Galileo space mission," *Celestial Mechanics and Dynamical Astronomy*, vol. 66, pp. 13-20, 1997.
- [2] D. E. Brownlee, P. Tsou, J. Anderson, M. Hanner, R. Newburn, Z. Sekanina, *et al.*, "Stardust: Comet and interstellar dust sample return mission," *Journal of Geophysical Research: Planets*, vol. 108, pp. 1-15, 2003.
- [3] W. H. Blume, "Deep impact mission design," *Space Science Reviews*, vol. 117, pp. 23-42, 2005.
- [4] K.-H. Glassmeier, H. Boehnhardt, D. Koschny, E. Kührt, and I. Richter, "The Rosetta mission: flying towards the origin of the solar system," *Space Science Reviews*, vol. 128, pp. 1-21, 2007.
- [5] A. Morbidelli, W. Bottke Jr, C. Froeschlé, and P. Michel, "Origin and Evolution of Near-Earth Objects," in *Asteroids III*, W. F. B. Jr., A. Cellino, P. Paolicchi, and R. P. Binzel, Eds., ed Tucson: University of Arizona Press, 2002, pp. 409-422.
- [6] M. J. Sonter, "The technical and economic feasibility of mining the near-earth asteroids," *Acta Astronautica*, vol. 41, pp. 637-647, 1997.
- [7] J. S. Lewis and M. L. Hutson, *Resources of near-Earth space*. Tucson Arizona: University of Arizona Press, 1993.
- [8] W. F. Bottke, *Asteroids III*. Tucson: University of Arizona Press, 2002.
- [9] J. P. Sanchez, D. Garcia Yarnoz, and C. McInnes, "Near-Earth asteroid resource accessibility and future capture mission opportunities," presented at the Global Space Exploration Conference. Paper GLEX-2012.11.1.5x12412, Washington, DC, 2012.
- [10] J. Sanchez and C. McInnes, "Asteroid resource map for near Earth space," *Journal of Spacecraft and Rockets*, vol. 48, pp. 153-165, 2011.
- [11] F. Tronchetti, "Private property rights on asteroid resources: Assessing the legality of the ASTEROIDS Act," *Space Policy*, vol. 30, pp. 193-196, 2014.
- [12] D. G. Andrews, K. Bonner, A. Butterworth, H. Calvert, B. Dagang, K. Dimond, *et al.*, "Defining a successful commercial asteroid mining program," *Acta Astronautica*, vol. 108, pp. 106-118, 2015.
- [13] A. Krolikowski and M. Elvis, "Making policy for new asteroid activities: In pursuit of science, settlement, security, or sales?," *Space Policy*, 2018.
- [14] K. Muzyka, "The Problems with an International Legal Framework for Asteroid Mining," in *Deep Space Commodities*, ed: Springer, 2018, pp. 123-140.
- [15] J. S. Lewis, *Asteroid mining 101: wealth for the new space economy*: Deep Space Industries, 2015.

-
- [16] Z. Hasnain, C. A. Lamb, and S. D. Ross, "Capturing near-Earth asteroids around Earth," *Acta Astronautica*, vol. 81, pp. 523-531, 2012.
- [17] N. Lladó, Y. Ren, J. J. Masdemont, and G. Gómez, "Capturing small asteroids into a Sun–Earth Lagrangian point," *Acta Astronautica*, vol. 95, pp. 176-188, 2014.
- [18] J. P. Sánchez and D. G. Yárnoz, "Asteroid retrieval missions enabled by invariant manifold dynamics," *Acta Astronautica*, vol. 127, pp. 667-677, 2016.
- [19] J. Sanchez and C. McInnes, "Asteroid resource map for near-Earth space," *Journal of Spacecraft and Rockets*, vol. 48, pp. 153-165, 2011.
- [20] G. F. Serio, A. Manara, P. Sicoli, and W. F. Bottke, "Giuseppe Piazzi and the discovery of Ceres," in *Asteroids III*, W. F. Bottke, A. Cellino, P. Paolicchi, and R. P. Binzel, Eds., ed Tucson: University of Arizona Press, 2002.
- [21] J. Neeley, B. Clark, M. Ockert-Bell, M. Shepard, J. Conklin, E. Cloutis, *et al.*, "The composition of M-type asteroids II: Synthesis of spectroscopic and radar observations," *Icarus*, vol. 238, pp. 37-50, 2014.
- [22] B. E. Clark, P. Helfenstein, J. Bell III, C. Peterson, J. Veverka, N. Izenberg, *et al.*, "NEAR infrared spectrometer photometry of Asteroid 433 Eros," *Icarus*, vol. 155, pp. 189-204, 2002.
- [23] M. K. Shepard, J. Richardson, P. A. Taylor, L. A. Rodriguez-Ford, A. Conrad, I. de Pater, *et al.*, "Radar observations and shape model of asteroid 16 Psyche," *Icarus*, vol. 281, pp. 388-403, 2017.
- [24] A. Andrews, R. Hudson, and D. Psaltis, "Optical-radar imaging of scale models for studies in asteroid astronomy," *Optics letters*, vol. 20, pp. 2327-2329, 1995.
- [25] P. Helfenstein, J. Veverka, P. Thomas, D. Simonelli, K. Klaasen, T. Johnson, *et al.*, "Galileo photometry of asteroid 243 Ida," *Icarus*, vol. 120, pp. 48-65, 1996.
- [26] S. Nozette and E. M. Shoemaker, "Back to the Moon, on to an asteroid: The Clementine mission," *Planetary Report*, vol. 13, pp. 10-11, 1993.
- [27] J. Veverka, B. Farquhar, M. Robinson, P. Thomas, S. Murchie, A. Harch, *et al.*, "The landing of the NEAR-Shoemaker spacecraft on asteroid 433 Eros," *Nature*, vol. 413, p. 390, 2001.
- [28] M. D. Rayman, P. A. Chadbourne, J. S. Culwell, and S. N. Williams, "Mission design for deep space 1: a low-thrust technology validation mission," *Acta astronautica*, vol. 45, pp. 381-388, 1999.
- [29] P. Thomas, "Sizes, shapes, and derived properties of the saturnian satellites after the Cassini nominal mission," *Icarus*, vol. 208, pp. 395-401, 2010.
- [30] D. Brownlee, "The Stardust mission: analyzing samples from the edge of the solar system," *Annual Review of Earth and Planetary Sciences*, vol. 42, pp. 179-205, 2014.
- [31] H. Kuninaka and J. i. Kawaguchi, "Lessons learned from round trip of Hayabusa asteroid explorer in deep space," in *Aerospace Conference, 2011 IEEE*, Big Sky, MT, USA, 2011, pp. 1-8.
- [32] M. Barucci, M. Fulchignoni, and A. Rossi, "Rosetta asteroid targets: 2867 Steins and 21 Lutetia," *Space Science Reviews*, vol. 128, pp. 67-78, 2007.

- [33] C. Russell, M. Barucci, R. Binzel, M. Capria, U. Christensen, A. Coradini, *et al.*, "Exploring the asteroid belt with ion propulsion: Dawn mission history, status and plans," *Advances in Space Research*, vol. 40, pp. 193-201, 2007.
- [34] X. Zou, C. Li, J. Liu, W. Wang, H. Li, and J. Ping, "The preliminary analysis of the 4179 Toutatis snapshots of the Chang'E-2 flyby," *Icarus*, vol. 229, pp. 348-354, 2014.
- [35] Y. Tsuda, M. Yoshikawa, M. Abe, H. Minamino, and S. Nakazawa, "System design of the Hayabusa 2—Asteroid sample return mission to 1999 JU3," *Acta Astronautica*, vol. 91, pp. 356-362, 2013.
- [36] D. S. Lauretta and O.-R. Team, "An overview of the OSIRIS-REx asteroid sample return mission," presented at the Lunar and Planetary Science Conference, Paper 2491, Woodlands, Texas, 2012.
- [37] J. Brophy, R. Gershman, D. Landau, J. Polk, C. Porter, D. Yeomans, *et al.*, "Asteroid return mission feasibility study," presented at the 47th AIAA/ASME/SAE/ASEE Joint Propulsion Conference & Exhibit, Paper 2011-5665, San Diego, California, 2011.
- [38] L. Fast, "Capture a 2m Diameter Asteroid, a Mission Proposal," presented at the AIAA SPACE 2011 Conference & Exposition, AIAA 2011-7116 Long Beach, California, 2011.
- [39] J. R. Brophy, L. Friedman, and F. Culick, "Asteroid retrieval feasibility," Keck Institute for Space Studies, California Institute of Technology, Jet Propulsion Laboratory, Pasadena, California 1457705567, 2012.
- [40] D. D. Mazanek, R. G. Merrill, J. R. Brophy, and R. P. Mueller, "Asteroid redirect mission concept: a bold approach for utilizing space resources," *Acta Astronautica*, vol. 117, pp. 163-171, 2015.
- [41] J. R. Brophy, "Legacy of the Asteroid Redirect Robotic Mission (ARRM)," presented at the The 35th International Electric Propulsion Conference, Georgia Institute of Technology, USA IEPC-2017-031, 2017.
- [42] J. P. Sanchez and C. R. McInnes, "On the ballistic capture of asteroids for resource utilisation," in *62nd International Astronautical Congress, IAC-11.C1.4.6*, CapeTown, SA, 2011.
- [43] J. P. Sanchez, D. Garcia Yarnoz, E. M. Alessi, and C. McInnes, "Gravitational capture opportunities for asteroid retrieval missions," presented at the 63rd International Astronautical Congress, IAC-12.C1.5.13x14763., Naples, Italy, 2012.
- [44] M. Tan, C. McInnes, and M. Ceriotti, "Low-energy near Earth asteroid capture using Earth flybys and aerobraking," *Advances in Space Research*, vol. 61, pp. 2099-2115, 2018.
- [45] M. Tan, C. McInnes, and M. Ceriotti, "Direct and indirect capture of near-Earth asteroids in the Earth–Moon system," *Celestial Mechanics and Dynamical Astronomy*, vol. 129, pp. 57-88, 2017.
- [46] M. Tan, C. R. McInnes, and M. Ceriotti, "Low-Energy Near-Earth Asteroid Capture Using Momentum Exchange Strategies," *Journal of Guidance, Control, and Dynamics*, vol. 41, pp. 632-643, 2017.
- [47] H. Yang, J. Li, and H. Baoyin, "Low-cost transfer between asteroids with distant orbits using multiple gravity assists," *Advances in Space Research*, vol. 56, pp. 837-847, 2015.

- [48] S. Gong and J. Li, "Asteroid capture using lunar flyby," *Advances in Space Research*, vol. 56, pp. 848-858, 2015.
- [49] J. P. Sanchez and C. McInnes, "Synergistic approach of asteroid exploitation and planetary protection," *Advances in Space Research*, vol. 49, pp. 667-685, 2012.
- [50] D. G. Yárnoz, J. Sanchez, and C. McInnes, "Easily retrievable objects among the NEO population," *Celestial Mechanics and Dynamical Astronomy*, vol. 116, pp. 367-388, 2013.
- [51] G. Tang and F. Jiang, "Capture of near-Earth objects with low-thrust propulsion and invariant manifolds," *Astrophysics and Space Science*, vol. 361, pp. 1-14, 2016.
- [52] G. Mingotti, J. Sánchez, and C. McInnes, "Combined low-thrust propulsion and invariant manifold trajectories to capture NEOs in the Sun–Earth circular restricted three-body problem," *Celestial Mechanics and Dynamical Astronomy*, vol. 120, pp. 309-336, 2014.
- [53] G. Mingotti, J.-P. Sanchez, and C. McInnes, "Low energy, low-thrust capture of near Earth objects in the Sun–Earth and Earth–Moon restricted three-body systems," in *SPACE Conferences & Exposition, AIAA 2014-4301*, Washington, 2014.
- [54] P. E. Verrier and C. R. McInnes, "Low-Energy Capture of Asteroids onto Kolmogorov–Arnold–Moser Tori," *Journal of Guidance, Control, and Dynamics*, vol. 38, pp. 330-335, 2014.
- [55] R. W. Farquhar, D. W. Dunham, Y. Guo, and J. V. McAdams, "Utilization of libration points for human exploration in the Sun–Earth–Moon system and beyond," *Acta Astronautica*, vol. 55, pp. 687-700, 2004.
- [56] A. Zimmer, "Investigation of vehicle reusability for human exploration of Near-Earth Asteroids using Sun–Earth Libration point orbits," *Acta Astronautica*, vol. 90, pp. 119-128, 2013.
- [57] M. Ceriotti and J. P. Sanchez, "Control of asteroid retrieval trajectories to libration point orbits," *Acta Astronautica*, vol. 126, pp. 342-353, 2016.
- [58] Y. M. Wang, D. Qiao, and P. Y. Cui, "Trajectory Design for the Transfer from the Lissajous Orbit of Sun-Earth System to Asteroids," *Applied Mechanics and Materials*, vol. 390, pp. 478-484, 2013.
- [59] Y. Gao, "Near-Earth asteroid flyby trajectories from the Sun-Earth L2 for Chang'e-2's extended flight," *Acta Mechanica Sinica*, vol. 29, pp. 123-131, 2013.
- [60] D. Folta, M. Woodard, and D. Cosgrove, "Stationkeeping of the First Earth-Moon Libration Orbiters: The ARTEMIS Mission," presented at the Proceedings of the AAS/AIAA Astrodynamics Specialist Conference, AAS 11-515, Girdwood, Alaska, 2011.
- [61] B. Hufenbach, K. Laurini, J. Piedboeuf, B. Schade, K. Matsumoto, F. Spiero, *et al.*, "The Global Exploration Roadmap," presented at the 62nd International Astronautical Congress, IAC-11-B3.1.8, Capetown, SA, 2011.
- [62] J. Olson, "Voyages: charting the course for sustainable human space exploration," NASA NP-2011-06-395-LaRC, 2012.
- [63] J. Brophy, F. Culick, L. Friedman, C. Allen, D. Baughman, J. Bellerose, *et al.*, "Asteroid retrieval feasibility study," *Keck Institute for Space Studies, California Institute of Technology, Jet Propulsion Laboratory*, 2012.

- [64] M. Lo and S. Ross, "The Lunar L1 Gateway: Portal to the stars and beyond," presented at the AIAA Space 2001 Conference and Exposition, A01-40254, Albuquerque, NM, U.S.A, 2001.
- [65] E. M. Alessi, G. Gómez, and J. J. Masdemont, "Leaving the Moon by means of invariant manifolds of libration point orbits," *Communications in Nonlinear Science and Numerical Simulation*, vol. 14, pp. 4153-4167, 2009.
- [66] K. E. Davis, R. L. Anderson, D. J. Scheeres, and G. H. Born, "The use of invariant manifolds for transfers between unstable periodic orbits of different energies," *Celestial Mechanics and Dynamical Astronomy*, vol. 107, pp. 471-485, 2010.
- [67] F. Salazar, C. de Melo, E. Macau, and O. Winter, "Three-body problem, its Lagrangian points and how to exploit them using an alternative transfer to L4 and L5," *Celestial Mechanics and Dynamical Astronomy*, vol. 114, pp. 201-213, 2012.
- [68] G. O'Neill, "The Colonization of Space," *Physics Today*, vol. 27(9), pp. 32-40, 1974.
- [69] G. DeFilippi Jr, "Station keeping at the L4 libration point: A three dimensional study," Master's thesis, AIR FORCE INST OF TECH WRIGHT-PATTERSON AFB OH SCHOOL OF ENGINEERING, 1977.
- [70] J. Lewis, "Construction materials for an SPS constellation in highly eccentric Earth orbit," in *Proceedings of the 2nd International Symposium*, Paris, 1991, pp. 174-179.
- [71] J. Hills, "Capturing asteroids into bound orbits around the earth: Massive early return on an asteroid terminal defense system," Los Alamos National Lab., NM (United States)1992.
- [72] K. Tanikawa, "Impossibility of the capture of retrograde satellites in the restricted three-body problem," *Celestial mechanics*, vol. 29, pp. 367-402, 1983.
- [73] J. B. Pollack, J. A. Burns, and M. E. Tauber, "Gas drag in primordial circumplanetary envelopes: A mechanism for satellite capture," *Icarus*, vol. 37, pp. 587-611, 1979.
- [74] J. K. Cline, "Satellite aided capture," *Celestial mechanics*, vol. 19, pp. 405-415, 1979.
- [75] B. Villac and D. J. Scheeres, "Escaping trajectories in the Hill three-body problem and applications," *Journal of guidance, control, and dynamics*, vol. 26, pp. 224-232, 2003.
- [76] M. E. Paskowitz and D. J. Scheeres, "Robust capture and transfer trajectories for planetary satellite orbiters," *Journal of guidance, control, and dynamics*, vol. 29, pp. 342-353, 2006.
- [77] E. A. Belbruno and J. K. Miller, "Sun-perturbed Earth-to-Moon transfers with ballistic capture," *Journal of Guidance, Control, and Dynamics*, vol. 16, pp. 770-775, 1993.
- [78] F. Topputo and E. Belbruno, "Computation of weak stability boundaries: Sun-Jupiter system," *Celestial Mechanics and Dynamical Astronomy*, vol. 105, p. 3, 2009.
- [79] E. Belbruno, *Capture dynamics and chaotic motions in celestial mechanics: With applications to the construction of low energy transfers*: Princeton University Press, 2004.
- [80] M. Tan, C. McInnes, and M. Ceriotti, "Capture of small near-Earth asteroids to Earth orbit using aerobraking," *Acta Astronautica (Accepted for publication)*.

- [81] M. Granvik, J. Vaubailon, and R. Jedicke, "The population of natural Earth satellites," *Icarus*, vol. 218, pp. 262-277, 2012.
- [82] H. Urrutxua, D. J. Scheeres, C. Bombardelli, J. L. Gonzalo, and J. Peláez, "Temporarily captured asteroids as a pathway to affordable asteroid retrieval missions," *Journal of Guidance, Control, and Dynamics*, vol. 38, pp. 2132-2145, 2015.
- [83] M. Granvik, R. Jedicke, B. Bolin, M. Chyba, G. Patterson, and G. Picot, "Earth's temporarily-captured natural satellites—The first step towards utilization of asteroid resources," in *Asteroids*, ed: Springer, 2013, pp. 151-167.
- [84] S. Brelsford, M. Chyba, T. Haberkorn, and G. Patterson, "Rendezvous missions to temporarily captured near Earth asteroids," *Planetary and Space Science*, vol. 123, pp. 4-15, 2016.
- [85] H. Urrutxua and C. Bombardelli, "A look at the capture mechanisms of the "temporarily captured asteroids" of the earth," in *26th International Symposium on Space Flight Dynamics, number ISSFD-2017*, 2017, pp. 1-7.
- [86] H. Urrutxua, D. J. Scheeres, C. Bombardelli, J. L. Gonzalo, and J. Peláez, "What does it take to capture an Asteroid? A case study on capturing Asteroid 2006 RH120," in *24th AAS/AIAA Space Flight Mechanics Meeting, Santa Fe, New Mexico*, 2014, pp. 26-30.
- [87] R. Shah, D. F. Woods, W. Faccenda, J. Johnson, R. Lambour, E. C. Pearce, *et al.*, "Asteroid Detection with the Space Surveillance Telescope," in *Proceedings of the AMOS Conference*, 2013.
- [88] G. Fedorets, M. Granvik, L. Jones, and R. Jedicke, "Discovering asteroids temporarily captured by the Earth with LSST," *IAU General Assembly*, vol. 22, 2015.
- [89] G. Fedorets, M. Granvik, and R. Jedicke, "Orbit and size distributions for asteroids temporarily captured by the Earth-Moon system," *Icarus*, vol. 285, pp. 83-94, 2017.
- [90] R. Jedicke, B. Bolin, W. F. Bottke, M. Chyba, G. Fedorets, M. Granvik, *et al.*, "Small asteroids temporarily captured in the Earth-Moon system," *Proceedings of the International Astronomical Union*, vol. 10, pp. 86-90, 2015.
- [91] T. A. Pavlak, "Trajectory design and orbit maintenance strategies in multi-body dynamical regimes," PhD thesis, Purdue University, 2013.
- [92] D. C. Folta, M. Woodard, K. Howell, C. Patterson, and W. Schlei, "Applications of multi-body dynamical environments: the ARTEMIS transfer trajectory design," *Acta Astronautica*, vol. 73, pp. 237-249, 2012.
- [93] M. W. Lo and J. S. Parker, "Unstable resonant orbits near earth and their applications in planetary missions," presented at the AIAA/AAS Astrodynamics Specialist Conference, Paper AIAA 2004-5304, Providence, RI., 2004.
- [94] M. Xu, T. Tan, and S. Xu, "Research on the transfers to Halo orbits from the view of invariant manifolds," *Science China Physics, Mechanics and Astronomy*, vol. 55, pp. 671-683, 2012.
- [95] K. E. Davis, R. L. Anderson, D. J. Scheeres, and G. H. Born, "Optimal transfers between unstable periodic orbits using invariant manifolds," *Celestial Mechanics and Dynamical Astronomy*, vol. 109, pp. 241-264, 2011.

-
- [96] W. S. Koon, M. W. Lo, J. E. Marsden, and S. D. Ross, "Shoot the moon," in *Proceedings of Spaceflight Mechanics 2000*, San Diego, CA, 2000, pp. 1017-1030.
- [97] W. S. Koon, M. W. Lo, J. E. Marsden, and S. D. Ross, *Dynamical systems, the three-body problem and space mission design*. New York: Springer-Verlag, 2011.
- [98] K. C. Howell and M. Kakoi, "Transfers between the Earth–Moon and Sun–Earth systems using manifolds and transit orbits," *Acta Astronautica*, vol. 59, pp. 367-380, 2006.
- [99] W. Koon, M. Lo, J. Marsden, and S. Ross, "Low Energy Transfer to the Moon," *Celestial Mechanics and Dynamical Astronomy*, vol. 81, pp. 63-73, 2001.
- [100] Y. Qi and S. Xu, "Study of lunar gravity assist orbits in the restricted four-body problem," *Celestial Mechanics and Dynamical Astronomy*, vol. 125, pp. 333-361, 2016.
- [101] P. A. de Sousa-Silva and M. O. Terra, "A survey of different classes of Earth-to-Moon trajectories in the patched three-body approach," *Acta Astronautica*, vol. 123, pp. 340-349, 2016.
- [102] F. Topputo, "On optimal two-impulse Earth–Moon transfers in a four-body model," *Celestial Mechanics and Dynamical Astronomy*, vol. 117, pp. 279-313, 2013.
- [103] H. B. Keller, *Numerical solution of two point boundary value problems*. Bristol, England, U.K.: SIAM Regional Conference Series in Applied Mathematics, J. W. Arrowsmith Ltd., 1976.
- [104] D. J. Grebow, "Trajectory design in the Earth-Moon system and lunar South Pole coverage," PhD thesis, Purdue University, 2010.
- [105] K. C. Howell, D. C. Davis, and A. F. Haapala, "Application of periapse maps for the design of trajectories near the smaller primary in multi-body regimes," *Mathematical Problems in Engineering*, vol. 2012, pp. 1-22, 2011.
- [106] S. Wagner and B. Wie, "Hybrid Algorithm for Multiple Gravity-Assist and Impulsive Delta-V Maneuvers," *Journal of Guidance, Control, and Dynamics*, vol. 38, pp. 2096-2107, 2015.
- [107] M. A. Minovitch, "The invention that opened the solar system to exploration," *Planetary and Space Science*, vol. 58, pp. 885-892, 2010.
- [108] J. A. Dunne and E. Burgess, "The voyage of Mariner 10," National Aeronautics and Space Administration, SP-4241978.
- [109] S. G. Turyshev, M. M. Nieto, and J. D. Anderson, "Lessons learned from the Pioneers 10/11 for a mission to test the Pioneer anomaly," *Advances in Space Research*, vol. 39, pp. 291-296, 2007.
- [110] N. J. Strange and J. M. Longuski, "Graphical method for gravity-assist trajectory design," *Journal of Spacecraft and Rockets*, vol. 39, pp. 9-16, 2002.
- [111] K. Wenzel, R. Marsden, D. Page, and E. Smith, "The ULYSSES mission," *Astronomy and Astrophysics Supplement Series*, vol. 92, p. 207, 1992.
- [112] D. Izzo, V. M. Becerra, D. R. Myatt, S. J. Nasuto, and J. M. Bishop, "Search space pruning and global optimisation of multiple gravity assist spacecraft trajectories," *Journal of Global Optimization*, vol. 38, pp. 283-296, 2007.

- [113] J. V. McAdams, D. W. Dunham, R. W. Farquhar, A. H. Taylor, and B. G. Williams, "Trajectory design and maneuver strategy for the MESSENGER mission to Mercury," *Journal of spacecraft and rockets*, vol. 43, pp. 1054-1064, 2006.
- [114] S. Bale, K. Goetz, P. Harvey, P. Turin, J. Bonnell, T. DudokádeáWit, *et al.*, "The FIELDS instrument suite for solar probe plus," *Space Science Reviews*, vol. 204, pp. 49-82, 2016.
- [115] K. Clark, J. Boldt, R. Greeley, K. Hand, I. Jun, R. Lock, *et al.*, "Return to Europa: overview of the Jupiter Europa orbiter mission," *Advances in space research*, vol. 48, pp. 629-650, 2011.
- [116] D. Qiao, H. Cui, and P. Cui, "Evaluating accessibility of near-earth asteroids via earth gravity assists," *Journal of Guidance, Control, and Dynamics*, vol. 29, pp. 502-505, 2006.
- [117] N. Eismont, M. Boyarskii, A. Ledkov, R. Nazirov, D. Dunham, and B. Shustov, "On the possibility of the guidance of small asteroids to dangerous celestial bodies using the gravity-assist maneuver," *Solar System Research*, vol. 47, pp. 325-333, 2013.
- [118] L. Casalino and G. Colasurdo, "Mars gravity assist to improve missions towards main-belt asteroids," *Acta Astronautica*, vol. 53, pp. 521-526, 2003.
- [119] Y. Chen, H. Baoyin, and J. Li, "Accessibility of main-belt asteroids via gravity assists," *Journal of Guidance, Control, and Dynamics*, vol. 37, pp. 623-632, 2014.
- [120] M. Vasile and P. D. Pascale, "Preliminary design of multiple gravity-assist trajectories," *Journal of Spacecraft and Rockets*, vol. 43, pp. 794-805, 2006.
- [121] C. Bao, H. Yang, B. Barsbold, and H. Baoyin, "Capturing near-Earth asteroids into bounded Earth orbits using gravity assist," *Astrophysics and Space Science*, vol. 360, p. 61, 2015.
- [122] P. A. Penzo and H. L. Mayer, "Tethers and asteroids for artificial gravity assist in the solar system," *Journal of Spacecraft and Rockets*, vol. 23, pp. 79-82, 1986.
- [123] J. R. Van Zandt, "Tethered asteroids," presented at the AIAA SPACE 2013 Conference and Exposition, Paper AIAA 2013-5302, San Diego, CA, 2013.
- [124] A. F. Prado, "Using tethered gravity-assisted maneuvers for planetary capture," *Journal of Guidance, Control, and Dynamics*, vol. 38, pp. 1852-1856, 2015.
- [125] D. Carrelli, D. O'Shaughnessy, T. Strikwerda, J. Kaidy, J. Prince, and R. Powell, "Autonomous aerobraking for low-cost interplanetary missions," *Acta Astronautica*, vol. 93, pp. 467-474, 2014.
- [126] Z. R. Putnam and R. D. Braun, "Drag-modulation flight-control system options for planetary aerocapture," *Journal of Spacecraft and Rockets*, vol. 51, pp. 139-150, 2013.
- [127] D. A. Spencer and R. Tolson, "Aerobraking cost and risk decisions," *Journal of Spacecraft and Rockets*, vol. 44, pp. 1285-1293, 2007.
- [128] R. Y. Jits and G. D. Walberg, "Blended control, predictor–corrector guidance algorithm: an enabling technology for Mars aerocapture," *Acta astronautica*, vol. 54, pp. 385-398, 2004.
- [129] D. T. Lyons, W. Sjogren, W. T. Johnson, D. Schmitt, and A. McDonald, "Aerobraking Magellan," in *Astrodynamicics 1991*, San Diego, CA, 1992, pp. 1821-1839.

- [130] D. T. Lyons, J. G. Beerer, P. Esposito, M. D. Johnston, and W. H. Willcockson, "Mars global surveyor: aerobraking mission overview," *Journal of Spacecraft and Rockets*, vol. 36, pp. 307-313, 1999.
- [131] G. Mingotti, F. Topputo, and F. Bernelli-Zazzera, "Optimal low-thrust invariant manifold trajectories via attainable sets," *Journal of guidance, control, and dynamics*, vol. 34, pp. 1644-1656, 2011.
- [132] D. Way, R. Powell, J. Masciarelli, B. Starr, and K. Edquist, "Aerocapture simulation and performance for the Titan Explorer mission," presented at the 39th AIAA/ASME/SAE/ASEE Joint Propulsion Conference and Exhibit, Paper AIAA 2003-4951 Huntsville, Alabama, 2003.
- [133] M. K. Lockwood, "Neptune aerocapture systems analysis," presented at the AIAA Atmospheric Flight Mechanics Conference and Exhibit, Paper AIAA 2004-4951 Providence, Rhode Island, 2004.
- [134] B. R. Starr and C. H. Westhelle, "Aerocapture Performance Analysis of a Venus Exploration Mission," presented at the AIAA Atmospheric Flight Mechanics Conference and Exhibit, Paper 2005-5913, San Francisco, CA, 2005.
- [135] R. R. Sostaric, C. Zumwalt, E. Garcia-Llama, R. Powell, and J. Shidner, "Trajectory guidance for Mars robotic precursors: aerocapture, entry, descent, and landing," presented at the International Planetary Probe Workshop (IPPW-8), JSC-CN-23876, Portsmouth, VA, 2011.
- [136] R. D. Braun, R. W. Powell, and J. Lyne, "Earth aerobraking strategies for manned return from mars," *Journal of Spacecraft and Rockets*, vol. 29, pp. 297-304, 1992.
- [137] M. Kumar and A. Tewari, "Trajectory and attitude simulation for aerocapture and aerobraking," *Journal of spacecraft and rockets*, vol. 42, pp. 684-693, 2005.
- [138] H. X. Baoyin, Y. Chen, and J. F. Li, "Capturing near earth objects," *Research in Astronomy and Astrophysics*, vol. 10, p. 587, 2010.
- [139] T. Heppenheimer, "Approximate analytic modeling of a ballistic aerobraking planetary capture," *Journal of Spacecraft and Rockets*, vol. 8, pp. 554-555, 1971.
- [140] S. D. Ross, "Near-earth asteroid mining," Department of Control and Dynamical Systems, Pasadena, CA, 2001.
- [141] E. M. Levin and E. M. Levin, "Dynamic analysis of space tether missions," ed San Diego, CA: American Astronomical Society Publication, 2007, pp. 11-17.
- [142] S. G. Tragesser, "Static formations using momentum exchange between satellites," *Journal of Guidance, Control, and Dynamics*, vol. 32, pp. 1277-1286, 2009.
- [143] C. Bombardelli, H. Urrutxua, M. Merino, J. Pelaez, and E. Ahedo, "The ion beam shepherd: A new concept for asteroid deflection," *Acta Astronautica*, vol. 90, pp. 98-102, 2013.
- [144] B. Wie, "Dynamics and control of gravity tractor spacecraft for asteroid deflection," *Journal of Guidance, Control, and Dynamics*, vol. 31, pp. 1413-1423, 2008.
- [145] C. R. McInnes, "Near Earth object orbit modification using gravitational coupling," *Journal of Guidance Control and Dynamics*, vol. 30, pp. 870-873, 2007.

- [146] C. R. McInnes, "Deflection of near-Earth asteroids by kinetic energy impacts from retrograde orbits," *Planetary and Space Science*, vol. 52, pp. 587-590, 2004.
- [147] M. Vasile and C. Colombo, "Optimal impact strategies for asteroid deflection," *Journal of Guidance, Control, and Dynamics*, vol. 31, pp. 858-872, 2008.
- [148] P. Michel, A. Cheng, and M. Küppers, "Asteroid Impact and Deflection Assessment (AIDA) mission: science investigation of a binary system and mitigation test," in *Proceeding of European Planetary Science Congress 2015*, Nantes, France, 2015, pp. 123-124.
- [149] G. H. Canavan and J. Rather, "Assessment of current and future technologies," in *Proceedings of the Near-Earth Interception Workshop*, 1992, pp. 227-236.
- [150] R. Nazirov and N. Eismont, "Gravitational maneuvers as a way to direct small asteroids to trajectory of a rendezvous with dangerous near-Earth objects," *Cosmic Research*, vol. 48, pp. 479-484, 2010.
- [151] K. E. Davis, "Locally optimal transfer trajectories between libration point orbits using invariant manifolds," MSc, University of Colorado at Boulder, 2009.
- [152] G. Gómez, M. Marcote, and J. J. Masdemont, "Trajectory correction manoeuvres in the transfer to libration point orbits," *Acta Astronautica*, vol. 56, pp. 652-669, 2005.
- [153] G. Gómez and J. Masdemont, "Some zero cost transfers between libration point orbits," *Advances in the Astronautical Sciences*, vol. 105, pp. 1199-1216, 2000.
- [154] B. Barden, K. Howell, and M. Lo, "Application of dynamical systems theory to trajectory design for a libration point mission," presented at the Astrodynamics Conference, Paper AIAA 96-3602, San Diego, CA, U.S.A, 1996.
- [155] H. Lei and B. Xu, "Transfers between libration point orbits of Sun–Earth and Earth–Moon systems by using invariant manifolds," *Journal of Engineering Mathematics*, vol. 98, pp. 163-186, 2016.
- [156] W. S. Koon, J. E. Marsden, and S. D. Ross, "Constructing a Low Energy Transfer between Jovian moons," in *Celestial Mechanics: Dedicated to Donald Saari for His 60th Birthday: Proceedings of an International Conference on Celestial Mechanics, December 15-19, 1999, Northwestern University, Evanston, Illinois*, 2002, p. 129.
- [157] W. S. Koon, M. W. Lo, J. E. Marsden, and S. D. Ross, "Low energy transfer to the Moon," in *Dynamics of Natural and Artificial Celestial Bodies*, ed: Springer, 2001, pp. 63-73.
- [158] L. Liou, J. Dankanich, and L. Alexander, "NASA in-space advanced chemical propulsion development in recent years," presented at the 45th AIAA/ASME/SAE/ASEE Joint Propulsion Conference & Exhibit, Paper AIAA 2009-5126, Denver, Colorado, 2009.
- [159] G. Woodcock, D. Byers, L. Alexander, and A. Krebsbach, "Advanced Chemical Propulsion Study," presented at the 40th AIAA/ASME/SAE/ASEE Joint Propulsion Conference and Exhibit, Paper AIAA 2004-3494 Fort Lauderdale, Florida, 2004.
- [160] G. Racca, A. Marini, L. Stagnaro, J. Van Dooren, L. Di Napoli, B. Foing, *et al.*, "SMART-1 mission description and development status," *Planetary and space science*, vol. 50, pp. 1323-1337, 2002.
- [161] J. T. Betts, "Survey of numerical methods for trajectory optimization," *Journal of guidance, control, and dynamics*, vol. 21, pp. 193-207, 1998.

- [162] R. H. Battin, *An introduction to the mathematics and methods of astrodynamics*. Reston, Virginia: AIAA Education Series, American Institute of Aeronautics and Astronautics, 1999.
- [163] P. Gurfil and P. K. Seidelmann, *Celestial mechanics and astrodynamics: theory and practice*. Berlin Heidelberg: Springer-Verlag, 2017.
- [164] V. Szebehely, *Theory of orbit: The restricted problem of three Bodies*. New York: Academic Press, 1967.
- [165] D. L. Richardson, "Analytic construction of periodic orbits about the collinear points," *Celestial Mechanics*, vol. 22, pp. 241-253, 1980.
- [166] G. Gómez, *Dynamics and Mission Design Near Libration Points, Vol I: Fundamentals: the Case of Collinear Libration Points* vol. 1. Singapore: World Scientific, 2001.
- [167] M. Hénon, "New families of periodic orbits in Hill's problem of three bodies," *Celestial Mechanics and Dynamical Astronomy*, vol. 85, pp. 223-246, 2003.
- [168] M. Hénon, "A family of periodic solutions of the planar three-body problem, and their stability," *Celestial mechanics*, vol. 13, pp. 267-285, 1976.
- [169] M. Hénon, "Numerical exploration of the restricted problem. VI. Hill's case: Non-periodic orbits," *Astronomy and Astrophysics*, vol. 9, pp. 24-36, 1970.
- [170] R. Broucke, "Periodic orbits in the restricted three body problem with earth-moon masses," Jet Propulsion Laboratory, California Institute of Technology, Report 82-1168, 1968.
- [171] K. Howell and H. Pernicka, "Numerical determination of Lissajous trajectories in the restricted three-body problem," *Celestial Mechanics*, vol. 41, pp. 107-124, 1987.
- [172] Z. Zhang and X. Hou, "Transfer orbits to the Earth–Moon triangular libration points," *Advances in Space Research*, vol. 55, pp. 2899-2913, 2015.
- [173] G. Gómez, A. Jorba, J. Masdemont, and C. Simó, "Study refinement of semi-analytical halo orbit theory," *Final Report, ESOC Contract*, 1991.
- [174] J. S. Parker, "Low-energy ballistic lunar transfers," Ph.D. Dissertation, University of Colorado at Boulder, 2007.
- [175] J. S. Parker, K. E. Davis, and G. H. Born, "Chaining periodic three-body orbits in the Earth–Moon system," *Acta Astronautica*, vol. 67, pp. 623-638, 2010.
- [176] J. S. Parker and G. H. Born, "Modeling a low-energy ballistic lunar transfer using dynamical systems theory," *Journal of Spacecraft and Rockets*, vol. 45, pp. 1269-1281, 2008.
- [177] H. Atkinson, C. Tickell, and D. Williams, "Report of the task force on potentially hazardous near Earth objects," British National Space Centre, London, 2000.
- [178] T. Gehrels, M. S. Matthews, and A. Schumann, *Hazards due to Comets and Asteroids* vol. 24. Tucson, Arizona: University of Arizona Press, 1994.
- [179] C. Gritzner, K. Dürfeld, J. Kasper, and S. Fasoulas, "The asteroid and comet impact hazard: risk assessment and mitigation options," *Naturwissenschaften*, vol. 93, pp. 361-373, 2006.

- [180] A. Harris, M. Boslough, C. Chapman, L. Drube, P. Michel, and A. Harris, "Asteroid Impacts and Modern Civilization: Can We Prevent a Catastrophe?," in *Asteroids IV*, P. Michel, F. E. DeMeo, and W. F. Bottke, Eds., ed Arizona: University of Arizona Press, 2015, pp. 835-854.
- [181] S. R. Chesley, P. W. Chodas, A. Milani, G. B. Valsecchi, and D. K. Yeomans, "Quantifying the risk posed by potential Earth impacts," *Icarus*, vol. 159, pp. 423-432, 2002.
- [182] K. Deb, A. Pratap, S. Agarwal, and T. Meyarivan, "A fast and elitist multiobjective genetic algorithm: NSGA-II," *IEEE transactions on evolutionary computation*, vol. 6, pp. 182-197, 2002.
- [183] D. E. C. Davis, "Multi-body trajectory design strategies based on periapsis Poincaré maps," PhD, Purdue University, 2011.
- [184] A. Haapala and K. Howell, "Trajectory design strategies applied to temporary comet capture including Poincaré maps and invariant manifolds," *Celestial Mechanics and Dynamical Astronomy*, vol. 116, pp. 299-323, 2013.
- [185] A. J. Krueger and R. A. Minzner, "A mid - latitude ozone model for the 1976 US Standard Atmosphere," *Journal of Geophysical Research*, vol. 81, pp. 4477-4481, 1976.
- [186] D. Rees, J. Barnett, and K. Labitzke, "COSPAR International Reference Atmosphere: 1986. Pt. 2: Middle atmosphere models," *Advances in space research*, vol. 10, p. 525, 1990.
- [187] D. A. Vallado, *Fundamentals of astrodynamics and applications*. New York: Springer, 2007.
- [188] S. Love and D. Brownlee, "Heating and thermal transformation of micrometeoroids entering the Earth's atmosphere," *Icarus*, vol. 89, pp. 26-43, 1991.
- [189] V. Svetsov, I. Nemtchinov, and A. Teterov, "Disintegration of large meteoroids in Earth's atmosphere: Theoretical models," *Icarus*, vol. 116, pp. 131-153, 1995.
- [190] M. Ceriotti, "Global optimisation of multiple gravity assist trajectories," PhD thesis, University of Glasgow, 2010.
- [191] B. Tauzin, E. Debayle, C. Quantin, and N. Coltice, "Seismoacoustic coupling induced by the breakup of the 15 February 2013 Chelyabinsk meteor," *Geophysical Research Letters*, vol. 40, pp. 3522-3526, 2013.
- [192] J. W. Birks, P. J. Crutzen, and R. G. Roble, "Frequent ozone depletion resulting from impacts of asteroids and comets," in *Comet/Asteroid Impacts and Human Society: An Interdisciplinary Approach*, P. Bobrowsky and H. Rickman, Eds., ed Berlin: Springer, 2007, pp. 225-245.
- [193] M. Lidov, "The evolution of orbits of artificial satellites of planets under the action of gravitational perturbations of external bodies," *Planetary and Space Science*, vol. 9, pp. 719-759, 1962.
- [194] G. Cook, "Luni-solar perturbations of the orbit of an earth satellite," *Geophysical Journal International*, vol. 6, pp. 271-291, 1962.
- [195] J. Danby, *Fundamentals of celestial mechanics (second ed)*. Va., U.S.A: Willman-Bell, Richmond, 1992.
- [196] E. W. Weisstein. (2002). *Sphere point picking*. Available: <http://mathworld.wolfram.com/SpherePointPicking.html>

- [197] D. Perna, M. Barucci, L. Drube, A. Falke, M. Fulchignoni, A. Harris, *et al.*, "A global response roadmap to the asteroid impact threat: the NEOSShield perspective," *Planetary and Space Science*, vol. 118, pp. 311-317, 2015.
- [198] A. Rao, *Dynamics of particles and rigid bodies: a systematic approach*. Cambridge: Cambridge University Press, 2005.
- [199] W. F. Bottke Jr, M. C. Nolan, H. J. Melosh, A. M. Vickery, and R. Greenberg, "Origin of the Spacewatch small Earth-approaching asteroids," *Icarus*, vol. 122, pp. 406-427, 1996.
- [200] W. Hartmann, "Impact strengths and energy partitioning in impacts into finite solid targets," in *Lunar and Planetary Science Conference*, 1988, pp. 451-452.
- [201] A. Fujiwara, G. Kamimoto, and A. Tsukamoto, "Destruction of basaltic bodies by high-velocity impact," *Icarus*, vol. 31, pp. 277-288, 1977.
- [202] D. P. O'Brien and R. Greenberg, "The collisional and dynamical evolution of the main-belt and NEA size distributions," *Icarus*, vol. 178, pp. 179-212, 2005.
- [203] D. R. Davis, C. R. Chapman, S. J. Weidenschilling, and R. Greenberg, "Collisional history of asteroids: Evidence from Vesta and the Hiryama families," *Icarus*, vol. 62, pp. 30-53, 1985.
- [204] D. D. Durda and S. F. Dermott, "The collisional evolution of the asteroid belt and its contribution to the zodiacal cloud," *Icarus*, vol. 130, pp. 140-164, 1997.
- [205] C. Okamoto and M. Arakawa, "Experimental study on the collisional disruption of porous gypsum spheres," *Meteoritics & Planetary Science*, vol. 44, pp. 1947-1954, 2009.
- [206] K. Holsapple, I. Glibin, K. Housen, A. Nakamura, and E. Ryan, "Asteroid impacts: Laboratory experiments and scaling laws," in *Asteroids III*. vol. 1, W. F. Bottke, A. Cellino, P. Paolicchi, and R. P. Binzel, Eds., ed, 2002, pp. 443-462.
- [207] E. V. Ryan, D. R. Davis, and I. Glibin, "A laboratory impact study of simulated Edgeworth–Kuiper belt objects," *Icarus*, vol. 142, pp. 56-62, 1999.
- [208] E. V. C. Ryan, "Catastrophic collisions: Laboratory impact experiments, hydrocode simulations, and the scaling problem," PhD, University of Arizona, 1992.
- [209] M. D. Jokic and J. M. Longuski, "Artificial gravity and abort scenarios via tethers for human missions to Mars," *Journal of Spacecraft and Rockets*, vol. 42, pp. 883-889, 2005.
- [210] M. Bangham, E. Lorenzini, and L. Vestal, "Tether transportation system study," NASA TP-1998-206959 NASA TP-1998-206959, 1998.
- [211] M. K. Bharti, "Momentum-Exchange Tether Propulsion System For Propellantless Orbital Manoeuvres: A Review," *International Journal of Research*, vol. 5, pp. 2463-2467, 2018.
- [212] M. D. Jokic and J. M. Longuski, "Design of tether sling for human transportation systems between Earth and Mars," *Journal of Spacecraft and Rockets*, vol. 41, pp. 1010-1015, 2004.
- [213] D. Smitherman, "Space Elevators, An Advanced Earth-Space Infrastructure for the New Millennium," NASA CP-2000-210429, 2000.

-
- [214] E. Lorenzini, M. Cosmo, M. Kaiser, M. Bangham, D. Vonderwell, and L. Johnson, "Mission analysis of spinning systems for transfers from low orbits to geostationary," *Journal of Spacecraft and Rockets*, vol. 37, pp. 165-172, 2000.
- [215] E. Kolemen, N. J. Kasdin, and P. Gurfil, "Multiple Poincaré sections method for finding the quasiperiodic orbits of the restricted three body problem," *Celestial Mechanics and Dynamical Astronomy*, vol. 112, pp. 47-74, 2012.
- [216] S. McGuire and C. O. Laux, "Experimental analysis of atomic Carbon and Carbon Monoxide production within a high temperature ablative boundary layer," in *55th AIAA Aerospace Sciences Meeting, AIAA 2017-0440*, Grapevine, Texas, 2017.
- [217] M. Rosen, "A Rocky Road to Mars: Asteroid grab would get humans back in space but perhaps no closer to the Red Planet," *Science News*, vol. 186, pp. 22-27, 2014.
- [218] M. B. Quadrelli, L. J. Wood, J. E. Riedel, M. C. McHenry, M. Aung, L. A. Cangahuala, *et al.*, "Guidance, navigation, and control technology assessment for future planetary science missions," *Journal of Guidance, Control, and Dynamics*, vol. 38, pp. 1165-1186, 2015.
- [219] R. Walker, D. Izzo, C. d. Negueruela, L. Summerer, M. Ayre, and M. Vasile, "Concepts for Near-Earth Asteroid deflection using spacecraft with advanced nuclear and solar electric propulsion systems," *Journal of the British Interplanetary Society*, vol. 58, pp. 268-278, 2005.